

# Irreversible Electroporation in Clinical Practice

Martijn R. Meijerink  
Hester J. Scheffer  
Govindarajan Narayanan  
*Editors*

 Springer

---

# Irreversible Electroporation in Clinical Practice

---

Martijn R. Meijerink • Hester J. Scheffer  
Govindarajan Narayanan  
Editors

# Irreversible Electroporation in Clinical Practice

 Springer

*Editors*

Martijn R. Meijerink  
Department of Radiology and Nuclear  
Medicine  
VU University Amsterdam  
Amsterdam  
The Netherlands

Hester J. Scheffer  
Department of Radiology and Nuclear  
Medicine  
VU University Amsterdam  
Amsterdam  
Noord-Holland  
The Netherlands

Govindarajan Narayanan  
Vascular and Interventional Radiology  
Miami University Hospital and Clinics  
Miami, FL  
USA

ISBN 978-3-319-55112-8      ISBN 978-3-319-55113-5 (eBook)  
<https://doi.org/10.1007/978-3-319-55113-5>

Library of Congress Control Number: 2017960205

© Springer International Publishing AG 2018

This work is subject to copyright. All rights are reserved by the Publisher, whether the whole or part of the material is concerned, specifically the rights of translation, reprinting, reuse of illustrations, recitation, broadcasting, reproduction on microfilms or in any other physical way, and transmission or information storage and retrieval, electronic adaptation, computer software, or by similar or dissimilar methodology now known or hereafter developed.

The use of general descriptive names, registered names, trademarks, service marks, etc. in this publication does not imply, even in the absence of a specific statement, that such names are exempt from the relevant protective laws and regulations and therefore free for general use.

The publisher, the authors and the editors are safe to assume that the advice and information in this book are believed to be true and accurate at the date of publication. Neither the publisher nor the authors or the editors give a warranty, express or implied, with respect to the material contained herein or for any errors or omissions that may have been made. The publisher remains neutral with regard to jurisdictional claims in published maps and institutional affiliations.

Printed on acid-free paper

This Springer imprint is published by Springer Nature  
The registered company is Springer International Publishing AG  
The registered company address is: Gewerbestrasse 11, 6330 Cham, Switzerland

---

# Contents

## Part I Introduction

- 1 History of Image-Guided Tumor Ablation . . . . .** 3  
Hester J. Scheffer
- 2 History of Electroporation . . . . .** 13  
Andrea Rolong, Rafael V. Davalos, and Boris Rubinsky

## Part II Preclinical Research

- 3 Multi-scale Biophysical Principles in Clinical Irreversible Electroporation . . . . .** 41  
Daniel C. Sweeney, Robert E. Neal II, and Rafael V. Davalos
- 4 Numerical Modelling for Prediction and Evaluation of Treatment Outcome . . . . .** 67  
Bor Kos and Damijan Miklavčič
- 5 The Effect of Irreversible Electroporation on Blood Vessels, Bile Ducts, Urinary Tract, Intestines, and Nerves . . . . .** 81  
Jantien A. Vogel, Laurien G.P.H. Vroomen, and Govindarajan Srimathveeravalli

## Part III Technique, Tips and Tricks

- 6 Anesthetic Management During Irreversible Electroporation Procedures . . . . .** 97  
Jenny M. Vieveen and R. Arthur Bouwman
- 7 Complications and Procedures to Enhance Safety . . . . .** 105  
Laurien G.P.H. Vroomen, K. Nielsen, A.H. Ruarus, and Hester J. Scheffer
- 8 Treatment Planning, Needle Insertion, Image Guidance, and Endpoint Assessment. . . . .** 115  
Lukas Philipp Beyer and Philipp Wiggermann

<b>9</b>	<b>Thermal Effects of Irreversible Electroporation</b> . . . . .	121
	Eran van Veldhuisen, J.A. Vogel, J.H. Klaessens, and R.M. Verdaasdonk	
<b>Part IV Clinical Practice</b>		
<b>10</b>	<b>Irreversible Electroporation of Liver Tumors</b> . . . . .	139
	Karin Nielsen, Hester J. Scheffer, M. Petrousjka van den Tol, and Anders Nilsson	
<b>11</b>	<b>Irreversible Electroporation of Pancreatic Tumors</b> . . . . .	167
	Martijn R. Meijerink, Anders Nilsson, Govindarajan Narayanan, and Robert Martin	
<b>12</b>	<b>Irreversible Electroporation for Perihilar Cholangiocarcinoma (Klatskin Tumors)</b> . . . . .	191
	Eva Roos, Laurien G.P.H. Vroomen, Eran van Veldhuisen, Robert-Jan Coelen, Thomas M. van Gulik, and Martijn R. Meijerink	
<b>13</b>	<b>Irreversible Electroporation of Kidney Tumours</b> . . . . .	201
	Jim Koukounaras, Helen Kavnoudias, and Kenneth R. Thomson	
<b>14</b>	<b>Irreversible Electroporation of Prostate Tumors</b> . . . . .	215
	Matthijs Scheltema and Jean de la Rosette	
<b>15</b>	<b>Irreversible Electroporation of Tumors Within the Pelvic Cavity</b> . . . . .	223
	Martijn R. Meijerink, Nicole van Grieken, and Laurien G.P.H. Vroomen	
<b>16</b>	<b>Irreversible Electroporation of Lung Tumors</b> . . . . .	239
	H. Kodama, Govindarajan Srimathveeravalli, and S.B. Solomon	
<b>Part V Future Perspectives</b>		
<b>17</b>	<b>From Local to Systemic Treatment: Leveraging Antitumor Immunity Following Irreversible Electroporation</b> . . . . .	249
	Anita G.M. Stam and Tanja D. de Gruijl	
<b>18</b>	<b>Future Perspectives of IRE</b> . . . . .	271
	Martijn R. Meijerink, Hester J. Scheffer, and Govindarajan Naranayan	
	<b>Index</b> . . . . .	281

---

**Part I**

**Introduction**

Hester J. Scheffer

---

## 1.1 Cancer: A Brief History

The oldest descriptions of cancer can be found in ancient manuscripts. Fossilized bone tumors and the records of Egyptian mummies provide material evidence. The oldest known account of cancer dates from approximately 3,000–2,500 B.C. It is possibly attributable to Imhotep, an Egyptian physician and architect. The papyrus describes eight cases of tumors or ulcers of the breast, which ancient physicians treated by cauterization with a tool called the “fire drill.” The papyrus continues the narrative by stating that “there is no effective treatment” [1].

Twelve centuries later, these tumors obtained their modern name – cancer. The word cancer is credited to the Greek physician Hippocrates (Kos, Greece, 460–370 B.C.). Considered the “father of medicine,” Hippocrates employed the words ‘carcinus’ and ‘carcinoma’ in his descriptions of non-ulcer forming and ulcer forming tumors. Carcinus refers to the familiar zodiac sign Cancer, the Crab. The Greeks used this term because of the tendril-like projections. Hippocrates believed that both cancer and depression developed when the four “humors” or bodily fluids – black bile, yellow bile, phlegm, and blood – fell out of balance with one another, allowing black bile to collect in excess in whichever part of the body the cancer affected. From Hippocrates onward, the humoral theory was adopted by the prominent Greek physicist Claudius Galenus in the second-century A.D. and by Roman and Persian physicians. This theory’ dominated and influenced Western medical science for the next 1300 years [2].

---

H.J. Scheffer

Department of Radiology and Nuclear Medicine, VU University Medical Center,  
De Boelelaan 1117, 1081 HV Amsterdam, Netherlands  
e-mail: [hj.scheffer@vumc.nl](mailto:hj.scheffer@vumc.nl)



The next great wave in cancer scholarship and understanding came with the Renaissance, when scholars began to refine their understanding of the human body. Following the development of the modern scientific method in the Renaissance, scientists began to apply this to the study of disease. The Belgium physician and anatomist Andreas Vesalius (1514–1564), considered the founder of modern human anatomy, used autopsies to identify and understand anatomic structures that had previously been a mystery. No matter how hard Vesalius sought to confirm Hippocrates's theory of black bile, he failed to find this sinister porter of cancer and depression. And so, in one of the most influential books on anatomy "de humani corporis fabrica" (1543), Galenus' theory of black bile as the explanation for cancer was finally dispelled [2].

This radical change in modern medicine was followed by Italian anatomist Giovanni Morgagni (1682–1771), who laid the foundations for scientific oncology by performing autopsies and relating the patient's illness to the pathology found after death. Scottish surgeon John Hunter (1728–1793) suggested that some cancer could be cured with surgery and described how the surgeon should decide upon which cancers to operate [3]. The invention of anesthesia in the nineteenth century allowed the practice of oncological surgery to flourish and physicians to develop standard surgical approaches. In 1871, the Austrian surgeon Theodor Billroth performed the first esophagectomy, followed in 1873 by the first laryngectomy and most famously, the first gastrectomy in 1881 [4]. The first pancreaticoduodenectomy was performed in 1898 by the Italian surgeon Alessandro Codivilla. American surgeon Allen Whipple refined the technique in 1935 to the procedure commonly referred to as the Whipple-procedure. By the late nineteenth century, several surgeons also started to perform elective resections of liver tumors. However, without knowledge of the segmental anatomy of the liver, these were all based on random resections resulting in extremely high mortality rates. In 1952 Jean-Louis Lortat-Jacob performed the first elective hepatic resection that was based on the segmental anatomy described by Couinaud [5]. By the late 1970s, the overall survival benefit of hepatic resection of colorectal liver metastases (CRLM) was established. Couinaud's anatomic knowledge, combined with advances in anesthesia and antiseptics, resulted in an impressive reduction of complications: mortality rates dropped from around 20% during the mid-1960s to 2–3% during the early 1990s.

The twentieth century also saw the emergence of two other mainstays of cancer therapy: systemic chemotherapy and external beam radiation therapy. In 1943, a German air raid in Bari, Italy, led to the destruction of 17 American warships. One of the ship's secret cargo consisted of 70-ton mustard gas bombs to be used in the battlefield. When the ship exploded, the deadly load dispersed into the air. The dissemination of the gas to the nearby harbor of Bari resulted in the death of almost a thousand people in the months following the explosion. Stewart Francis Alexander, a Lieutenant Colonel and an expert in chemical warfare, investigated the aftermath. Autopsies of the victims suggested that pro-found lymphoid and myeloid suppression had developed after exposure. In his

report, Alexander theorized that since mustard gas all but ceased the division of certain types of somatic cells whose nature was to divide fast, it could also potentially be put to use in helping to suppress the division of certain types of cancerous cells [6]. Using this information, two pharmacologists from the Yale School of medicine, Louis Goodman and Alfred Gilman, injected mustine, a related agent (the prototype nitrogen mustard anticancer chemotherapeutic) into a patient with non-Hodgkin's lymphoma. They observed a dramatic reduction in the patient's tumor masses [7]. Although the effect lasted only a few weeks, this was the first step to the realization that cancer could be treated by pharmacological agents [8]. This success was soon followed by Sidney Farber, often named the father of chemotherapy, who was the first to achieve a remission in a child with acute myeloid leukemia using the folic acid-antagonist aminopterin in 1948 [2]. After this discovery, an extensive search for other chemotherapeutic agents began, and many different chemotherapeutics were developed. The early chemotherapy regimens were life-threatening procedures and resulted in a temporary response at best, but some of these agents are still in use. For example, fluorouracil (5-FU), still one of the mainstays of chemotherapy for colorectal liver metastases, was first described in 1957. Recently, targeted therapies such as kinase inhibitors and monoclonal antibodies have been added to the arsenal of systemic therapies.

In 1895, Wilhelm Conrad Röntgen discovered the basic properties of ionizing radiation (X-rays) and the possibility of using radiation in medicine. During early practical work and scientific investigation, experimenters noticed that prolonged exposure to X-rays created inflammation and, more rarely, tissue damage on the skin. Emil Grubbe, a medical student, hypothesized that the destruction of skin as a side effect of radiation could be used to treat tumors. On March 29, 1896, he bombarded the breast of an aged lady, Rose Lee, in which a painful recurrence after mastectomy had developed. The treatment resulted in significant tumor shrinkage. This first radiation treatment indicated the foundation of the field of radiation oncology [9]. The discovery of Radium in 1898 by Marie Curie resulted in the speculation whether it could be used for therapy in the same way as X-rays. Radium was soon seen as a way to treat disorders that were not affected enough by X-ray treatment because it could be applied in a multitude of ways in which X-rays could not [10]. By the 1930s, radiation oncologists were able to achieve permanent remission of several types of cancer in a significant fraction of patients. Further improvement came with the introduction of megavoltage linear accelerators in the 1950s. Nowadays, the three main divisions of radiation therapy are external beam radiation therapy, brachytherapy, and systemic radioisotope therapy. The past years, a more precise method of external beam radiation has been developed: stereotactic ablative radiotherapy (SABR). SABR refers to highly focused radiation treatment, delivering an intense dose concentrated on the tumor with submillimeter accuracy, while limiting the dose to the surrounding organs. SABR is increasingly used to treat lung, liver, brain, and pancreatic tumors (Fig. 1.1).

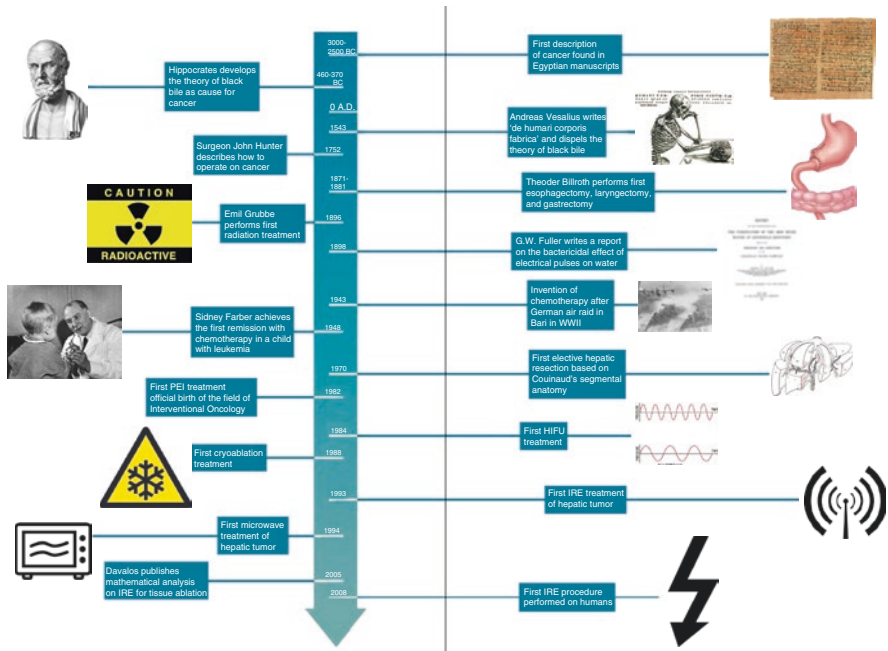


Fig. 1.1 Historical landmarks in oncology

## 1.2 Image-Guided Tumor Ablation: A Brief History

Decades of intensive cancer research have resulted in continuously improved surgical, chemotherapeutic, and radiation treatments. This has led to a dramatic improvement in overall cancer survival. However, despite the advances of surgical techniques, many tumors are still considered unsuitable for surgical resection, especially primary and secondary liver tumors; for example, only 20–30% of the patients with CRLM are found eligible for surgery because of unfavorable tumor location, disease extent or insufficient hepatic reserve, and comorbidity [11]. The use of radiotherapy for liver tumors is traditionally limited due to the low tolerance of normal liver tissue to radiation, which results in radiation-induced liver disease in a significant proportion of patients [12]. Furthermore, although it greatly improves overall survival, chemotherapy generally has a temporary effect and rarely leads to complete regression on its own.

### 1.2.1 Percutaneous Ethanol Ablation

In order to be able to treat some of these unresectable tumors, forward thinking surgeons, radiologists, and interventional radiologists started to consider and realize the potential to treat solid tumors using a completely new modality: “tumor ablation”,

with the help of electrodes or probes inserted into tumors, delivering chemicals or energy in order to achieve local control. Historically, percutaneous ethanol injection (PEI) was the first percutaneous ablative therapy to be clinically applied in the early 1980s. Ethanol causes thrombosis and disruption of the endothelium of small blood vessels and induces cell death due to dehydration. The official birth of percutaneous interventional oncology was marked by the first papers on PEI of small hepatic and abdominal tumors and parathyroid hyperplasias [13, 14]. In two subsequent papers, Livraghi and Ebara and colleagues demonstrated PEI to be cheap, safe, and effective in the treatment of hepatocellular carcinoma (HCC) [15, 16]. However, in the treatment of metastatic disease PEI proved less effective, since the heterogeneous and often fibrous nature of metastatic tumors restricts the diffusion of ethanol. For a similar reason, other injectable agents such as chemotherapeutic drugs and hot saline did not provide great efficacy for the treatment of metastatic liver disease. Different methods for ablation based on the deposition of physical energy therefore came into being.

### 1.2.2 Radiofrequency Ablation

Of the different ablation techniques, radiofrequency ablation (RFA) is currently the most widely employed technique. While the clinical use of RFA is relatively new, the biological effects of radiofrequency currents were already recognized long before their therapeutic use was investigated. In 1891, D'Arsonval demonstrated that when radiofrequency waves passed through tissue, they caused an increase in tissue temperature [17]. In 1910, the British urologist Edwin Beer described a new method for the treatment of bladder neoplasms using cauterization through a cystoscope [18], followed in 1911 by William Clark who described the use of oscillatory desiccation in the treatment of malignant tumors that were accessible for minor surgical procedures [19]. However, presumably because of the lack of image guidance, it was not until 1990 that two independent investigators, McGahan and Rossi, used a modification of prior radiofrequency techniques to create coagulation via the percutaneous route using specifically designed needles [20, 21]. In 1993 this technique was used for the first time to ablate liver tumors in humans [22]. RFA uses a needle applicator that emits an alternating electric current, which results in the generation of heat and ultimately protein denaturation resulting in cell death. Over the past 10 years, manufacturers have designed more powerful generators, developed special programs for heat deposition, and improved needle designs such as the deployable prongs and the saline-cooled applicator, which caused less tissue charring, both considerably increasing coagulation volumes. Nowadays, RFA has reached a high level of reliability for the treatment of HCCs up to 5–6 cm in size, of hepatic metastases up to 3–4 cm and, of some extrahepatic malignancies, such as lung, kidney, and bone neoplasms [23–26].

### 1.2.3 High-Intensity Focused Ultrasound

High-intensity focused ultrasound (HIFU) represents another thermal tumor ablation technique. The biological effects of ultrasound were known long before its use for diagnostic imaging was proposed. During the First World War, the French physicist Paul Langevin worked on a detection method for submarines. He reported that “fish placed in the beam in the neighborhood of the source operating in a small tank were killed immediately, and certain observers experienced a painful sensation on plunging the hand in this region”. In 1942, John Lynn was the first to use HIFU to create focal ablation lesions *in vivo*. In the late 1950s, William and Francis Fry developed a four-element HIFU transducer which was used for the first clinical HIFU treatments of Parkinsonism and hyperkinesis in 1958 by Russell Meyers. In the late 1980s, when ultrasound imaging became widely available, US-HIFU was intensely investigated for the ablation of liver tumors. In 1993, Hynynen and coworkers proposed the use of magnetic resonance (MR) for therapy guidance. The combination of MR guidance and HIFU ablation was coined MR-HIFU and marked the beginning of a renewed interest in this treatment modality.

### 1.2.4 Cryoablation

Extremely cold temperatures have been used to decrease inflammation and to relieve pain since the time of the ancient Egyptians. In the nineteenth century an English physician, James Arnott, used a combination of ice and salt to produce tissue necrosis for tumors of the cervix and breast by topic application [27]. Liquid air and carbon dioxide were subsequently employed as cryogens for the treatment of tumors, based on the principle used for air conditioning and refrigeration; atmospheric gases warm when compressed and cool during expansion. Following many experimental studies using liquid nitrogen as cryogen [28], the first clinical experiences with the use of cryotherapy were reported by the late 1980s. The key development was the fusion of cryoablation with real-time image guidance to verify the extent of treatment and to measure the size of the ice ball created by freezing [29]. Interstitial hepatic cryosurgery initially started as an intraoperative procedure, mostly because of the large size of cryoprobes. Thanks to the subsequent development of argon-based cryoablation systems with much thinner cryoprobes and decreased treatment times, minimally invasive cryoablation techniques, including the percutaneous approach under cross-sectional image guidance, have been introduced for – predominantly – kidney, lung, and bone malignancies [30].

### 1.2.5 Laser Ablation

Laser ablation (or laser-induced interstitial thermotherapy) uses laser for thermal tumor destruction. The neodymium: yttrium-aluminum-garnet (Nd: YAG) laser system was initially used to treat head and neck tumors through precise surgical

dissections rather than for tumor destruction. The first experimental application of laser hyperthermia for the treatment of liver neoplasms was reported in 1987 [31]. Recent improvements in laser-induced thermotherapy allow larger areas of coagulative necrosis than the earlier systems [32, 33]. However, the clinical acceptance of laser ablation has been limited, in part due to the technical complexity of the method requiring several fiber placements compared to the other easier-to-perform thermal ablation methods.

### 1.2.6 Microwave Ablation

Microwave ablation (MWA) is the most recently introduced thermal ablation technique. It uses a monopolar antenna causing water molecules in the tissue to vibrate at a higher frequency than with RFA. This generates frictional heat in the water molecules and leads to thermal coagulation of tissue. The first reports about US-guided percutaneous MWA for the treatment of unresectable HCC were published in 1994 [34]. Microwave energy has demonstrated several advantages over RFA [35]. Microwaves readily penetrate through biologic materials, including those with low electrical conductivity, such as lung, bone, and dehydrated or charred tissue. Consequently, microwave power can produce continuous, extremely high (>150 °C) temperatures, which improves ablation efficacy by increasing thermal conduction into the surrounding tissue. Multiple antennas can be operated simultaneously [36–38]. On the other hand, the distribution of microwave energy is inherently more difficult to control, which can lead to unintended injuries to other tissues [39, 40].

Modern approaches take advantage of the vastly superior armamentarium of imaging strategies nowadays available. Advances in the technique combined with improved localization now make it possible to be much more aggressive and effective in attempting to achieve local control of unresectable primary or metastatic tumors. Ablative therapies have gained widespread attention and, in many cases, broad clinical acceptance as methods for treating focal malignancies in a wide range of tumor types and tissues, including primary and secondary malignancies of the liver, kidney, lung, and bone [35, 41–44]. Each minimally invasive ablation technique has their own advantages and disadvantages and particular applications [45]. However, all the currently used effective ablative modalities are thermal techniques. Because these methods depend on thermal injury, they inadvertently carry some risk of damage to the adjacent extracellular environment like blood vessels and bile ducts, which can lead to serious complications. Other common complications of thermal ablation are perforation of adjacent bowel structures or the diaphragm. Another disadvantage of thermal ablation is that the extent of the treated area is difficult to control because blood circulation has a strong local effect on the distribution of heat. As a result, temperatures near large vessels decrease, which can lead to incomplete ablation of tumors located near these vessels. Due to this so-called heat-sink effect, the chance of complete ablation is effectively decreased to up

to 50% for RFA near large vessels. In recent years, a new method of tumor ablation has emerged that addresses the limitations of thermal ablation: irreversible electroporation.

## References

1. Breasted JH. The Edwin Smith surgical papyrus: published in facsimile and hieroglyphic translation with translation and commentary in two volumes. Chicago: University of Chicago Press, University of Chicago Oriental Institute Publications; 1991.
2. Mukherjee S. The emperor of all maladies: a biography of cancer. New York: Scribner; 2011.
3. Moore W. The knife man: the extraordinary life and times of John Hunter, father of modern surgery. London: Bantam Press; 2005.
4. Nuland B. Doctors: the biography of modern medicine. New York: Knopf; 1988.
5. Lortat-Jacob J, Robert H. Well defined technique for right hepatectomy. Paris: La presse medicale; 1952.
6. Li JJ. Laughing gas, viagra and lipitor: the human stories behind the drugs we use. New York: Oxford University Press; 2006.
7. Gilman A. The initial clinical trial of nitrogen mustard. *Am J Surg.* 1963;105:574–8.
8. Fenn J, Udelsman R. First use of intravenous chemotherapy cancer treatment: rectifying the record. *J Am Coll Surg.* 2011;212(3):413–7.
9. MacKee GM. X-rays and radium in the treatment of diseases of the skin. Philadelphia: Lea & Febiger; 1921.
10. Metzbaum M. Radium: its value in the treatment of lupus, rodent ulcer, and epithelioma, with reports of cases. *Int Clin.* 1905;4(14):21–31.
11. Leporrier J, Maurel J, Chiche L, Bara S, Segol P, Launoy G. A population-based study of the incidence, management and prognosis of hepatic metastases from colorectal cancer. *Br J Surg.* 2006;93:465–74.
12. Emami B, Lyman J, Brown A. Tolerance of normal tissue to therapeutic irradiation. *Int J Radiat Oncol Biol Phys.* 1991;21:109–22.
13. Solbiati L, Giangrande A, De Pra L, Bellotti E, Cantu P, Ravetto C. Percutaneous ethanol injection of parathyroid tumours under US guidance: treatment for secondary hyperparathyroidism. *Radiology.* 1985;155:607–10.
14. Livraghi T, Festi D, Monti F, Salmi A, Vettori C. US-guided percutaneous ethanol injection of small hepatic and abdominal tumours. *Radiology.* 1986;161:309–12.
15. Livraghi T, Salmi A, Bolondi L, Marin G, Arienti V, Monti F. Small hepatocellular carcinoma: percutaneous alcohol injection – results in 23 patients. *Radiology.* 1988;1(168):313–7.
16. Ebara M, Otho M, Sugiura N, Okuda K, Kondo F, Kondo Y. Percutaneous ethanol injection for the treatment of small hepatocellular carcinoma: study of 95 patients. *J Gastroenterol Hepatol.* 1990;5:616–25.
17. D'Arsonval M. Action physiologique des courants alternatifs. *C R Soc Biol.* 1891;43:283–6.
18. Beer E. Removal of neoplasms of the urinary bladder. A new method employing frequency (Oudin) currents through a catheterizing cystoscope. *JAMA.* 1910;54:1768.
19. Clark W. Oscillatory desiccation in the treatment of accessible malignant growths and minor surgical conditions. *J Adv Ther.* 1911;29:169–83.
20. McGahan J, Browning P, Brock J, Tesluk H. Hepatic ablation using radiofrequency electrocautery. *Investig Radiol.* 1990;25:267–70.
21. Rossi S, Fornari F, Pathies C, Buscarini L. Thermal lesions induced by 480 KHz localized current field in guinea pig and pig liver. *Tumori.* 1990;76:54–7.
22. McGahan J, Schneider P, Brock J, Tesluk H. Treatment of liver tumors by percutaneous radiofrequency electrocautery. *Semin Interv Radiol.* 1993;10:143–9.

23. Solbiati L, Livraghi T, Goldberg S. Percutaneous radiofrequency ablation of hepatic metastases from colorectal cancer: long-term results in 117 patients. *Radiology*. 2001;221:159–66.
24. Belfiore G, Moggio G, Tedeschi E. CT-guided radiofrequency ablation: a potential complementary therapy for patients with unresectable primary lung cancer – a preliminary report of 33 patients. *AJR Am J Roentgenol*. 2004;183:1003–11.
25. Mayo-Smith W, Dupuy D. Adrenal neoplasms: CT-guided radiofrequency ablation. Preliminary results. *Radiology*. 2004;231:225–30.
26. Rosenthal D, Hornicek F, Torriani M, Gebhardt M, Mankin H. Osteoid osteoma: percutaneous treatment with radiofrequency energy. *Radiology*. 2003;229:171–5.
27. Gage A. History of cryosurgery. *Semin Surg Oncol*. 1998;14:99–109.
28. Dutta P, Montes M, Gage A. Large volume freezing in experimental hepatic cryosurgery. Avoidance of bleeding in hepatic freezing by an improvement in the technique. *Cryobiology*. 1979;16:50–5.
29. Ravikumar T, Kane R, Cady B. Hepatic cryosurgery with intraoperative ultrasound monitoring for metastatic colon carcinoma. *Arch Surg*. 1987;122:403.
30. Permpongkosol S, Nielsen M, Solomon S. Percutaneous renal cryoablation. *Urology*. 2006;68:19–25.
31. Hashimoto D. Application of the laser thermal effect to the therapy of liver neoplasms. *Nippon Rinsho*. 1987;45:888–96.
32. Pacella C, Bizzarri G, Francica G. Percutaneous laser ablation in the treatment of hepatocellular carcinoma with small tumours: analysis of factors affecting the achievement of tumour necrosis. *J Vasc Interv Radiol*. 2005;16:1447–57.
33. Vogl T, Straub R, Eichler K, Sollner O, Mack M. Colorectal carcinoma metastases in liver: laser-induced interstitial thermotherapy – local tumour control rate and survival data. *Radiology*. 2004;230:450–8.
34. Seki T, Kubota Y, Wakabayashi M. Percutaneous transhepatic microwave coagulation therapy for hepatocellular carcinoma proliferating in the bile duct. *Dig Dis Sci*. 1994;39:663–6.
35. Ahmed M, Brace CL, Lee FT, Goldberg SN. Principles of and advances in tumor ablation. *Radiology*. 2011;258(2):351–69.
36. Brace C, Laeseke P, Sampson L, Frey T, van der Weide D, Lee FJ. Microwave ablation with a single small-gauge triaxial antenna: in vivo porcine liver model. *Radiology*. 2007;242:435–40.
37. Goldberg S, Hahn P, Tanabe K. Percutaneous radiofrequency tissue ablation: does perfusion-mediated tissue cooling limit coagulation necrosis? *J Vasc Interv Radiol*. 1998;9:101–11.
38. Ahmed M, Lobo S, Weinstein J. Improved coagulation with saline solution pretreatment during radiofrequency tumor ablation in a canine model. *J Vasc Interv Radiol*. 2002;13:717–24.
39. Strickland A, Clegg P, Cronin N. Experimental study of large-volume microwave ablation in the liver. *Br J Surg*. 2002;89:1003–7.
40. Wolf F, Grand D, Machan J, Dipetrillo T, Mayo-Smith W, Dupuy D. Microwave ablation of lung malignancies: effectiveness, CT findings, and safety in 50 patients. *Radiology*. 2008;247:871–9.
41. Gillams AR, Lees WR. Five-year survival in 309 patients with colorectal liver metastases treated with radiofrequency ablation. *Eur Radiol*. 2009;19(5):1206–13.
42. Livraghi T, Solbiati L, Meloni M, Gazelle G, Halpern E, Goldberg S. Treatment of focal liver tumors with percutaneous radio-frequency ablation: complications encountered in a multicenter study. *Radiology*. 2003;226(2):441–51.
43. Dupuy D, DiPetrillo T, Gandhi S, Ready N, Ng T, Donat W, et al. Radiofrequency ablation followed by conventional radiotherapy for medically inoperable stage I non-small cell lung cancer. *Chest*. 2006;129(3):738–45.
44. Gervais D, McGovern F, Arellano R, McDougal W, Mueller P. Renal cell carcinoma: clinical experience and technical success with radio-frequency ablation of 42 tumors. *Radiology*. 2003;226(2):417–24.
45. Davalos RV, Mir LM, Rubinsky B. Tissue ablation with irreversible electroporation. *Ann Biomed Eng*. 2005;33(2):223–31.



Andrea Rolong, Rafael V. Davalos, and Boris Rubinsky

---

## 2.1 Introduction

Electroporation phenomena can be traced back to the eighteenth century when red spots on human animal skin (Lichtenberg figures) were observed in the areas where electric fields were applied. Once the cause of this phenomenon was understood and control over the parameters that produce electric fields was achieved, a quick adoption of the use of pulsed electric fields to kill microbes was seen in the area of food and water sterilization. Biomedical applications soon followed where electric fields began to be used to control movement of biological material: cells were brought in close proximity and fused together through membrane destabilization (electrofusion), DNA material was introduced into cells through transient pores in the membrane (electrogenetherapy), and chemotherapeutic drugs were directly delivered to cells (electrochemotherapy). These applications fall under the energy regime known as reversible electroporation in which temporary cell membrane destabilization is achieved. Irreversible electroporation (IRE) uses an energy regime much higher than that of reversible electroporation and induces cell death via various mechanisms. Since the postulation that IRE can be used to ablate substantial volumes in such a manner that it does not induce significant traditional thermal damage, it has been widely investigated moving from in vitro studies, to in vivo animal studies, and finally to human patients through clinical trials. Its nonthermal mechanism to induce cell death makes it an attractive modality to safely treat unresectable tumors.

---

A. Rolong • R.V. Davalos (✉)

Department of Biomedical Engineering and Mechanics, Virginia Tech – Wake Forest University School of Biomedical Engineering and Sciences, Virginia Tech, Blacksburg, VA 24061, USA  
e-mail: [davalos@vt.edu](mailto:davalos@vt.edu)

B. Rubinsky

Department of Mechanical Engineering, University of California, Berkeley, CA 94720, USA

Electroporation is the phenomenon in which cell membrane permeability to ions and otherwise non-permeant molecules is increased by exposing the cell to short high electric field pulses. Such increase in permeability is related to the formation of nanoscale defects or pores in the cell membrane; this led to the adoption of the term *electroporation* to describe this occurrence. The goal of this chapter is to present a historical review of the use of electric fields leading to the field of electroporation from the first reports of these events in the eighteenth century to modern applications in minimally invasive surgery.

Time period	Advancement in the field
1754	J.A. Nollet performed experiments with electric fields and noticed formation of red spots on human and animal skin in the areas where sparks were applied. These can be explained as thermal Joule heating effects [1] or as damage to the capillaries by irreversible electroporation [2, 3]
1780	Luigi Galvani discovered “animal electricity” when a dead frog’s muscle twitched after being placed on an iron grating and having a bronze hook touch its spinal cord. Alessandro Volta explained the phenomenon as DC current. This led to the invention of a voltaic pile (first device able to produce steady electric current)
1802	J.W. Ritter performs experiments in electrophysiology and observes a contraction that occurs after a strong current passes through a stretch of muscle–nerve sample and is interrupted (Ritter’s opening tetanus) [4]
1898	G.W. Fuller performs what can be considered the first work on irreversible electroporation phenomena as bactericidal processing of water samples [5]
1903	A.D. Rockwell reports on experiments performed in the late 1800s using Leyden jars [6]; these could now be explained as hemolysis induced by irreversible electroporation [7]
1913	A.J. Jex-Blake evaluates the lethal effects of electricity and lightning [8]. It is currently accepted that some of the injuries caused by lightning, such as Lichtenberg figures on the skin, are due to irreversible electroporation [9]. These figures are believed to have the same origins as Nollet’s red spots (mentioned above)
1936	G.M. McKinley concludes that damage caused to living tissues by high-frequency fields (10–100 MHz) cannot be from thermal origin alone, particularly in the case of nervous tissue. <i>He proposes that this alternate mechanism associated with electric fields can be used as a minimally invasive method to selectively ablate specific tissues</i> [10]
1946	J.E. Nyrop publishes a paper in <i>Nature</i> in which a large portion of bacteria in a liquid suspension is destroyed at sublethal temperatures by the application of high radiofrequency electric fields [11]
1951	A.L. Hodgkin explains the Ritter’s opening tetanus as “...(the breakdown)... of the insulating properties of the membrane ... under the influence of the abnormally high potential difference” which alludes to what is now referred to as irreversible electroporation [12]
1956	B. Frankenhaeuser and L. Widén explain the change in normal nerve conductivity that occurs after electric pulses are applied on nerve nodes; they refer to it as anode break excitation [13]. In their study, amplitudes of up to ten times the normal threshold were obtained and pulse duration increased from <1 to >100 ms. They state the phenomenon is known since at least 1898 [14]

Time period	Advancement in the field
1957	Stämpfli and Willi describe irreversible and reversible electroporation on a frog nerve membrane [15]. Stämpfli reports that under certain conditions, membrane breakdown is irreversible whereas in others it is reversible [16]. He compares the phenomenon to the breakdown of the dielectric field of a capacitor
1961	H. Doevenspeck [17] describes commercial installations using electrical pulses to break apart cellular components for industrial food-related processing of animal meat through nonthermal means, which resemble irreversible electroporation. They report that these electric pulses can inactivate microorganisms with what is considered a nonthermal effect producing a small increase in temperature of at most 30 °C
1967	Pivotal papers by Sale and Hamilton on the bactericidal action of electric fields which set the basis for the field of irreversible electroporation. They contain the foundation of many of the future studies in electroporation in general [18–20]
1974	U. Zimmerman and his group determine that the electric field in cell counters induces cell membrane breakdown. Their methodology, which combines experimentation in Coulter type counters and between parallel plates with the solution of Laplace's equation, produced some of the first systematic data on the electrical parameters required for electroporation in cells. The critical membrane potential difference leading to membrane breakdown was found to be about 1 V. Results were published in a series of papers [21, 22]. They also suggest employing erythrocytes and lymphocytes as drug and enzyme carrier systems
1977	K. Kinoshita and T. Tsong [23] propose the permeabilization of the cell membrane due to the application of electric pulses is related to the formation of several pores. In experiments with red blood cells, they show that the size of the pores can be varied and that they eventually reseal
1978	S.V. Belov reports on what is probably the first case in which IRE of living tissues is intentionally pursued [24]. In an investigation of coagulation electro-surgical devices, he suggests that surgical coagulation is actually related to cell membrane breakdown due to pulses that have a “high ratio of peak to mean voltages.” The research was performed on frog leg muscle where histological analysis and measurements of changes in electrical resistance were used to show the damage to the cell membrane in tissue without producing a thermal effect
1982	The use of <b>reversible electroporation to produce fusion between cells</b> is described in a paper by Zimmermann [25]
1982	Neumann and his collaborators coin the term <i>electroporation</i> to describe the membrane breakdown induced by electric fields and introduce the use of <b>reversible electroporation to insert genes into cells</b> [26]
1984	After the design by H. Potter et al. [27] of an electroporation cuvette suitable for cell suspensions, microbiology researchers started to employ electrophoresis power supplies in order to perform gene transfection by electroporation
1987	S. Orlowski, L.M. Mir, and colleagues [28] and M. Okino and H. Mohri [29] independently report on the use of reversible electroporation to transiently permeabilize cells and thereby <b>introduce cytotoxic agents into malignant cells for the treatment of cancer</b>
1987–1988	An important series of studies in the field of <b>irreversible electroporation of tissue</b> began with the 1987 [30] and 1988 [31] papers by R.C. Lee and his coinvestigators on tissue trauma induced by electrical discharge

Time period	Advancement in the field
1989	By performing electrical conductance measurements K.T. Powell et al. [32] demonstrate that <b>frog skin can be reversibly electroporated</b>
1991	The first report on the use of <b>reversible electroporation to introduce plasmid DNA into a living tissue</b> was published by Titomirov et al. [33]
1991	L.M. Mir and colleagues publish two breakthrough papers on the use of reversible electroporation to treat cancer by facilitating the diffusion of anticancer drugs, such as bleomycin, in the malignant cells. They coin the term <i>electrochemotherapy</i> to describe this procedure [34] and report on the first clinical trial in the field of electroporation [35]
1993	Prausnitz et al. publish the first studies on <b>skin electroporation as transdermal drug delivery</b> [2, 36]
1990–1999	The study of the contribution of <b>irreversible electroporation to tissue damage during electrical shock</b> trauma continued since it was first proposed in the 1980s and was led primarily by R.C. Lee [37–39]. They suggest that irreversibly electroporated <b>cell membranes could be therapeutically sealed with surfactants</b> [40]
1997	Piñero et al. show in vitro that electroporation not only caused <b>necrosis</b> but it also induced cell death with features compatible with <b>apoptosis</b> [41]
1997	K.H. Schoenbach et al. [42, 43] report the first in vitro study on the use of very <b>high-voltage pulses of “submicrosecond” duration</b>
1998	Treatment planning is performed using <b>numerical methods to determine electric field distribution</b> . This was pioneered for the case of in vivo reversible electroporation by D. Miklavcic et al. [44]
1998	L.H. Ramirez et al. [45] report that <b>blood flow is blocked in the area where the electric field is applied</b> during tissue reversible electroporation. The phenomenon is later referred to as <i>the vascular lock</i> by Gehl et al. [46]
2000	Al-Khadra et al. report on the role of electroporation on defibrillation [47]. Jex-Blake had previously cited works of the eighteenth century in which animals were recovered from heart failure induced by electrical current by means of another electrical shock (defibrillation term not coined at the time)
2003	R.V. Davalos and B. Rubinsky file a provisional <b>US patent application</b> [48] followed by a non-provisional application in 2004 which proposes the <b>use of classical IRE</b> (pulses longer than 5 $\mu$ s) <b>as a tissue ablation method</b> . They point out that IRE can be easily applied in areas where perfusion is high (e.g., in the vicinity of blood vessels), as opposed to thermal methods of ablation
2004	C. Yao et al. [49] investigate the use of special pulses, referred to as <i>steep pulsed electric field</i> (SPEF), to kill cells in vitro and to inhibit tumor growth in vivo. Their SPEF pulses consist of a fast rising edge (rise time $\sim$ 200 ns) followed by a slow exponential decay ( $\tau \sim$ 200 $\mu$ s), originated from a capacitance discharge. They propose and demonstrate (in vitro and with delayed tumor growth in mice) that intracellular effects from the rising slope together with the plasma membrane effects from the falling slope can be used to destroy both cell nucleus and membrane
2005	R.V. Davalos, L.M. Mir, and B. Rubinsky publish a paper demonstrating that <b>IRE</b> can be used <b>as an independent tissue ablation method</b> [50] not necessarily accompanied by thermal effects and that such feature has important implications in post-treatment healing
2007	IRE is performed on pigs under experimental conditions relatively close to those of a clinical scenario [51]. IRE was applied in liver using 18-gauge stainless-steel needles positioned with the assistance of ultrasound sonography. The size and shape of the lesions is explained in a treatment planning procedure by Edd and Davalos [52]

Time period	Advancement in the field
2007	Al-Sakere et al. [53, 54] performs in vivo IRE of tumors subcutaneously inoculated in mice and studies the immune reactions. They achieved 92% complete regression reusing a protocol that consisted of 80 pulses of 100 $\mu$ s at 0.3 Hz with a field magnitude of 2,500 V/cm
2007	J. Lavee et al. publish a study with pigs in which IRE of the atrium is performed in order to analyze its applicability for the <b>treatment of atrial fibrillation</b> as an alternative to methods based on thermal ablation [55]. The demarcation between ablated and normal tissue was clear and sharp
2010	G. Onik and B. Rubinsky report on the first human clinical trial [56] where 16 patients with prostate cancer were treated with IRE in a series of outpatient procedures. Potency and continence was preserved in all patients who were continent and potent prior to treatment
2011	A clinical trial that included 38 patients with advanced liver, lung, and kidney tumors, where a total of 69 tumors were treated, is performed by Thompson et al. in Australia [57]
2015	In the largest evaluation to date, 200 patients with locally advanced pancreatic adenocarcinoma (stage III), underwent either IRE alone ( $n = 150$ ) or pancreatic resection combined with IRE for treatment margin enhancement ( $n = 50$ ) [58]

Note: The above table is not an all-inclusive summary of the all the studies performed on electroporation across the various areas of food processing, water sterilization, and biomedicine but rather a summary of key findings and what is believed to be the first report on each

### 2.1.1 The Lichtenberg Phenomenon

Probably the first scientific description of a phenomenon indicative of irreversible electroporation in tissue can be found in the 1754 book of J.A. Nollet “*Recherches sur les causes particulieres des phénomènes électriques*” [59]. In experiments with electrical fields, Nollet noticed the formation of red spots on the skin of humans and animals in areas where electrical sparks were applied. This same phenomenon was studied by J.P. Reilly [1], and, according to him, the red spots may be the consequence of stratum corneum degradation due to thermal damage. However, while thermal Joule heating effects cannot be ruled out, it is probable that those red spots were in fact caused by damage to the capillaries by irreversible electroporation. Erythemas are common in skin electroporation [2, 3], and even though some heating is always expected, it does not seem likely that the electrical generators at the time (static electricity generators were invented by Otto von Guericke in 1663) would be able to cause significant heating.

Interest in the effect of electricity in biological materials emerged throughout the eighteenth century. In 1780 Luigi Galvani showed that when a dead frog was placed on an iron grating and a bronze hook touched the spinal cord, the frog’s muscle twitched. He described the phenomenon as “animal electricity” but it was Alessandro Volta who found the correct explanation: the presence of two different metals in the same electrolyte creates a current. This led to the invention of the voltaic pile—the first device able to produce steady electric current and a basic element used in later discoveries on electromagnetism [60].

Observations on the effects of electric fields on tissue made in the early twentieth century may be related to electroporation. In 1913 A.J. Jex-Blake discussed the lethal effects of human made electricity and lightning [8]. He argues that burns from electricity, as observed in industrial accidents, are related to thermal effects, whereas electrical injuries from lightning do not seem to be all from thermal origin. It is now accepted that some of the damaging effects of lightning are caused by irreversible electroporation [31].

An astonishing nonlethal effect of lightning on humans is the emergence of red Lichtenberg figures on the skin that disappear in a few days. These figures have probably the same origin as Nollet's red spots. It is thought that following the dielectric breakdown of the skin and subsequent massive electron shower, red blood cells are extravasated into the superficial layers of the skin from the underlying capillaries [9] thus forming Lichtenberg figures.

---

## 2.2 Pulsed Electric Fields and Water Sterilization

The first work focusing on an irreversible electroporation phenomenon may be found in the 1898 study by G.W. Fuller titled "Report on the investigations into the purification of the Ohio river water at Louisville Kentucky" [5]. He discusses an experiment in which multiple high-voltage discharges are observed to kill bacteria on a water sample. Temperature was not found to increase significantly because of the treatment which, based on how irreversible electroporation is currently used for sterilization of fluids, indicates that Fuller's report on a bactericidal effect is most likely due to irreversible electroporation.

A 2001 publication titled "Water purification by electrical discharges" describes three types of electrical discharges commonly reported for water purification: contact glow discharge electrolysis, dielectric barrier discharges (silent discharges), and pulsed corona discharges [61]. In contact glow discharge electrolysis, a thin wire anode in contact with the water surface is charged with a continuous DC voltage, while the cathode is dipped in water and isolated from anode through porous glass. A vapor sheath forms around the anode through which current flows as a glow discharge and charged species in the plasma (present in the discharge gap or vapor sheath around the anode) are accelerated due to the steep potential gradient; they enter the liquid phase with very high energy. A dielectric barrier discharge reactor involves the use of electrodes; at least one of them is covered with a thin layer of dielectric material such as glass or quartz [62]. For water treatment applications using this type of reactor, a layer of water around one of the electrodes acts as a dielectric. An AC voltage of around 15 kV is usually applied across the electrodes. Free electrons and other ions in the discharge gap are accelerated under the influence of the applied electric field. An electron avalanche (streamer) is produced through repetition of the process of the free electrons. Lastly, a pulsed corona discharge reactor entails a pulse generator and a reactor. The reactor contains metallic electrodes usually in a needle-plate arrangement where the needle is connected to a high-voltage terminal and the plate is grounded. The needle is covered with an

insulator where only the tip is exposed so that an intense electric field may be obtained. Electrical discharges in all of these reactors take place in the gas phase in close proximity to the water surface which allows for plasma chemical reactions to take place. High-energy electrons produced in electrical discharges face inelastic collisions with other molecules in the environment which result in either the excitation, dissociation, electron capture, or ionization of target molecules. Here, the primary reactant is  $\text{H}_2\text{O}$  which leads to the formation of free radicals,  $\text{OH}^*$  in particular and these in turn destroy pollutants in the water [61].

More recent publications have continued to investigate the use of pulsed electric fields as an affordable and efficient alternative to decontaminate water without the need for chemicals or more expensive processing. A conducting nanosponge made of polyurethane coated with carbon nanotubes and silver nanowires was presented by C. Liu et al. to electroporate bacteria and viruses in water [63], a follow-up study by the same group reported on a similar method of water purification but with the use of copper nanowires instead of silver and with static electricity as the power source for electroporation [64].

---

### 2.3 Pulsed Electric Fields and the Food Industry

The field of electroporation has advanced with research carried out simultaneously in the areas of biomedicine and food processing technology. In food technology, irreversible electroporation is referred to as *pulsed electric field* processing or *electroplasmolysis* in reference to the lysis of cell membranes to extract their contents and to the bactericidal effect in these types of treatments. The nonthermal bactericidal effect of electric fields remained an area of research in the food industry through the first and second half of the twentieth century and continues today [65–67]. During the first half of the twentieth century, it was not obvious to researchers whether electric fields had a bactericidal effect beyond those expected from thermal or electrochemical causes. For instance, A.J.H. Sale and W.A. Hamilton cite a review published in 1949 that finds accounts both for and against such nonthermal effects of electric fields [68]. In 1961, H. Doevenspeck [17] describes the use of electric pulses to disrupt cellular components for industrial food-processing of meat through nonthermal means—thus resembling irreversible electroporation. These involve the electrical discharge of electric pulses from carbon electrodes through the treated material. The paper does not specifically refer to the breakdown of the cell membrane; nor does it provide specific values for the electric pulses used. Still, the outcome reported is clearly nonthermal disruption of the cell membrane. Doevenspeck also reported results showing that these electric pulses can inactivate microorganisms with a nonthermal effect; treatments produced a small increase in temperature of at most 30 °C.

The interest in the bactericidal effect of electric fields motivated three outstanding and influential papers by Sale and Hamilton which set the basis for the field of irreversible electroporation and contain many of the observations and methodology used in subsequent studies on electroporation [18–20]. The aim of the first paper

was to demonstrate that high field electric pulses of direct current (DC) can kill cells without a thermal effect. They assessed the nonthermal bactericidal effect using ten very short (2–20  $\mu\text{s}$ ) DC electric pulses separated by long intervals of a few seconds in order to minimize the temperature rise. A systematic study with several types of bacteria and two species of yeast demonstrated that the effect was not related to the cells' growth stage, the pH, electrolysis, nor heating. The measured temperature rise was at most 10  $^{\circ}\text{C}$ . They concluded that the electric field magnitude is the first parameter that affects cell killing followed by the total time the field is applied. The electric fields needed to completely ablate the cells were found to be rather substantial: 6 kV/cm for *Saccharomyces cerevisiae* and 16 kV/cm for *Escherichia coli*.

In the paper that followed [19], Hamilton and Sale explain that the mechanism by which the pulsed electric fields kill the cells is through the irreversible loss of the membrane's function as a semipermeable barrier. The paper reports leakage of cell contents in the medium of *Escherichia coli* suspension as a measure of the loss of cell membrane integrity; this was detected with spectroscopy. It also demonstrated membrane damage which led to lysis of erythrocytes and protoplasts. Electron microscopy of *E. coli* and erythrocytes show that complete membrane breakdown did not occur which suggests that either the damage was confined to particular areas that were not identified, or there are other mechanisms that contribute to cell death without requiring complete and irreversible loss of membrane integrity.

In the third study [20] Sale and Hamilton show that the electric field magnitude to induce lysis of various organisms ranges from 3.1 to 17 kV/cm (for 50% lysis with a protocol of ten pulses of 20  $\mu\text{s}$ ), while the equivalent induced transmembrane voltages only range from 0.7 to 1.15 V. They suggest that the transmembrane potential induced by the external field may cause “conformational changes in the membrane structure resulting in the observed loss of its semipermeable properties.”

In order to compute the induced transmembrane voltage, Sale and Hamilton employed a model in which the cell was considered to be a conductive sphere isolated from the external conductive medium by a thin dielectric layer. They used equations derived from those previously described by J.C. Maxwell for calculating the conduction through a suspension of spheres [69, 70]. The transmembrane voltage ( $V_m$ ) is highest at the poles facing the electrodes (i.e., direction of the electric field,  $\mathbf{E}$ ), and its value at any point on the cell is given by the *Schwann equation* [71].

---

## 2.4 Pulsed Electric Fields and Medicine

It is unsurprising that the first systematic work on what is now known as reversible and irreversible electroporation was done on nerves since research on stimulation of nerves with electricity goes as far back as the work of Galvani. In 1956, B. Frankenhaeuser and L. Widén published a study that attempted to explain the phenomenon of *anode break excitation* [13]. The phenomenon was described as a change in the normal nerve conductivity behavior when electric pulses are applied on nerve nodes with (as expressed in their study) amplitudes that are up to ten times the normal threshold and pulse durations of less than 1 ms to more than 100 ms.



The authors state that the actual phenomenon is known since at least 1898 [14]. Indicative of reversible and irreversible electroporation, they explain the phenomenon writing “It is, therefore, concluded that the strong (electrical) shock damaged to a large extent the nodes... and that these nodes were more or less inactivated.” And that “It may be concluded that the effect caused by the strong shock is to a fair extent reversible.” A previous study by Hodgkin [12] as well as several others were cited in support of their conclusion.

R. Stämpfli in collaboration with A. F. Huxley and others produced a series of studies in the 1950s which explored reversible and irreversible electroporation on the nerve membrane a frog. Stämpfli and Willi [15] write: “We had confirmed the observation of Frankenhaeuser and Widén [13], showing that anode break excitation in myelinated nerve can be elicited by strong positive pulses. We were able to show that such pulses produce a breakdown of membrane resistance and potential, if they increase the membrane potential by 70–110 mV, which corresponds to a voltage gradient of approximately half a million V/cm across the membrane. If only one short pulse is given the membrane recovers immediately after the breakdown like an electrolytic condenser. If very strong positive pulses on the order of 10 V are applied, the membrane is destroyed irreversibly.” Stämpfli reported that 5-s pulses induced membrane potentials of about 120–140 mV in a single insulated Ranvier node of a frog nerve fiber (corresponding to voltage gradients across the membrane of about 500,000 V/cm) and that these can cause breakdown of the membrane resistance. Under certain conditions, the breakdown is reversible; in others it is irreversible [16]. He described the phenomenon similar to the breakdown of the dielectric field of a capacitor.

Research during the 1970s and 1980s was primarily done in the field of reversible electroporation and focused on developing new uses and fundamental understanding of the mechanisms driving this phenomenon.

In 1972 E. Neumann and K. Rosenheck showed that electric pulses with a magnitude of 18–24 kV/cm and 150  $\mu$ s duration, produced reversible permeabilization of the cell membrane of bovine medullary chromaffin cells which secrete epinephrine, norepinephrine, ATP, and proteins [72]. Experiments showed that the largest increase in temperature was 6 °C (from initial 0 °C) and that the observed effect of reversible permeabilization was thus nonthermal. The authors relate such phenomenon to the physiological release of hormones and neurotransmitters in neurons instead of recognizing the increase in transmembrane potential induced by the external electric field resulting in reversible electroporation.

U. Zimmerman and colleagues, possibly unaware of previous studies by Sale and Hamilton, determined that electric fields induce cell membrane breakdown and that this could be the cause of discrepancies in the readings of an electrical cell counter. They developed a methodology combining experimentation in Coulter type counters and between parallel plates with the solution of Laplace's equation; this produced some of the first systematic data on the electrical parameters required for cell electroporation. They explored the dependence of cell membrane breakdown in human and bovine red blood cells, as expressed by the presence of intracellular contents in the extracellular solution, to increasing pulse amplitude and length.

They found the highest degree of membrane breakdown for a pulse length of about 50–100  $\mu\text{s}$  and electric field strength of about 2.6–2.8 kV/cm. The critical membrane potential difference leading to membrane breakdown was found to be about 1 V. Results from this group of studies were published in a couple of papers starting in 1974 [21, 22]. The parameters from this series of papers are relevant to irreversible electroporation. A practical outcome of their work is the idea of employing erythrocytes and lymphocytes as drug and enzyme carrier systems. In addition, they showed that the effects were not thermal and found different asymptotic values for human and bovine red blood cells. The latter phenomenon suggested the possibility for different irreversible electroporation thresholds for various types of cells.

### 2.4.1 Electrochemotherapy

K. Kinoshita and T. Tsong [23] proposed, from osmotic mass transfer experiments with red blood cells, the permeabilization of the cell membrane from application of electric pulses forms several pores with radii of a few angstroms. They showed that the size of these pores can be varied and that they eventually reseal and proposed the use of permeabilized cells as carriers of chemical species through the circulatory system. After evaluating the time it takes for the cells to reseal as a function of temperature, they found that impermeability is rapidly regained at 37 °C while cells remain highly permeable at 3 °C even after 20 h following the application of pulses.

M. Okino and H. Mohri [29] and S. Orlowski et al. [28] proposed the use of reversible electroporation to reversibly permeabilize cells in order to introduce cytotoxic agents into malignant cells for a more effective treatment of cancer.

In 1989, electrical conductance experiments performed by K.T. Powell et al. [32] demonstrated that frog skin can be reversibly electroporated. The report did not show how that could influence the passage of drugs through the skin but it may have influenced the following discovery in 1993 by M.R. Prausnitz et al. [36] in which transdermal drug delivery was achieved by electroporation.

L.M. Mir published two breakthrough papers in 1991 on the use of reversible electroporation to treat cancer by facilitating the infiltration of anticancer drugs, such as bleomycin, into malignant cells. They coined the term *electrochemotherapy* to describe this procedure [34] and reported on the first clinical trial in the field of electroporation [35]. M. Belehradek et al. reported on the results from this first clinical phase I–II trial in which good tolerance by the patients, lack of toxicity, and overall antitumor effects were observed. These served as the initial encouragement for further studies and developments on electrochemotherapy in clinical oncology [73].

Electrochemotherapy is now one of the most solid applications of reversible electroporation, and it is being used clinically to treat cancer patients. Probably the most updated review information on the topic can be found in [74–76].

Skin electroporation and its use for drug delivery emerged as an important aspect of reversible electroporation of tissue. The study that established skin electroporation for transdermal drug delivery was published in 1993 [36], and multiple reviews

have been written on this application of tissue electroporation [77] including a recent report on in vivo real-time monitoring of this technique [78].

In 1998 [45] a remarkable occurrence observed during tissue reversible electroporation was reported: blood flow is blocked in the area where the electric field is applied. This phenomenon, referred to as *the vascular lock* [46], has been noticed in muscle [46], liver [45], and tumors [79]. Disruption of blood flow can affect drug delivery [46] and be followed by ischemia, which could also be beneficial in the treatment of tumors [80]. Furthermore, the use of electroporation to intentionally interrupt blood flow has been proposed to temporarily or permanently reduce perfusion to target areas [81, 82]. Gehl et al. [46] suggested two mechanisms that would explain why such vascular lock is produced: (1) the electrical stimulus induces an immediate reflex vasoconstriction of afferent arterioles mediated by the sympathetic system, and (2) the permeabilization of endothelial cells causes an increase of interstitial pressure and a decrease of intravascular pressure that leads to vascular collapse.

L.M. Mir published a review article on the considerations for in vivo electroporation, specifically for electrochemotherapy and for DNA electrotransfer in gene therapy [83]. He discusses the different methods of investigation to determine the electric field distribution in vivo. Delivery of high intrinsic cytotoxicity drugs and the participation of the host immune response in electrochemotherapy are further discussed as well as vascular effects of electric pulses, choosing between intratumoral or intravenous injection of the drug, proper dosage, treatment effect on tumor margin, an overview of clinical trials, and challenges and considerations for the future of the field. Similarly, the field of DNA electrotransfer was evaluated, and questions that remained unanswered were presented in the study as call for continued research in the different effects and applications of pulsed electric fields in vivo.

J. Gehl and colleagues also pioneered the use of reversible electroporation to load cancer cells with calcium. Various studies have been published, and results place the technique as an efficient anticancer treatment [84, 85]. Calcium electroporation can induce cell death through ATP depletion; this decrease in ATP could be due to cellular use, decreased production due to the effects of calcium on the mitochondria, and extracellular release through the permeabilized membrane [84]. Electroporation with calcium has shown similar results to electrochemotherapy which could make it a more affordable option to the use of expensive cytotoxic drugs [85]; furthermore, a higher concentration of calcium in the extracellular space could lower the electric field required for successful transfer and subsequent cell death [86].

## 2.4.2 Electrofusion

The use of reversible electroporation to produce fusion between cells is described in the paper by Zimmermann [25]. In 1989, a publication on electroporation and electrofusion [87] by Neumann et al. described the kinetics of electrofusion, electrofusion of lipid bilayers, the role of proteases in electrofusion of mammalian cells, and

the mechanism of electroporation and electrofusion in erythrocyte membranes, among others. One of the main biomedical applications of electrofusion is in the production of hybridomas to create antibodies in large amounts. Electrofusion has been deemed to have advantages over conventional methods of cell fusion induced by chemicals due to its high degree of control and increased efficiency. A more recent review on cell fusion is by M. Kandušer and M. Ušaj [88].

### 2.4.3 Electrogenetherapy

The first ones to coin the term electroporation were Neumann and his collaborators in a publication from 1982. They used this term to describe the membrane breakdown from the use of pulsed electric fields and introduced the use of reversible electroporation for the insertion of genes into cells [26]. They also presented a classical thermodynamic analysis of the formation of pores during electroporation. It is interesting to note that this paper which focuses on reversible electroporation cautions against the use of irreversible parameters during the procedure. During the two decades following this work, irreversible electroporation was studied primarily as an upper limit to reversible electroporation in the context of applications of reversible electroporation. Research in the application of electric pulses has led to numerous other publications in the field of electroporation.

H. Potter et al. [27] designed an electroporation cuvette suitable for cell suspensions which led microbiology researchers to employ electrophoresis power supplies in order to perform gene transfection by electroporation. Commercial generators were soon developed specifically intended for electroporation and now this transfection technique is very common in microbiology laboratories. Summaries on the technique and its applications can be found in several publications, e.g., [87, 89].

The first report on the use of reversible electroporation to introduce plasmid DNA into a living tissue was published in 1991 by A.V. Titomirov et al. [33]. Gene delivery to cells in tissue, mediated by reversible electroporation, has become an area of major importance to biotechnology and medicine. It has also found applications in the treatment of cancer [90, 91]. Some of the reviews and edited books written on this particular use of reversible electroporation include [33, 92–94].

### 2.4.4 Irreversible Electroporation

In the 1930s, the thermal effect of electric fields on biological materials was thoroughly investigated [95, 96]. From G.M. McKinley's 1936 report [10], and from experiments performed during the 1920s and 1930s by other researchers, it was concluded that damage caused to living tissues by high-frequency fields (10–100 MHz) cannot be only from thermal origin. *McKinley even proposed that this special “agent” (referring to the electric field) could be used as a minimally invasive ablative method that is selective to specific tissues.* Even though there is not enough methodological data to conclude that electroporation was being

performed in his study using chick embryos, the paper proposed that electric fields produce other mechanisms of damage to biological cells in addition to those caused by thermal means.

A.L. Hodgkin [12] proposed that the Ritter's opening tetanus phenomenon is associated with the breakdown of the insulating properties of the membrane under the influence of an abnormally high potential difference. This explanation describes a phenomenon equivalent to what is now referred to as irreversible electroporation. Even the wording suggests the concept of breakdown of a cell membrane viewed as a dielectric layer. Actually, the notion that the cell membrane could be modeled as a thin dielectric layer had appeared earlier; in 1925, H. Fricke [97] was able to reasonably guess a value of 30 nm for the membrane thickness (actual 7 nm) by analyzing the passive electrical properties of red blood cells under the assumption that cell membrane acts electrically as a thin dielectric layer. After this it was reasonable to expect that some sort of dielectric rupture phenomenon could exist in the case of living cells as it happens in most dielectrics. A common breakdown mechanism in dielectrics is the *avalanche breakdown*: when the dielectric is subjected to a sufficiently high electric field, some bound electrons are freed and accelerated, and then those electrons can liberate additional electrons during collisions in a process that leads to a dramatic conductivity increase and, in some cases, to permanent physical damage of the dielectric material. Now it is accepted that electroporation is not due to dielectric rupture by electron avalanche [98], but the idea that membrane breakdown could be caused by excessive transmembrane voltage surely helped to understand some experimental observations that are related to electroporation.

These highlights from research in the first half of the twentieth century suggest that during this period further observations on the effects of electric fields on biological materials were made that were consistent with the phenomenon of irreversible electroporation. The concept that the cell membrane is a dielectric and that it can break down under the application of an electric field seems to have become accepted. Perhaps the central characteristics of the findings relevant to irreversible electroporation during this period is the realization that while electricity can induce damage to biological materials through thermal effects, there is also another mechanism associated with electricity that induces damage and which is not thermal. In addition evidence seems to be building that electric fields can produce irreversible damage to the cell membrane.

Irreversible electroporation was initially considered as the upper limit of reversible electroporation and, as such, something to be avoided since the aim for reversible electroporation is to create transient pores in the cell membrane while maintaining cell viability.

Related to the above paragraph, it is convenient to note that most researchers cite necrosis due to excessive permeabilization and consequent disruption of the osmotic balance as the killing mechanism of electroporation. However, in the late 1990s, two independent papers were published in which it was shown in vitro that electroporation not only caused necrosis but it also induced cell death with features compatible with apoptosis [41, 99]. In both papers, it is reported that electroporation leads to chromosomal DNA fragmentation which is considered to be an explicit

indication of late apoptosis. Another interesting outcome of the paper by J. Piñero et al. [41], the authors refer to the use of electrochemotherapy for treating solid tumors which may indicate that the abstract was actually proposing the use of irreversible electroporation for treating tumors. Since the understanding within the scientific community was that irreversible electroporation would induce tissue necrosis and not apoptosis, it had been considered a deleterious side effect of reversible electroporation and was to be avoided to prevent instantaneous necrosis leading to massive tumor necrosis and possible ulceration [100].

### 2.4.5 Nonthermal Irreversible Electroporation for Tissue Ablation

In 2003, R.V. Davalos and B. Rubinsky filed a provisional US patent application on the use of classical irreversible electroporation type of pulses (5  $\mu$ s or longer) as a tissue ablation method. With a subsequent paper in 2005, R.V. Davalos, L.M. Mir, and B. Rubinsky published the founding paper suggesting that IRE can be applied in such a manner to induce cell death and ablate tissue while mitigating deleterious thermal effects. This approach would avoid the deleterious effects of massive necrosis as described above and spare important tissue structures, such as the extracellular membrane, to facilitate healthy tissue regeneration. This paper laid the foundation that IRE can be applied as an independent tissue ablation modality.

This approach of delivering the IRE pulses to minimize what is traditionally considered thermal damage marked the beginning of a series of studies in the use of IRE as a technique to treat cancerous tumors which are considered otherwise inoperable due to their proximity to sensitive structures. Several of these are discussed below and show the progression of the field from animal clinical cases into human clinical trials until the latest studies of today.

A series of papers carried out by Rubinsky's group confirmed their hypothesis through treatment of hepatocarcinomas by means of irreversible electroporation. Edd et al. demonstrated that IRE can selectively ablate areas of non-pathological rodent livers [101]. In this study, the histological assessment 3 h after pulses were applied showed some interesting features: the treated areas exhibited microvascular occlusion, endothelial cell necrosis, and diapedeses, resulting in ischemic damage to parenchyma and massive pooling of erythrocytes in the hepatic sinusoids. Hepatocytes displayed blurred cell borders, pale eosinophilic cytoplasm, variable pyknosis, and vacuolar degeneration. On the other hand, large blood vessel architecture was preserved.

J. Edd and R.V. Davalos described how mathematical modeling aided by computer methods can be employed to predict the shape and extent of the lesion created by IRE [52]. The basic principle for such modeling is that any specific tissue region is electroporated if the electric field magnitude is higher than a certain value. Such threshold is specific to the sort of tissue and the features of the IRE pulses (e.g., number of pulses and duration of the pulses). Once this threshold is experimentally obtained, by using numerical methods on computers, it is possible to predict the

distribution of the field magnitude in a tissue according to the electrode configuration and the applied voltages to those electrodes. This methodology for treatment planning was pioneered for the case of *in vivo* reversible electroporation by D. Miklavcic's group [44].

### 2.4.6 Effects of IRE in Animals

Experiments in live mammals have elucidated some of the characteristic features of IRE and have aided in the clinical adoption of this ablation modality to treat human patients. The nonthermal mechanism to induce cell death is still considered to be the most attractive feature of the use of IRE to ablate tumors.

E. Maor et al. presented the results from a pilot study in which IRE (ten 100  $\mu$ s pulses of 3,800 V/cm) was applied to the carotid artery of rats that were kept alive for 28 days after the procedure [102]. Histology showed that the connective matrix of the blood vessels remained intact, whereas the number of vascular smooth muscle cells (VSMC) was significantly decreased without pathological observable consequences such as aneurysm, thrombus formation, or necrosis. These findings seem to indicate that IRE can be applied safely to the vicinity of large blood vessels. Moreover, the fact that VSMC population was significantly reduced suggests that IRE could be the basis for treating pathologies such as restenosis and atherosclerotic processes. As a matter of fact, Maor and coinvestigators also performed research on the use of IRE for treating cardiac restenosis [103].

G. Onik et al. applied *in vivo* IRE to canine prostates by means of percutaneous needle electrodes placed under ultrasound guidance [104]. Macroscopic observation of the induced lesions revealed a very distinct narrow zone of transition from normal viable tissue to complete necrosis. Nearby structures such as the urethra, vessels, nerves, and rectum were not affected by the IRE procedure despite the fact that these areas were deliberately included in the region covered by the high electric field.

Gonzalez et al. performed IRE procedures on pigs under experimental conditions relatively close to those of a clinical scenario [105]. An incision was made to expose the liver, and IRE was applied by using 18 gauge needles that were positioned with the assistance of ultrasound sonography. Following the surgical procedure, animals were sacrificed at 24 h, 3, 7, and 14 days, and liver samples were excised for histopathological analysis. All 14 animals survived the IRE procedure. It was observed that upon application of the IRE pulses, a variable degree of generalized muscle contraction occurred in each animal, and such degree appeared to be related to the administered amount of muscle relaxant (Pancuronium in this study). Immediately following pulse application, sonography showed a markedly hypoechoic area in the expected location of the IRE lesion, and at 24 h, the ultrasound image showed the area was now uniformly hyperechoic. Histological analysis showed that the IRE ablated area is continuously necrotic and that the transition between this area and the adjacent untreated normal parenchyma is abrupt; macroscopic histological analysis also showed that large vascular structures were mainly unaffected. All animals manifested peripheral lymphadenopathy in the drainage area of the ablated tissue.

B. Al-Sakere et al. [53] performed *in vivo* IRE of tumors subcutaneously inoculated in mice and studied the immune reactions. The objective of the study was to elucidate the role of the immune system in the ablation of tumors by means of IRE. They concluded that the immune system is not required in order to successfully ablate tumors by IRE, and thus IRE is a feasible option to consider for the treatment of immunodepressed cancer patients. This study was preceded by an investigation of multiple electroporation protocols that led to complete regression of tumors inoculated in mice [54]. Optimal results were obtained by using protocols that increased the number of pulses from the traditional eight pulses delivered at 1 Hz for ECT. Their best results consisted of 80 pulses of 100  $\mu$ s at 0.3 Hz (an interval of 3.3 s between pulses) with a field magnitude of 2,500 V/cm. With this protocol, complete regression was achieved in 12 out of 13 treated tumors, and no thermal effects were observed.

E.W. Lee et al. showed the potential of IRE to produce an ablation zone with sharper delineation than other ablation modalities [106] in their 2010 review of IRE procedures using image guidance. Ultrasound can be used to place the needles in the target location; computed tomography (CT) and magnetic resonance imaging (MRI) can be used pre- and post-IRE to visualize the tumor region and confirm successful ablation. Histological analysis shows a demarcation between the ablated and live tissue in the micrometer range (on the order of one- to two-cell thickness) [107].

In 2011, two separate studies from R.V. Davalos' group reported on the first clinical cases of the use of IRE to treat naturally occurring cancerous tissue in animal patients. P.A. Garcia et al. [108] used non-thermal irreversible electroporation and adjuvant fractionated radiotherapy to treat a canine patient with an inoperable, spontaneous malignant intracranial glioma. No adverse effects were reported after an IRE protocol with 50- $\mu$ s-pulses delivered in 20 pulse trains with a voltage-to-distance ratio of 1,000 and 1,250 V/cm that resulted in a  $\sim$ 75% reduction of tumor volume after 48 h and allowed for subsequent fractionated radiotherapy which began on the 16th day after IRE treatment. Complete remission was achieved for 149 days at which point death ensued from radiation encephalopathy. R.E. Neal II et al. [109] reported on the treatment of a canine patient with a focal histiocytic sarcoma of the coxofemoral joint that was causing sciatic neuropathy and bilateral pelvic limb lameness. The original size of the neoplasm was greater than 136 mL located in heterogeneous tissue composed of bone, muscle, arteries, and the sciatic nerve. Complete remission was achieved 6 months after IRE treatment and chemotherapy. Both relapsed and suspected chemoresistant tumors were completely ablated using IRE alone with minimal damage to healthy tissues.

#### **2.4.7 Application of IRE for Human Tumor Ablation**

In the first human clinical trial, 16 patients with prostate cancer were treated with IRE. G. Onik and B. Rubinsky reported on this in 2010 [56] where a series of outpatient procedures were performed. All patients were continent immediately and all patients who were potent before the procedure were potent after the procedure.



Two patients who had bilateral areas treated required 6 months for full return of potency. Color Doppler ultrasound showed intact flow within the neurovascular bundle immediately after the procedure. Postoperative biopsies taken from the area of previously known cancer in 15 patients showed no evidence for cancer. There was one patient with a negligible PSA who refused a post-operative biopsy and one in whom a micro-focus of Gleason 6 cancer was found outside the treated area. This patient was successfully retreated with focal cryosurgery. An important finding from this study is that vascular elements were patent and intact nerve bundles were observed; these structures were surrounded by necrotic and fibrotic tissue.

In 2011, another clinical trial that included 38 patients was performed by Thompson in Australia [57]. The patients presented with advanced liver, lung, or kidney tumors where a total of 69 tumors were treated. Complete tumor ablation was observed in 66% of the treatments with the highest percent of failure (or incomplete treatment) observed for lung and kidney tumors. Both unipolar and bipolar electrodes were used for treatments with 90 pulses of 70  $\mu$ s duration, delivered in nine sets of ten pulses per site of delivery. Complications of treatment included cardiac arrhythmias; after four patients experienced this particular problem, ECG-synchronized delivery of pulses was then adopted but two additional patients experienced arrhythmias despite of this synchronization. Fifteen of 18 treatments resulted in complete tumor ablation for patients with hepatocellular carcinoma. This early success suggested that liver tumors may be the optimal target for IRE ablation.

A study of 44 patients who underwent 48 IRE treatments for hepatocellular carcinoma (14 ablations), colorectal metastases (20 ablations), and other types of metastases (ten ablations) presented a local, recurrence-free survival of 97.4%, 94.6%, and 59.5% at 3, 6, and 12 months, respectively. Recurrence rates were higher for tumors larger than 4 cm [110].

IRE has also been used to treat locally advanced pancreatic adenocarcinoma. A study from 2012 evaluated the efficacy of IRE for downstaging and control of this disease [111]. IRE was performed in 14 patients where the mean tumor size was 3.3 cm. One patient received two treatments and three patients presented with metastatic disease. Results showed only one case of pancreatitis that was attributed to a complication from IRE treatment. Post-IRE scans immediately after treatment and 24 h later showed that vascular patency was preserved. Patients with metastatic disease eventually died from disease progression, but two patients who were successfully treated did not show any sign of disease for 11 and 14 months.

A multicenter clinical trial of 27 patients with locally advanced pancreatic cancer (LAPC) was treated with IRE with or without simultaneous partial resection [112]. Surgical IRE was performed on all patients with the exception of one who underwent percutaneous IRE. No cases of pancreatitis nor fistula formation were reported, but there was one 90-day mortality due to hepatic and renal failure and four other cases with possible IRE-related complications. There was no evidence of disease recurrence in 26 of the 27 patients still alive by the 90-day follow-up. Additionally, a significant decrease in the use of narcotics to control pain in patients was reported in comparison to pre-IRE treatment. The study showed efficacy and relative safety of the use of IRE to treat locally advanced pancreatic cancer.

Two subsequent multicenter, prospective institutional review board (IRB)-approved evaluations reported in 2014 and 2015 focused on the use of IRE to treat locally advanced cancers. The former [113] evaluated 107 patients treated with 117 IRE procedures who presented with tumors involving vascular structures (<5 mm in proximity to major vessels); this vascular invasion made the tumors unresectable and not amenable for thermal ablation. Patient treatment was comprised of 84 ablations for pancreatic cancer, 17 for liver tumors, and the rest included lung, kidney, mediastinal, pelvic, and prostate. Complications occurred more often for pancreatic cancers and open surgery; the most common were bleeding, venous thromboembolism, and biliary complications. The local recurrence-free survival was calculated to be 12.7 months, and no significant vascular complications were encountered. The study published last year [58] presents the case of 200 LAPC patients (stage III), comprising the largest evaluation to date, who underwent either IRE alone ( $n = 150$ ) or pancreatic resection combined with IRE for treatment margin enhancement ( $n = 50$ ). IRE was successfully completed in all patients; they had initially undergone induction chemotherapy and 52% were additionally given chemoradiation therapy for a median of 6 months prior to IRE. Six patients experienced local recurrence as reported with a median follow-up of 29 months. A median overall survival of 24.9 months ranging from 4.9 to 85 months was calculated for this group of patients which consolidates IRE with adjuvant chemotherapy and chemoradiotherapy as the combination therapy to induce the longest-term LAPC disease control as currently reported in the literature.

IRE treatment has been successfully performed through laparotomy [112, 114], laparoscopy [110], and percutaneous incision [111, 115]. Percutaneous treatment has shown the least amount of complications from IRE procedures [113] due to its less-invasive nature which in turn promotes a faster recovery. This led to a particular study on percutaneous IRE of LAPC using a dorsal approach [116] motivated by the impediment to use the ventral approach on the 67-year-old patient with a stage III pancreatic tumor. Electrode placement in the 5-cm tumor located in close proximity to collateral vessels and duodenum was performed through the dorsal approach since the most commonly used ventral approach would pose high risk of complications from the procedure alone. This is the first report on the success of this particular dorsal approach and thus provides an alternative in IRE method of delivery for patients with tumors of intricate morphologies involving critical structures.

IRE has also been used to treat renal tumors. Aside from the first study aforementioned by Thomson et al. [57] and an almost simultaneous study also published in 2011 by Pech et al. [117], the largest study on the use of IRE to ablate renal tumors was reported by Trimmer et al. [118] in which 20 patients with T1a renal carcinoma ( $n = 13$ ), indeterminate masses ( $n = 5$ ), or benign masses ( $n = 2$ ) underwent CT-guided IRE. Mean tumor size was  $2.2 \text{ cm} \pm 0.7$ . All patients were successfully treated with no major complications although seven patients presented with minor complications that included difficult-to-control pain, urinary retention, and self-limiting perinephric hematomas. Incomplete ablation caused two patients to undergo salvage therapy at 6 weeks; all 15 patients imaged at 6 months had no evidence of recurrence; and only one patient was observed to experience recurrence at 1 year

post-IRE. This study reinforced the safety of the use of IRE to treat renal tumors despite suffering from selection bias—all tumors were small in size and distant from major blood vessels or critical structures.

A recent review on the use of IRE to treat renal tumors was published earlier this year [119]. The authors warrant consideration when applying the same parameters used for IRE ablations of the liver to treat renal masses. Two phase I and II prospective clinical trials plan to assess the safety and efficacy of IRE in the treatment of renal cancer [120]. Wendler et al. reported on the “IRENE trial” that will evaluate completeness of ablation in renal tumors at 28 days after percutaneous IRE by performing histopathological analysis of tissue samples from partial resection. MRI will be performed after 2, 7, and 28 days from IRE procedure, and image analysis will be done to compare and evaluate any changes [120]. Wagstaff et al. report on a similar protocol with a smaller sample size (ten patients instead of 20) in which there will be no inclusion limitation based on tumor size but only patients who are expected to undergo radical nephrectomy will be included in the study [121]. Objectives of this study include evaluating the safety and efficacy of renal mass ablation with IRE through histopathology of resection specimens, as well as the efficacy of MRI and CEUS imaging of ablation zone. Preliminary results from the first three patients enrolled in the IRENE trial were recently published [122]. Renal cell carcinoma tumors of 15–17 mm were treated with IRE; results describe a new distribution of the ablation zone with negative margins for all three tumors, complete tumor necrosis for two of them, and residual tumor of unclear malignancy in the center of one of them. Results will continue to be gathered as part of these clinical trials which will help in the optimization of IRE parameters to successfully treat renal tumors. If it is concluded that IRE does not present great advantage over other more commonly used ablation techniques, a niche application of IRE could include central renal tumors in close proximity to blood vessels and collecting system in which the nonthermal mode of ablation can be exploited [119].

#### 2.4.8 Other Applications of IRE

Nononcologic applications of IRE could include treatment of hypertension through renal sympathetic nerve denervation [123]; this possibility comes from previous successes in this area by radiofrequency ablation [124, 125] which gave an indication to some of the advantages that could be obtained through the use of IRE where heat sink effects and undesired vascular complications can be avoided. IRE may also be used to prevent arterial restenosis following angioplasty; this was shown through a series of studies from Rubinsky’s group [103, 126, 127] that confirmed ablation of vascular smooth muscle cells by endovascular IRE where the elastic lamina remained intact and the endothelial layer is allowed to regenerate. Vascular connective tissue matrix remained undamaged while no aneurysm nor thrombus formation was observed; these findings highlight the implications of the use of IRE in the treatment of cardiovascular disorders.

Another application of IRE is in the area of tissue engineering. A study published early last year evaluated its feasibility to introduce pores in bacterial cellulose scaffolds by delivering pulsed electric fields of high enough magnitude to kill the bacteria in specific locations and at particular times during cellulose production [128]. The use of IRE to decellularize organs has also been investigated [129]; results point toward potential applications in the fields of tissue engineering and regenerative medicine where the inherent mechanisms of IRE to nonthermally ablate tissue while sparing the extracellular matrix, blood vessels, and nerves, could have major implications. Similarly, these characteristics of IRE have also found an application for wound healing and scarless skin regeneration [130, 131], organ regeneration [132], and as an antiseptic for burn wounds [133].

---

## References

1. Reilly JP. Applied bioelectricity: from electrical stimulation to electropathology. New York: Springer; 1998.
2. Prausnitz MR. A practical assessment of transdermal drug delivery by skin electroporation. *Adv Drug Deliv Rev.* 1999;35:61–76.
3. Vanbever R, Pr at V. In vivo efficacy and safety of skin electroporation. *Adv Drug Deliv Rev.* 1999;35:77–88.
4. Noad HM. Lectures on electricity; comprising galvanism, magnetism, electro-magnetism, magneto- and thermo- electricity, and electo-physiology. 3rd ed. London: George Knight and Sons; 1849.
5. Fuller GW. Report on the investigations into the purification of the Ohio river water at Louisville Kentucky. New York: D. Van Nostrand Company; 1898.
6. Rockwell AD. The medical and surgical uses of electricity: including the X-ray, Finsen light, vibratory therapeutics, and high-frequency currents. New York: E.B. Treat & Company; 1903.
7. Abidor IG, Li LH, Hui SW. Studies of cell pellets: II. Osmotic properties, electroporation, and related phenomena: membrane interactions. *Biophys J.* 1994;67:427–35.
8. Jex-Blake AJ. Death by electric currents and by lightning. The Goulstonian lectures for 1913. *Br Med J.* 1913;11:425–552., 492–498, 548–552, 601–603.
9. O’Keefe Gatewood M, Zane RD. Lightning injuries. *Emerg Med Clin North Am.* 2004;22:369–403.
10. McKinley GM. Short electric wave radiation in biology. In: Duggar BM, editor. Biological effects of radiation, vol. 1. New York: McGraw-Hill Book Co; 1936. p. 541–58.
11. Nyrop JE. A specific effect of high-frequency electric currents on biological objects. *Nature.* 1946;157:51–2.
12. Hodgkin AL. The ionic basis of electrical activity in nerve and muscle. *Biol Rev Camb Philos Soc.* 1951;26:339–409.
13. Frankenhaeuser B, Wid n L. Anode break excitation in desheathed frog nerve. *J Physiol.* 1956;131:243–7.
14. Biedermann W. Electro-physiology, vol. 2. London: Macmillan; 1898.
15. St mpfli R, Willi M. Membrane potential of a Ranvier node measured after electrical destruction of its membrane. *Exp Dermatol.* 1957;13:297–8.
16. St mpfli R. Reversible electrical breakdown of the excitable membrane of a Ranvier node. *An Acad Bras Cienc.* 1957;30:57–63.
17. Doevenspeck H. Influencing cells and cell walls by electrostatic impulses. *Fleishwirtschaft.* 1961;13:986–7.

18. Sale AJH, Hamilton WA. Effects of high electric fields on microorganisms. 1. Killing of bacteria and yeasts. *Biochim Biophys Acta*. 1967;148:781–8.
19. Hamilton WA, Sale AJH. Effects of high electric fields on microorganisms. 2. Mechanism of action of the lethal effect. *Biochim Biophys Acta*. 1967;148:789–800.
20. Sale AJH, Hamilton WA. Effects of high electric fields on microorganisms. 3. Lysis of erythrocytes and protoplasts. *Biochim Biophys Acta*. 1968;163:37–43.
21. Zimmermann U, Pilwat G, Riemann F. Dielectric breakdown of cell membranes. *Biophys J*. 1974;14:881–99.
22. Riemann F, Zimmermann U, Pilwat G. Release and uptake of haemoglobin and ions in red blood cells induced by dielectric breakdown. *Biochim Biophys Acta*. 1975;394:449–62.
23. Kinoshita KJ, Tsong TY. Formation and resealing of pores of controlled sizes in human erythrocyte membrane. *Nature*. 1977;268:438–41.
24. Belov SV. Effects of high-frequency current parameters on tissue coagulation. *Biomed Eng*. 1978;12:209–11.
25. Zimmermann U. Electric field-mediated fusion and related electrical phenomena. *Biochim Biophys Acta*. 1982;694:227–77.
26. Neumann E, Schaeffer-Ridder M, Wang Y, Hofschneider PH. Gene transfer into mouse lymphoma cells by electroporation in high electric fields. *EMBO J*. 1982;1:841–5.
27. Potter H, Weir L, Leder P. Enhancer-dependent expression of human kappa immunoglobulin genes introduced into mouse pre-B lymphocytes by electroporation. *Proc Natl Acad Sci U S A*. 1984;81:7161–5.
28. Orłowski S, Belehradek JJ, Paoletti C, Mir LM. Transient electroporation and stable transformation of cells in culture. Increase of the cytotoxicity of anticancer drugs. *Biochem Pharmacol*. 1988;34:4727–33.
29. Okino M, Mohri H. Effects of a high-voltage electrical impulse and an anticancer drug on *in vivo* growing tumors. *Jpn J Cancer Res*. 1987;78:1319–21.
30. Lee RC, Kolodney MS. Electrical injury mechanisms: electrical breakdown of cell membranes. *Plast Reconstr Surg*. 1987;80:672–9.
31. Lee RC, Gaylor DC, Bhatt D, Israel DA. Role of cell membrane rupture in the pathogenesis of electrical trauma. *J Surg Res*. 1988;44:709–19.
32. Powell KT, Morgenthaler AW, Weaver JC. Tissue electroporation. Observation of reversible electrical breakdown in viable frog skin. *Biophys J*. 1989;56:1163–71.
33. Titomirov AV, Sukharev S, Kistanova E. *In vivo* electroporation and stable transformation of skin cells of newborn mice by plasmid DNA. *Biochim Biophys Acta*. 1991;1088:131–4.
34. Mir LM, Orłowski S, Belehradek JJ, Paoletti C. Electrochemotherapy potentiation of antitumor effect of bleomycin by local electric pulses. *Eur J Cancer*. 1991;27:68–72.
35. Mir LM, Belehradek M, Domenge C, Orłowski S, Poddevin B, Belehradek JJ, et al. Electrochemotherapy, a new antitumor treatment: first clinical trial. *C R Acad Sci III*. 1991;313:613–8.
36. Prausnitz MR, Bose VG, Langer R, Weaver JC. Electroporation of mammalian skin: a mechanism to enhance transdermal drug delivery. *Proc Natl Acad Sci U S A*. 1993;90:10504–8.
37. Bhatt DL, Gaylor DC, Lee RC. Rhabdomyolysis due to pulsed electric fields. *Plast Reconstr Surg*. 1990;86(1):1–11., pp. 1–11.
38. Abramov GS, Bier M, Capelli-Schellpfeffer M, Lee RC. Alteration in sensory nerve function following electrical shock. *Burns*. 1996;22:602–6.
39. Bier M, Hammer SM, Canaday DJ, Lee RC. Kinetics of sealing for transient electropores in isolated mammalian skeletal muscle cells. *Bioelectromagnetics*. 1999;20:194–201.
40. Lee RC, River LP, Pan FS, Ji L, Wollmann RL. Surfactant-induced sealing of electroporation-induced skeletal muscle membranes *in vivo*. *Proc Natl Acad Sci U S A*. 1992;89:4524–8.
41. Piñero J, Lopez-Baena M, Ortiz T, Cortes F. Apoptotic and necrotic cell death are both induced by electroporation in HL60 human promyeloid leukaemia cells. *Apoptosis*. 1997;2:330–6.
42. Schoenbach KH, Peterkin FE, Alden RWI, Beebe SJ. The effect of pulsed electric fields on biological cells: experiments and applications. *IEEE Trans Plasma Sci*. 1997;25:284–92.

43. Schoenbach KH, Beebe SJ, Buescher ES. Intracellular effect of ultrashort electrical pulses. *Bioelectromagnetics*. 2001;22:440–8.
44. Miklavcic D, Beravs K, Semrov D, Cemazar M, Demsar F, Sersa G. The importance of electric field distribution for effective in vivo electroporation of tissues. *Biophys J*. 1998;74:2152–8.
45. Ramirez LH, Orłowski S, An D, Bindoula G, Dzodic R, Ardouin P, et al. Electrochemotherapy on liver tumours in rabbits. *Br J Cancer*. 1998;77:2104–11.
46. Gehl J, Skovsgaard T, Mir LM. Vascular reactions to in vivo electroporation: characterization and consequences for drug and gene delivery. *Biochim Biophys Acta*. 2002;1569:51–8.
47. Al-Khadra A, Nikolski V, Efimov IR. The role of electroporation in defibrillation. *Circ Res*. 2000;87:797–804.
48. Davalos RV, Rubinsky B. Tissue ablation with irreversible electroporation. US Application 10/571,162. Filed: 12/24/04 Issued 11/1/11 Patent No. 8,048,067. 2004.
49. Yao C, Sun C, Mi Y, Xiong L, Wang S. Experimental studies on killing and inhibiting effects of steep pulsed electric field (SPEF) to target cancer cell and solid tumor. *IEEE Trans Plasma Sci*. 2004;32:1626–33.
50. Davalos RV, Mir LM, Rubinsky B. Tissue ablation with irreversible electroporation. *Ann Biomed Eng*. 2005;33:223.
51. Rubinsky B, Onik G, Mikus P. Irreversible electroporation: a new ablation modality – clinical implications. *Technol Cancer Res Treat*. Feb 2007;6:37–48.
52. Edd JF, Davalos RV. Mathematical modeling of irreversible electroporation for treatment planning. *Technol Cancer Res Treat*. 2007;6:275–86.
53. Al-Sakere B, Bernat C, Andre F, Connault E, Opolon P, Davalos RV, et al. A study of the immunological response to tumor ablation with irreversible electroporation. *Technol Cancer Res Treat*. 2007;6:301–6.
54. Al-Sakere B, André F, Bernat C, Connault E, Opolon P, Davalos RV, et al. Tumor ablation with irreversible electroporation. *PLoS One*. 2007;2:e1135.
55. Lavee J, Onik G, Mikus P, Rubinsky B. A novel nonthermal energy source for surgical epicardial atrial ablation: irreversible electroporation. *Heart Surg Forum*. 2007;10:E162–7.
56. Onik G, Rubinsky B, editors. *Irreversible electroporation: first patient experience focal therapy of prostate cancer (irreversible electroporation)*. Berlin: Springer; 2010. p.^pp. Pages
57. Thomson KR, Cheung W, Ellis SJ, Federman D, Kavnoudias H, Loader-Oliver D, et al. Investigation of the safety of irreversible electroporation in humans. *J Vasc Interv Radiol*. 2011;22:611–21.
58. Martin RCG, Kwon D, Chalikhonda S, Sellers M, Kotz E, Scoggins C, et al. Treatment of 200 locally advanced (stage III) pancreatic adenocarcinoma patients with irreversible electroporation: safety and efficacy. *Ann Surg*. 2015;262:486–94.
59. Nollet JA. *Recherches sur les causes particulieres des phénomènes électriques*. Paris: Chez H.L. Guerin & L.F. Delatour; 1754.
60. Ivorra A, Rubinsky B. Historical review of irreversible electroporation in medicine. In: Boris Rubinsky, editor. *Irreversible electroporation*. Springer, Berlin; 2010. p. 1–21.
61. Malik MA, Ghaffar A, Malik SA. Water purification by electrical discharges. *Plasma Sources Sci Technol*. 2001;10:82.
62. Eliasson B, Hirth M, Kogelschatz U. Ozone synthesis from oxygen in dielectric barrier discharges. *J Phys D Appl Phys*. 1987;20:1421.
63. Liu C, Xie X, Zhao W, Liu N, Maraccini PA, Sassoubre LM, et al. Conducting nanosponge electroporation for affordable and high-efficiency disinfection of bacteria and viruses in water. *Nano Lett*. 2013;13:4288–93.
64. Liu C, Xie X, Zhao W, Yao J, Kong D, Boehm AB, et al. Static electricity powered copper oxide nanowire microbical electroporation for water disinfection. *Nano Lett*. 2014;14:5603–8.
65. Toepfl S, Mathys A, Heinz V, Knorr D. Review: potential of high hydrostatic pressure and pulsed electric fields for energy efficient and environmentally friendly food processing. *Food Rev Intl*. 2006;22:405–23.
66. Saulis G. Electroporation of cell membranes: the fundamental effects of pulsed electric fields in food processing. *Food Eng Rev*. 2010;2:52–73.

67. Mahnič-Kalamiza S, Vorobiev E, Miklavčič D. Electroporation in food processing and biorefinery. *J Membr Biol.* 2014;247:1279–304.
68. Burton H. A survey of literature on bacterial effects of short electromagnetic waves. Shinfield: National Institute for Research in Dairying; 1949.
69. Maxwell JC. A treatise on electricity and magnetism. 3rd ed. Oxford: Clarendon Press; 1904.
70. Cole KS. Electric impedance of suspensions of spheres. *J Gen Physiol.* 1928;12:29–36.
71. Miklavcic D, Kotnik T. Electroporation for electrochemotherapy and gene therapy. In: Rosch PJ, Markov MS, editors. *Bioelectromagnetic medicine.* New York: Informa Health Care; 2004. p. 637–56.
72. Neumann E, Rosenheck K. Permeability changes induced by electric impulses in vesicular membranes. *J Membr Biol.* 1972;29:279–90.
73. Belehradek M, Domenge C, Luboinski B, Orlowski S, Belehradek J, Mir LM. Electrochemotherapy, a new antitumor treatment. First clinical phase I–II trial. *Cancer.* 1993;72:3694–700.
74. Mali B, Jarm T, Snoj M, Sersa G, Miklavcic D. Antitumor effectiveness of electrochemotherapy: a systematic review and meta-analysis. *Eur J Surg Oncol (EJSO).* 2013;39:4–16.
75. Queirolo P, Marincola F, Spagnolo F. Electrochemotherapy for the management of melanoma skin metastasis: a review of the literature and possible combinations with immunotherapy. *Arch Dermatol Res.* 2014;306:521–6.
76. Miklavčič D, Mali B, Kos B, Heller R, Serša G. Electrochemotherapy: from the drawing board into medical practice. *Biomed Eng Online.* 2014;13:29.
77. Prausnitz MR, Mitragotri S, Langer R. Current status and future potential of transdermal drug delivery. *Nat Rev Drug Discov.* 2004;3:115–24.
78. Blagus T, Markelc B, Cemazar M, Kosjek T, Preat V, Miklavcic D, et al. In vivo real-time monitoring system of electroporation mediated control of transdermal and topical drug delivery. *J Control Release.* 2013;172:862–71.
79. Sersa G, Cemazar M, Parkins CS, Chaplin DJ. Tumour blood flow changes induced by application of electric pulses. *Eur J Cancer.* 1999;35:672–7.
80. Sersa G, Jarm T, Kotnik T, Coer A, Podkrajsek M, Sentjurc M, et al. Vascular disrupting action of electroporation and electrochemotherapy with bleomycin in murine sarcoma. *Br J Cancer.* 2008;98:388–98.
81. Rubinsky B, Edd J, Horowitz L. Electroporation to interrupt blood flow. USA Patent 12/163727. 2004.
82. Palanker D, Vankov A, Freyvert Y, Huie P. Pulsed electrical stimulation for control of vasculature: temporary vasoconstriction and permanent thrombosis. *Bioelectromagnetics.* 2008;29:100–7.
83. Mir LM. Therapeutic perspectives of in vivo cell electropermeabilization. *Bioelectrochemistry.* 2001;53:1–10.
84. Frandsen SK, Gissel H, Hojman P, Tramm T, Eriksen J, Gehl J. Direct therapeutic applications of calcium electroporation to effectively induce tumor necrosis. *Cancer Res.* 2012;72:1336–41.
85. Frandsen SK, Gissel H, Hojman P, Eriksen J, Gehl J. Calcium electroporation in three cell lines: a comparison of bleomycin and calcium, calcium compounds, and pulsing conditions. *Biochim Biophys Acta (BBA) Gen Subj.* 2014;1840:1204–8.
86. Hansen EL, Sozer EB, Romeo S, Frandsen SK, Vernier PT, Gehl J. Dose-dependent ATP depletion and cancer cell death following calcium electroporation, relative effect of calcium concentration and electric field strength. *PLoS One.* 2015;10:e0122973.
87. Neumann E, Sowers AE, Jordan CA, editors. *Electroporation and electrofusion in cell biology.* New York: Plenum Press; 1989. p. pp. Pages
88. Kanduser M, Usaj M. Cell electrofusion: past and future perspectives for antibody production and cancer cell vaccines. *Expert Opin Drug Deliv.* 2014;11:1885–98.
89. Nickoloff JA, editor. *Electroporation protocols for microorganisms.* Totowa: Humana Press; 1995. p. pp. Pages
90. Daud AI, DeConti RC, Andrews S, Urbas P, Riker AI, Sondak VK, et al. Phase I trial of interleukin-12 plasmid electroporation in patients with metastatic melanoma. *J Clin Oncol.* 2008;26:5896–903.

91. Tamura T, Sakata T. Application of in vivo electroporation to cancer gene therapy. *Curr Gene Ther.* 2003;3:59–64.
92. Jaroszeski MJ, Gilbert R, Nicolau C, Heller R. Delivery of genes in vivo using pulsed electric fields. *Methods Mol Med.* 2000;37:173–86.
93. Mir LM, Moller PH, André F, Gehl J. Electric pulse-mediated gene delivery to various animal tissues. *Adv Genet.* 2005;54:83–114.
94. Andre F, Mir L. DNA electrotransfer: its principles and an updated review of its therapeutic applications. *Gene Ther.* 2004;11:S33–42.
95. Christie RV, Binger CA. An experimental study of Diathermy IV. Evidence for the penetration of high frequency currents through the living body. *J Exp Med.* 1927;46:715–34.
96. Weinberg ED, Ward GE. Diathermy and regeneration of bone. *Arch Surg.* 1934;28:1121–9.
97. Fricke H. A mathematical treatment of the electric conductivity and capacity of disperse systems. II. The capacity of a suspension of conducting spheroids surrounded by a non-conducting membrane for a current of low frequency. *Phys Rev.* 1925;26:678–81.
98. Crowley JM. Electrical breakdown of biomolecular lipid membranes as an electromechanical instability. *Biophys J.* 1973;13:711–24.
99. Hofmann F, Ohnimus H, Scheller C, Strupp W, Zimmermann U, Jassoy C. Electric field pulses can induce apoptosis. *J Membr Biol.* 1999;169:103–9.
100. Miklavcic D, Semrov D, Mekić H, Mir LM. A validated model of in vivo electric field distribution in tissues for electrochemotherapy and for DNA electrotransfer for gene therapy. *Biochim Biophys Acta.* 2000;1523:73–83.
101. Edd J, Horowitz L, Davalos RV, Mir LM, Rubinsky B. In-vivo results of a new focal tissue ablation technique: irreversible electroporation. *IEEE Trans Biomed Eng.* 2006;53:1409–15.
102. Maor E, Ivorra A, Leor J, Rubinsky B. The effect of irreversible electroporation on blood vessels. *Technol Cancer Res Treat.* 2007;6:307–12.
103. Maor E, Ivorra A, Leor J, Rubinsky B. Irreversible electroporation attenuates neointimal formation after angioplasty. *IEEE Trans Biomed Eng.* 2008;55:2268–74.
104. Onik G, Rubinsky B, Mikus P. Irreversible electroporation: implications for prostate ablation. *Technol Cancer Res Treat.* 2007;6:295–300.
105. Gonzalez CA, Rojas R, Villanueva C, Rubinsky B. Inductive phase shift spectroscopy for volumetric brain edema detection: an experimental simulation. *2007 Ann Int Conf IEEE Eng Med Biol Soc.* 2007;1–16:2346–9.
106. Lee EW, Thai S, Kee ST. Irreversible electroporation: a novel image-guided cancer therapy. *Gut Liver.* 2010;4(Suppl 1):S99–s104.
107. Lee EW, Chen C, Prieto VE, Dry SM, Loh CT, Kee ST. Advanced hepatic ablation technique for creating complete cell death: irreversible electroporation. *Radiology.* 2010;255:426–33.
108. Garcia PA, Pancotto T, Rossmeisl JH, Hena-Guerrero N, Gustafson NR, Daniel GB, et al. Non-thermal irreversible electroporation (N-TIRE) and adjuvant fractionated radiotherapeutic multimodal therapy for intracranial malignant glioma in a canine patient. *Technol Cancer Res Treat.* 2011;10:73–83.
109. Neal RE 2nd, Rossmeisl JH Jr, Garcia PA, Lanz OI, Hena-Guerrero N, Davalos RV. Successful treatment of a large soft tissue sarcoma with irreversible electroporation. *J Clin Oncol.* 2011;29:e372–7.
110. Cannon R, Ellis S, Hayes D, Narayanan G, Martin RC 2nd. Safety and early efficacy of irreversible electroporation for hepatic tumors in proximity to vital structures. *J Surg Oncol.* 2013;107:544–9.
111. Narayanan G, Hosein PJ, Arora G, Barbery KJ, Froud T, Livingstone AS, et al. Percutaneous irreversible electroporation for downstaging and control of unresectable pancreatic adenocarcinoma. *J Vasc Interv Radiol.* 2012;23:1613–21.
112. Martin RC 2nd, McFarland K, Ellis S, Velanovich V. Irreversible electroporation therapy in the management of locally advanced pancreatic adenocarcinoma. *J Am Coll Surg.* 2012;215:361–9.
113. Martin RC, Philips P, Ellis S, Hayes D, Bagla S. Irreversible electroporation of unresectable soft tissue tumors with vascular invasion: effective palliation. *BMC Cancer.* 2014;14:1–9.



114. Martin RC 2nd, McFarland K, Ellis S, Velanovich V. Irreversible electroporation in locally advanced pancreatic cancer: potential improved overall survival. *Ann Surg Oncol*. 2013;20(Suppl 3):S443–9.
115. Bagla S, Papadouris D. Percutaneous irreversible electroporation of surgically unresectable pancreatic cancer: a case report. *J Vasc Intervent Radiol JVIR*. 2012;23:142–5.
116. Scheffer HJ, Melenhorst MCAM, Vogel JA, van Tilborg AAJM, Nielsen K, Kazemier G, et al. Percutaneous irreversible electroporation of locally advanced pancreatic carcinoma using the dorsal approach: a case report. *Cardiovasc Intervent Radiol*. 2014;38:760–5.
117. Pech M, Janitzky A, Wendler JJ, Strang C, Blaschke S, Dudeck O, et al. Irreversible electroporation of renal cell carcinoma: a first-in-man phase I clinical study. *Cardiovasc Intervent Radiol*. 2011;34:132–8.
118. Trimmer CK, Khosla A, Morgan M, Stephenson SL, Ozayar A, Cadeddu JA. Minimally invasive percutaneous treatment of small renal tumors with irreversible electroporation: a single-center experience. *J Vasc Interv Radiol*. 2015;26:1465–71.
119. Narayanan G, Doshi MH. Irreversible Electroporation (IRE) in renal tumors. *Curr Urol Rep*. 2016;17:1–7.
120. Wendler JJ, Porsch M, Nitschke S, Kollermann J, Siedentopf S, Pech M, et al. A prospective phase 2a pilot study investigating focal percutaneous irreversible electroporation (IRE) ablation by NanoKnife in patients with localised renal cell carcinoma (RCC) with delayed interval tumour resection (IRENE trial). *Contemp Clin Trials*. 2015;43:10–9.
121. Wagstaff PG, de Bruin DM, Zondervan PJ, Savci Hejjink CD, Engelbrecht MR, van Delden OM, et al. The efficacy and safety of irreversible electroporation for the ablation of renal masses: a prospective, human, in-vivo study protocol. *BMC Cancer*. 2015;15:165.
122. Wendler JJ, Ricke J, Pech M, Fischbach F, Jürgens J, Siedentopf S, et al. First delayed resection findings after Irreversible Electroporation (IRE) of human localised renal cell carcinoma (RCC) in the IRENE pilot phase 2a trial. *Cardiovasc Intervent Radiol*. 2015;39:239–50.
123. Deipolyi AR, Golberg A, Yarmush ML, Arellano RS, Oklu R. Irreversible electroporation: evolution of a laboratory technique in interventional oncology. *Diagn Interv Radiol*. 2014;20:147–54.
124. Bunte MC, Infante de Oliveira E, Shishehbor MH. Endovascular treatment of resistant and uncontrolled hypertension: therapies on the horizon. *JACC Cardiovasc Interv*. 2013;6:1–9.
125. Krum H, Schlaich M, Whitbourn R, Sobotka PA, Sadowski J, Bartus K, et al. Catheter-based renal sympathetic denervation for resistant hypertension: a multicentre safety and proof-of-principle cohort study. *Lancet*. 373:1275–81.
126. Maor E, Ivorra A, Rubinsky B. Non thermal irreversible electroporation: novel technology for vascular smooth muscle cells ablation. *PLoS One*. 2009;4:e4757.
127. Maor E, Ivorra A, Mitchell JJ, Rubinsky B. Vascular smooth muscle cells ablation with endovascular nonthermal irreversible electroporation. *J Vasc Interv Radiol*. 2010;21:1708–15.
128. Baah-Dwomoh A, Rolong A, Gatenholm P, Davalos R. The feasibility of using irreversible electroporation to introduce pores in bacterial cellulose scaffolds for tissue engineering. *Appl Microbiol Biotechnol*. 2015;99:4785–4794., pp. 1–10.
129. Sano M, Neal R, Garcia P, Gerber D, Robertson J, Davalos R. Towards the creation of decellularized organ constructs using irreversible electroporation and active mechanical perfusion. *Biomed Eng Online*. 2010;9:83.
130. Golberg A, Broelsch GF, Bohr S, Mihm MC, Austen WG, Albadawi H, et al. Non-thermal, pulsed electric field cell ablation: a novel tool for regenerative medicine and scarless skin regeneration. *Technology*. 2013;1:1–7.
131. Golberg A, Khan S, Belov V, Quinn KP, Albadawi H, Felix Broelsch G, et al. Skin rejuvenation with non-invasive pulsed electric fields. *Sci Rep*. 2015;5:10187., 05/12/online.
132. Golberg A, Bruinsma BG, Jaramillo M, Yarmush ML, Uygun BE. Rat liver regeneration following ablation with irreversible electroporation. *Peer J*. 2016;4:e1571.
133. Golberg A, Broelsch GF, Vecchio D, Khan S, Hamblin MR, Austen WG Jr, et al. Eradication of multidrug-resistant *A. baumannii* in burn wounds by antiseptic pulsed electric field. *Technology*. 2014;2:153–60.

---

## Part II

# Preclinical Research

---

# Multi-scale Biophysical Principles in Clinical Irreversible Electroporation

# 3

Daniel C. Sweeney, Robert E. Neal II, and Rafael V. Davalos

---

## 3.1 Introduction

Irreversible electroporation (IRE) is a focal ablation methodology that involves generating brief, but intense, electric fields in a target tissue. These electric fields operate on the cell level to electrically perforate—or permeabilize—the cell membrane while maintaining the structural integrity of the extracellular components [12]. The development of IRE technology significantly improved the outcomes of patients with late-stage pancreatic cancer. A study investigating such outcomes found that the median survival of stage III pancreatic cancer patients rose from 6–13 to 24.9 months in a 200-person study following IRE treatment [31], roughly doubling patient post-treatment survival.

The movement of electrons and other charged moieties is central to the mechanisms driving the clinical efficacy of IRE, which are motivated by an electrical potential (voltage) gradient. Similar to heat conduction, such a gradient is usually established using one electrode/s from which the electrons flow (source) and one or more electrode that accept the flow of electrodes (sinks). The geometry of the source and sink electrodes largely determine the distribution of electric field within a target tissue during an IRE procedure. It is imperative that the clinician has a conceptual understanding of how electric fields are distributed when treating a patient with IRE, and we seek to provide the context and intuitive understanding of the phenomena motivating IRE treatment in this chapter.

One of the central considerations inherent in any procedure involving the application of electric fields is that they are difficult to visualize in real time. Visualization

---

D.C. Sweeney (✉) • R.V. Davalos  
Department of Biomedical Engineering and Mechanics, Virginia Tech,  
330 Kelly Hall, Blacksburg, VA, USA  
e-mail: [sweeneyd@vt.edu](mailto:sweeneyd@vt.edu)

R.E. Neal II  
Angio Dynamics Inc., Queensbury, NY, USA

is difficult for any electric field distribution because it represents the force that can be exerted on a unit electrical charge positioned at every point. For the case of the electric fields generated in IRE procedures, these fields represent the force acting on a charged particle, rather than the movement of the particle itself, and therefore may only be evaluated indirectly. While monitoring electron flow [27] and the small changes in temperature generated during IRE [5], clinicians have largely relied on treatment planning algorithms and empirical or a priori knowledge of the tumor anatomy and physiology to determine the order in which ablations should occur and their positioning within the tissue to optimally destroy the target tissue while minimizing collateral damage to healthy tissue.

Several mathematical techniques form the foundation for the clinically relevant treatment planning for IRE procedures. Analytical techniques are useful for gaining an intuitive understanding of the biophysical mechanisms associated with IRE. These techniques, however, are not able to capture many of the geometric complexities of biological tissue and have little clinical use outside of gaining a clinical intuition about how electric fields behave in such materials. Analytical techniques will be discussed at the cellular level, and, while not explicitly accurate for every example, it is our hope that the conceptual lessons learned from these mathematical formulations will give the reader an intuitive understanding of why and how IRE is performed the way it is.

The finite element method (FEM) is the workhorse of IRE treatment planning and will be utilized to outline the tissue-level considerations in the second part of this chapter. In IRE procedures, FEM modeling is especially useful because real, patient-specific tumor, organ, and tissue geometries are used to plan individual- and tumor-specific ablations. In a typical model, images from 3-D medical imaging modalities—such as MRI or CT scans—are reconstructed into 3-D geometries and then subdivided into smaller sections or finite elements. The governing physical principles are then solved on each element. These elements are then used to reconstruct piecewise functions that allow the relevant physical quantities to be determined at every point within the whole geometry. For example, in a typical IRE procedure, a clinician might image a tumor and send the scans to an engineer who will reconstruct the scans into their 3-D geometries. Once reconstructed, the engineer will insert models of electrodes into the tissue and determine how the electric field should be applied to which electrodes in which order for optimal tissue ablation [16]. The engineer will send the reconstructed model back to the clinician prior to treatment so that they are able to perform the treatment in the optimal manner.

---

## 3.2 Electric Fields

Electromagnetic fields appear ubiquitously throughout the biological realm; chemical gradients directly give rise to electric fields, appearing in fields from developmental biology to wound healing. Modern electrodynamic theory was developed by James Clerk Maxwell in the mid-nineteenth century [32] and has subsequently been adapted and developed to explain electrical phenomena observed in biological interactions.

Within a tissue, the local electric field intensity is directly related to the ablation field [12]. If modeled accurately, it can provide invaluable information to the medical operator toward the visualization of the expected final lesion volume and how it will change in relation to adjusting ablation parameters (geometry, pulse number, length, voltage, etc.). Therefore, the assumptions, considerations, and solutions critical to mathematically modeling electroporation are developed below with the goals of compiling and reviewing the essential concepts that have driven the advancement of electroporation.

### 3.2.1 Pulse Characteristics

The electric fields generated for clinical use have included many different wave shapes, including triangular, ramp, sinusoidal, and exponential, though typically treatments are delivered using square pulses. However, typically square pulses are used for IRE treatment, and it is important to discuss the terminology associated with such waveforms before delving into the physical concepts relevant to IRE. Figure 3.1 schematically demonstrates the terminology commonly used to refer to an IRE pulse waveform. The polarity of a waveform (e.g., monopolar or bipolar) refers to whether its amplitude varies only in the positive direction or both in the positive and negative directions. The pulse width refers to the total “on-time,” or time where the pulse is nonzero, and may be used to describe portions of the waveform in either the positive or negative direction, or both, depending on the context. The intra-pulse delay describes how much time passes before the completion of one pulse and the beginning of another, though it typically is used to describe the delay between pulses of opposite polarity in bipolar pulses. IRE treatment generally involves delivering tens to hundreds of pulses with a set amount of time between each pulse treatment repetition, and the inter-pulse delay is the amount of time between each pulse. The amplitude describes the magnitude of the potential in

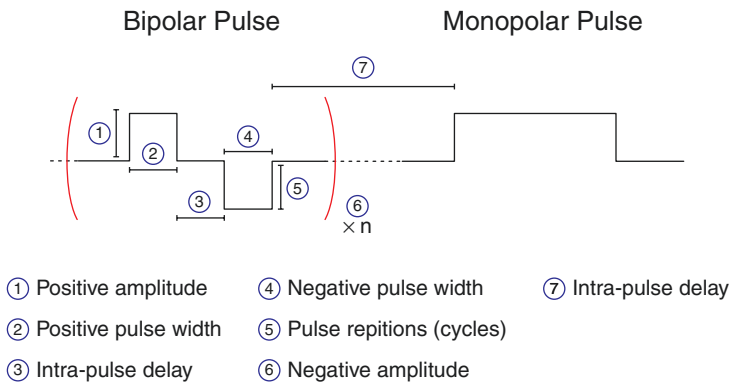


**Fig. 3.1** Anatomy of bipolar and monopolar square electrical pulses. Waveforms commonly used in IRE are shown schematically to indicate terminology. A train of  $n$  bipolar pulses are shown followed by a single monopolar pulse

a single direction, measured from the sink electrode. These parameters may vary from treatment to treatment, but typically 80 pulses with pulse widths of 100  $\mu\text{s}$  and repeated at once per second 1 Hz are used for an IRE treatment.

### 3.2.2 Ohm's Law

The relationship between an electrical potential  $V$  and the flow of electrical current  $I$  is frequently described as  $V = IR$  where  $R$  is the degree to which a given material will resist the flow of current (resistance), which is the one-dimensional form of Ohm's law. Indeed, Ohm's law must be generalized to accurately represent geometries when considering complex tissue shape factors encountered when applying Ohm's law in more than one dimension. In multiple dimensions, the electrical field  $\mathbf{E}$  arises from a potential drop between two points connected by path  $\mathbf{l}$ . The potential drop across that path provides the electric field along the orientation of  $\mathbf{l}$  for every point along the path on each electrode and through tissue as

$$\Delta V = - \int_{x_1}^{x_2} \mathbf{E} \cdot d\mathbf{l}. \quad (3.1)$$

The electrical current is defined as the density of electrons flowing through a closed surface. Similar to the flow of a fluid driven by a pressure head, the flow of electrons is driven by a potential difference. In the fluid analogy, the total pressure head is equal to the integral of the pressure gradient at each point in the fluid flow. Similarly, electrical current flow is described by Eq. 3.1 in much the same manner: the total potential drop across a material is given by the electric field at every point integrated between the beginning and ending points.

Further extending the idea of electrical current using the fluid analogy, if we define the electrical current through a unit of volume, similar to a control volume in fluid dynamics, we obtain a current density  $\mathbf{J}$ . If  $\mathbf{J}$  is defined at every point in a fluid flow, and we integrate across the entire fluid volume  $\Omega$  (Fig. 3.2a), we can obtain a flow density  $\mathbf{J}$  that gives the density of fluid (or electrons) and in which direction it is flowing. In order to measure such a density, we must define a surface in two-dimensional space through which  $\mathbf{J}$  is flowing (Fig. 3.2b). For a simple fluid flow, this surface might be the cross section of a pipe. Abstracting this to an arbitrary unit surface  $\partial\Omega$ , the flux integral

$$I = \oint_{\Omega} \mathbf{J} \cdot d\Omega \quad (3.2)$$

gives the current  $I$  as the integral of the current flow density  $\mathbf{J}$  through an arbitrary closed surface  $\partial\Omega$ . For a one-dimensional electron flow through a known cross section, Ohm's law is given as  $V = IR$ . However, visualizing two- and three-dimensional current paths and electric field distributions between two surfaces is slightly more complicated because the current does not travel homogeneously through the material but rather as a distribution such that the current density is spread throughout the entire ohmic material. Thus, the electrical current can be broken into its

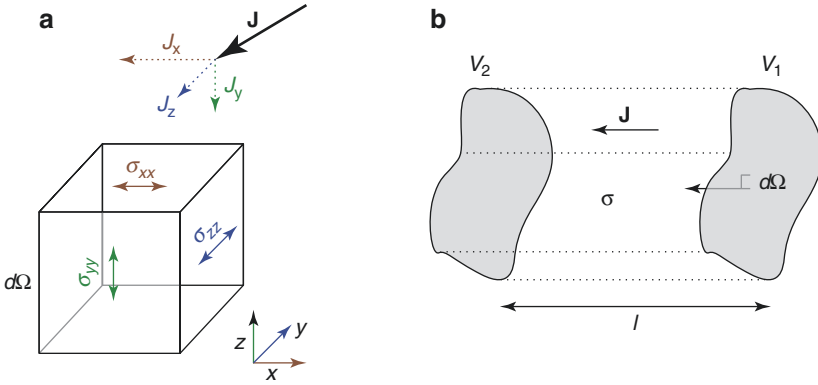


**Fig. 3.2** Phenomenological relationship between electrical conductivity  $\sigma_{ij}$  and electrical current density  $\mathbf{J} = \langle J_x, J_y, J_z \rangle$ . (a) Each component of the total electric current density vector  $\mathbf{J}$  may experience a different conductivity through each unit component  $d\Omega$  within an ohmic material. (b) A potential drop  $\Delta V = V_1 - V_2$  between conducting surfaces separated by an ohmic material with conductivity  $\sigma$  results in a current density  $\mathbf{J}$  through that material and an electric field of uniform intensity  $|\mathbf{E}| = \Delta V/l$

vector components  $\mathbf{J} = \langle J_x, J_y, J_z \rangle$  where  $J_x$ ,  $J_y$ , and  $J_z$  are magnitudes of electrical current density flowing in each the  $x$ ,  $y$ , and  $z$  directions.

**3.2.2.1 Electrical Conductivity**

For an arbitrary geometry in the domain  $\Omega$ , exposed to electric field  $\mathbf{E}$ , a current density  $\mathbf{J}$  will develop in each of the  $x$ ,  $y$ , and  $z$  directions. Thus,  $\mathbf{J}$ , described as the flow of electrons (electrical current) or ions (ionic current) per unit volume, is motivated by the electric field distribution within a given material  $\Omega$ . For low-frequency or DC electric fields, we can relate  $\mathbf{E}$  to  $\mathbf{J}$  through Ohm’s law on  $\Omega$  as

$$\mathbf{J} = \underline{\sigma} \mathbf{E}. \tag{3.3}$$

where

$$\mathbf{E} = \begin{bmatrix} E_x \\ E_y \\ E_z \end{bmatrix}, \underline{\sigma} = \begin{bmatrix} \sigma_{xx} & \sigma_{xy} & \sigma_{xz} \\ \sigma_{yx} & \sigma_{yy} & \sigma_{yz} \\ \sigma_{zx} & \sigma_{zy} & \sigma_{zz} \end{bmatrix}, \mathbf{J} = \begin{bmatrix} J_x \\ J_y \\ J_z \end{bmatrix}.$$

Because the electrical potential drop as well as the current flow can occur in each spatial dimension, the conductivity  $\underline{\sigma}$  must be represented as a  $3 \times 3$  matrix (also called the conductivity tensor) that describes how the electric field in each direction can impact the current flows, or is conducted, in each dimension. For current flowing as the result of a potential drop within an arbitrary material in Cartesian coordinates, we can write

$$\begin{bmatrix} J_x \\ J_y \\ J_z \end{bmatrix} = \begin{bmatrix} \sigma_{xx} & \sigma_{xy} & \sigma_{xz} \\ \sigma_{yx} & \sigma_{yy} & \sigma_{yz} \\ \sigma_{zx} & \sigma_{zy} & \sigma_{zz} \end{bmatrix} \begin{bmatrix} E_x \\ E_y \\ E_z \end{bmatrix},$$

to show these interactions explicitly, where the subscripts on  $E$  and  $J$  indicate the direction of that vector component (i.e.,  $J_x$  is the current density in the  $x$  direction) and the subscripts on  $\sigma$  are the ratio of each electric field component to each current density component (i.e.,  $\sigma_{xy}$  is the ratio of the electric field component  $E_x$  divided by the current density component  $J_y$ ). For a typical material,  $\underline{\sigma}$  is generally symmetrical, meaning that

$$\underline{\sigma} = \begin{bmatrix} \sigma_{xx} & \sigma_{xy} & \sigma_{xz} \\ \sigma_{yx} & \sigma_{yy} & \sigma_{yz} \\ \sigma_{zx} & \sigma_{zy} & \sigma_{zz} \end{bmatrix} = \begin{bmatrix} \sigma_{xx} & 0 & 0 \\ 0 & \sigma_{yy} & 0 \\ 0 & 0 & \sigma_{zz} \end{bmatrix}. \quad (3.4)$$

### 3.2.2.2 Permittivity

Rather than simply allowing electron flow, a material may become polarized in the presence of an electric field at high frequencies. This behavior is known as permittivity. A material's permittivity describes its ability to become polarized in an electric field. This effect is due to the realignment of molecular dipoles motivated by the applied electric field. Permittivity is generally expressed relative to the permittivity of free space  $\epsilon_0$ . Because it takes time for molecules to rearrange when the electric field is applied and removed (Fig. 3.3), the permittivity of a material gives rise to the transient response and may be thought of as the ability of a material to store electrical energy. Such properties are ideal in electrical components such as capacitors that are designed for this purpose. The capacitive current  $\mathbf{J}_c$  through a material in a domain  $\Omega$  with relative permittivity  $\underline{\epsilon}_r$  is given as

$$\mathbf{J}_c = \epsilon_0 \underline{\epsilon}_r \frac{\partial \mathbf{E}}{\partial t}. \quad (3.5)$$

Similar to conductivity,  $\underline{\epsilon}_r$  is given by the permittivity tensor

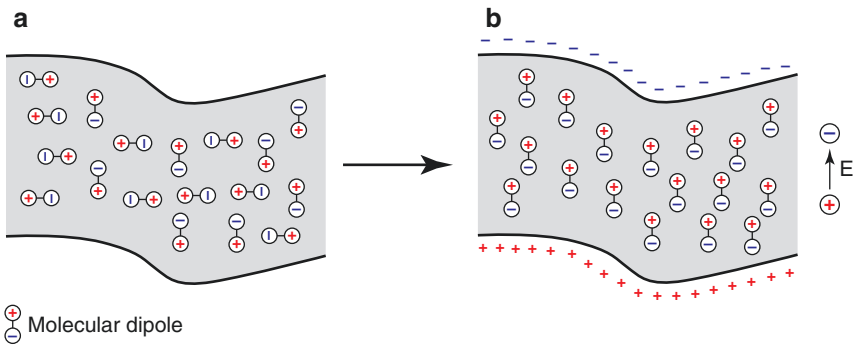


**Fig. 3.3** Permittivity describes the extent to which a dielectric material composed of molecular dipoles or polarizable molecules to reorganize exposed to an electric field. The dipoles that are normally randomly distributed in a material (a) will realign with respect to the electric field  $\mathbf{E}$  within a material (b). This results in the production of a capacitive current  $\mathbf{J}_c$ .



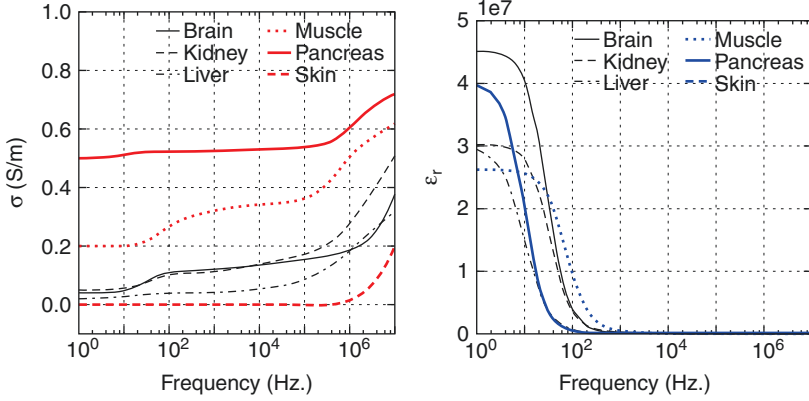


**Fig. 3.4** Conductivity and relative permittivity of common tissues treated using electroporation-based therapies. The electrical conductivity  $\sigma$  (left) and relative permittivity  $\epsilon_r$  (right) of common tissues are plotted for frequencies from 1 Hz to 1 MHz [17]

$$\underline{\epsilon}_r = \begin{bmatrix} \epsilon_{xx} & \epsilon_{xy} & \epsilon_{xz} \\ \epsilon_{yx} & \epsilon_{yy} & \epsilon_{yz} \\ \epsilon_{zx} & \epsilon_{zy} & \epsilon_{zz} \end{bmatrix}, \quad (3.6)$$

which indicates how the capacitive current in each direction is generated through how the electric field changes in each direction over time. A material that exhibits such polarization properties is called a dielectric, and its relative permittivity  $\epsilon_r$  may also be referred to as its dielectric constant. Oftentimes, a material can be considered isotropic, or possessing uniform material properties in every direction. Even if a material is not entirely isotropic on a molecular level, it may be considered such if the bulk conductivity, permittivity, and permeability are presented on a scale at which the material appears macroscopically homogeneous, such as in liver. In such cases, the tissue conductivity and permittivity can be determined generally throughout as a function of frequency, as depicted in Fig. 3.4. Introducing the capacitive current's dependence on angular frequency  $\omega = 2\pi f$  (where  $f$  is given in Hz.) in a uniform material as  $\mathbf{J}_c = \epsilon_r \epsilon_0 \omega \mathbf{E}$ , we can write an equation stating that no current is generated within any point within the bulk of the material. This is known as the current continuity condition and can be written as [36]

$$(\sigma + j\epsilon_r \epsilon_0 \omega) \nabla \cdot \mathbf{E} = 0, \quad (3.7)$$

where  $j = \sqrt{-1}$  is an imaginary number. By solving for  $\mathbf{E}$ , we obtain a modified expression similar to Ohm's law that accounts for the time-dependent changes present when the signal changes in time. This transient quantity, analogous to a tissue's ohmic resistance, is known as the tissue's impedance  $Z$ . However, in the course of integration, several spatial dependencies must be considered, though, if conductivity and permittivity are constant in space and time, the spatial component of the material's impedance may be represented by the shape function  $K$ . In this case, the impedance of a tissue is given as

$$Z = \frac{1}{K(\sigma + j\epsilon_r\epsilon_0\omega)}. \quad (3.8)$$

Shape functions will be discussed further in the following section, though the transient response of a material may be estimated using Eq. 3.8 to estimate the impedance of a material with uniform, static conductivity and permittivity. Because biological tissue's properties change relatively slowly compared to the duration of the applied electric field in a typical IRE procedure, the electrical properties are considered quasi-static and are estimated at low frequencies (DC-1 kHz).

### 3.2.2.3 Shape Functions

For a material with no transient response in more than one dimension, we adapt Ohm's law to multiple dimensions using a shape factor  $K$  such that the total resistance of the material  $R$  is given by

$$R = \frac{1}{K\sigma}. \quad (3.9)$$

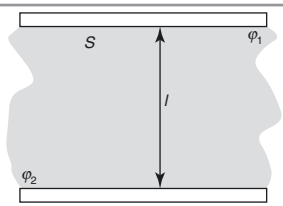
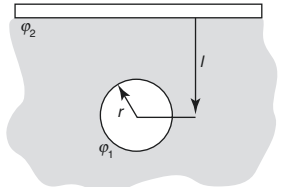
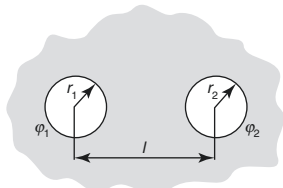
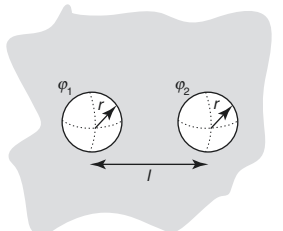
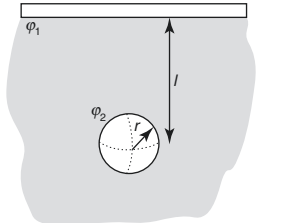
Representing Ohm's law in this manner greatly simplifies the estimation of tissue properties from the electric field distribution using readily measurable quantities, voltage  $V$  and current  $I$ . Shape factors calculated for several common electrode geometries in an electrically homogenous material are given in Table 3.1. For example, in the case of an ohmic material separated by two large conducting plates, the shape factor given in Table 3.1 is  $K = A/l$ , where  $A$  is the surface area of the plates and  $l$  is the distance between them. In this case, the resistance of the material is given as  $R = l/(A\sigma)$ , which corresponds to the general resistance of a short cylinder.

This example illustrates two particularly useful concepts in developing an intuition with regard to how electric fields behave. If the area of the electrodes in this geometry is increased, the total effective resistance of the system is decreased, meaning that more total current will flow through the material. However, the current going through the system may be decreased if the distance separating the two plates is increased. These relationships are intuitively true in a given geometry, and their interplay is helpful in understanding a material's response in the presence of an electric field.

### 3.2.3 Laplace's Equation

Given a homogenous material exposed to an electric field, the conductivity (and permittivity, in the case of a dielectric) may be divided from both the right- and left-hand sides of the continuity equation, leaving  $\nabla \cdot \mathbf{E} = 0$ . Considering the definition of an electric field  $\mathbf{E} = -\nabla\phi$ , the general form of an electrostatic field can be solved by Laplace's equation as

**Table 3.1** Shape functions for calculating the electrical resistance in a tissue for a given electrode configuration

Electrode geometry		Shape factor ( $K$ )
<i>Parallel plates</i> of surface area $A$ separated by a material of length $l$		$\frac{A}{l}$
<i>Cylinder and plate</i> for which $d \gg r$ and $A \gg r, d$ and $d$ is the cylinder length		$\frac{2\pi d}{\cosh^{-1}(l/r)}$
<i>Parallel cylinders</i> of length $d$ in an infinite material for which $l \gg r_1, r_2$		$\frac{2\pi l}{\cosh^{-1}\left(\frac{2l^2 - 2r_1^2 - 2r_2^2}{r_1 r_2}\right)}$
<i>Two spheres</i> in an infinite material and for which $r_2 \geq r_1$		$\frac{4\pi r_2}{\frac{r_2}{r_1} \left(1 - \frac{(r_1/l)^4}{1 - (r_2/l)^4}\right) - \frac{2r_2}{l}}$
<i>Sphere and plate</i> in a semi-infinite material and for which $l > r$		$\frac{4\pi r}{1 - r/(2l)}$

Adapted from Bergman et al. [4]

To calculate resistance, use  $R = 1/(\sigma K)$  where  $K$  is the shape function listed in the right column

$$\nabla^2 \varphi = 0 \tag{3.10}$$

where  $\varphi$  is the local electric potential field and the Laplacian operator is defined for Cartesian coordinates as  $\nabla^2 \varphi = \varphi_{xx} + \varphi_{yy} + \varphi_{zz}$ . From a physical perspective, Laplace's equation indicates that no electric field source exists within the material

**Table 3.2** Typical electrical properties of cellular components of an isolated cell

Parameter	Variable	Value	Unit	Reference
Permittivity of free space	$\epsilon_0$	$8.854 \times 10^{-12}$	$As/Vm$	
Extracellular (saline) relative permittivity	$\epsilon_e$	75		[6]
Extracellular (saline) conductivity	$\sigma_e$	1.25	$S/m$	Measured
Cell membrane relative permittivity	$\epsilon_m$	7		[22]
Cell membrane conductivity	$\sigma_m$	$3 \times 10^{-7}$	$S/m$	[19]
Cell membrane thickness	$d_m$	4	$nm$	[3]
Cytoplasm relative permittivity	$\epsilon_i$	60		[21]
Cytoplasm conductivity	$\sigma_i$	0.5	$S/m$	[22]
Cell radius	$r$	10	$\mu m$	

Adapted from Čemažar et al. [8]

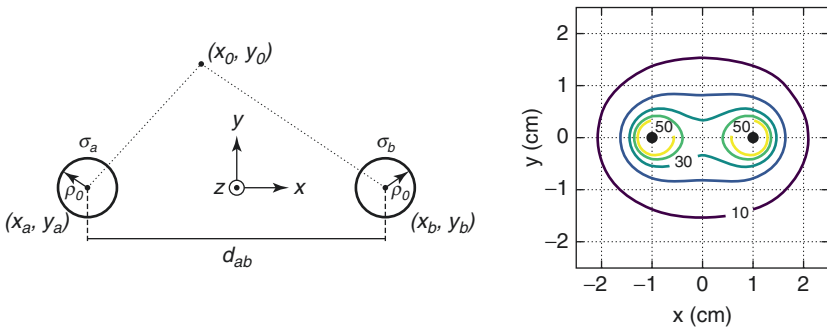


**Fig. 3.5** The solution to Laplace’s equation for two infinitely long cylindrical electrodes. The solution to Laplace’s equation is given for the case of 1.0 V applied across 0.1 cm (ID) cylindrical electrodes spaced 2.0 cm apart. Contours are given for 10, 20, 30, 40, and 50 V/cm (Adapted from Mahnic-Kalamiza et al. [28])

and can only exist at the boundaries. From here, modeling the electric field distribution for a particular geometry is performed by solving Laplace’s equation in each subdomain with a given material property using the isopotential and current continuity boundary conditions giving an electric field distribution. For the case of two cylindrical electrodes, the solution to Laplace’s equation is shown in Fig. 3.5.

**3.2.3.1 Parallel Plate Electrodes**

The simplest geometry for which an electric field may be calculated is that of two conductive parallel plates of surface area  $A$  separated by distance  $d$  (with the condition that  $A \gg d$ ). The electric field intensity within the material may then be approximated along a single dimension as  $\mathbf{E} = -\nabla\varphi \approx -\Delta V/d$ . By scaling the total current  $I$  for a unit surface area on the conducting electrode as  $I/A$ , Ohm’s law confirms the shape factor given in Table 3.1, yielding

$$\Delta V = RI = \frac{l}{A\sigma} I,$$

after rearrangement. It is important to note that though the electric field is equivalent to the voltage-to-distance ratio in the case of parallel plate electrodes, this is not always the case, and the reader should exercise prudence when applying the principles herein described for more complex geometries.

### 3.2.3.2 Two Cylindrical Electrodes

Electrode configurations consisting of two or more cylindrical, needle electrodes are almost ubiquitously used in ECT, GET, and IRE. An analytical solution exists for the electric field intensity as a function of position around the electrode insertions in the plane perpendicular to the exposed conductors. The electric field due to two long, cylindrical electrodes of equal radius  $r_a = r_b = \rho_0$  placed at positions  $(x_a, y_a)$  and  $(x_b, y_b)$  with their centers offset by distance  $d_{ab}$  is given as

$$E(x_0, y_0) = \frac{\varphi_{ab}}{2 \log \frac{d_{ab} + \sqrt{d_{ab}^2 - 4\rho_0^2}}{2\rho_0}} \cdot \sqrt{\left( \frac{x'_a - x}{(x'_a - x)^2 + (y'_a - y)^2} - \frac{x'_b - x}{(x'_b - x)^2 + (y'_b - y)^2} \right)^2 + \left( \frac{y'_a - y}{(x'_a - x)^2 + (y'_a - y)^2} - \frac{y'_b - y}{(x'_b - x)^2 + (y'_b - y)^2} \right)^2} \quad (3.11)$$

for the general form of the analytical solution for two electrodes [9, 28] to Eq. 3.10, with constants as

$$\begin{aligned} x'_a &= x_a + |e| \cdot \sin \theta_1, \theta_1 = \arctan \frac{y_b - y_a}{x_b - x_a}, \\ x'_b &= x_b + |e| \cdot \sin \theta_2, \theta_2 = \arctan \frac{y_a - y_b}{x_a - x_b}, \\ y'_a &= y_a + |e| \cdot \cos \theta_1, \\ y'_b &= y_b + |e| \cdot \cos \theta_2, e = \frac{d}{2} - \sqrt{\left(\frac{d}{2}\right)^2 - \rho_0^2}. \end{aligned}$$

From this calculation, several particularly important phenomena arise that may not be obvious. From inspection of Eq. 3.11, we recognize that the electric field does not decay linearly between the two electrodes—i.e., the voltage-to-distance ratio does not provide a valid representation of the local electric field intensity,

dramatically overestimating the treatment result. The electric field intensity distribution for this geometry is plotted in Fig. 3.5, and it quickly becomes clear that the shape of the electric field in this configuration appears to resemble the two-dimensional projection of a peanut or an infinity symbol: the electric field intensity is greatest near the electrode and decays radially between them. Consequently, any electric field-dependent phenomenon will occur first at the electrode-tissue interface first before propagating throughout the remaining exposed tissue.

The two-needle electrode geometry may be extrapolated to an arbitrary number of electrodes placed around a target tissue volume. For  $N$  electrodes positioned around a tissue mass, the electric field distribution is given by the superposition of the electric fields generated by each electrode, depending on the geometry and the sequence in which the electric field is applied [14] (Fig. 3.12). However, there are several important consequences of arranging electrodes in arrays and then energizing pairs of them in sequence. By energizing any pair electrodes following a different pair, the total electric field experienced within the total tissue is a sum of the electric fields generated by each of the electrode pairs. While this may not significantly impact the electric field distribution in a tissue with static conductivity and permittivity, the electrical properties of biological tissue change as a function of electric field intensity, temperature, and time. In a realistic procedure, the electric field distribution between any two sets of electrodes in an array will be dependent on the electric field distribution generated between the previously energized electrode pairs. This will effectively manifest as unequal resistances measured between two otherwise geometrically similar electrode pairs. Though IRE schemes are designed to largely account for these differences, they will nevertheless be present, and similar resistance measurements should not be expected.

---

### 3.3 Cell-Level Phenomena

In general, biological tissue has a very hierarchical structure; a tissue's smaller scale components dictate its gross anatomical form. Specifically, in the case of electroporation-based treatments and therapies, the biophysical action of the treatment at a molecular level dictates the cellular effects which, in turn, dictate the tissue and organ-level outcome of the treatment. It is because of this structure that attaining a holistic understanding of electroporation processes at the cellular level helps caregivers exploit the relevant physical mechanisms to attain more accurate and clinically advantageous treatment plans and protocols.

#### 3.3.1 Transmembrane Potential and the Schwan Equation

The cellular membrane functionally separates the interior of a cell from its external environment, thereby establishing chemical gradients that the cell utilizes for generating action potentials, nutrient uptake, and waste export. These chemical gradients establish an osmotic gradient across the relatively impermeant membrane. Due to the electrical charge distribution within many of these molecules, the chemical gradient established across the cell membrane also establishes a large electric

potential difference ( $\sim 70$  mV). When an electric field is applied across a cell, opposing charges gather at opposing sides of the membrane and generate an electrically induced pressure across the membrane. When this pressure surpasses a threshold, defects in the membrane are expanded and allow molecular transport into and out of the cell. This is the mechanistic basis for electroporation.

In 1957, H. P. Schwan developed the expression now carrying his name for the transmembrane potential induced by an exogenous electric field applied to a spherical cell [41]. The Schwan equation is commonly employed to provide an intuitive, analytical description of the mechanism giving rise to electroporation phenomenon. The formulation of the Schwan equation considers concentric spherical regions to represent a cell. The transmembrane potential is the difference in potential in the radial direction across the thin region separating the center region of the concentric spheres defining the membrane boundaries; in other words, the membrane is modeled as the dielectric shell. In such a case, the transmembrane potential is defined as

$$\varphi_m(r, \theta) = f_s ER \cos(\theta), \quad (3.12)$$

where

$$f_s = \frac{2\sigma_e \left[ 3d_m R^2 \sigma_i + (3d_m^2 R - d_m^3)(\sigma_m - \sigma_i) \right]}{2R^3 (\sigma_m + 2\sigma_i) \left( \sigma_m + \frac{1}{2}\sigma_i \right) - 2(R - d_m)^3 (\sigma_e - \sigma_m)(\sigma_i - \sigma_m)}.$$

In this case, the cell membrane has a thickness of  $d_m$ , and the radius of the cell to the internal surface of the membrane is  $R$ . The conductivity of the cytoplasm, membrane, and extracellular medium are given as  $\sigma_i$ ,  $\sigma_m$ , and  $\sigma_e$ , respectively. In reality, there is a time dependence on the induced transmembrane potential  $\varphi_m$ . This time dependence can be approximated through further simplifications performed under the conditions that the membrane diameter is much smaller than the radius of the cell ( $d_m \ll R$ ). Through substitution of  $\sigma + j\epsilon_e \epsilon_0 \omega$  for  $\sigma$  in order to obtain the transient components of the transmembrane potential given by the Schwan equation and if the permittivities of the internal and the external electrolytic media are negligible ( $\epsilon_i \approx \epsilon_e \approx 0$ ), and the conductivities of the internal and external media are significantly greater than that of the membrane ( $\sigma_m \ll \sigma_i, \sigma_e$ ), the membrane charging time constant  $\tau$  is given by

$$\tau = \frac{R\epsilon_m}{2d_m \left( \frac{\sigma_i \sigma_e}{\sigma_i + 2\sigma_e} \right) + R\sigma_m}.$$

We may now rewrite the time-dependent Schwan equation as

$$\varphi_m(r, \theta, t) = f_s Er \cos(\theta) \left( 1 - \exp\left(-\frac{t}{\tau}\right) \right), \quad (3.13)$$

which demonstrates how the transmembrane potential depends on the geometric contributions of the cell shape  $f_s$ , the exponential dependence on time  $t$ , and the polar

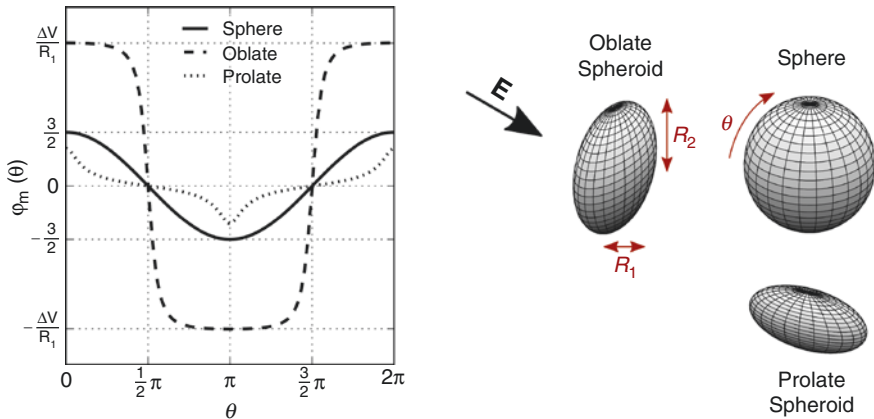


**Fig. 3.6** The surface area of the cell membrane experiencing a significantly increased transmembrane potential  $\varphi_m(\theta)$  is increased for cell geometries perpendicular to the electric field. The transmembrane potentials induced on spherical and oblate and prolate spheroidal cells are plotted and indicate that the greater the projection of the cell surface parallel to the electric field, the greater the area on the cell membrane that experiences significantly increase transmembrane potentials (Adapted from Kotnik and Miklavcic [26])

position  $\theta$ . We must consider that cell geometry and orientation with respect to the electric field affect the induced transmembrane potential. The transmembrane potentials resulting from extending our analysis to prolate and oblate spheroidal geometries with interior membranes (shells) are shown in Fig. 3.6 [25, 26]. The transmembrane potential profiles shown in Fig. 3.6 highlight how the regions of the cell surface perpendicular to the electric field experience the greatest transmembrane potential, resulting in the greatest probability of electroporation in these areas. It is important to note that the transmembrane potential expression is similar for prolate, oblate, and spherical cells; the oblate geometry experiences a considerably larger surface area of the membrane to larger transmembrane potentials than the prolate geometry. In practical terms, this indicates that cells positioned with their long axes perpendicular to the electric field (oblate) will exhibit a significantly greater average membrane permeabilization than if their long axis is parallel to the electric field.

### 3.3.2 Pore Generation in Bilayer Lipid Membranes

In 1979, Abidor et al. were able to link the increased conductivity and molecular transport observed post-exposure in bilayer membranes to membrane defects arising from the colloidal nature of lipid bilayers [1], and in so doing, developed the biophysical explanation underpinning modern electroporation theory.

An intact bilayer membrane will form spontaneously in an aqueous material. Once formed, a membrane is subject to thermodynamic fluctuations that govern its structural properties at the molecular level; the distance between charged lipid head groups fluctuates while maintaining the hydrophobic membrane core because of the random thermodynamic motion of the lipid molecules [24]. Representing these



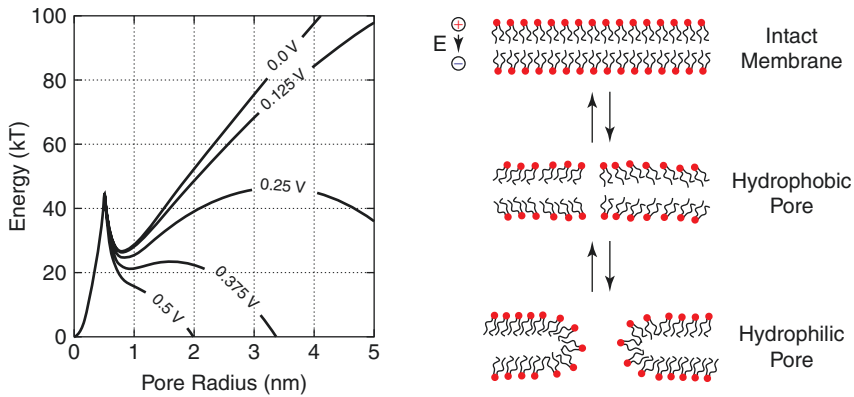


**Fig. 3.7** Energy of pore formation becomes favorable with increasing transmembrane potential. A membrane defect that forms as a result of normal thermal fluctuations of the cell membrane increase in radius is forced to expand in the presence of an increased transmembrane potential—a hydrophilic pore—and eventually cause the lipid head groups to invert when the defect has reached a critical radius  $r = r_*$  to energetically stabilize the structure, forming a hydrophobic pore

random fluctuations as a statistical distribution, it becomes conceivable that there is a small probability that the random motion of the lipid molecules in the bilayer membrane will generate a defect in the membrane structure in which an intramolecular space will form that is large enough to permit a molecule to penetrate the hydrophobic core and emerge on the opposite side (Fig. 3.7). Though not explicitly detailed here, the derivation of the following interfacial physics calculation is detailed in [1, 20, 29, 30] for interested readers. In 1999, DeBruin et al. simplified the explanation of the second type of defects that form as hydrophilic pores by introducing a quadratic term to represent the energy of this enlarged defect—termed a hydrophobic pore—rather than the modified Bessel functions used previously [13] (Fig. 3.7).

Once the radius of a defect reaches a critical value, denoted  $r = r^*$ , the lipid head groups invert and energetically stabilize the pore, bridging the two membrane leaflets and creating a hydrophilic pore. This stabilization is reflected as a local minimum in the energy function  $r_m > r^*$  and indicates that, once hydrophilic pores are formed, they tend to aggregate at  $r = r_m$  before collapsing back to an intact membrane. Physically, these dynamics are captured by modeling a hydrophobic pore using the quadratic term proposed by DeBruin et al. such that a global minimum energy is achieved at  $r = 0$ , where the hydrophobic pore of radius is normalized to the radius at which the hydrophilic-hydrophobic transition occurs  $r^*$ . The energy associated with that transition is denoted as  $E(r_*) = E_*$ . The hydrophilic pore energy is developed by considering a dielectric material separating two bulk phases of a conducting material. The term  $\pi a_p r^2 \phi_m^2$  represents the electrical energy that motivates the transition of a hydrophobic to hydrophilic pore, similar to a discrete capacitor. The inside of a hydrophilic pore is associated with a linear tension  $2\pi r \gamma$ , and whole membrane experiences a surface tension  $\pi r^2 \Gamma$ . An additional term is added here as a quartic term to represent the steric interactions of the lipid head groups in

the pore with  $C$  as the interaction constant. Together, with the introduction of an exogenous electric field added to the energy function

$$E_{pore}(r) = \begin{cases} E_* \left( \frac{r}{r_*} \right)^2 - \pi a_p r^2 \phi_m^2 & 0 \leq r \leq r_* \\ 2\pi r \gamma - \pi r^2 \Gamma - \pi a_p r^2 \phi_m^2 + \left( \frac{C}{r} \right)^4 & r_* < r \ll d_m \end{cases}, \quad (3.14)$$

where  $\phi_m$  is the transmembrane potential and  $a_p$  accounts for the difference in dielectric properties between an intact membrane and the surrounding aqueous environment, estimated as [1, 38]

$$a_p = \frac{(\epsilon_w - \epsilon_l)\epsilon_0}{2d_m}.$$

Figure 3.7 shows the altered pore energy function arising from increased transmembrane potentials. It is of note that dramatic deformation for  $r > r_*$  occurs at potentials  $\sim 200$  mV and has been estimated experimentally to be between 0.2 and 1 V [39].

## 3.4 Electric Field Distribution in Gross Tissue

Through our discussion of the effects of an electric field on a single cell, we can expand the discussion to multicellular and tissue-level systems. With the understanding that the electric field intensity, frequency, and waveform are the most easily manipulated parameters to adjust for electrode arrays of a fixed geometry, and that the transmembrane potential both directly depends on the magnitude of the applied electric field and drives electropore formation, a tissue-level perspective of the effect of electric fields in vitro may be quickly developed. With the electric field intensity driving electroporative processes, such as IRE, it becomes critical to predict the electric field distribution within a biological tissue. At frequencies  $< 10$  kHz, it is commonly assumed that the electric field distribution may be approximated using the Laplace equation. In this case, the tissue is only considered resistive, with no capacitive component. While this assumption provides an incomplete model for tissue, it is nonetheless widely used and provides valuable information. The typical frequency content of an electrical signal used in clinical applications of electroporation is below 10 kHz, and, as such, our discussion will focus on the tissue response within this range.

### 3.4.1 Deviations in Electrode Geometry

Idealized plate electrodes are considered completely planar, while cylindrical electrodes are considered perfectly cylindrical and parallel. However, in reality,

scenarios present where it becomes necessary to account for slight variations in intraoperative electrode placement and positioning. For example, electrodes may be placed slightly skew, or a particularly dense tissue region may cause electrode bowing or off-parallel insertion when using needle electrodes. Though these variations may appear slight, they may result in suboptimal, incomplete, or excessive ablation.

### 3.4.1.1 Bowing and Angulation

Inserting and maintaining parallel two-needle electrodes into a highly structured tissue, even with guides and sharpened ends, may prove challenging due to multiple tissue layers, dense connective tissue, or soft tissue deformation during treatment. This angulation results in an intensification of the electric field and current density toward the conducting surfaces in closest proximity Fig. 3.8. Significant angulation may result in the incomplete ablation of tissue regions where the conducting surfaces of the electrodes are farthest apart and, though complete ablation occurs around the surfaces of electrodes in close proximity, unwanted heat may be generated in this region due to the increased current density driving increased Joule heating (discussed later). Though addressed individually, these aberrations may be

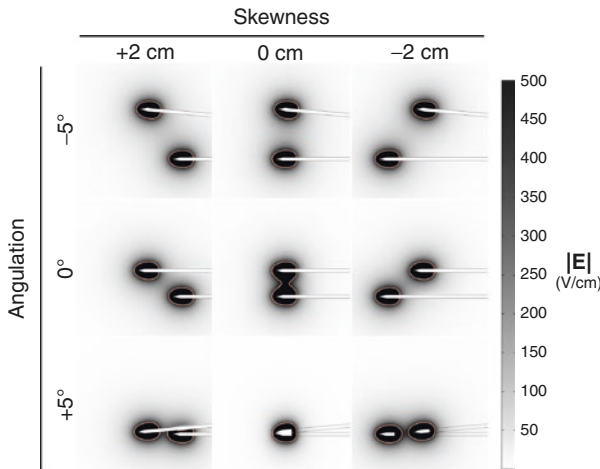


**Fig. 3.8** Angulation and skewness of exposed electrode surfaces can significantly impact the electric field intensities driving electroporation within the target tissue region. In simulated, isotropic liver tissue ( $\sigma = 0.1$  S/m,  $\epsilon_r = 80$ ), cylindrical needle electrodes with radii of 1 mm and sharp conical tips are inserted 10 cm into the simulated tissue mass. One centimeter of the conducting surface of the electrodes, excluding the tip, was exposed on each electrode, and simulations are given at steady state, without considering dynamic conductivity tissue responses to the electric field or temperature. 1.5 kV were applied to the two electrodes, which are spaced 1 cm apart in the central image

compounded and result in over- and under-exposed tissue regions to be suboptimally or ineffectively treated.

When electrodes deform along their length during placement—called bowing—regions of tissue may experience increased or decreased electric field intensities because the electrodes are closer or further apart, respectively. Bowing, similar to angulation, may cause regions of underexposed tissue to remain insufficiently permeabilized to effectively enhance molecular transport or to induce cell death. Overexposed regions will experience increased Joule heating and may be more susceptible to unintended thermal damage.

#### **3.4.1.2 Skewness**

For an ideal placement, electrodes are often placed in the same plane and focally ablate the tissue region between the exposed conductors. However, scenarios present where electrodes may not be inserted to exactly the same depth because of sensitive tissue structures or other such anatomical consideration. In this case, it is imperative to consider the ratio of the characteristic length of the exposed conducting surface on the electrodes to the distance between them. If not properly handled, skew electrodes can either cause an underestimation of the tissue treatment volume because a greater distance than expected separates the two electrode surfaces. However, if well considered, a skewed electrode placement can confer the benefit of being able to more elegantly deliver the electric field intensities necessary for IRE to a tissue region with complexities such as vascularity or anisotropy.

Generally, though, for an isotropic tissue, angulation will result in an overestimate of the ablation volume because the physical distance separating the two electrodes will be greater. This greater distance may not matter for slightly skew configurations of a few millimeters but will significantly impact the treatment volume when the distance between electrode surfaces is more than about half of their height of the electrode. However, if the two electrodes are placed in close lateral proximity (i.e., the shaft of the two electrodes are close together) and separated by roughly the distance similar to that of the exposed electrode surface, the ablation volume will appear ellipsoidal along the axis of the electrode shafts.

In general, the ratio of conductor surface areas to the distance separating them indicates whether the electrodes generate an electric field with a conduction shape function that will more closely resemble a point source and a semi-infinite plane or a parallel electrode configuration. Small differences in exposed surface area will not significantly impact the electric field, so long as the electrodes are approximately symmetric around a central axis. It is important to recognize the distortions that may be present under these circumstances.

#### **3.4.1.3 Tissue Inhomogeneity**

Tissue structure and orientation are complicated by the presence of multiple tissues performing multiple tasks in close proximity; a tissue's electrical properties are derived from this structural organization. Therefore, a tissue's physiology must be carefully considered in pretreatment planning for IRE procedures.

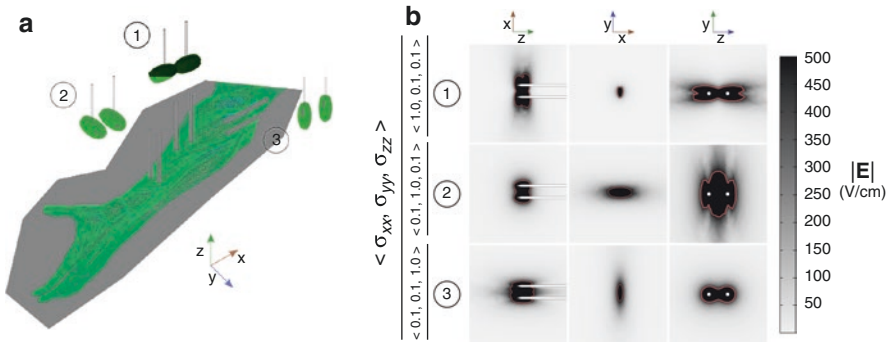


**Fig. 3.9** A tissue exhibiting anisotropic conductivity will distort the expected electric field depending on the electrode placement. Electrodes were inserted into simulated anisotropic tissue (muscle;  $\epsilon_r = 80$ ;  $\underline{\sigma} = \langle \sigma_{xx}, \sigma_{yy}, \sigma_{zz} \rangle$ ) at the points shown in (a), and the lesion geometries around the electrodes are indicated by the surfaces around the electrode tips. The electric field distortions generated in the  $xy$ -,  $yz$ -, and  $xz$ -planes as a result of different anisotropic conductivities are shown in (b). The electric field was generated using an applied potential of 1.5 kV, and the 500 V/cm electromagnetic intensity isosurface of the resultant electromagnetic field distribution is shown. The axis indicator refers to the electrode positioning of the images with the electric field isosurfaces rather than the orientation in (a); this orientation is conserved in (b)

#### 3.4.1.4 Anisotropic Tissue

Electrical anisotropies arise from asymmetric distributions and orientations of tissue and its constituents that allow electrical current to flow in one direction more easily than another Fig. 3.9. Physically, these anisotropies mean that the conductivity tensor  $\sigma_{ij}$  is not equal in each coordinate direction ( $\sigma_{xx} \neq \sigma_{yy} \neq \sigma_{zz}$ ) and that the electric field distribution will be distorted because the electron flow will be directed according to the particular anisotropy. For example, muscle tissue is highly anisotropic as the muscle fibers stretch along the contractile axis of the tissue. This structure allows electrical current to flow more easily along the contractile axis with the fiber alignment, rather than against it.

#### 3.4.1.5 Vascularization and Perfused Tissue

During exposure to electric fields, fluid flow and the vascular structure itself generate inhomogeneities within the tissue that complicate the prediction of its response Fig. 3.10. If the perfusate is an electrolyte, for example, blood flowing through the portal vein in the liver, it may conduct electric current better than the surrounding tissue and result in a large anisotropy along the axis of fluid flow at the local vessel region. Conversely, the vascular walls produce a large capacitance that introduces a nontrivial time dependence into the electric field distribution that might not be present in relatively homogeneous bulk tissue, like the lobe of a liver.

### 3.4.2 Joule Heating

Thermal considerations are critical when planning and delivering IRE treatment to a target tissue region. While delivering electric current to a tissue, it may be

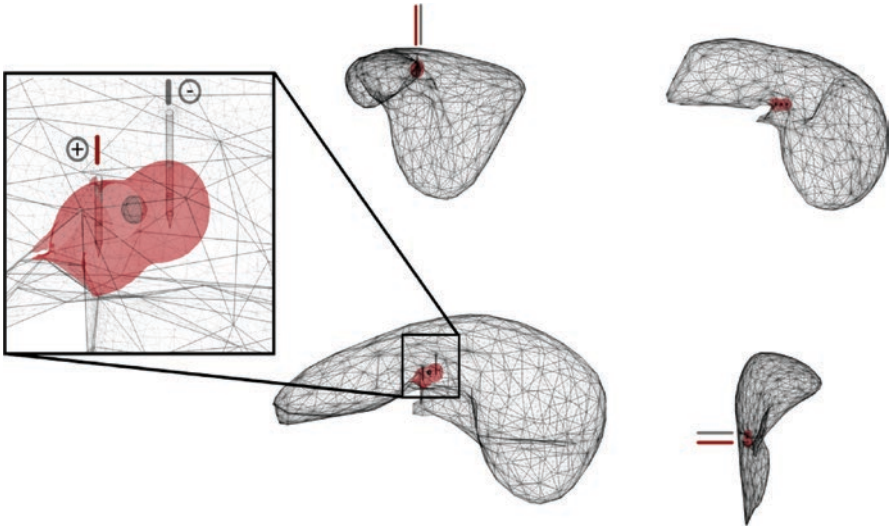


**Fig. 3.10** The electric field surrounding tumor tissue embedded in normal vascularized tissue (liver) will distort the electric field delivered to the target tissue. A simulated liver tissue with static electrical properties (to emphasize the effect of inhomogeneous tissue) is shown with the gallbladder, hepatic ducts, liver lobule tissue, and falciform ligament each exhibiting different electrical properties. The electric field surface shown for a potential ablation zone is shown from the (b) right dorsal sagittal, (c) left dorsal sagittal, and (d) superior transverse perspectives. Distortions in the electric field occur at the tissue-tissue and tissue-air boundaries

important to deliver series of pulses, but it is critical to understand that thermal energy is generated when electrical current travels through a resistive material. When electrical energy is consumed by a material, the rate at which it is consumed is given by the rate of energy conversion (power  $\wp$ )

$$\wp = \mathbf{J} \cdot \mathbf{E} = \sigma |\mathbf{E}|^2.$$

In the case of biological tissue undergoing IRE treatment, this energy delivered to the tissue is largely transformed into heat. It is desirable for the thermal damage sustained by a tissue to remain minimal so that protein denaturation does not occur and the structural integrity of the proteinaceous stromal components is not compromised [11, 18, 35].

For a particular point in space, the heat generated in a unit volume of tissue  $Q$  is given as  $Q = \wp$ , assuming perfect conversion from electrical energy to heat (i.e.,  $Q = \sigma |\mathbf{E}|^2$ ). Thus, the material conductivity  $\sigma$  directly impacts the heating of the tissue as a result of the electrical energy. Generally, the temperature distribution and the change in temperature for a region of tissue undergoing IRE treatment are calculated by Pennes bioheat Eq. 3.10 with an added term to account for Joule heating, which is given by

$$\rho c_p \frac{\partial T}{\partial t} = \nabla \cdot (\mathbf{k} \nabla T) + \dot{q}_m + \dot{q}_p + \sigma |\mathbf{E}|^2 \quad (3.15)$$

where  $\rho$  is the density of the material,  $c_p$  is the heat capacity of the material,  $T$  is temperature,  $\dot{q}_m$  is the heat generated from metabolic processes within the tissue, and  $\dot{q}_p$  is the heat added to the tissue by a perfusate.

### 3.4.2.1 Dynamic Conductivity

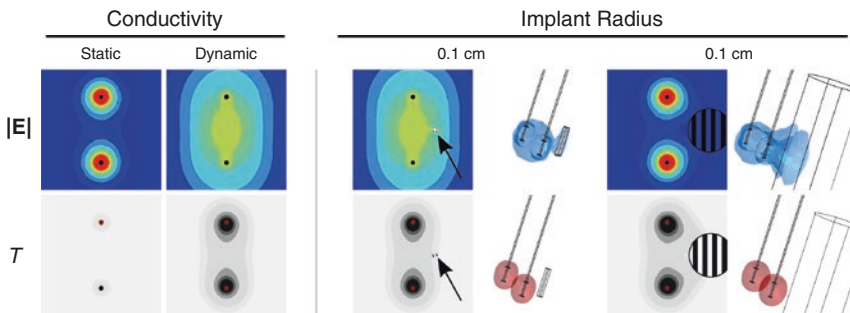
The cell membrane serves as a barrier across which chemical and electrical potential gradients are established to drive cellular processes. When cells become electroporated, the membrane develops pores which permit the diffusive exchange of normally impermeant molecules between the intracellular and extracellular environment. This affects the electrical properties of a bulk tissue by both increasing the conductivity of the extracellular material [23, 37] from the cytoplasm and opening previously unavailable intracellular current pathways.

The bulk electrical conductivity of a tissue changes as a result of increased cellular permeability during application of electric fields to a target tissue from empirically determined local electric field intensity as a function of the local electric field intensity and temperature for a given point in space is given by

$$\sigma_D(E, T) = (1 + \alpha(T - T_0)) \left[ \sigma_0 + (\sigma_{\max} - \sigma_0) \exp(-A \exp(-B|E|)) \right]$$

where  $T$  is the temperature,  $T_0$  is the initial temperature,  $\alpha$  is the conductivity-temperature coefficient ( $\sim 1-3 \text{ \%}/^\circ\text{C}$ ) [34],  $\sigma_0$  is the initial electrical conductivity,  $\sigma_{\max}$  is the electrical conductivity obtained when the tissue is maximally permeabilized,  $E$  is the electric field intensity, and  $A$  and  $B$  are curve-fitting terms [34].

To illustrate the impact of intraoperative electrical conductivity changes arising from temperature changes and exposure to electric fields, a simulated liver tissue is shown in Fig. 3.11 to demonstrate the altered electric field and temperature



NOTE: The same values were used for the contours across all images

**Fig. 3.11** Dynamic conductivity and large conductive obstructions dramatically distort the electric field distribution. Biological tissues increase their conductivity in applied electric fields as cells become electroporated. The electric field for the cases of static ( $\sigma$ ) and dynamic conductivity  $\sigma(|E|, T)$  are plotted in the right panel. The left shows the distortions in electric field created by the presence of an electrically conductive object near the electrodes delivering IRE pulses with larger obstructions affecting the electric field distribution more than small obstructions. Temperature distributions are also given for each scenario and indicate that the temperature distribution is similar to the electric field distribution

distributions. It is important to note that the tissue was considered without perfusion and metabolic components to isolate the impact of the electric field, geometry, and temperature on the conductivity distribution throughout the tissue. The left panel shows a static homogenous conductivity ( $\sigma = 0.15$  S/m) and a dynamic conductivity based on the dependence given by Sect. 4.2.1. While in the case of a static conductivity  $\sigma$ , the electric field distribution closely mirrors that predicted by Eq. 3.11; when a dynamic conductivity  $\sigma(\mathbf{E}, T)$  is used, the electric field is distorted, and the electric field intensity becomes more evenly distributed across the tissue between the electrodes because the current flowing between the electrodes is able to be distributed across a larger, more conductive region. The increased conductivity of this region will necessarily permit more current under equipotential pulses and is responsible for the change in resistance measured between the first pulse and the last pulse in a train [15].

### 3.4.2.2 Pulse Number

IRE has typically been performed using a recommended  $70\text{--}90 \times 100$   $\mu\text{s}$  pulse delivered once every 1.0 s (1 Hz) at voltages that depend on the target tissue, desired ablation volume, and electrode geometry [2, 42]. This setting was chosen because it delivers the optimal number of pulses to achieve efficient cell death throughout the tissue volume while mitigating thermal damage resulting from Joule heating [10, 35]. Delivering more pulses will result in a growth of the ablation zone due to the conductivity changes in the tissue and the greater probability that cells within the ablation zone will be destroyed; though this could dramatically impact the thermal damage to the tissue. With increasing pulse number, the ablation zone size will initially make significant increases with pulse number during the first  $\sim 70\text{--}90$  but only marginally impact its size for the following pulses. However, increasing pulse number, for equivalent-length pulses below the capacity of the tissue to diffuse the heat generated by a single pulse, also increases the heat generated in that tissue. Delivering a train of hundreds of pulses may not, effectually, impact the efficacy of IRE to kill cells but will certainly increase the heat generated within and around the electrodes and ablation region [35]. For this reason, it is critical to balance the pulse number with minimal thermal damage to the tissue.

Several strategies to minimize tissue heating during IRE procedures have previously been employed. Simply adding inter-pulse delays between each pulse allows some heat to diffuse away from the ablated tissue and results in less overall temperature rise. In a similar vein, performing a train of pulses in rapid succession followed by a longer delay achieves a similar effect, though with potentially larger ablations generated within each cycle. Actively cooling the ablation region using a heat sink would further mitigate IRE's thermal effects by actively drawing excess heat out of the tissue instead of allowing it to passively diffuse. Though the specific details of these methodologies are not outlined here, increasing pulse number also increases the concern for undesired thermal effects and spurs the need for effective cooling.



### 3.4.2.3 Conductive Implants

Metallic surgical implants (stents, bone screws, etc.) or instruments (other electrodes, hemostats, etc.) have become commonplace, and it must be understood that introducing such a material to an electrical environment will distort the electric field distribution at an extent proportional to its size and conductivity relative to the size and conductivity of the affected tissue. For example, small objects (treatment seeds) will have a trivial impact, whereas larger objects (stents) will have a greater effect. The conducting metallic surface will result in the buildup of surface charge which diverts the flow of electrons with respect to that obstruction. However, a conducting obstruction on the order of the same diameter as the needle electrodes does not significantly distort the final ablation volume, and it has been shown that such structures do not impede the safe and effective delivery of IRE treatment [33, 40]. Similarly, the temperature distribution in a tissue is relatively unchanged for small conductive obstructions, with larger obstructions impacting the temperature distribution more significantly, assuming they begin at the same temperature as the surrounding tissue. However, if these obstructions begin at cooler temperatures, they may serve as heat sinks for heat transfer and ultimately generate lower temperatures throughout the ablation region, if heating becomes a concern.

### 3.4.2.4 Electrode Exposure Length

The exposed length of the conductive electrode surface can also impact the electric field distribution in an ablation region. For example, if only a small portion of the electrode is exposed, and the electrodes are far apart, the electric field will appear similar to that of an electric field applied between two spherical electrodes. However, for longer electrode exposure lengths, the area between the electrodes will begin to more closely resemble Fig. 3.5 and have a larger ablation zone in the direction parallel to the length of the electrodes.

### 3.4.2.5 Electrode Arrays and Pulse Sequences

It is possible to use multiple electrodes positioned in an array to perform IRE focal ablation [7]. By grounding one (or multiple) electrode, and energizing another, an electric field is generated inside the target tissue, as in the case of two-needle electrode. Electrical pulses are often applied between each adjacent electrode combination to ablate a larger volume of tissue, but it is important to consider the consequences of these serial pulsing combinations, such as the one shown in Fig. 3.12a. Realizing that the tissue conductivity is dynamic and dependent on the local electric field intensity and temperature, it becomes clear that if a region of tissue has been electroporated previously, it will not have the same electrical properties with additional exposure. Indeed, additional electrical pulses delivered to the tissue will depend on the previous electrified state of the tissue. Figure 3.12b shows a cross-section of the electric field intensity and temperature distributions in simulated liver tissue with steady conductivity ( $\sigma = 0.5 \text{ S/m}$ ) and dynamic conductivity given by Sect. 4.2.1. Considering the more realistic case of dynamic conductivity, the electric field is distorted from what is predicted from simple models, and the

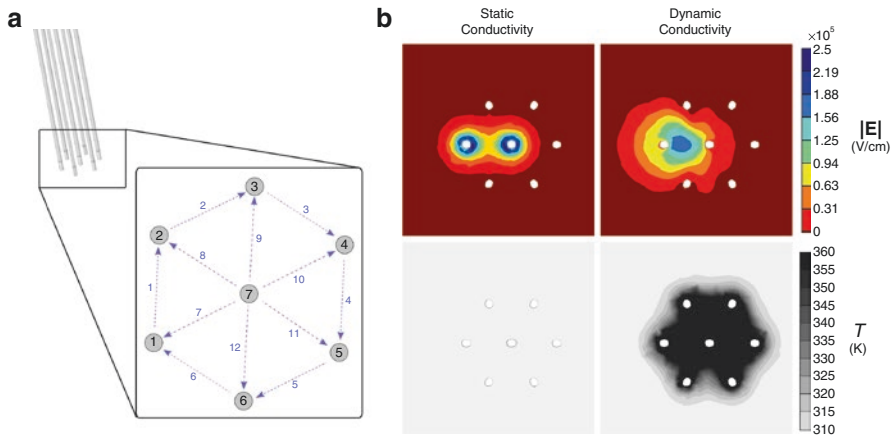


**Fig. 3.12** The electric field and temperature distributions generated within a tissue during electroporation change the tissue conductivity and therefore depend on the tissue's previous electric field exposure and temperature. A pulsing scheme for a 7-electrode array (blue) generates electric fields between every combination of two electrodes in the typical circular electrode array shown (1 cm between electrodes). The electric field and temperature distributions are shown at the completion of each serial pulsing step

temperature has risen dramatically beyond what the static model predicts. In order to induce minimal thermal damage during treatment, it is imperative that the dynamic response of a tissue to an electric field be considered during treatment planning and application.

### Conclusion

An intuitive understanding of how electric fields behave in biological tissue involves understanding how electric fields are distributed within a tissue, impact the constituent cells within that tissue, and abstract that cellular impact back to measurable tissue-level properties. An understanding of these properties results in more accurate treatment planning prior to treatment and better clinical response to any intraoperative complications. IRE treatment is a complex, multi-scale, biophysical treatment modality that, when its biophysical mechanisms are appreciated and it is implemented in a well-considered manner, has been shown to provide clinically viable treatment options for patients that would otherwise not exist.

### References

1. Abidor I, Arakelyan V, Chernomordik L, Chizmadzhev Y, Pastushenko V, Tarasevich M. 246 – electric breakdown of bilayer lipid membranes I. The main experimental facts and their qualitative discussion. *Bioelectrochem Bioenerg.* 1979;6(1):37–52.
2. Al-Sakere B, André F, Bernat C, Connault E, Opolon P, Davalos RV, Rubinsky B, Mir LM. Tumor ablation with irreversible electroporation. *PLoS One.* 2007;2(11):e1135.

3. Alberts B. *Molecular biology of the cell*. 4th ed. New York: Garland Science; 2002.
4. Bergman TL, Incropera FP, Lavine AS. *Fundamentals of heat and mass transfer*. Hoboken: Wiley; 2011.
5. Bhonsle SP, Arena CB, Sweeney DC, Davalos RV. Mitigation of impedance changes due to electroporation therapy using bursts of high-frequency bipolar pulses. *Biomed Eng Online*. 2015;14(Suppl 3):S3.
6. Buchner R, Hefter GT, May PM. Dielectric relaxation of aqueous NaCl solutions. *Chem Eur J*. 1999;103(1):1–9.
7. Campana LG, Cesari M, Dughiero F, Forzan M, Rastrelli M, Rossi CR, Sieni E, Tosi AL. Electrical resistance of human soft tissue sarcomas: an ex vivo study on surgical specimens. *Med Biol Eng Comput* 2016;54.5:773–87.
8. Čemažar J, Douglas TA, Schmelz EM, Davalos RV. Enhanced contactless dielectrophoresis enrichment and isolation platform via cell-scale microstructures. *Biomicrofluidics*. 2016;10(1):014109.
9. Corović S, Pavlin M, Miklavcic D. Analytical and numerical quantification and comparison of the local electric field in the tissue for different electrode configurations. *Biomed Eng Online*. 2007;6:37.
10. Davalos R, Rubinsky B, Mir L. Theoretical analysis of the thermal effects during in vivo tissue electroporation. *Bioelectrochemistry*. 2003;61(1–2):99–107.
11. R. V. Davalos, S. Bhonsle, R. E. Neal. Implications and considerations of thermal effects when applying irreversible electroporation tissue ablation therapy. *Prostate*. 2015;1118(Jan):n/a–n/a.
12. Davalos RV, Mir LM, Rubinsky B. Tissue ablation with irreversible electroporation. *Ann Biomed Eng*. 2005;33(2):223–31.
13. DeBruin KA, Krassowska W. Modeling electroporation in a single cell. I. Effects of field strength and rest potential. *Biophys J*. 1999;77(3):1213–24.
14. Dev SB, Dhar D, Krassowska W. Electric field of a six-needle Array electrode used in drug and DNA delivery in vivo: analytical versus numerical solution. *IEEE Trans Biomed Eng*. 2003;50(11):1296–300.
15. Dunki-Jacobs EM, Philips P, Martin RCG. Evaluation of resistance as a measure of successful tumor ablation during irreversible electroporation of the pancreas. *J Am Coll Surg*. 2014;218(2):179–87.
16. Edd JF, Davalos RV. Mathematical modeling of irreversible electroporation for treatment planning. *Technol Cancer Res Treat*. 2007;6(4):275–86.
17. Gabriel S, Lau R, Gabriel C. The dielectric properties of biological tissues: II. Measurements in the frequency range 10 Hz to 20 GHz. *Phys Med Biol*. 1996;41:2251.
18. Garcia P, Rossmeis J, Neal REI, Ellis T, Davalos R. A parametric study delineating irreversible electroporation from thermal damage based on a minimally invasive intracranial procedure. *Biomedica*. 2011;10:34.
19. Gascoyne PRC, Pethig R, Burt JPH, Becker FF. Membrane changes accompanying the induced differentiation of friend murine erythroleukemia cells studies by dielectrophoresis. *Biochim Biophys Acta Biomembr*. 1993;1149(1):119–26.
20. Glaser RW, Leikin SL, Chernomordik LV, Pastushenko VF, Sokirko AI. Reversible electrical breakdown of lipid bilayers: formation and evolution of pores. *Biochim Biophys Acta*. 1988;940:275–87.
21. Hölzel R, Lamprecht I. Dielectric properties of yeast cells as determined by electrorotation. *Biochim Biophys Acta Biomembr*. 1992;1104(1):195–200.
22. Hu Q, Joshi RP, Beskok A. Model study of electroporation effects on the dielectrophoretic response of spheroidal cells. *J Appl Phys*. 2009;106(2):024701.
23. Ivorra A, Villemejeane J, Mir LM. Electrical modeling of the influence of medium conductivity on electroporation. *Phys Chem Chem Phys: PCCP*. 2010;12(34):10055–64.
24. Kashchiev D, Exerowa D. Bilayer lipid membrane permeation and rupture due to hole formation. *Biochim Biophys Acta*. 1983;732(1):133–45.
25. Kotnik T, Bobanovic F, Miklavcic D. Applied electric fields—a theoretical analysis. *Bioelectrochem Bioenerg*. 1997;43:285–91.

26. Kotnik T, Miklavcic D. Analytical description of transmembrane voltage induced by electric fields on spheroidal cells. *Biophys J.* 2000;79(2):670–9.
27. Kranjc M, Bajd F, Sersa I, Woo EJ, Miklavcic D. Ex vivo and in silico feasibility study of monitoring electric field distribution in tissue during electroporation based treatments. *PLoS One.* 2012;7(9):3–10.
28. Mahnic-Kalamiza S, Kotnik T, Miklavcic D. Educational application for visualization and analysis of electric field strength in multiple electrode electroporation. *BMC Med Educ.* 2012;12:102.
29. Marcelja S. Structural contribution to solute-solute interaction. *Croat Chem Acta.* 1977;49(2):347–58.
30. Marcelja S, Radic N. Repulsion of interfaces due to boundary water. *Chem Phys Lett.* 1976;42(1):129–30.
31. Martin RCG, Kwon D, Chalikhonda S, Sellers M, Kotz E, Scoggins C, McMasters KM, Watkins K. Treatment of 200 locally advanced (stage III) pancreatic adenocarcinoma patients with irreversible electroporation. *Ann Surg.* 2015;262(3):486–94.
32. Maxwell JC. A dynamical theory of the electromagnetic field. *Philos Trans R Soc Lond.* 1865;155(0):459–512.
33. Melenhorst MCAM, Scheffer HJ, Vroomen LGPH, Kazemier G, van den Tol MP, Meijerink MR. Percutaneous irreversible electroporation of unresectable hilar cholangiocarcinoma (Klatskin tumor): a case report. *Cardio Vasc Interv Radiol.* 2016;39(1):117–21.
34. Neal RE, Garcia PA, Robertson JL, Davalos RV. Experimental characterization and numerical modeling of tissue electrical conductivity during pulsed electric fields for irreversible electroporation treatment planning. *IEEE Trans Biomed Eng.* 2012;59(4):1076–85.
35. Neal RE, Millar JL, Kavnoudias H, Royce P, Rosenfeldt F, Pham A, Smith R, Davalos RV, Thomson KR. In vivo characterization and numerical simulation of prostate properties for non-thermal irreversible electroporation ablation. *Prostate.* 2014;74:458–68.
36. Neff HP. *Introductory electromagnetics.* New York: Wiley; 1991.
37. Pavlin M, Kanduser M, Rebersek M, Pucihar G, Hart FX, Magjarevic R, Miklavcic D. Effect of cell electroporation on the conductivity of a cell suspension. *Biophys J.* 2005;88(6):4378–90.
38. Powell KT, Weaver JC. Transient aqueous pores in bilayer membranes: a statistical theory. *Bioelectrochem Bioenerg.* 1986;211:211–27.
39. Rols MP, Teissie J. Modulation of electrically induced permeabilization and fusion of Chinese hamster ovary cells by osmotic pressure. *Biochemistry.* 1990;29(19):4561–7.
40. Scheffer HJ, Vogel JA, van den Bos W, Neal RE, van Lienden KP, Besselink MGH, van Gemert MJC, van der Geld CWM, Meijerink MR, Klaessens JH, Verdaasdonk RM. The influence of a metal stent on the distribution of thermal energy during irreversible electroporation. *PLoS One.* 2016;11(2):e0148457.
41. Schwan H. P. *Electrical properties of tissue and cell suspensions.* In: *Advances in biological and medical physics*, Vol. 5. New York: Academic; 1957. p. 147.
42. Wendler JJ, Fischbach K, Ricke J, Jürgens J, Fischbach F, Köllermann J, Porsch M, Baumunk D, Schostak M, Liehr U-b, Pech M. Irreversible electroporation (IRE): standardization of terminology and reporting criteria for analysis and comparison. *Pol J Radiol.* 2016;81:54–64.

Bor Kos and Damijan Miklavčič

---

## 4.1 Numerical Methods and Models for Treatment Planning

Irreversible electroporation is in many ways similar to radiation therapy. The initial required action is physical, while the final resolution of the outcome occurs through a biological mechanism. In the area of radiation therapy, the physical quantity, which determines the outcome of the therapy, is the delivered radiation dose, which is most commonly delivered in fractions over a span of consecutive days. The general workflow for radiation therapy is that a radiation oncologist determines the gross tumour volume (GTV – i.e. the total volume of the tumour tissue) and the clinical target volume (CTV – i.e. the GTV and surrounding safety margin). An additionally larger volume called planning target volume (PTV) is defined, which aims to compensate for errors in image segmentation, patient positioning, etc. These volumes are then transferred to the radiation physicist to prepare and optimize the treatment plan for each individual patient [7].

Since IRE is a relatively new treatment, it can be useful to use established terminology when developing the methods and protocols for treatment, since this can only improve the clarity and ease the acceptance of these technologies. Because IRE requires the insertion of electrodes to the target clinical volume, application of the treatment over a longer therapy is not feasible, even though there is some evidence that delivering electrical pulses in separate bursts with a relatively short rest period in between can contribute to increase probability of cell kills [50]. Unlike with radiotherapy, fractionation of the treatment is not possible, but a radiological evaluation of treatment outcome might be possible as early as 2 days after treatment [13].

---

B. Kos, PhD (✉) • D. Miklavčič, PhD  
Department of Biomedical Engineering, University of Ljubljana, Ljubljana, Slovenia  
e-mail: [bor.kos@fe.uni-lj.si](mailto:bor.kos@fe.uni-lj.si)

**Table 4.1** Parallelism and similarities between radiotherapy and irreversible electroporation

Radiotherapy	Irreversible electroporation
Simulation – medical imaging (CT or a combination of CT with PET) of the patient	Mathematical model of electroporation: measurement of tissue properties and tissue-level models of electroporation
Treatment planning: delineation of target volumes, definition of dose constraints, calculation of a suitable plan by numerical modelling and optimization – number of fractions, position and intensity of the beams	Treatment planning: medical imaging of the patient, delineation of target volumes, construction of the mathematical model geometry, calculation of a suitable plan by numerical modelling and optimization – number and positions of electrodes, number of pulses, delivered voltage for each electrode pair
Set-up verification: medical imaging is used for verifying the position of the patient and target tissues; in subsequent sessions, lasers and tattoo marks are used together with patient anatomy casts	Set-up verification: optimal electrode positions are registered on the original medical images; electrode positions are verified using ultrasound, CT or CBCT imaging
Treatment delivery and monitoring: radiation is delivered according to the treatment plan in several fractions, while imaging is used to control for breathing movement	Treatment plan delivery and monitoring: after electrode insertion, electric pulses are delivered in sync with the heartbeat. Current and voltage are measured to control for possible errors during electric pulse delivery
Response assessment: post-treatment measurement of tumour size or biological tumour markers with medical imaging	Response assessment: post-treatment measurement of tumour size or biological tumour markers with medical imaging, compared to pretreatment medical images

Adapted for irreversible electroporation from Pavliha et al. [52]

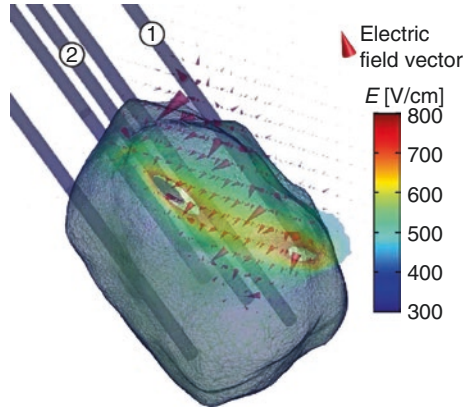
To continue building the framework of treatment panning, we can look at the similarities and differences between radiotherapy and IRE treatment planning (Table 4.1). In radiotherapy, the physical quantity which determines the local outcome is the absorbed dose in the target tissue expressed in gray (Gy). In IRE, the respective physical quantities are pulsed electric fields expressed in V/m, pulse duration, pulse delivery period and number of pulses. While radiation passes through the body in a straight line and is absorbed in relation with the tissue density, the electric field at the frequencies used in IRE exists between the electrodes and is inhomogeneous. The electric field distribution is dependent on the geometry of the electrodes and the distance between them; the electric properties of tissue, which vary between individuals and can change with different pathological states of tissue; and the delivered voltage [14, 56, 59]. The mathematical description of the electric field is given by the following two equations:

$$-\nabla(\sigma\nabla V) = 0$$

$$E = -\nabla V$$

where  $\nabla$  is the gradient operator,  $V$  is the electric potential,  $\sigma$  is the electric conductivity and  $E$  is the electric field strength [54]. An illustration of the electric field in a

**Fig. 4.1** Electric field around a tumour. The *arrows* show the electric field direction (scaled in size by field strength) around an active electrode pair indicated by numbers 1 and 2. The gradient slice plot shows the electric field magnitude in a horizontal plane (electrodes are angled). The electric field is highly inhomogeneous around the electrodes



non-homogeneous tissue surrounding a tumour is given in Fig. 4.1. Additionally, the conductivity of tissues is affected by the effects of electroporation. Namely, it increases with increasing electric field [14, 36]. Therefore, the electric field in tissue is governed by a partial differential equation, which determines the different methods that can be used to model these fields in tissue.

Finite element method is most commonly used to solve differential equations for this kind of mathematical problems [28]. The finite element method involves discretizing the computational domain into a mesh of elements, which can be of various shapes. The assumption is that the underlying quantity changes little enough over the element and that the physical quantity can be then described by relatively simple functions. The elements can follow the contours of the geometry, which is typically very complex and irregular in the case of tumours in tissue. Many different FEM solvers exist, both open-source (FEniCS, freeFEM) and commercial (COMSOL, Matlab, AceFEM) software implementations are available.

Regardless of the type of software implementation used, the first step in the treatment planning process is building a computational model, which is a description of the patients' anatomy and a numerical representation of the clinical target volume and surrounding tissues. A patient-specific model can be made using geometrical approximations with simplified shapes (e.g. ellipsoids) or based on actual medical images. To use medical images, segmentation and then appropriately meshing the segmented images to a three-dimensional model or directly to a three-dimensional mesh need to be performed. The segmentation in itself is a complex task: it can be performed either manually (very time-consuming) or automatically (requires complex algorithms and expert validation). Automatic segmentation has been well described for liver and liver vessel tissues [42, 45, 53], prostate [12, 25, 48] and kidney [11, 67]. The tumour tissue mostly requires manual segmentation. For automatic segmentation, there are several packages developed and available to use (ITK-SNAP, Slicer, Visifield). Automatic segmentation also typically requires a manual validation by a radiologist. Once segmentation is finished, it has to be transformed into a computational mesh. Again, there are several open-source (TetGen)

and commercial (Mimics/3matic, Simpleware, Comsol Multiphysics) tools available, which can transform segmented medical images directly into a volumetric mesh for finite element analysis.

Then however, the virtual electrodes need to be inserted into the model. This involves a complex task of modifying the existing mesh to include the electrodes. To avoid this mesh modification, the electrode geometry can be approximated by selecting appropriate mesh elements to change to the electrode domain, or the geometry can be built by building the electrodes themselves and then assigning material parameters to each element individually through look-up tables [6]. Irrespective of the kind of implementation, it is important to implement the electroporation-dependent conductivity in the model, since it significantly affects the predicted currents and also the size of the IRE lesion. When comparing the size of effect from a model without any increase in conductivity vs a model with increase in conductivity, the latter will always predict a larger volume of effect and also better match experimentally obtained lesions [14, 21, 46, 47, 64, 66].

---

## 4.2 Modelling the Effect of Different Pulse Parameters on Treatment Result

Although IRE is typically referred to as a nonthermal procedure, it brings a non-negligible temperature rise in play. The currently available AngioDynamics NanoKnife system can deliver pulses of up to 3 kV and 50 A in amplitude, which equals a pulse power of up to 150 kW. However the duty cycle (ratio between pulse duration and period of pulse delivery) is typically below  $10^{-4}$ , since the pulses are delivered with cardiac synchronization and they are typically less than 100  $\mu$ s long. Therefore, the average power of an irreversible electroporation treatment is on the order of 15 W or less.

The thermal energy that pulses deliver will heat the tissue surrounding the active electrode pair. Because tissue generally has a positive thermal coefficient for conductivity, which is in the range of 1–2%/K, hotter tissue will draw more current and cause even more heating in the tissue. The heating of tissue can contribute to the gradual increase in the delivered current through the course of the treatment (Fig. 4.1). An average temperature rise of 10 °C in the whole treated volume will therefore cause an increase in current of 10–20% (Fig. 4.2).

Temperature in tissue is most often modelled using the Pennes' bioheat equation. This equation features the diffusion equation, whereby heat diffuses in the opposite direction of the temperature gradient. It also includes terms for heating from metabolic heat generation, which is negligible in comparison with the heating from electric pulses, and cooling from blood perfusion. Blood perfusion itself is also affected by temperature and is reduced dramatically once a certain temperature threshold is reached due to protein coagulation [27, 28]. Blood perfusion is affected directly and quickly by electric pulses themselves, which restrict blood flow in all but the largest vessels, as well as microcirculation [30]. Consequently, when modelling thermal



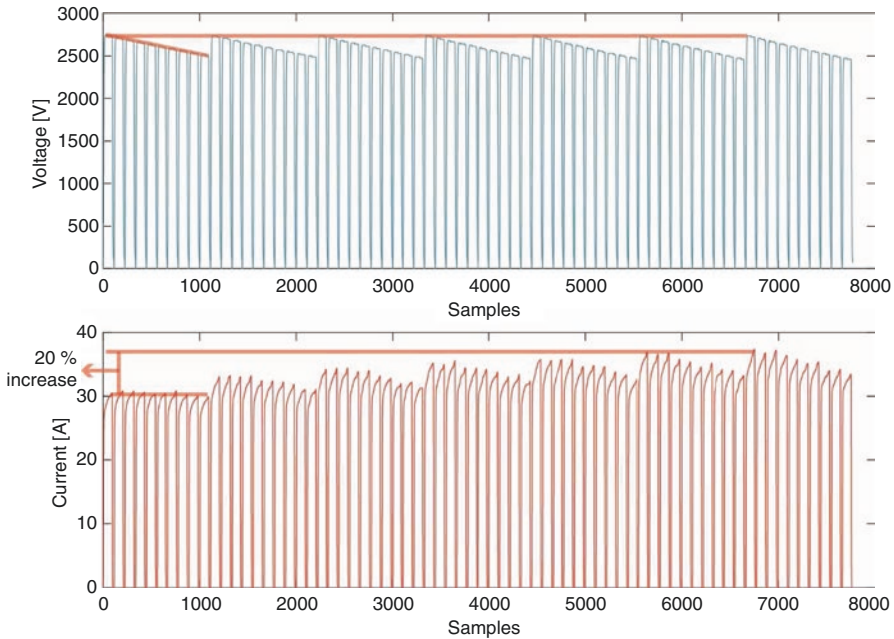


**Fig. 4.2** Voltage and current during an IRE procedure in the liver. Pulses are delivered in trains of 10 pulses, and then the drop in voltage requires the machine to recharge. The current in the first train can be seen to remain constant even though the voltage is decreasing, which can be attributed to some effects of electroporation. In the last train, the current is 20% higher than the initial current (Current data from case presented in Kos et al. [33])

effect of irreversible electroporation, perfusion can be included as normal in bioheat modelling, but care must be taken to reduce the perfusion in areas affected by irreversible electroporation.

The thermal effect of IRE pulses can be modelled from the temperature rise itself by the use of the Arrhenius integral, which is often used in processes where thermal damage occurs. The Arrhenius integral is a mathematical model describing the capability of tissue to withstand higher temperatures for a shorter time. The thermal damage is modelled as a time-dependent process, where a certain activation energy is required for the process to begin. The higher the temperature, the faster the rate of the thermal damage occurs. Depending on the selection of the pulse parameters, the thermal damage can represent a smaller or larger part of actual tissue damage [20, 21, 33]. Even if thermal damage is not contraindicated by the presence of some critical tissue, thermal heating and associated effects can be limited by selecting an appropriate number of pulses to achieve the desired effect.

There is some evidence that increasing the number of pulses can increase the volume of the treated region to a certain extent, but after about 200 pulses, the increase starts to plateau [62]. This suggests that there could be an optimal number of pulses which would enable a high efficacy of the electroporation treatment while keeping the total volume of thermal damage low. To model the dependency of the

electroporation effect on the number of pulses, different mathematical models have been proposed [17, 23]. Currently, the Peleg-Fermi model of cell death [55] has given results most consistent with experimental data [17, 20, 33]. The model was first developed to describe microbial inactivation due to pulsed electric fields [55] but has been expanded by Golberg and Rubinsky to mammalian cells. With this model it is important to note that the parameters of the model, i.e. critical electric field and the shape constant, are dependent on the number of pulses used [57]. However, they should not be used outside of the range of pulses on which the data was calibrated on.

---

### 4.3 Optimization of Treatment Plans

The goal of treatment plan preparation through optimization of electrode positions and amplitude of pulses is to ensure adequate target volume coverage and to minimize exposure and damage to surrounding critical or vulnerable structures due to irreversible electroporation and thermal damage [71]. In radiotherapy, various methods are used for radiation delivery, but newer methods such as intensity-modulated radiation therapy and volumetric modulated arc therapy require ever more complex treatment planning techniques [10, 31, 63, 68]. Here, the main goal is to optimize the treatment to ensure maximum sparing of surrounding healthy tissue, while maintaining an adequate dose of radiation in the CTV.

In contrast to radiation therapy, IRE has fewer difficulties in ensuring nearby critical structures are not affected because the electric field is very localized. Also the transition regions between ablated and non-ablated tissue thin [4, 5, 46, 47]. Optimization in general can be performed on a varying number of parameters. A full parameter list would include six degrees of freedom for each electrode (by ensuring electrode parallelism only three degrees of freedom are required for all electrodes) and one degree of freedom for each electrode pair used in the treatment. A four electrode system with parallel electrodes would therefore have 21 parameters (positions of each electrode, direction of all electrodes and voltage between six electrode pairs). This represents a large parameter space, which cannot be searched using brute force approaches. An approach using genetic algorithms has been proposed and tested [70], but if the electrode positions are fixed, also local gradient-based optimization of only voltages is feasible and time-efficient [19].

---

### 4.4 2D vs 3D Modelling and Treatment Planning Tools

When we consider any numerical method implementation for solving differential equations, it is beneficial to look for possible symmetries and choose the lowest applicable number of dimensions for the model. It is therefore desirable to use 2D modelling for ease of implementation, display, etc. With a 2D geometry that the

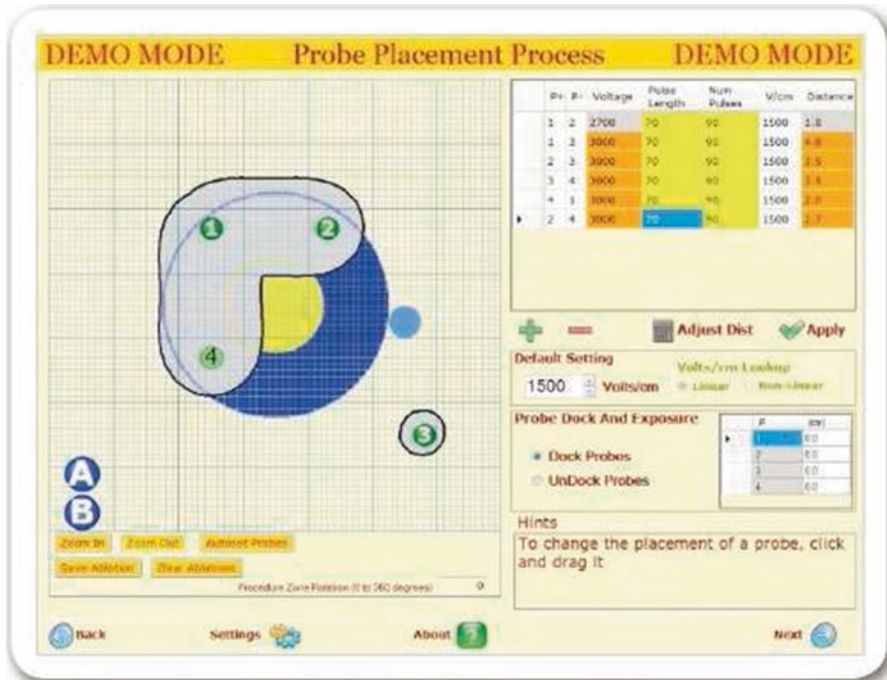
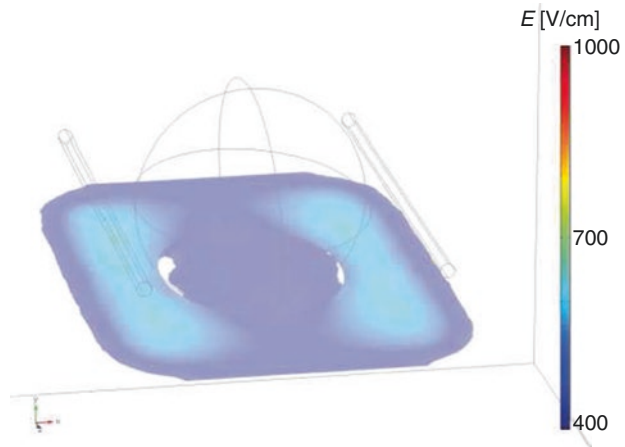


**Fig. 4.3** 2D prediction of irreversible electroporation effect in the NanoKnife pulse generator. The GTV is indicated by a *yellow ellipse*. The dimensions of this ellipse can be set by the user. The CTV (GTV plus tumour margin) is an offset of the CTV and is shown in *blue*. The electrode positions and distances can be set by the user, indicated by the numbers in *circles* on the left-hand side panel. The generator sets the voltage based on the distances between electrodes and a specified voltage-to-distance setting (Image courtesy of AngioDynamics, Inc. and its affiliates)

actual geometry is approximated by a 2D cross-section, the planning is done on this geometry with the assumption that it will also suffice for coverage of the whole CTV. The current software on the AngioDynamics NanoKnife pulse generator bases the delivered voltage on the distance between electrodes, which can be specified on a two-dimensional cross-section (Fig. 4.3).

The predicted lesion is shown in grey on the image. This prediction is based on the results of two numerical studies [16, 18]. The predicted lesion assumes a constant and homogeneous conductivity of the CTV and does not take into account the changes in tissue conductivity due to electroporation neither due to heating. Since the tumour conductivity is generally larger than that of normal tissues [26, 29, 39, 49, 56], this is quite a drastic simplification. Consequently a high voltage-to-distance ratio is recommended for irreversible electroporation treatments. Nearby high-conductivity regions, such as blood vessels, also present a possible pitfall for complete CTV coverage. This was already anticipated by [18] and was also later shown by other groups [9, 22, 43]. Additionally, it is possible that, even for strictly optimized 2D results of total coverage of the tumour, when an actual 3D model is considered,

**Fig. 4.4** Slice plot of the electric field in a prolate spheroid tumour model. The electric field was optimized for field delivery with two electrodes to at least 400 V/cm in a 2D cross-section, but the coverage is less than 90% in the 3D model (Reproduced with permission from Kos and Miklavčič [32])



the coverage could be below optimal [32]. This is illustrated in Fig. 4.4 where coverage was optimized 100% of the area in the 2D cross-section and which resulted in coverage below the desired electric field strength.

Due to the listed limitations of a 2D approach, it is necessary to use very high voltage-to-distance ratios for IRE therapies, to ensure that an adequate electric field is present in the CTV. The drawback of this approach is that the total volume that is achievable by any electrode configuration is limited. The electric current exceeding maximum deliverable by the pulse generator is another possible drawback, but this can be avoided by using a shorter electrode exposure and/or moving electrodes between pulse sets.

The possible solution to the challenges listed above is to use a fully 3D model for treatment planning. This allows for full inclusion of tissue heterogeneity, gives a better and clearer prediction of affected regions in the direction normal to the 2D plane and allows complete inclusion of distinctly three-dimensional structures such as blood vessels and other important critical structures. A 3D approach is, for example, used by the Visifield treatment planning tool that is being developed ([www.visifield.com](http://www.visifield.com), University of Ljubljana). It also allows for automatic segmentation of the liver with liver vessels, prostate and manual segmentation of tumours and other tissues [44, 51]. The patient-specific model is built from the segmented images, and the numerical computation uses dynamic conductivity to solve the electric field to the best of accuracy [33, 34, 70]. The numerical modelling is performed completely automatically and therefore very user-friendly and does not require in-depth engineering knowledge [44]. The output also includes cumulative coverage curves for each tissue used in the case, which is the electroporation equivalent of a dose-volume histogram (Fig. 4.5). The downside of using the 3D approach is a longer time needed to prepare a treatment plan and less flexibility to adapt the plan interactively during the treatment.

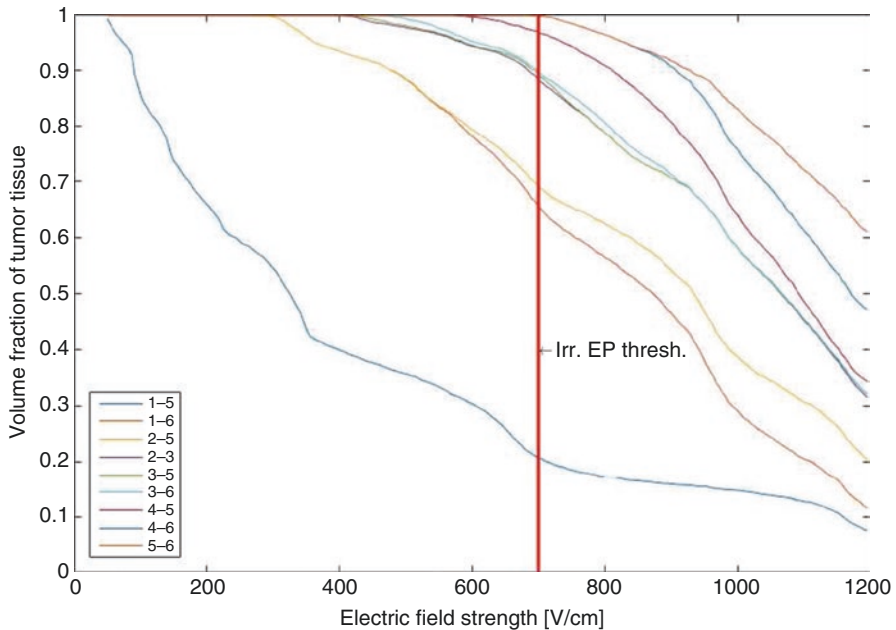


**Fig. 4.5** Cumulative coverage with electric field for the tumour tissue. The *horizontal axis* shows electric field strength, while the *vertical axis* shows the volume fraction of tissue where the electric field threshold is at least as high as indicated on the *horizontal axis*. Electric field threshold for irreversible electroporation taken from Sel et al. [59] (Data adapted for irreversible electroporation from Edhemovic et al. [19])

## 4.5 Statistical Methods for Evaluating Treatment Outcomes

Currently, most research on irreversible electroporation effects is focused on finding threshold electric fields, above which complete tissue ablation is expected [15, 16, 46, 47, 58, 59]. However, this is complicated by the fact that different tissues most probably have different electric field thresholds and the number of pulses also significantly affects these thresholds [57, 62]. To rectify these issues, Golberg and Rubinsky [23] have proposed modifying an existing model of cell death, which was initially developed for modelling microbial deactivation after pulsed electric field treatment [55]. This kind of modelling allows to present the computed results in terms of probability of cell kill, and the modelling of probability of adverse effects is already an active research area in the field of radiotherapy treatment planning [40, 69].

To develop successful models of probability of tissue damage, it is important to validate them at different levels of complexity. The initial study by Golberg and Rubinsky [23] used data from *in vitro* experiments; however the initial data only contained data points for up to 10 pulses. Irreversible electroporation treatments

usually employ a larger number of pulses; therefore it was necessary to validate these models also within a larger parameters space. With a larger number of pulses, the Peleg-Fermi model was still the best for the description of final cell kill probability; however the parameter values were found to be different from those initially published [17]. This approach has also been translated to treating tissues with irreversible electroporation [20, 61].

Another difference between *in vitro* and *in vivo* quantization would be the contribution of the immune system. It has been suggested that there is an immune response present after IRE treatments [2, 8, 41]. Therefore, the modelling of the role of the immune system in the resolution of final IRE effects should be an interesting topic of future research.

---

## 4.6 Fusion with Navigation Systems

In contrast to radiotherapy with external beams, IRE cannot be controlled as well for position, since electrode insertion is still performed by hand. Following a treatment plan for electrode placement can be difficult to achieve in practice even with CT guidance. If strict adherence to the plan cannot be maintained, the final coverage of the CTV with electric field is affected [34]. The solutions to this issue are the use of optical or electromagnetic instrument tracking for guidance of electrode insertion. Optical navigation has already been used for guiding electrodes in electrochemotherapy [24]. With optical navigation, the electrode insertion point and direction can easily be controlled during treatment; however this approach is most suited to treatment in areas where there is limited movement between the planning scan and the actual treatment execution. Electromagnetic navigation has been developed and tested for guidance of radiofrequency ablation electrodes [1, 3, 65], so it should be possible to adapt this approach to use in irreversible electroporation as well.

Another option is guidance using intraoperative cone-beam CT and fusion of the intraoperative images with preoperative planning images. This approach would allow good adherence to a preoperative treatment plan. This kind of approach is already in use for guidance of interventions such as radiofrequency ablation or trans-arterial chemoembolization. Adapting this for irreversible electroporation should be possible with no additional software or equipment.

In the future a possible development would be to use an interoperative CT scan to precisely locate electrodes and adjust the treatment plan relatively quickly of the procedure with known final electrode positions. This could be achieved if reasonably quick recalculations would be available giving the performing physician online information on the projected treatment volumes. Another approach, which however requires more development, would be to use MRI imaging to directly visualize the electric fields during IRE treatment, as has already been demonstrated to be feasible using a research MRI scanner [35, 37, 38, 60].

**Acknowledgments** This work was supported by the Slovenian Research Agency under different grants (Research project Z3-7126, Research programme P2-0249, Research project J3-5505). The work was performed in the scope of LEA EBAM.

## References

1. Abi-Jaoudeh N, Kruecker J, Kadoury S, et al. Multimodality image fusion-guided procedures: technique, accuracy, and applications. *Cardiovasc Intervent Radiol*. 2012;35:986–98. doi:[10.1007/s00270-012-0446-5](https://doi.org/10.1007/s00270-012-0446-5).
2. Al-Sakere B, Bernat C, Andre F, et al. A study of the immunological response to tumor ablation with irreversible electroporation. *Technol Cancer Res Treat*. 2007;6:301–6.
3. Amalou H, Wood BJ. Electromagnetic tracking navigation to guide radiofrequency ablation of a lung tumor. *J Bronchology Interv Pulmonol*. 2012;19:323–7. doi:[10.1097/LBR.0b013e31827157c9](https://doi.org/10.1097/LBR.0b013e31827157c9).
4. Appelbaum L, Ben-David E, Feroja M, et al. Irreversible electroporation ablation: creation of large-volume ablation zones in in vivo porcine liver with four-electrode arrays. *Radiology*. 2013;270:416–24. doi:[10.1148/radiol.13130349](https://doi.org/10.1148/radiol.13130349).
5. Appelbaum L, Ben-David E, Sosna J, et al. US findings after irreversible electroporation ablation: radiologic-pathologic correlation. *Radiology*. 2012;262:117–25. doi:[10.1148/radiol.11110475](https://doi.org/10.1148/radiol.11110475).
6. Aström M, Zrinzo LU, Tisch S, et al. Method for patient-specific finite element modeling and simulation of deep brain stimulation. *Med Biol Eng Comput*. 2009;47:21–8. doi:[10.1007/s11517-008-0411-2](https://doi.org/10.1007/s11517-008-0411-2).
7. Atun R, Jaffray DA, Barton MB, et al. Expanding global access to radiotherapy. *Lancet Oncol*. 2015;16:1153–86. doi:[10.1016/S1470-2045\(15\)00222-3](https://doi.org/10.1016/S1470-2045(15)00222-3).
8. Bastianpillai C, Petrides N, Shah T, et al. Harnessing the immunomodulatory effect of thermal and non-thermal ablative therapies for cancer treatment. *Tumour Biol J Int Soc Onco Dev Biol Med*. 2015;36:9137–46. doi:[10.1007/s13277-015-4126-3](https://doi.org/10.1007/s13277-015-4126-3).
9. Ben-David E, Ahmed M, Feroja M, et al. Irreversible electroporation: treatment effect is susceptible to local environment and tissue properties. *Radiology*. 2013;269:738–47. doi:[10.1148/radiol.13122590](https://doi.org/10.1148/radiol.13122590).
10. Bevilacqua V, Mastronardi G, Piscopo G. Evolutionary approach to inverse planning in coplanar radiotherapy. *Image Vis Comput*. 2007;25:196–203.
11. Chao J, Shi F, Xiang D, et al. 3D fast automatic segmentation of kidney based on modified AAM and random forest. *IEEE Trans Med Imaging*. 2016;35:1395–407. doi:[10.1109/TMI.2015.2512606](https://doi.org/10.1109/TMI.2015.2512606).
12. Cheng R, Turkbey B, Gandler W, et al. Atlas based AAM and SVM model for fully automatic MRI prostate segmentation. *Conf Proc Annu Int Conf IEEE Eng Med Biol Soc IEEE Eng Med Biol Soc Annu Conf*. 2014;2014:2881–5. doi:[10.1109/EMBC.2014.6944225](https://doi.org/10.1109/EMBC.2014.6944225).
13. Chung DJ, Sung K, Osuagwu FC, et al. Contrast enhancement patterns after irreversible electroporation: experimental study of CT perfusion correlated to histopathology in normal porcine liver. *J Vasc Interv Radiol JVIR*. 2016;27:104–11. doi:[10.1016/j.jvir.2015.09.005](https://doi.org/10.1016/j.jvir.2015.09.005).
14. Corovic S, Lackovic I, Sustaric P, et al. Modeling of electric field distribution in tissues during electroporation. *Biomed Eng Online*. 2013;12:16. doi:[10.1186/1475-925X-12-16](https://doi.org/10.1186/1475-925X-12-16).
15. Corović S, Zupanic A, Kranjc S, et al. The influence of skeletal muscle anisotropy on electroporation: in vivo study and numerical modeling. *Med Biol Eng Comput*. 2010;48:637–48. doi:[10.1007/s11517-010-0614-1](https://doi.org/10.1007/s11517-010-0614-1).
16. Davalos R, Mir L, Rubinsky B. Tissue ablation with irreversible electroporation. *Ann Biomed Eng*. 2005;33:223–31. doi:[10.1007/s10439-005-8981-8](https://doi.org/10.1007/s10439-005-8981-8).
17. Dermal J, Miklavčič D. Mathematical models describing Chinese hamster ovary cell death due to electroporation in vitro. *J Membr Biol*. 2015;248:865–81. doi:[10.1007/s00232-015-9825-6](https://doi.org/10.1007/s00232-015-9825-6).
18. Edd JF, Davalos RV. Mathematical modeling of irreversible electroporation for treatment planning. *Technol Cancer Res Treat*. 2007;6:275–86.
19. Edhemovic I, Gadzije EM, Breclj E, et al. Electrochemotherapy: a new technological approach in treatment of metastases in the liver. *Technol Cancer Res Treat*. 2011;10:475–85.
20. Garcia PA, Davalos RV, Miklavcic D. A numerical investigation of the electric and thermal cell kill distributions in electroporation-based therapies in tissue. *PLoS One*. 2014;9:e103083. doi:[10.1371/journal.pone.0103083](https://doi.org/10.1371/journal.pone.0103083).

21. Garcia PA, Rossmeisl JH Jr, Neal RE 2nd, et al. A parametric study delineating irreversible electroporation from thermal damage based on a minimally invasive intracranial procedure. *Biomed Eng Online*. 2011;10:34. doi:[10.1186/1475-925X-10-34](https://doi.org/10.1186/1475-925X-10-34).
22. Golberg A, Bruinsma BG, Uygun BE, Yarmush ML. Tissue heterogeneity in structure and conductivity contribute to cell survival during irreversible electroporation ablation by “electric field sinks”. *Sci Rep*. 2015;5:8485. doi:[10.1038/srep08485](https://doi.org/10.1038/srep08485).
23. Golberg A, Rubinsky B. A statistical model for multidimensional irreversible electroporation cell death in tissue. *Biomed Eng Online*. 2010;9:13. doi:[10.1186/1475-925X-9-13](https://doi.org/10.1186/1475-925X-9-13).
24. Grosej A, Kos B, Cemazar M, et al. Coupling treatment planning with navigation system: a new technological approach in treatment of head and neck tumors by electrochemotherapy. *Biomed Eng Online*. 2015;14(Suppl 3):S2. doi:[10.1186/1475-925X-14-S3-S2](https://doi.org/10.1186/1475-925X-14-S3-S2).
25. Guo Y, Gao Y, Shen D. Deformable MR prostate segmentation via deep feature learning and sparse patch matching. *IEEE Trans Med Imaging*. 2016;35:1077–89. doi:[10.1109/TMI.2015.2508280](https://doi.org/10.1109/TMI.2015.2508280).
26. Haemmerich D, Schutt D, Wright A, et al. Electrical conductivity measurement of excised human metastatic liver tumours before and after thermal ablation. *Physiol Meas*. 2009;30:459–66. doi:[10.1088/0967-3334/30/5/003](https://doi.org/10.1088/0967-3334/30/5/003).
27. Haemmerich D, Wood BJ. Hepatic radiofrequency ablation at low frequencies preferentially heats tumour tissue. *Int J Hyperth Off J Eur Soc Hyperthermic Oncol N Am Hyperth Group*. 2006;22:563–74. doi:[10.1080/02656730601024727](https://doi.org/10.1080/02656730601024727).
28. Hall SK, Ooi EH, Payne SJ. A mathematical framework for minimally invasive tumor ablation therapies. *Crit Rev Biomed Eng*. 2014;42:383–417.
29. Halter RJ, Zhou T, Meaney PM, et al. The correlation of in vivo and ex vivo tissue dielectric properties to validate electromagnetic breast imaging: initial clinical experience. *Physiol Meas*. 2009;30:S121–36. doi:[10.1088/0967-3334/30/6/S08](https://doi.org/10.1088/0967-3334/30/6/S08).
30. Jarm T, Cemazar M, Miklavcic D, Sersa G. Antivascular effects of electrochemotherapy: implications in treatment of bleeding metastases. *Expert Rev Anticancer Ther*. 2010;10:729–46. doi:[10.1586/era.10.43](https://doi.org/10.1586/era.10.43).
31. Kierkels RGJ, Visser R, Bijl HP, et al. Multicriteria optimization enables less experienced planners to efficiently produce high quality treatment plans in head and neck cancer radiotherapy. *Radiat Oncol Lond Engl*. 2015;10:87. doi:[10.1186/s13014-015-0385-9](https://doi.org/10.1186/s13014-015-0385-9).
32. Kos B, Miklavčič D. 2-d vs 3-d: the importance of modelling in three dimensions for planning electroporation-based treatments. In: Lacković I, Vasic D, editors. 6th European Conference of the International Federation for Medical and Biological Engineering. Dubrovnik: Springer International Publishing; 2015. p. 829–32.
33. Kos B, Voigt P, Miklavcic D, Moche M. Careful treatment planning enables safe ablation of liver tumors adjacent to major blood vessels by percutaneous irreversible electroporation (IRE). *Radiol Oncol*. 2015;49:234–41. doi:[10.1515/raon-2015-0031](https://doi.org/10.1515/raon-2015-0031).
34. Kos B, Zupanic A, Kotnik T, et al. Robustness of treatment planning for electrochemotherapy of deep-seated tumors. *J Membr Biol*. 2010;236:147–53. doi:[10.1007/s00232-010-9274-1](https://doi.org/10.1007/s00232-010-9274-1).
35. Kranjc M, Bajd F, Sersa I, et al. Ex vivo and in silico feasibility study of monitoring electric field distribution in tissue during electroporation based treatments. *PLoS One*. 2012;7:e45737. doi:[10.1371/journal.pone.0045737](https://doi.org/10.1371/journal.pone.0045737).
36. Kranjc M, Bajd F, Serša I, Miklavčič D. Magnetic resonance electrical impedance tomography for measuring electrical conductivity during electroporation. *Physiol Meas*. 2014;35:985–96. doi:[10.1088/0967-3334/35/6/985](https://doi.org/10.1088/0967-3334/35/6/985).
37. Kranjc M, Bajd F, Sersa I, Miklavcic D. Magnetic resonance electrical impedance tomography for monitoring electric field distribution during tissue electroporation. *IEEE Trans Med Imaging*. 2011;30:1771–8. doi:[10.1109/TMI.2011.2147328](https://doi.org/10.1109/TMI.2011.2147328).
38. Kranjc M, Markelc B, Bajd F, et al. In situ monitoring of electric field distribution in mouse tumor during electroporation. *Radiology*. 2015;274:115–23. doi:[10.1148/radiol.14140311](https://doi.org/10.1148/radiol.14140311).
39. Lazebnik M, Popovic D, McCartney L, et al. A large-scale study of the ultrawideband microwave dielectric properties of normal, benign and malignant breast tissues obtained from cancer surgeries. *Phys Med Biol*. 2007;52:6093–115. doi:[10.1088/0031-9155/52/20/002](https://doi.org/10.1088/0031-9155/52/20/002).



40. Lee T-F, Chao P-J, Chang L, et al. Developing multivariable normal tissue complication probability model to predict the incidence of symptomatic radiation pneumonitis among breast cancer patients. *PLoS One*. 2015;10:e0131736. doi:[10.1371/journal.pone.0131736](https://doi.org/10.1371/journal.pone.0131736).
41. Li X, Xu K, Li W, et al. Immunologic response to tumor ablation with irreversible electroporation. *PLoS One*. 2012;7:e48749. doi:[10.1371/journal.pone.0048749](https://doi.org/10.1371/journal.pone.0048749).
42. López-Mir F, Naranjo V, Angulo J, et al. Liver segmentation in MRI: a fully automatic method based on stochastic partitions. *Comput Methods Prog Biomed*. 2014;114:11–28. doi:[10.1016/j.cmpb.2013.12.022](https://doi.org/10.1016/j.cmpb.2013.12.022).
43. Marčan M, Kos B, Miklavčič D. Effect of blood vessel segmentation on the outcome of electroporation-based treatments of liver tumors. *PLoS One*. 2015;10:e0125591. doi:[10.1371/journal.pone.0125591](https://doi.org/10.1371/journal.pone.0125591).
44. Marčan M, Pavliha D, Kos B, et al. Web-based tool for visualization of electric field distribution in deep-seated body structures and planning of electroporation-based treatments. *Biomed Eng Online*. 2015;14(Suppl 3):S4. doi:[10.1186/1475-925X-14-S3-S4](https://doi.org/10.1186/1475-925X-14-S3-S4).
45. Marčan M, Pavliha D, Music MM, et al. Segmentation of hepatic vessels from MRI images for planning of electroporation-based treatments in the liver. *Radiol Oncol*. 2014;48:267–81. doi:[10.2478/raon-2014-0022](https://doi.org/10.2478/raon-2014-0022).
46. Neal RE 2nd, Millar JL, Kavnoudias H, et al. In vivo characterization and numerical simulation of prostate properties for non-thermal irreversible electroporation ablation. *Prostate*. 2014;74(5):458–68. doi:[10.1002/pros.22760](https://doi.org/10.1002/pros.22760).
47. Neal RE, Garcia PA, Kavnoudias H, et al. In vivo irreversible electroporation kidney ablation: experimentally correlated numerical models. *IEEE Trans Biomed Eng*. 2015;62:561–9. doi:[10.1109/TBME.2014.2360374](https://doi.org/10.1109/TBME.2014.2360374).
48. Nouranian S, Mahdavi SS, Spadinger I, et al. A multi-atlas-based segmentation framework for prostate brachytherapy. *IEEE Trans Med Imaging*. 2015;34:950–61. doi:[10.1109/TMI.2014.2371823](https://doi.org/10.1109/TMI.2014.2371823).
49. O'Rourke AP, Lazebnik M, Bertram JM, et al. Dielectric properties of human normal, malignant and cirrhotic liver tissue: in vivo and ex vivo measurements from 0.5 to 20 GHz using a precision open-ended coaxial probe. *Phys Med Biol*. 2007;52:4707–19. doi:[10.1088/0031-9155/52/15/022](https://doi.org/10.1088/0031-9155/52/15/022).
50. Pakhomova ON, Gregory BW, Khorokhorina VA, et al. Electroporation-induced electrosensitization. *PLoS One*. 2011;6:e17100. doi:[10.1371/journal.pone.0017100](https://doi.org/10.1371/journal.pone.0017100).
51. Pavliha D, Kos B, Marčan M, et al. Planning of electroporation-based treatments using web-based treatment-planning software. *J Membr Biol*. 2013;246:833–42. doi:[10.1007/s00232-013-9567-2](https://doi.org/10.1007/s00232-013-9567-2).
52. Pavliha D, Kos B, Županič A, et al. Patient-specific treatment planning of electrochemotherapy: procedure design and possible pitfalls. *Bioelectrochemistry*. 2012;87:265–73. doi:[10.1016/j.bioelechem.2012.01.007](https://doi.org/10.1016/j.bioelechem.2012.01.007).
53. Pavliha D, Mušič MM, Serša G, Miklavčič D. Electroporation-based treatment planning for deep-seated tumors based on automatic liver segmentation of MRI images. *PLoS One*. 2013;8:e69068. doi:[10.1371/journal.pone.0069068](https://doi.org/10.1371/journal.pone.0069068).
54. Pavšelj N, Miklavčič D. Finite element modeling of in vivo electroporation. In: Rubinsky B, editor. *Irreversible electroporation*. Berlin: Springer; 2010. p. 183–202.
55. Peleg M. A model of microbial survival after exposure to pulsed electric fields. *J Sci Food Agric*. 1995;67:93–9. doi:[10.1002/jsfa.2740670115](https://doi.org/10.1002/jsfa.2740670115).
56. Peyman A, Kos B, Djokić M, et al. Variation in dielectric properties due to pathological changes in human liver. *Bioelectromagnetics*. 2015;36:603–12. doi:[10.1002/bem.21939](https://doi.org/10.1002/bem.21939).
57. Pucihar G, Krmelj J, Reberšek M, et al. Equivalent pulse parameters for electroporation. *IEEE Trans Biomed Eng*. 2011;58:3279–88. doi:[10.1109/TBME.2011.2167232](https://doi.org/10.1109/TBME.2011.2167232).
58. Qin Z, Jiang J, Long G, et al. Irreversible electroporation: an in vivo study with dorsal skin fold chamber. *Ann Biomed Eng*. 2013;41:619–29. doi:[10.1007/s10439-012-0686-1](https://doi.org/10.1007/s10439-012-0686-1).
59. Sel D, Cukjati D, Batiuskaitė D, et al. Sequential finite element model of tissue electroporation. *IEEE Trans Biomed Eng*. 2005;52:816–27. doi:[10.1109/TBME.2005.845212](https://doi.org/10.1109/TBME.2005.845212).

60. Serša I, Kranjc M, Miklavčič D. Current density imaging sequence for monitoring current distribution during delivery of electric pulses in irreversible electroporation. *Biomed Eng Online*. 2015;14(Suppl 3):S6. doi:[10.1186/1475-925X-14-S3-S6](https://doi.org/10.1186/1475-925X-14-S3-S6).
61. Sharabi S, Kos B, Last D, et al. A statistical model describing combined irreversible electroporation and electroporation-induced blood-brain barrier disruption. *Radiol Oncol*. 2016;50:28–38. doi:[10.1515/raon-2016-0009](https://doi.org/10.1515/raon-2016-0009).
62. Sharabi S, Last D, Guez D, et al. Dynamic effects of point source electroporation on the rat brain tissue. *Bioelectrochemistry*. 2014;99:30–9. doi:[10.1016/j.bioelechem.2014.06.001](https://doi.org/10.1016/j.bioelechem.2014.06.001).
63. Song T, Staub D, Chen M, et al. Patient-specific dosimetric endpoints based treatment plan quality control in radiotherapy. *Phys Med Biol*. 2015;60:8213–27. doi:[10.1088/0031-9155/60/21/8213](https://doi.org/10.1088/0031-9155/60/21/8213).
64. Srimathveeravalli G, Cornelis F, Mashni J, et al. Comparison of ablation defect on MR imaging with computer simulation estimated treatment zone following irreversible electroporation of patient prostate. *SpringerPlus*. 2016;5:219. doi:[10.1186/s40064-016-1879-0](https://doi.org/10.1186/s40064-016-1879-0).
65. Venkatesan AM, Kadoury S, Abi-Jaoudeh N, et al. Real-time FDG PET guidance during biopsies and radiofrequency ablation using multimodality fusion with electromagnetic navigation. *Radiology*. 2011;260:848–56. doi:[10.1148/radiol.11101985](https://doi.org/10.1148/radiol.11101985).
66. Wimmer T, Srimathveeravalli G, Gutta N, et al. Planning irreversible electroporation in the porcine kidney: are numerical simulations reliable for predicting empiric ablation outcomes? *Cardiovasc Intervent Radiol*. 2015;38:182–90. doi:[10.1007/s00270-014-0905-2](https://doi.org/10.1007/s00270-014-0905-2).
67. Yang G, Gu J, Chen Y, et al. Automatic kidney segmentation in CT images based on multi-atlas image registration. *Conf Proc Annu Int Conf IEEE Eng Med Biol Soc IEEE Eng Med Biol Soc Annu Conf*. 2014;2014:5538–41. doi:[10.1109/EMBC.2014.6944881](https://doi.org/10.1109/EMBC.2014.6944881).
68. Zarepisheh M, Long T, Li N, et al. A DVH-guided IMRT optimization algorithm for automatic treatment planning and adaptive radiotherapy replanning. *Med Phys*. 2014;41:61711. doi:[10.1118/1.4875700](https://doi.org/10.1118/1.4875700).
69. Zehentmayr F, Söhn M, Exeli A-K, et al. Normal tissue complication models for clinically relevant acute esophagitis ( $\geq$  grade 2) in patients treated with dose differentiated accelerated radiotherapy (DART-bid). *Radiat Oncol Lond Engl*. 2015;10:121. doi:[10.1186/s13014-015-0429-1](https://doi.org/10.1186/s13014-015-0429-1).
70. Zupanic A, Kos B, Miklavcic D. Treatment planning of electroporation-based medical interventions: electrochemotherapy, gene electrotransfer and irreversible electroporation. *Phys Med Biol*. 2012;57:5425–40. doi:[10.1088/0031-9155/57/17/5425](https://doi.org/10.1088/0031-9155/57/17/5425).
71. Županič A, Miklavčič D. Optimization and numerical modeling in irreversible electroporation treatment planning. In: Rubinsky B, editor. *Irreversible electroporation*. Berlin: Springer; 2010. p. 203–22.

---

# The Effect of Irreversible Electroporation on Blood Vessels, Bile Ducts, Urinary Tract, Intestines, and Nerves

# 5

Jantien A. Vogel, Laurien G.P.H. Vroomen,  
and Govindarajan Srimathveeravalli

---

## 5.1 Introduction

Surgical resection is the definitive treatment option for patients with primary or metastatic cancers, resulting in the best possible patient outcomes when resection is achieved with negative margins. However, involvement of vital structures such as blood vessels and genitourinary or gastrointestinal tract often poses a contraindication to safe and successful surgical resection.

In light of the limitations of surgical resection for tumors involving the vital structures, a number of locoregional therapies have been developed in the last 20 years. Focal ablation, which has gained increased attention in the recent years, is a local technique that uses energy to destroy tumor tissue. Of focal ablation techniques, thermal ablation using radiofrequency ablation (RFA) or microwave ablation (MWA) is most frequently used. The intent of thermal ablation is to destroy malignant cells; however, extracellular proteins will also be heated and could be denatured, leading to permanent damage to the tissue infrastructure including vital structures [1]. Consequently, thermal ablation is contraindicated adjacent to the

---

J.A. Vogel and L.G.P.H. Vroomen contributed equally

J.A. Vogel (✉)  
Department of Surgery, Academic Medical Center,  
Meibergdreef 9, 1105, AZ, Amsterdam, The Netherlands  
e-mail: [j.a.vogel@amc.uva.nl](mailto:j.a.vogel@amc.uva.nl)

L.G.P.H. Vroomen  
Department of Radiology and Nuclear Medicine, VU University Medical Center,  
de Boelelaan 1117, 1081, HV, Amsterdam, The Netherlands

G. Srimathveeravalli  
Department of Radiology, Interventional Radiology Service, Memorial Sloan-Kettering  
Cancer Center, 1275 York Avenue, New York, NY 10065, USA

Department of Radiology, Weil Cornell Medical College, New York, NY, USA

biliary tree, major blood vessels, intestines, nerves, and the urinary tract [2–4]. Moreover, lesions adjacent to major blood vessels pose a challenge to thermal techniques due to the “heat sink” effect: the cooling effect of blood flow in vessels greater than 3 mm, leading to incomplete ablation [5, 6].

Irreversible electroporation (IRE) potentially circumvents the abovementioned limitations. By applying the electric field *in situ*, irreversible cell damage could be achieved, leading to cell death without substantially raising the temperature of the tissue [7]. Considering that the primary working mechanism of IRE is nonthermal, the extracellular matrix should theoretically remain intact while all cells are destroyed within the ablation zone [8]. As a result, the structural integrity of inlaying and adjacent vital structures including bile ducts, blood vessels, urinary tract, prostate, intestines, and nerves should also be retained due to the preservation of the collagen framework followed by regeneration [9]. Several animal model and clinical studies investigating this hypothesis are presented below.

---

## 5.2 Blood Vessels

### 5.2.1 Preclinical Studies

The impact of large blood vessels adjacent to the tumor on the efficacy of IRE formed the topic of investigation of four preclinical studies [10–13]. In a porcine model of liver cancer, Charpentier et al. [12] reported that IRE achieved hepatocyte necrosis extending to the margin of the large hepatic veins, without evidence of heat sink. In another porcine model of liver cancer, Lee et al. [13] reported that IRE achieved uniform ablation not sparing perivascular tissue in tumor tissue contiguous to hepatic veins, as seen on computer tomography (CT) evaluation, gross pathology, as well as histopathology evaluation. When triphenyltetrazolium chloride vitality staining was used by Au et al. [10] 10 min after IRE, the demarcated ablation zone was seen to be unaffected by large blood vessels or bile ducts, and there was little change thereafter. Lastly, Ben-David et al. [11] reported no influence on the shape or size of the ablation zone by the presence of blood vessels. Despite generally positive findings, the effect of large blood vessels on the efficacy of IRE remains inconclusive. Although Charpentier et al. [12] found that IRE did not cause a heat sink, they also reported a more irregular ablation zone in the liver hilum than in intrahepatic zones, potentially because the liver hilum is located in proximity of large blood vessels. When an *in vivo* rat model was used, Golberg et al. [14] reported that IRE in the proximity of larger vessels and clustered vessel structures had less effect than IRE in the tissue parenchyma or in the proximity of smaller vessels, suggesting either a heat sink or, as they stated, an “electric field sink.”

Other preclinical studies studied the effect of IRE on blood vessel patency, focusing on tissue with blood vessels traversing the ablation zone [11, 13, 15–21]. Nine studies ablating tissue with traversing blood vessels demonstrated the preservation of large vessels [16–18], intact architecture [11, 19], and color flow angiography on 2D ultrasound imaging [18] without signs of thrombosis [18, 20]. However, signs of acute vasculitis such as leukocyte, lymphocyte, and neutrophil infiltration in the

vessel wall, endothelial damage [13, 16, 17, 19, 21], transient loss of smooth muscle cells, and occasional interruption of blood flow and occlusion by erythrocytes and fibrin deposition [19] were also reported, mainly in the smaller vessels. Although the primary aim of the study of Lee et al. [13] mentioned above was to study the effect of the presence of blood vessels on IRE rather than IRE on blood vessel patency, they also reported a transient narrowing of large vessels in 9 out of 23 cases, which resolved after 4 weeks.

Studies investigating IRE-related injury to large blood vessels in the treatment zone are limited. In two studies where IRE was directly applied to vessels, the carotid artery was examined [22, 23]. At 24 h after ablation, no difference was seen between IRE-treated vessels and control vessels in morphology or the number of cells in the tunica media. After 7–28 days, a lower number (75%) of vascular smooth muscle cells were present in the tunica media of IRE-treated vessels compared to controls. However, no signs of thrombosis, aneurysm formation, or vascular rupture were reported, and there was no change in vessel diameter [22]. After 24 h, endothelial damage seemed to have recovered [23].

### 5.2.2 Clinical Studies

Clinical studies have focused on evaluating the effect of IRE on vessel patency in close proximity to the ablation zone.

In a study by Narayanan et al. [24], 101 patients with 129 lesions of various malignancies were included (liver [100], pancreas [18], kidney [3], pelvis [1], aortocaval lymph nodes [2], adrenal [2], lung [1], retroperitoneal [1], and surgical bed of a prior Whipple procedure [1]). Observed abnormal IRE-associated vascular changes on imaging were (i) thrombosis of the left portal vein at 1-month follow-up ( $n = 1$ ), (ii) non-occlusive thrombus in the main portal vein at 24-h follow-up ( $n = 1$ ), and (iii) mild vessel narrowing (<20% of original caliber) involving the superior branch of right portal vein, main right portal vein, and right hepatic vein, respectively, at 24-h follow-up ( $n = 3$ ). All these were noted in the venous system, with the highest prevalence of changes in the portal vein. This may be related to flow dynamics within the portal venous system making it more susceptible to vascular damage [24]. The distance between the treatment area and vessel wall did not appear to be a significant factor in postprocedural vessel patency [24]. Long-term follow-up revealed no late vascular deviations in the majority of vessels [24].

Vessel spasm was noted by Scheffer et al. [25], who presented a case report of a 67-year-old patient with locally advanced pancreatic carcinoma (LAPC) (stage III) who was percutaneously treated with IRE. On contrast-enhanced CT, a spastic but patent hepatic and splenic artery was visible immediately following the removal of the electrodes.

Recently, Martin et al. [26] published findings from a study comparing outcomes between open IRE alone ( $n = 150$ ) and pancreatic resection plus IRE ( $n = 50$ ) in 200 patients with LAPC (stage III). Noted vascular complications were a deep venous thrombosis ( $n = 1$ ), pseudoaneurysm ( $n = 1$ ), hepatic arterial thrombosis ( $n = 1$ ), and a non-occlusive superior mesenteric vein/portal vein thrombosis (SMV) ( $n = 1$ ) (all

Clavien-Dindo grade II). A patient in the in situ group with prior complete portal vein thrombosis/SMV occlusion died within 90 days after the procedure because of liver failure. Similarly, Philips et al. [26] reported two cases of bleeding and one case of progressive portal vein thrombosis after a total of 167 IRE procedures in various unresectable tumors (with a majority being liver [39.5%] and pancreatic [35.5%] lesions). Progression of vessel thrombosis may be stimulated by IRE, most likely through edema after the ablation procedure [27].

It remains a matter of debate whether or not IRE is a safe procedure in the vicinity of blood vessels. The most commonly reported vessel-related complication post-IRE is thrombosis, with the portal vein being the most affected site. IRE may also cause hemorrhage. Administration of anticoagulants of which the effect could be easily reversed (e.g., heparin) may be considered postprocedurally in order to minimize the risk of thrombus formation. Nonetheless, data on this are lacking. In addition, needle placement in direct contact with blood vessels may result in thrombosis or hemorrhage as a result of a thermal effect since heat development during IRE seems unavoidable [28–30]. Consequently, direct contact (>2 mm) between the active electrode tip and blood vessels should be avoided [31].

---

## 5.3 Biliary System

### 5.3.1 Preclinical Studies

In preclinical studies, preservation of bile ducts post-IRE is noted without any sign of bile leakage [15, 16, 18]; however, there are signs of acute cholecystitis [17] and occasional apoptotic cells [1].

### 5.3.2 Clinical Studies

To assess biliary complications after percutaneous IRE of 22 hepatic tumors (in 11 patients) located within 1 cm from major bile ducts, Silk et al. [28] retrospectively examined all pre- and postprocedural CT images for signs of bile duct dilatation, obstruction, or leakage (Fig. 5.1). In addition, serum bilirubin and alkaline phosphatase values were evaluated to identify possible biliary injury. In their review, an increase of preexisting or new-onset biliary duct dilatation was detected in three patients. However, the reported dilatation was secondary to tumor progression in two out of three cases. Only the subsegmental bile duct prominence, which developed in the third patient who had no laboratory signs of bile duct injury, was considered directly related to the IRE procedure. This adverse event might be the result of a thermal effect since retrospective assessment of the CT images revealed that one needle was placed in direct contact with the bile duct [28].

Similarly, Kingham et al. [32] evaluated the safety of IRE for patients with malignant liver tumors that were located near (<1 cm) major hepatic veins or

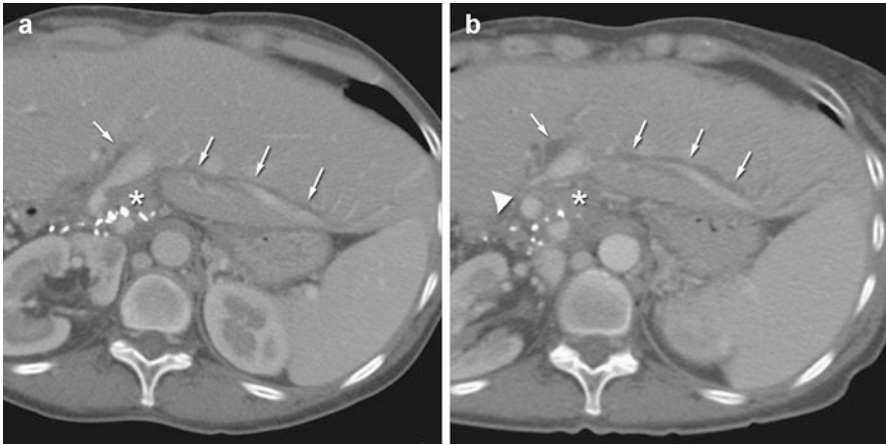


**Fig. 5.1** (a–d) Representative tumor locations (*arrowheads*), bile ducts (*arrows*), and immediate follow-up imaging after IRE treatment showing ablation cavity (*asterisks*). Tumors included in the study were located  $\leq 1$  cm from the common hepatic duct (a) or a primary branch (b) [28]

portal pedicles. Twenty-eight patients with 65 tumors were included, of whom 22 patients [79%] were treated with an open approach and 6 [21%] were treated percutaneously. Post-IRE, one grade I portal vein thrombosis occurred (1.5%), with no biliary dilation. Additionally, Hosein and colleagues [33] examined all available follow-up CT scans and detected no vessel stenosis, thrombosis, or shunting within or adjacent to the treatment zones. Biliary strictures were also not observed on postprocedural imaging.

A prospective analysis was performed by Cannon et al. [34] who analyzed the safety of IRE for hepatic tumors in close proximity to major vascular or biliary structures or to adjacent organs. Forty-four patients (20 colorectal liver metastases, 14 hepatocellular carcinoma, and 10 other metastases) underwent 48 IRE procedures. Biliary complications were stent occlusion and cholangitis due to biliary stent occlusion. During follow-up, neither biliary stricture nor portal vein thrombosis was reported.

Lastly, Dollinger et al. [35] evaluated biliary complications after IRE of hepatic tumors in 24 patients (53 tumors). Bile ducts were located within a radius of 1.0 cm of the ablation zone. Subacute follow-up MR images (i.e., 1–3 days post-IRE) showed 15 bile duct injuries: narrowing ( $n = 8$ ) and dilatation ( $n = 7$ ). Further, three patients showed transient abnormalities of laboratory values (bilirubin, 1.6–5.2 mg/dL) at subacute follow-up.

The abovementioned clinical data corroborate the referenced animal data, advocating the relative safety of hepatic IRE in proximity of blood vessels and bile ducts. However, bile ducts adjacent to the target area may be negatively affected, leading to cholangitis and biliary obstruction. Therefore, prophylactic biliary protection is recommended prior to the procedure since placement of a plastic biliary endoprosthesis or percutaneous transhepatic cholangiography drain

may be more difficult post-IRE due to extensive swelling of the ampullary area (unpublished data) [36].

---

## 5.4 Pancreas

### 5.4.1 Preclinical Studies

Preclinical studies in swine have demonstrated the feasibility and relative safety of IRE in pancreatic tissue [37–40]. In all studies, IRE ablations in pancreas were performed in healthy swine. No immediate complications were seen [37–40]. In the days following IRE, a transient increase in white blood cell count, normalizing on the second [39] or third [37] day; a transient increase in amylase and lipase, normalizing on the second [39], third [37], or 14th day [40]; lactate dehydrogenase, normalizing on the 14th day [40]; and aspartate transaminase, normalizing on the 14th day [40] or remaining elevated throughout the 14 days of evaluation [37] was seen. Blood urea nitrogen and creatinine remained within normal limits for all animals [37]. Some animals developed ascites, with a similar increase in amylase and lipase on day 1 which decreased after; however, no clinical signs of pancreatitis were observed and this finding was confirmed on pathologic evaluation [39]. In the study by Bower et al., all animals experienced a transient hypoglycemia 1–3 h postoperatively which began to resolve after 5 h and was normalized on the first postoperative day [37].

### 5.4.2 Clinical Studies

In the clinical setting, Martin et al. [41] performed a prospective multi-institutional pilot evaluation of 27 patients undergoing open IRE for LAPC (stage III). IRE related complications ( $n = 4$ ) were progression of a portal vein thrombus, a new-onset complete portal vein thrombosis, a duodenotomy leak after removal of a metal stent at the time of operation, and a duodenal leak after transduodenal needle placement.

In addition, Paiella et al. [42] reported two IRE-related adverse events in one patient after pancreatic IRE: an abscess within the pancreas accompanied by a pancreaticoduodenal fistula. Invasive treatment was not necessary since the patient responded well to broad-spectrum antibiotic therapy.

Trueba-Arguiñarena et al. [30] treated a 66-year-old patient with IRE for the management of a malignant pancreatic adenocarcinoma that involved the celiac artery. Pre-IRE, contrast-enhanced CT revealed thrombosis of the splenic and mesenteric vein with abundant collateral circulation from the intestinal venous return and a patent portal vein. Five days postprocedural, fluid in the right abdomen and edema in the wall of ascending colon was detected on imaging, which was probably due to collateral vein damage by needle placement compromising the venous



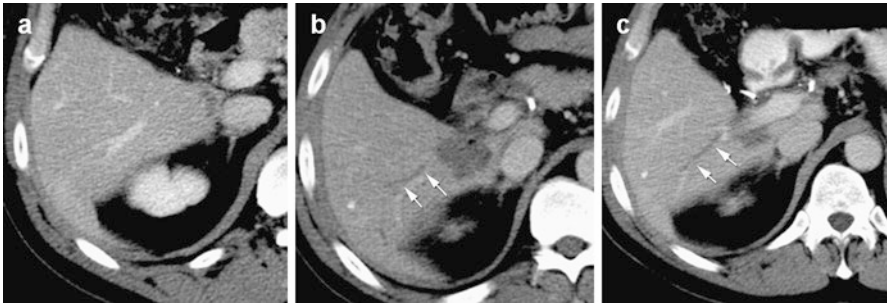


**Fig. 5.2** A 52-year-old man with colorectal metastases underwent IRE treatment for two tumor locations. (a) Initial contrast-enhanced CT scan (portal venous phase) performed before treatment shows baseline duct width. (b) Follow-up CT scan performed immediately after the procedure shows ablation cavity and a prominent segmental duct (*arrowheads*). (c) Follow-up CT scan performed 1 month later still shows bile duct dilatation (*arrowheads*) [28]

drainage. This complication was successfully treated with diuretics and resolved during follow-up. Nine days post-IRE, the patient presented with an episode of hematemesis that required blood transfusion and was related to six transgastrially inserted electrodes.

Furthermore, Scheffer et al. prospectively investigated the safety of percutaneous IRE for LAPC (stage III) in 25 patients [36]. Twenty-three adverse events occurred in 10 out of 25 patients, with a median grade of Common Terminology Criteria for Adverse Events (CTCAE) grade I (range, I–III). Within 90 days post-IRE, three out of ten patients with no previous biliary protection developed new-onset biliary obstruction (grade III) requiring additional treatment. The placement of the biliary endoprosthesis or percutaneous transhepatic cholangiography drainage was challenging in two out of three patients due to extensive swelling of the ampullary area (Fig. 5.2). Moreover, one patient developed stenosis of the superior mesenteric artery 6 weeks post-IRE. Lastly, two grade IV complications occurred, one edematous pancreatitis with bile leakage and hemodynamic instability and one life-threatening hemorrhage caused by a duodenal ulcer.

In a study by Kluger et al. [43], prospective data of consecutive patients who received IRE for T4 pancreatic tumors were analyzed to determine treatment safety, using the Clavien-Dindo classification. A total of 50 patients underwent 53 IRE procedures for primary treatment ( $n = 29$ ) or margin extension ( $n = 24$ ). Post-procedural mortality (i.e., within 90 days post-IRE) occurred in six patients, five of whom were in the primary treatment control group. Among the direct IRE-related complications, the authors reported upper gastrointestinal hemorrhage (grade III;  $n = 3$ ), duodenal ulceration/perforation (grade III;  $n = 1$ ), biliary obstruction (grade III;  $n = 1$ ), duodenal and bile duct necrosis (grade V;  $n = 1$ ), duodenal-cutaneous fistula (grade V;  $n = 1$ ), portal vein thrombosis (grade V;  $n = 1$ ), and bleeding of the gastroduodenal artery (grade V;  $n = 1$ ). Although there were no significant differences in the incidences of grade III–IV complications

based on the modifiable IRE parameters, needle placement, tumor size, or primary treatment versus margin extension, some complications in patients receiving treatment in margins seemed to be secondary to the injury of normal pancreatic tissue.

Pancreatic IRE is generally well tolerated; however, major adverse events could occur. It is suggested to place electrodes mainly in tumor tissue and circumvent electrode placement – or ablation- of healthy pancreatic tissue in order to avoid IRE-induced pancreatitis since IRE may cause self-digestion of the pancreas itself. The procedure could be performed percutaneously or using an open approach. The choice is at the discretion of the physician. Although complication rates appear similar between the two techniques, both approaches have advantages over each other [36, 44]. The advantage of percutaneous IRE over open IRE is the ability to use CT guidance during the procedure, which gives the surgeon or radiologist the ability to determine the exact three-dimensional tumor measurements and its vicinity to surrounding structures. In addition, percutaneous IRE is less invasive than open IRE since the open approach requires laparotomy. On the contrary, open IRE enables real-time differentiation between resectable and unresectable tumors and the detection of metastases that are not yet visible on imaging.

---

## 5.5 Urinary Tract

### 5.5.1 Preclinical Studies

For IRE in urologic tumors, the main concerns are the patency of traversing nerves and the urinary collecting system. In preclinical performance of IRE around urinary collecting systems, microscopic evaluation showed a completely destroyed urothelium but intact extracellular matrix [45–49]. However, when evaluated with fluoroscopy, impeded peristaltic segments were observed [47]. There were no signs of leakage or damage of the collecting system when ablating kidneys [45, 48, 50], no signs of kidney failure [50], and no signs of cicatrization, shrinkage, or ulceration of the renal pelvis and calyces [50]. A transient increase in serum creatinine was seen but was within the standard values [50].

### 5.5.2 Clinical Studies

Human data regarding renal IRE is scarce; nonetheless, preliminary data suggest safety of IRE in the management of renal tumors with preservation of renal function. Thomson et al. [51] treated ten malignant kidney lesions (in seven patients) that were unresponsive to alternative treatment methods. One patient with a previously damaged ureter by RFA developed a ureteric stricture after IRE, requiring a ureteric stent. Although the ureter or collecting system was centrally located in all target lesions, no other strictures were observed. Additionally, transient hematuria (<24 h) occurred in two patients after direct puncture of the renal pelvis by an

18-gauge needle electrode; however, it resolved spontaneously. In a retrospective study by Trimmer et al. [52], 20 patients underwent CT-guided IRE of T1a renal carcinoma ( $n = 13$ ) or small benign or indeterminate renal masses. Post-IRE, no major adverse events occurred. However, minor complications, i.e., postprocedural pain ( $n = 2$ ), perinephric hematomas ( $n = 2$ ), and urinary retention secondary to anesthesia ( $n = 3$ ), were noted in 35% (7/20).

Regarding focal IRE of the prostate, Valerio et al. [53] described a cohort of 34 men with a median follow-up of 6 months (range, 1–24), of whom potency and continence were preserved in 95% and 100%, respectively, post-IRE. A study by Ting et al. [54] examining IRE for localized prostate cancer corroborated these findings. Functional follow-up was comparable to Valerio et al., and there was no significant impairment of urinary, sexual, or bowel function after 6-month follow-up. These data are very promising and may have important clinical implications in minimizing complications after focal prostatic therapy.

---

## 5.6 Nerves

### 5.6.1 Preclinical Studies

IRE's effect on nerves has mainly been investigated by applying IRE directly to sciatic and femoral nerves. Two studies showed that immediately after injury, nerve continuity was preserved [55, 56]. In one of these, by Li et al. where IRE was performed on the sciatic nerve, the authors reported immediate signs of disintegrated myelin sheet [55] and immediate complete paralysis with a reduced nerve conduction velocity. However, these were temporary; the myelin sheet regenerated and the paralyzed foot recovered normal function after 7 weeks. In another study, where IRE was also performed on the sciatic nerve, the authors reported loss of Schwann cells after 3 days [57] but these also regenerated 2 weeks. One study reported that 2 months after IRE treatment on the sciatic nerve, the compound muscle action potential (CMAP) remained lowered in half of the animals [58]; this finding was different from Li et al. in which proximal and distal CMAP recovered 7–10 weeks after IRE, respectively.

In one study where IRE was applied on the vertebrae, no neurologic defects were detected when IRE was performed directly over the posterior cortex or pedicles where the nerves exited the central nerve system [59].

### 5.6.2 Clinical Studies

To date, there are very few articles describing the preliminary results of IRE to treat locoregional pelvic tumor recurrences that are otherwise unsuitable for established treatment options due to the vicinity of major nerves, prostate, or ureter.

The first article, by Niessen et al. [60], presented a case report of a 56-year-old woman who was referred for IRE treatment of a large advanced local recurrence of

endometrial tumor (maximum tumor diameter was 14.9 cm) with infiltration of the sacral bone and nerve plexus. Two ablation procedures were performed to cover the complete target lesion. After the first procedure, no neural symptoms were observed, such as aggravated back pain, sensory deficit, loss of leg strength, or paresthesia. Unfortunately, a mild 4+ paresis of the right extensor hallucis longus (L4 to S1) occurred after the second procedure, which resolved 4 weeks post-IRE. Neurological examination revealed no sensory loss or impairment of bladder function.

Vroomen et al. [61] (<https://www.ncbi.nlm.nih.gov/pubmed/28470395>) presented findings in a series of eight patients (nine tumors) who underwent percutaneous IRE to treat the recurrence of various tumors (primary rectal [ $n = 4$ ], anal [ $n = 1$ ], sigmoid [ $n = 1$ ], cervical carcinoma [ $n = 1$ ], and renal cell carcinoma [ $n = 1$ ]) after a median follow-up of 12 months (range, 4–36). One delayed hemorrhage occurred after restarting anticoagulation therapy 3 days post-IRE. Three patients showed lower limb motor loss with sensory involvement; partial recovery occurred in one patient. Two patients developed a hypotonic bladder, with complete recovery in one. Additionally, two patients showed upper limb motor loss with sensory involvement, which recovered partially in both.

In conclusion, IRE may represent a suitable technique to treat lesions that are located in the vicinity of neural structures. Nevertheless, loss of permanent function may occur. Intraoperative neurophysiologic monitoring (IONM) during percutaneous IRE may be helpful to identify impending neural damage and to prevent permanent function loss since neural structures in the vicinity of the target area are often poorly visualized [62]. Future studies should evaluate its potential utility during IRE.

## Conclusion

These preclinical and clinical studies provide a background of evidence suggesting that IRE may have a suitable role in the treatment of patients who are less than ideal candidates for current thermal ablation modalities due to tumor location in proximity to vital structures. Although theoretically IRE has a nonthermal working mechanism, some studies describe the thermal potential of IRE [29, 63–65]. To avoid potential thermal damage, electrodes should be placed in a way where there is no direct contact between the active tip of the needle and a vital structure. Nevertheless, the clinical data are consistent with the animal models of IRE and support the hypothesis that vascular structures in and around the treatment zone are not significantly affected by this modality. The ability to destroy tissue up to the vessel and biliary wall without damage to the vessel and biliary tree, respectively, gives IRE the potential to overcome the issue of local recurrences near these vital structures which, as noted above, is the clinical limitation of the thermal ablation. Further, data regarding IRE for the treatment of malignant lesions adjacent to neural structures, as well as renal and prostatic tumors, are very promising and support the assessment of the safety and efficacy of IRE in larger studies.

## References

1. Long G, Bakos G, Shires PK, Gritter L, Crissman JW, Harris JL, Clymer JW. Histological and finite element analysis of cell death due to irreversible electroporation. *Technol Cancer Res Treat.* 2014;13(6):561–9. doi:[10.7785/ctrtexpress.2013.600253](https://doi.org/10.7785/ctrtexpress.2013.600253).
2. Date RS, Siriwardena AK. Radiofrequency ablation of the pancreas. II: Intra-operative ablation of non-resectable pancreatic cancer. A description of technique and initial outcome. *JOP.* 2005;6(6):588–92.
3. Tanabe KK, Curley SA, Dodd GD, Siperstein AE, Goldberg SN. Radiofrequency ablation: the experts weigh in. *Cancer.* 2004;100(3):641–50. doi:[10.1002/cncr.11919](https://doi.org/10.1002/cncr.11919).
4. Howard JH, Tzeng CW, Smith JK, Eckhoff DE, Bynon JS, Wang T, Arnoletti JP, Heslin MJ. Radiofrequency ablation for unresectable tumors of the liver. *Am Surg.* 2008;74(7):594–600. discussion 600–591
5. Goldberg SN, Hahn PF, Tanabe KK, Mueller PR, Schima W, Athanasoulis CA, Compton CC, Solbiati L, Gazelle GS. Percutaneous radiofrequency tissue ablation: does perfusion-mediated tissue cooling limit coagulation necrosis? *J Vasc Interv Radiol.* 1998;9(1 Pt 1):101–11.
6. Lu DS, Raman SS, Vodopich DJ, Wang M, Sayre J, Lassman C. Effect of vessel size on creation of hepatic radiofrequency lesions in pigs: assessment of the heat sink effect. *AJR Am J Roentgenol.* 2002;178(1):47–51. doi:[10.2214/ajr.178.1.1780047](https://doi.org/10.2214/ajr.178.1.1780047).
7. Rubinsky B. Irreversible electroporation in medicine. *Technol Cancer Res Treat.* 2007;6(4):255–60.
8. Scheffer HJ, Nielsen K, van Tilborg AA, Vieveen JM, Bouwman RA, Kazemier G, Niessen HW, Meijer S, van Kuijk C, van den Tol MP, Meijerink MR. Ablation of colorectal liver metastases by irreversible electroporation: results of the COLDFIRE-I ablate-and-resect study. *Eur Radiol.* 2014;24(10):2467–75. doi:[10.1007/s00330-014-3259-x](https://doi.org/10.1007/s00330-014-3259-x).
9. Phillips MA, Narayan R, Padath T, Rubinsky B. Irreversible electroporation on the small intestine. *Br J Cancer.* 2012;106(3):490–5. doi:[10.1038/bjc.2011.582](https://doi.org/10.1038/bjc.2011.582).
10. Au JT, Kingham TP, Jun K, Haddad D, Gholami S, Mojica K, Monette S, Ezell P, Fong Y. Irreversible electroporation ablation of the liver can be detected with ultrasound B-mode and elastography. *Surgery.* 2013;153(6):787–93. doi:[10.1016/j.surg.2012.11.022](https://doi.org/10.1016/j.surg.2012.11.022).
11. Ben-David E, Appelbaum L, Sosna J, Nissenbaum I, Goldberg SN. Characterization of irreversible electroporation ablation in in vivo porcine liver. *AJR Am J Roentgenol.* 2012;198(1):W62–8. doi:[10.2214/ajr.11.6940](https://doi.org/10.2214/ajr.11.6940).
12. Charpentier KP, Wolf F, Noble L, Winn B, Resnick M, Dupuy DE. Irreversible electroporation of the liver and liver hilum in swine. *HPB: Off J Int Hepato Pancreato Biliary Assoc.* 2011;13(3):168–73. doi:[10.1111/j.1477-2574.2010.00261.x](https://doi.org/10.1111/j.1477-2574.2010.00261.x).
13. Lee YJ, Lu DSK, Osuagwu F, Lassman C. Irreversible electroporation in porcine liver: short- and long-term effect on the hepatic veins and adjacent tissue by ct with pathological correlation. *Investig Radiol.* 2012;47(11):671–5.
14. Golberg A, Bruinsma BG, Uygun BE, Yarmush ML. Tissue heterogeneity in structure and conductivity contribute to cell survival during irreversible electroporation ablation by electric field sinks. *Sci Rep.* 2015;5:8485. doi:[10.1038/srep08485](https://doi.org/10.1038/srep08485).
15. Appelbaum L, Ben-David E, Sosna J, Nissenbaum Y, Goldberg SN. US findings after irreversible electroporation ablation: radiologic-pathologic correlation. *Radiology.* 2012;262(1):117–25. doi:[10.1148/radiol.11110475](https://doi.org/10.1148/radiol.11110475).
16. Lee EW, Chen C, Prieto VE, Dry SM, Loh CT, Kee ST. Advanced hepatic ablation technique for creating complete cell death: irreversible electroporation. *Radiology.* 2010;255(2):426–33. doi:[10.1148/radiol.10090337](https://doi.org/10.1148/radiol.10090337).
17. Lee EW, Loh CT, Kee ST. Imaging guided percutaneous irreversible electroporation: ultrasound and immunohistological correlation. *Technol Cancer Res Treat.* 2007;6(4):287–94.
18. Liu Y, Xiong Z, Zhou W, Hua Y, Li C, Yao C. Percutaneous ultrasound-guided irreversible electroporation: a goat liver study. *Oncol Lett.* 2012;4(3):450–4. doi:[10.3892/ol.2012.781](https://doi.org/10.3892/ol.2012.781).

19. Edd JF, Horowitz L, Davalos RV, Mir LM, Rubinsky B. In vivo results of a new focal tissue ablation technique: irreversible electroporation. *IEEE Trans Biomed Eng.* 2006;53(7):1409–15. doi:[10.1109/tbme.2006.873745](https://doi.org/10.1109/tbme.2006.873745).
20. Chen X, Ren Z, Zhu T, Zhang X, Peng Z, Xie H, Zhou L, Yin S, Sun J, Zheng S. Electric ablation with irreversible electroporation (IRE) in vital hepatic structures and follow-up investigation. *Sci Rep.* 2015;5:16233. doi:[10.1038/srep16233](https://doi.org/10.1038/srep16233).
21. Choi YS, Kim HB, Chung J, Kim HS, Yi JH, Park JK. Preclinical analysis of irreversible electroporation on rat liver tissues using a microfabricated electroporator. *Tissue Eng Part C Methods.* 2010;16(6):1245–53. doi:[10.1089/ten.TEC.2009.0803](https://doi.org/10.1089/ten.TEC.2009.0803).
22. Maor E, Ivorra A, Leor J, Rubinsky B. The effect of irreversible electroporation on blood vessels. *Technol Cancer Res Treat.* 2007;6(4):307–12.
23. Maor E, Ivorra A, Leor J, Rubinsky B. Irreversible electroporation attenuates neointimal formation after angioplasty. *IEEE Trans Biomed Eng.* 2008;55(9):2268–74. doi:[10.1109/tbme.2008.923909](https://doi.org/10.1109/tbme.2008.923909).
24. Narayanan G, Bhatia S, Echenique A, Suthar R, Barbery K, Yrizarry J. Vessel patency post irreversible electroporation. *Cardiovasc Intervent Radiol.* 2014;37(6):1523–9. doi:[10.1007/s00270-014-0988-9](https://doi.org/10.1007/s00270-014-0988-9).
25. Scheffer HJ, Melenhorst MC, Vogel JA, van Tilborg AA, Nielsen K, Kazemier G, Meijerink MR. Percutaneous irreversible electroporation of locally advanced pancreatic carcinoma using the dorsal approach: a case report. *Cardiovasc Intervent Radiol.* 2015;38(3):760–5. doi:[10.1007/s00270-014-0950-x](https://doi.org/10.1007/s00270-014-0950-x).
26. Martin RC 2nd, Kwon D, Chalikhonda S, Sellers M, Kotz E, Scoggins C, McMasters KM, Watkins K. Treatment of 200 locally advanced (stage III) pancreatic adenocarcinoma patients with irreversible electroporation: safety and efficacy. *Ann Surg.* 2015;262(3):486–494.; discussion 492–484. doi:[10.1097/SLA.0000000000001441](https://doi.org/10.1097/SLA.0000000000001441).
27. Philips P, Hays D, Martin RC. Irreversible electroporation ablation (IRE) of unresectable soft tissue tumors: learning curve evaluation in the first 150 patients treated. *PLoS One.* 2013;8(11):e76260. doi:[10.1371/journal.pone.0076260](https://doi.org/10.1371/journal.pone.0076260).
28. Silk MT, Wimmer T, Lee KS, Srimathveeravalli G, Brown KT, Kingham PT, Fong Y, Durack JC, Sofocleous CT, Solomon SB. Percutaneous ablation of peribiliary tumors with irreversible electroporation. *J Vasc Interv Radiol: JVIR.* 2014;25(1):112–8. doi:[10.1016/j.jvir.2013.10.012](https://doi.org/10.1016/j.jvir.2013.10.012).
29. van den Bos W, Scheffer HJ, Vogel JA, Wagstaff PG, de Bruin DM, de Jong MC, van Gemert MJ, de la Rosette JJ, Meijerink MR, Klaessens JH, Verdaasdonk RM. Thermal energy during irreversible electroporation and the influence of different ablation parameters. *J Vasc Interv Radiol.* 2016;27(3):433–43. doi:[10.1016/j.jvir.2015.10.020](https://doi.org/10.1016/j.jvir.2015.10.020).
30. Trueba-Arguinarena FJ, de Prado-Otero DS, Poves-Alvarez R. Pancreatic adenocarcinoma treated with irreversible electroporation case report: first experience and outcome. *Medicine.* 2015;94(26):e946. doi:[10.1097/md.0000000000000946](https://doi.org/10.1097/md.0000000000000946).
31. Scheffer HJ, Nielsen K, de Jong MC, van Tilborg AA, Vieveen JM, Bouwman AR, Meijer S, van Kuijk C, van den Tol PM, Meijerink MR. Irreversible electroporation for nonthermal tumor ablation in the clinical setting: a systematic review of safety and efficacy. *J Vasc Interv Radiol.* 2014;25(7):997–1011.; quiz 1011. doi:[10.1016/j.jvir.2014.01.028](https://doi.org/10.1016/j.jvir.2014.01.028).
32. Kingham TP, Karkar AM, D'Angelica MI, Allen PJ, Dematteo RP, Getrajdman GI, Sofocleous CT, Solomon SB, Jarnagin WR, Fong Y. Ablation of perivascular hepatic malignant tumors with irreversible electroporation. *J Am Coll Surg.* 2012;215(3):379–87. doi:[10.1016/j.jamcollsurg.2012.04.029](https://doi.org/10.1016/j.jamcollsurg.2012.04.029).
33. Hosein PJ, Echenique A, Loaiza-Bonilla A, Froud T, Barbery K, Rocha Lima CM, Yrizarry JM, Narayanan G. Percutaneous irreversible electroporation for the treatment of colorectal cancer liver metastases with a proposal for a new response evaluation system. *J Vasc Interv Radiol.* 2014;25(8):1233–1239. e1232. doi:[10.1016/j.jvir.2014.04.007](https://doi.org/10.1016/j.jvir.2014.04.007).
34. Cannon R, Ellis S, Hayes D, Narayanan G, Martin RC 2nd. Safety and early efficacy of irreversible electroporation for hepatic tumors in proximity to vital structures. *J Surg Oncol.* 2013;107(5):544–9. doi:[10.1002/jso.23280](https://doi.org/10.1002/jso.23280).

35. Dollinger M, Zeman F, Niessen C, Lang SA, Beyer LP, Muller M, Stroszczynski C, Wiggermann P. Bile duct injury after irreversible electroporation of hepatic malignancies: evaluation of MR imaging findings and laboratory values. *J Vasc Interv Radiol*. 2015; doi:[10.1016/j.jvir.2015.10.002](https://doi.org/10.1016/j.jvir.2015.10.002).
36. Scheffer HJ, Vroomen LG, de Jong MC, Melenhorst MC, Zonderhuis BM, Daams F, Vogel JA, Besselink MG, van Kuijk C, Witvliet J, de van der Schueren MA, de Gruijl TD, Stam AG, van den Tol PM, van Delft F, Kazemier G, Meijerink MR. Ablation of locally advanced pancreatic cancer with percutaneous irreversible electroporation: Results of the phase I/II PANFIRE study. *Radiology*. 2017;282(2):585–597. doi:[10.1148/radiol.2016152835](https://doi.org/10.1148/radiol.2016152835). Epub 2016 Sep 6
37. Bower M, Sherwood L, Li Y, Martin R. Irreversible electroporation of the pancreas: definitive local therapy without systemic effects. *J Surg Oncol*. 2011;104(1):22–8. doi:[10.1002/jso.21899](https://doi.org/10.1002/jso.21899).
38. Charpentier KP, Wolf F, Noble L, Winn B, Resnick M, Dupuy DE. Irreversible electroporation of the pancreas in swine: a pilot study. *HPB (Oxford)*. 2010;12(5):348–51. doi:[10.1111/j.1477-2574.2010.00174.x](https://doi.org/10.1111/j.1477-2574.2010.00174.x).
39. Fritz S, Sommer CM, Vollherbst D, Wachter MF, Longerich T, Sachsenmeier M, Knapp J, Radeleff BA, Werner J. Irreversible electroporation of the pancreas is feasible and safe in a porcine survival model. *Pancreas*. 2015;44(5):791–8. doi:[10.1097/mpa.0000000000000331](https://doi.org/10.1097/mpa.0000000000000331).
40. Wimmer T, Srimathveeravalli G, Gutta N, Ezell PC, Monette S, Kingham TP, Maybody M, Durack JC, Fong Y, Solomon SB. Comparison of simulation-based treatment planning with imaging and pathology outcomes for percutaneous CT-guided irreversible electroporation of the porcine pancreas: a pilot study. *J Vasc Intervent Radiol: JVIR*. 2013;24(11):1709–18. doi:[10.1016/j.jvir.2013.05.056](https://doi.org/10.1016/j.jvir.2013.05.056).
41. Martin RC 2nd, McFarland K, Ellis S, Velanovich V. Irreversible electroporation therapy in the management of locally advanced pancreatic adenocarcinoma. *J Am Coll Surg*. 2012;215(3):361–9. doi:[10.1016/j.jamcollsurg.2012.05.021](https://doi.org/10.1016/j.jamcollsurg.2012.05.021).
42. Paiella S, Butturini G, Frigerio I, Salvia R, Armatura G, Bacchion M, Fontana M, D’Onofrio M, Martone E, Bassi C. Safety and feasibility of irreversible electroporation (IRE) in patients with locally advanced pancreatic cancer: results of a prospective study. *Dig Surg*. 2015;32(2):90–7. doi:[10.1159/000375323](https://doi.org/10.1159/000375323).
43. Kluger MD, Epelboym I, Schrope BA, Mahendraraj K, Hecht EM, Susman J, Weintraub JL, Chabot JA. Single-institution experience with irreversible electroporation for T4 pancreatic cancer: first 50 patients. *Ann Surg Oncol*. 2016;23(5):1736–43. doi:[10.1245/s10434-015-5034-x](https://doi.org/10.1245/s10434-015-5034-x).
44. Vogel JA, Rombouts SJ, de Rooij T, van Delden OM, Dijkgraaf MG, van Gulik TM, van Hooft JE, van Laarhoven HW, Martin RC, Schoorlemmer A, Wilmlink JW, van Lienden KP, Busch OR, Besselink MG. Induction Chemotherapy followed by resection or irreversible electroporation in locally advanced pancreatic cancer (IMPALA): A prospective cohort study. *Ann Surg Oncol*. 2017. doi:[10.1245/s10434-017-5900-9](https://doi.org/10.1245/s10434-017-5900-9). [Epub ahead of print]
45. Deodhar A, Monette S, Single GW Jr, Hamilton WC Jr, Thornton R, Maybody M, Coleman JA, Solomon SB. Renal tissue ablation with irreversible electroporation: preliminary results in a porcine model. *Urology*. 2011;77(3):754–60. doi:[10.1016/j.urology.2010.08.036](https://doi.org/10.1016/j.urology.2010.08.036).
46. Olweny EO, Kapur P, Tan YK, Park SK, Adibi M, Cadeddu JA. Irreversible electroporation: evaluation of nonthermal and thermal ablative capabilities in the porcine kidney. *Urology*. 2013;81(3):679–84. doi:[10.1016/j.urology.2012.11.026](https://doi.org/10.1016/j.urology.2012.11.026).
47. Srimathveeravalli G, Silk M, Wimmer T, Monette S, Kimm S, Maybody M, Solomon SB, Coleman J, Durack JC. Feasibility of catheter-directed intraluminal irreversible electroporation of porcine ureter and acute outcomes in response to increasing energy delivery. *J Vasc Intervent Radiol: JVIR*. 2015;26(7):1059–66. doi:[10.1016/j.jvir.2015.01.020](https://doi.org/10.1016/j.jvir.2015.01.020).
48. Tracy CR, Kabbani W, Cadeddu JA. Irreversible electroporation (IRE): a novel method for renal tissue ablation. *BJU Int*. 2011;107(12):1982–7. doi:[10.1111/j.1464-410X.2010.09797.x](https://doi.org/10.1111/j.1464-410X.2010.09797.x).
49. Wimmer T, Srimathveeravalli G, Silk M, Monette S, Gutta N, Maybody M, Erinjery JP, Coleman JA, Solomon SB, Sofocleous CT. Feasibility of a modified biopsy needle for irreversible electroporation ablation and periprocedural tissue sampling. *Technol Cancer Res Treat*. 2015; doi:[10.1177/1533034615608739](https://doi.org/10.1177/1533034615608739).

50. Wendler JJ, Pech M, Porsch M, Janitzky A, Fischbach F, Buhtz P, Vogler K, Huhne S, Borucki K, Strang C, Mahnkopf D, Ricke J, Liehr UB. Urinary tract effects after multifocal nonthermal irreversible electroporation of the kidney: acute and chronic monitoring by magnetic resonance imaging, intravenous urography and urinary cytology. *Cardiovasc Intervent Radiol*. 2012;35(4):921–6. doi:[10.1007/s00270-011-0257-0](https://doi.org/10.1007/s00270-011-0257-0).
51. Thomson KR, Cheung W, Ellis SJ, Federman D, Kavnoudias H, Loader-Oliver D, Roberts S, Evans P, Ball C, Haydon A. Investigation of the safety of irreversible electroporation in humans. *J Vasc Interv Radiol*. 2011;22(5):611–21. doi:[10.1016/j.jvir.2010.12.014](https://doi.org/10.1016/j.jvir.2010.12.014).
52. Trimmer CK, Khosla A, Morgan M, Stephenson SL, Ozayar A, Cadeddu JA. Minimally invasive percutaneous treatment of small renal tumors with irreversible electroporation: a single-center experience. *J Vasc Interv Radiol*. 2015;26(10):1465–71. doi:[10.1016/j.jvir.2015.06.028](https://doi.org/10.1016/j.jvir.2015.06.028).
53. Valerio M, Strickert PD, Ahmed HU, Dickinson L, Ponsky L, Shnier R, Allen C, Emberton M. Initial assessment of safety and clinical feasibility of irreversible electroporation in the focal treatment of prostate cancer. *Prostate Cancer Prostatic Dis*. 2014;17(4):343–7. doi:[10.1038/pcan.2014.33](https://doi.org/10.1038/pcan.2014.33).
54. Ting F, Tran M, Bohm M, Siriwardana A, Van Leeuwen PJ, Haynes AM, Delprado W, Shnier R, Stricker PD. Focal irreversible electroporation for prostate cancer: functional outcomes and short-term oncological control. *Prostate Cancer Prostatic Dis*. 2016;19(1):46–52. doi:[10.1038/pcan.2015.47](https://doi.org/10.1038/pcan.2015.47).
55. Li W, Fan Q, Ji Z, Qiu X, Li Z. The effects of irreversible electroporation (IRE) on nerves. *PLoS One*. 2011;6(4):e18831.
56. Wong SSM, Hui JWY, Chan AWH, Chu CM, Rowlands DK, Yu SCH. Irreversible electroporation of the femoral neurovascular bundle: imaging and histologic evaluation in a swine model. *J Vasc Interv Radiol*. 2015;26(8):1212–1220.e1211.
57. Schoellnast H, Monette S, Ezell PC, Deodhar A, Maybody M, Erinjeri JP, Stubblefield MD, Single GW Jr, Hamilton WC Jr, Solomon SB. Acute and subacute effects of irreversible electroporation on nerves: experimental study in a pig model. *Radiology*. 2011;260(2):421–7. doi:[10.1148/radiol.11103505](https://doi.org/10.1148/radiol.11103505).
58. Schoellnast H, Monette S, Ezell PC, Maybody M, Erinjeri JP, Stubblefield MD, Single G, Solomon SB. The delayed effects of irreversible electroporation ablation on nerves. *Eur Radiol*. 2013;23(2):375–80. doi:[10.1007/s00330-012-2610-3](https://doi.org/10.1007/s00330-012-2610-3).
59. Tam AL, Abdelsalam ME, Gagea M, Ensor JE, Moussa M, Ahmed M, Goldberg SN, Dixon K, McWatters A, Miller JJ, Srimathveeravalli G, Solomon SB, Avritscher R, Wallace MJ, Gupta S. Irreversible electroporation of the lumbar vertebrae in a porcine model: is there clinical-pathologic evidence of neural toxicity? *Radiology*. 2014;272(3):709–19. doi:[10.1148/radiol.14132560](https://doi.org/10.1148/radiol.14132560).
60. Niessen C, Jung EM, Schreyer AG, Wohlgemuth WA, Trabold B, Hahn J, Rechenmacher M, Stroszczyński C, Wiggemann P. Palliative treatment of presacral recurrence of endometrial cancer using irreversible electroporation: a case report. *J Med Case Rep*. 2013;7:128. doi:[10.1186/1752-1947-7-128](https://doi.org/10.1186/1752-1947-7-128).
61. Vroomen LGPH, Scheffer HJ, Melenhorst MCAM, van Grieken N, van den Tol MP, Meijerink MR. Irreversible Electroporation to Treat Malignant Tumor Recurrences Within the Pelvic Cavity: A Case Series. *Cardiovasc Intervent Radiol*. 2017 May 3. doi:[10.1007/s00270-017-1657-6](https://doi.org/10.1007/s00270-017-1657-6).
62. Marshall RH, Avila EK, Solomon SB, Erinjeri JP, Maybody M. Feasibility of intraoperative nerve monitoring in preventing thermal damage to the “Nerve at Risk” during image-guided ablation of tumors. *Cardiovasc Intervent Radiol*. 2015; doi:[10.1007/s00270-015-1287-9](https://doi.org/10.1007/s00270-015-1287-9).
63. Faroja M, Ahmed M, Appelbaum L, Ben-David E, Moussa M, Sosna J, Nissenbaum I, Goldberg SN. Irreversible electroporation ablation: is all the damage nonthermal? *Radiology*. 2013;266(2):462–70. doi:[10.1148/radiol.12120609](https://doi.org/10.1148/radiol.12120609).
64. Dunki-Jacobs EM, Philips P, Martin RC 2nd. Evaluation of thermal injury to liver, pancreas and kidney during irreversible electroporation in an in vivo experimental model. *Br J Surg*. 2014;101(9):1113–21. doi:[10.1002/bjs.9536](https://doi.org/10.1002/bjs.9536).
65. Scheffer HJ, Vogel JA, van den Bos W, Neal RE 2nd, van Lienden KP, Besselink MG, van Gemert MJ, van der Geld CW, Meijerink MR, Klaessens JH, Verdaasdonk RM. The influence of a metal stent on the distribution of thermal energy during irreversible electroporation. *PLoS One*. 2016;11(2):e0148457. doi:[10.1371/journal.pone.0148457](https://doi.org/10.1371/journal.pone.0148457).



---

## Part III

# Technique, Tips and Tricks

---

# Anesthetic Management During Irreversible Electroporation Procedures

# 6

Jenny M. Vieveen and R. Arthur Bouwman

Irreversible electroporation (IRE) has evolved as a promising technique for tumor ablation. High-voltage electrical field pulses generated between electrodes surrounding the tumor induce cell death by permanently increasing the cell membrane permeability. For anesthesiologists involved in IRE procedures, these high-voltage electrical pulses pose specific intra-procedural challenges, and several precautions have to be taken into account in order to safely perform IRE procedures. In this chapter, we will discuss all these specific details from the extremely high-voltage electrical pulses, necessary precautions, and potential complications that may occur during the procedure.

---

## 6.1 Cardiovascular Effects of IRE: Arrhythmias and Hypertension

Irreversible electroporation uses multiple series of high-voltage electrical pulses that are locally deposited via electrodes placed around the tumor. Electroporation increases membrane permeability which allows ion transport to occur over the cellular membrane. Should these (uncontrolled) ion transports occur in cardiac tissue, arrhythmias or even fibrillation may occur. Deodhar et al. [1] performed unsynchronized electroporation close to the heart in swine and showed that fatal

---

J.M. Vieveen, MD

Department of Anesthesiology, VU University Medical Center, Amsterdam, The Netherlands

R.A. Bouwman, MD, PhD (✉)

Department of Anesthesiology, Catharina Hospital, Eindhoven, The Netherlands

e-mail: [arthur.bouwman@catharinaziekenhuis.nl](mailto:arthur.bouwman@catharinaziekenhuis.nl)

© Springer International Publishing AG 2018

M.R. Meijerink et al. (eds.), *Irreversible Electroporation in Clinical Practice*,  
[https://doi.org/10.1007/978-3-319-55113-5\\_6](https://doi.org/10.1007/978-3-319-55113-5_6)

97

ventricular arrhythmias occurred during IRE treatment. Also, in humans during treatment in close proximity to the heart, IRE treatment induced cardiac arrhythmias (Fig. 6.1).

These arrhythmias can largely be prevented by the use of synchronized irreversible electroporation. Hereby the electrical pulses are delivered synchronously to the heart rhythm during the absolute refractory period of the heart. This synchronization is achieved by attaching a preprogrammed commercial ECG monitor which analyzes the ECG rhythm to detect the R wave. Then the irreversible electroporation generator delivers a pulse 50 ms after each R wave.

Nielsen et al. [2] describe 28 patients treated with open or percutaneous irreversible electroporation using ECG synchronization (Table 6.1). In two IRE procedures, a minor self-limiting cardiac arrhythmia (ventricular extrasystole and a bigeminy) was observed. The ventricular extrasystole was seen during an open IRE procedure apical in the liver near the left diaphragm. After the abortion of the procedure, the rhythm normalized, and the ablation could be successfully continued after removal of the electrode that was closest to the heart. The bigeminy with premature ventricular complexes occurred during a pancreatic



**Fig. 6.1** Electrocardiograph (ECG) trace during irreversible electroporation (IRE) treatment of a hepatic tumor below the heart. The synchronizer was not used, and ventricular capture of the IRE pulse resulted in a loss of the arterial pulse because of insufficient time for filling of the left ventricle (Adapted from Ball et al.)

**Table 6.1** Complications related to the general procedure during and after IRE in 28 patients

Treatment site	Complication	N	Grade	Intervention
Liver (open procedure)	Arrhythmia	1	I	Electrode removal
	Postoperative hemorrhage	1	III	Re-laparotomy
	Pain	2	II, III	Oral, IV, and neuraxial analgesics
	Pneumonia	1	II	Antibiotics
	Peripheral edema	1	II	Compression stockings
Liver (percutaneous)	Pneumothorax	2	II	Chest tube
Pancreas	Arrhythmia	1	I	None
	Pancreatitis + bile leakage	1	III	Drainage, antibiotics
Kidney	Hematuria	1	I	None
Pelvis	Nerve function loss	1	II/III	Rehabilitation, physiotherapy

Adapted from Nielsen et al. [2]

ablation but disappeared within 5 min at the end of the procedure. In both cases, there was no hemodynamic instability.

In most patients, a transient increase in blood pressure can be observed during electroporation. This increase involves both systolic and diastolic pressure and is generally mild to moderate (20–45 mmHg), but severe increases in blood pressure up to 200 mmHg have been reported. Nielsen et al. [2] describes a median rise of 44 mmHg of the systolic blood pressure and 19 mmHg of the diastolic pressure. Increases in blood pressure were most pronounced during pancreatic procedures and were accompanied by increase in heart rate. Blood pressure increases responded well to additional propofol and remifentanyl. Also Martin et al. [3] were confronted with intraoperative hypertension, but much higher pressures were reported (median systolic BP 190, range 185–215 and median diastolic 98, range 91–115). Blood pressure was largely unresponsive to various types of antihypertensives with minimal to insufficient effects.

The exact mechanism causing this elevation in both blood pressure and heart rate remains unclear, but stimulation of the autonomous nerve system is a likely explanation.

### 6.1.1 Precautions

As previously mentioned, the use of synchronized irreversible electroporation helps to avoid most cardiac arrhythmias. It is recommended to attach the synchronizing device to the patient before placing the patient in the CT scanner or covering the patient in sterile drapes. This allows evaluation of the quality of the ECG signal and proper function of the synchronization before starting the IRE procedure. Furthermore, it is strongly recommended during IRE procedures to attach a patient to an external defibrillator in order to avoid delays in treatment when arrhythmias requiring defibrillation should occur. This may be especially relevant during percutaneous procedures with patient in the CT scanner and when it is impossible to reach the patient to apply defibrillator pads.

Considering the above irreversible electroporation is contraindicated for patients with a history of cardiac arrhythmias requiring anti-arrhythmic therapy and/or pacemaker/implantable cardioverter-defibrillator. Uncontrolled hypertension, congestive heart failure and active coronary artery disease are relatively contra indication for IRE procedures. Because there is definite rise in both systolic and diastolic blood pressure as well as a slight increase in heart rate, these patients are at risk for cardiac complications. In case of these relative contraindications, the benefits and risks of IRE treatment should be carefully weighed in the individual patient.

---

## 6.2 Muscle Contractions

Electrical stimulation during IRE elicits muscular contractions, which can be severe due to the rapid and high-voltage pulses that are used during IRE. As a consequence, IRE procedures require complete relaxation of the patient during

irreversible electroporation and thus general anesthesia is necessary. As reported by Ball et al. [4] contractions of the entire upper body can be observed in inadequately paralyzed patients undergoing IRE. Moreover, even if complete muscular relaxation is ensured, local muscle contractions around the electrode insertion can still be observed. These local contractions are more profound during percutaneous procedures, especially when electrodes are placed through large muscles.

In our opinion to ensure procedural safety, IRE procedures require close monitoring of neuromuscular function to ensure deep neuromuscular block. A neuromuscular monitoring device should be connected and calibrated before administration of muscle relaxants. Before electrical pulses are initiated, close communication within the IRE team should confirm the presence of deep neuromuscular (e.g., typically train of four (TOF) ratio of zero). Obviously, at the end of the procedure, adequate reversal of the neuromuscular block should be confirmed. If necessary, antagonists may be necessary.

---

### 6.3 Laboratory Results

As IRE induces cell death via destructing cellular membrane integrity, initial concerns for disturbances in acid-base balance and electrolytes were postulated. In the study of Ball et al. [4], disturbances in acid-base balance and associated hyperkalemia were indeed observed in 4 patients out of 21 patients. The disturbances were mild, and cancellation of the procedure was not required. In the study from Nielsen et al. [2], blood tests were performed to measure serum electrolytes, renal function, and hepatic or pancreatic enzymes. No significant electrolyte abnormalities were observed in any patient.

Liver and pancreatic enzymes were elevated directly after IRE procedures on the liver and pancreas, respectively. On the first day after the procedure, the highest level of the enzyme disturbances was reached.

Chen et al. describes liver function damage occurring 2 h to 2 days after treatment of the liver with IRE in female pigs and a mild inflammatory response. But after 2 days, the elevated enzymes and white blood cell count starts to return back to normal and were completely resolved after 14 days.

From available evidence until now, it can be concluded that IRE does not seem to induce major disturbances in the acid-base and electrolytes and no additional precautions are warranted. However, enzyme elevation as a sign of damage of the organ targeted by IRE can be observed, but these elevations are generally also classified as mild.

---

### 6.4 Seizures

Since irreversible electroporation works through electrical pulses, it could potentially provoke an epileptic seizure by the electrical discharge to the brain.

Therefore the manufacturer of IRE notes epilepsy or a previous seizure in the medical past as a contraindication for the treatment, although it is not certain if IRE indeed can induce a seizure.

During electroconvulsive therapy in case of therapy-resistant depression, seizures are induced by application of electrical pulses of 5 Hz or more to the brain. When ECG synchronization is used during IRE, the change that a pulse frequency of 5 Hz is reached is diminished and unlikely. In order to explore the occurrence of seizure activity induced by IRE treatment, we investigated the effect of IRE in non-epileptic patients by using a simplified EEG monitor and looking at cerebral activity. No background brain activity was observed in five out of six patients and none of the patients showed reactive cerebral response on an electrical pulse (Fig. 6.2).

During their IRE procedures, all patients were under general anesthesia with propofol according to our local IRE protocol. As propofol is known for its antiepileptic property, the depth of the anesthesia may have precluded seizure activity in response to IRE.

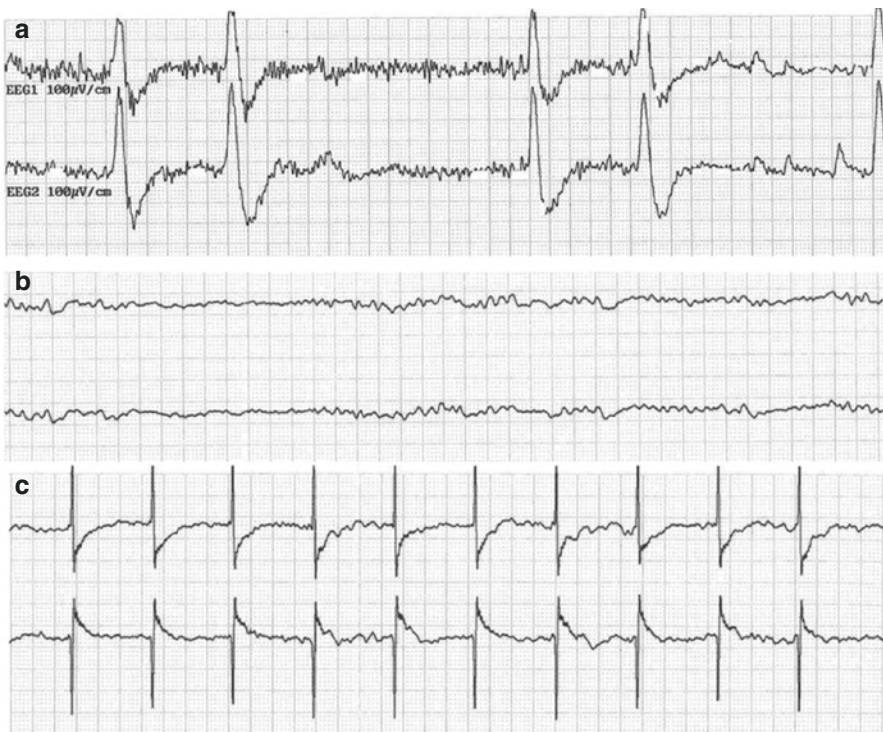


**Fig. 6.2** Simplified electroencephalographic (EEG) trace during irreversible electroporation, (a) before induction of anesthesia, (b) after induction of anesthesia, (c) during IRE. During IRE EEG artifacts can be observed, which return to baseline directly after the pulse (Adapted from Nielsen et al. [2])

Based on these observations, it seems justified to conclude that the chance to reach minimal frequency necessary to induce a seizure is limited by the use of an ECG synchronizer. And secondly, as general anesthesia increases the seizure threshold, potential seizure activity may suppress. Therefore, it seems safe to use IRE in patients with a medical history of epilepsy, but it should be kept in mind that the number of observations and the experience of IRE in these patients are limited and clearly more studies are required, before safe application of IRE in patients with epilepsy can be recommended.

## 6.5 Patient Position

IRE can be performed both percutaneous and via open procedure. Percutaneous procedures mostly take place, at least in our hospital, in the CT scanning room. This setting and the position of the patient will challenge the anesthesiologist.

According to the location of the lesion that will be treated with IRE, the patient will be in prone, supine, or lateral position. Optimal support of the patient may be challenged by the constraints of the CT scanner. Unlike the setting in the operation theater, patients need to fit through the CT scanner with all monitoring cables and venous access lines in situ. This may be especially challenging when a prone position is required.

In the supine position, however, the biggest challenge is the placement of the arms above the head, which poses a considerable risk of plexus brachialis damage. In order to avoid image artifacts, the radiologists often request to position the arms folded above the head to ensure a clear view of the treatment area. In the study of Ball et al. [4] 2 patients out of 12 suffered from transient brachial plexus neuropraxia, after which positioning of the arms was optimized. A foam face pillow, designed for prone position, was placed on top of the patient's head after which the arms were folded on top of the pillow.

In our clinic, patients are placed with their head on a regular bed pillow, and the arms are folded above the head (Fig. 6.3). After padding the elbows, padded straps are used to adjust the arms and prevent them from sliding.

Before the start of the procedure, it is of utmost importance to check whether the patient can freely move in and out of the CT scanner without the patient touching the CT scanner, displacing or disconnecting monitor leads or venous access lines.



**Fig. 6.3** Open IRE procedure (a) and percutaneous procedure (b) (adapted from Nielsen et al. [2]). Arm position during percutaneous IRE procedure in the CT scanner (c)

## 6.6 Postoperative Pain

Both Nielsen et al. [2] and Ball et al. [4] describe a group of patients who underwent percutaneous electroporation. Patients who received an open procedure with additional IRE were all provided with an epidural for postoperative pain. And since their postoperative pain couldn't be related to IRE only, it is difficult to relate postoperative pain to the IRE procedure itself in this group.

Most of the percutaneous treated patients reported the posttreatment pain as mild. The median maximum reported VAS was 3 with a range between 0 and 9. In most patients, post-procedural pain could well be managed with oral analgesics. The most painful procedure seems the IRE of the pancreas with reported VAS scores up to 9. This may very well be explained by the close anatomical relation of the pancreas with coeliac plexus in addition to the post-procedural reactive pancreatitis that is induced by IRE treatment of pancreatic tissue. However, using a multimodal pain treatment postoperative pain was effectively managed in most patients.

---

## References

1. Deodhar A, Dickfeld T, Single GW, Hamilton WC Jr, Thornton RH, Sofocleous CT, Maybody M, Gonen M, Rubinsky B, Solomon SB. Irreversible electroporation near the heart: ventricular arrhythmias can be prevented with ECG synchronization. *Am J Roentgenol.* 2011;196(3):W330–5.
2. Nielsen K, Scheffer HJ, Vieveen JM, van Tilborg AAJM, Meijer S, van Kuijk C, van Tol MP, Meijerink MR, Bouwman RA. Anaesthetic management during open and percutaneous irreversible electroporation. *Br J Anaesth.* 2014;113(6):985–92.
3. Martin RCG, Schwartz E, Adams JA, Farah I, Derhake BM. Intra-operative anesthesia management in patients undergoing surgical irreversible electroporation of the pancreas, liver, kidney and retroperitoneal tumors. *Anesth Pain Med.* 2015;5(3):e22786.
4. Ball C, Thomson KR, Kavnoudias H. Irreversible electroporation: a new challenge in “out of operating theater” anesthesia. *Anesth Analg.* 2010;110(5):1305–9.



---

## Complications and Procedures to Enhance Safety

# 7

Laurien G.P.H. Vroomen, K. Nielsen, A.H. Ruarus,  
and Hester J. Scheffer

As ablative techniques are used more than ever in oncologic treatment, increasing knowledge about the possible adverse effects has arisen. It is well known that thermal ablation of lesions in the proximity of critical structures, like major bile ducts, nerves, intestines, ureters, and vessels, has an unacceptable complication rate due to thermal damage and can therefore be contraindicated in selected cases [1–3].

Irreversible electroporation has been developed to address the tumors that are located in an area that is unsuitable for thermal ablation. Since the cellular destruction is, at least theoretically, triggered by a nonthermal mechanism, IRE is considered to conserve proteins and the underlying connective tissue [4–8]. Preclinical and early clinical data have demonstrated that IRE can destroy tumor tissue while preserving the structural integrity of major bile ducts, the urinary tract, and larger vessels (see Chap. 5: *The Effect of Irreversible Electroporation on Blood Vessels, Bile Ducts, Urinary Tract, Intestines, and Nerves*) [9, 10]. Hence, IRE shows promise for the safe ablation of difficult-to-reach tumors [11–15]. However, physicians should be aware of potential adverse events that may negatively affect patient outcome. Awareness, early identification, and the implementation of preventive and intervening measures may reduce the incidence and severity of complications [16].

This chapter will address the general complications that are associated with IRE and suggest safety-enhancing procedures. Several general anesthesiology-related issues, such as pain management and the use of synchronized pulsing with the

---

K. Nielsen, MD, PhD

Department of Surgery, VU University Medical Center,  
de Boelelaan 1117, 1081, HV, Amsterdam, The Netherlands

L.G.P.H. Vroomen, MD (✉) • A.H. Ruarus, MD • H.J. Scheffer, MD, PhD

Department of Radiology and Nuclear Medicine, VU University Medical Center,  
de Boelelaan 1117, 1081, HV, Amsterdam, The Netherlands

e-mail: [la.vroomen@vumc.nl](mailto:la.vroomen@vumc.nl)

ardiac cycle to prevent arrhythmias, have been discussed in Chap. 6 (*Anesthetic Management During Irreversible*,

*Electroporation Procedures*). Organ-specific complications are summarized here but discussed more extensively in the various chapters in part IV.

IRE-related complications can be divided into three categories:

- General risks associated with the procedure
- Risks associated with probe placement
- Risks associated with the pulsed electrical field

---

## 7.1 Risks Associated with the General Procedure

Patient selection is crucial for treatment success in any type of tumor [17]. A multidisciplinary team should evaluate eligibility of the patients, based on (1) medical history and physical examination, with specific emphasis on contraindications for IRE, (2) laboratory assessment, and (3) appropriate preprocedural imaging to assess the stage of the disease (number, size, and location of lesion[s]). Patients with poor functional reserve (American Society of Anesthesiologists [ASA] performance status >3) at baseline should not be considered candidates for IRE.

A board-certified interventional radiologist, trained by one of the IRE proctors, should perform the IRE procedure. The preferred approach for IRE is topic of ongoing debate. Both methods have distinct advantages and disadvantages and none has proven yet to be generally superior over the other. Treatment approach should therefore be based on the experience of the performing physician. Since the open approach requires laparotomy, it enables the use of intraoperative ultrasound (US) for real-time differentiation between resectable and inoperable tumors and detection of micro-metastases. Furthermore, it gives the surgeon the possibility to manipulate overlying structures to protect them from damage.

The advantage of the less invasive percutaneous IRE-procedure is the use of CT-guidance. This allows for three-dimensional tumor measurements and evaluation of its relation to surrounding structures. Determining exact inter-electrode distances and electrode angulations is more accurate than with the US-guided open approach. The length of hospital stay is in favor of the percutaneous procedure due to lower complication rates. Nonetheless, both approaches mandate extensive experience with image-guided tumor ablation.

In postoperative bedridden patients, thromboembolic complications can occur, which can represent a dangerous event in terms of mortality and morbidity with high social impact and costs. Postprocedural administration of low-molecular-weight heparin (LMWH) until the patient has regained daily activity has proven to be an effective and safe method to prevent these events [18]. After major abdominal surgery there is evidence to even continue LMWH for a month after surgery [19].

Infection is a major concern after oncological interventions, depending on the site treatment and is more often encountered after open procedures [20]. Maximum sterile precautions are therefore mandatory. The issue of prophylactic antibiotic

agents for tumor ablation is controversial, with some operators administering them universally and others only in selected cases. There have been no randomized controlled trials on antibiotic agent use in patients undergoing tumor ablation; at present, most of the published data pertaining to this topic relate to the personal experience of various groups [21].

Although percutaneous tumor ablation is generally considered a clean procedure, pancreatic and hepatic IRE in the presence of a biliary enteric anastomosis, biliary stent placement, and after sphincterotomy should qualify as clean-contaminated procedures, due to retrograde enteric bacterial communication with the biliary tract. In these procedures, prophylactic antibiotics are usually recommended [20]. Furthermore, if during an IRE procedure stomach or bowel is traversed, an additional dose of antibiotics is often administered. In the absence of definitive scientific evidence, many practitioners continue the empirical use of prophylaxis.

Different infectious complications, like pneumonia, surgical site infections or urinary tract infections more frequently occur in patients who underwent laparotomy. Adequate precautions should be taken, like early urinary catheter removal, early mobilization and physical therapy, and adequate pain management (see Chap. 6).

The protracted extended-arm positioning required for CT-guided IRE is known to cause postural perioperative peripheral nerve injury (PPNI). Optimum patient positioning with the limbs preferably placed in natural position without stretching nerves, muscles, tendons, and vessels is helpful to reduce the risk of neural impairment [22]. To achieve safe and optimum positioning, foam wedges, cushions, vacuum bag systems, or dedicated positioning molds can be used.

---

## 7.2 Risks Associated with Probe Placement

The key to a successful and safe ablation is meticulous treatment planning and per-procedural imaging. The required number of electrodes and their configuration should be determined based on features such as tumor shape and size, and its relation to critical structures that are at risk for injury [17].

During open IRE surrounding structures are often visible and can be moved or manipulated by the surgeon to some extent. The position of the electrodes is confirmed by intraoperative ultrasound, as is the relation of the probes to structures within the target organ. Eligibility for IRE should be questioned in case of transmucosal tumor invasion into surrounding intestines like the duodenum, considering the risk for ulceration and/or bleeding [23, 24]. Since bowel transgression may contaminate the sterile ablation zone, traversing the duodenum or colon with one or more probes should preferably be avoided during percutaneous IRE. Pneumo-, hydro-, and balloon-dissection as well as the so-called lever technique are safe, low-cost, and technically easy-to-perform maneuvers during percutaneous IRE to create space between intra-abdominal structures (Fig. 7.1). As previously stated, supplementary antibiotic prophylaxis is recommended if traversing the intestinal tract is inevitable.

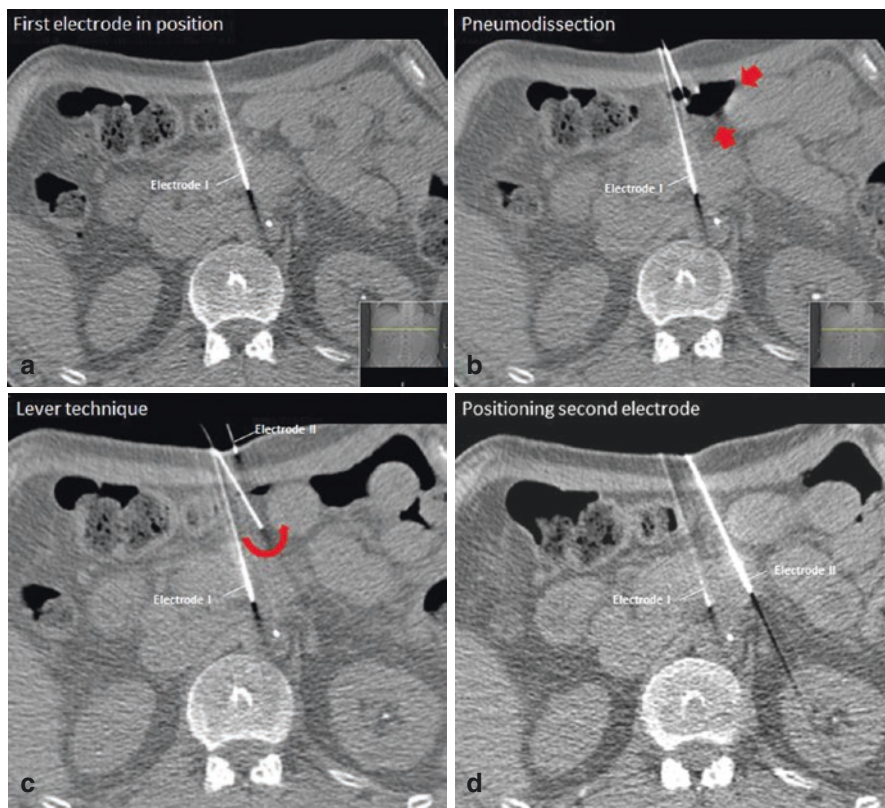


**Fig. 7.1** CT fluoroscopy images during IRE. (a) Positioning the first electrode. (b) Pneumodissection with CO<sub>2</sub> (red arrows) to obtain distance from the adjacent small bowel. (c) Lever technique with the pneumodissection needle (curved red arrow) which is deviating the small bowel laterally during the introduction of the second electrode. (d) Positioning of the second electrode passing by the small bowel

CT imaging is crucial for probe placement during percutaneous interventions, but tumor delineation is often poor on unenhanced CT. When using an intravenous contrast agent the interventionist is restricted to a certain time-window after administration. Since the maximum dose of intravenous contrast material is already reached after one or two contrast injections, repetitive monitoring is precluded. Repeated imaging is mandatory during the multiple probe placements required for IRE. To allow repeated and real-time visualization of the tumor and adjacent vessels without exceeding the contrast threshold, a flush catheter can be placed in the proximal abdominal aorta (for pancreatic IRE) or in the superior mesenteric artery (for hepatic IRE) prior to the procedure. Through this catheter, small amounts of diluted contrast are administered allowing accurate contrast enhanced imaging throughout the ablation. This improves safety and accuracy of electrode placement, while reducing the total dose of contrast administration (Fig. 7.2) [25].

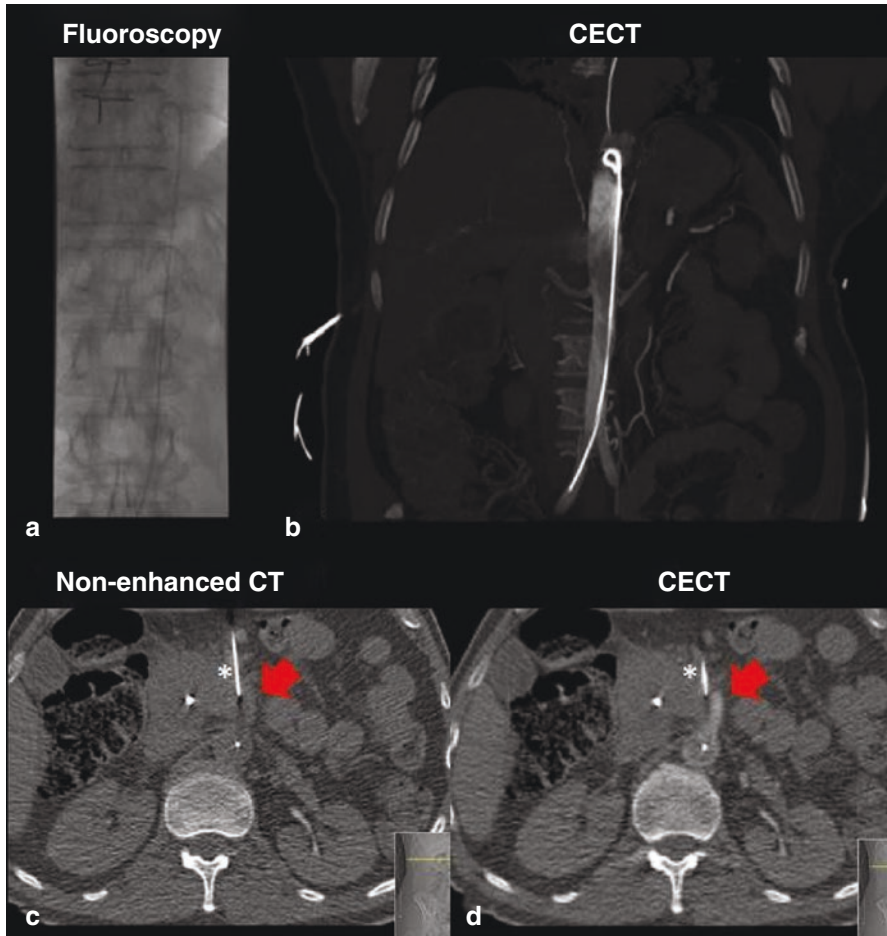


**Fig. 7.2** (a) Flush catheter placed in the abdominal aorta cranial of the visceral arteries. (b) Flush catheter used to inject small amounts of contrast on CT to allow repeated and real-time visualization of the tumor and adjacent vessels. (c) Nonenhanced CT with flush catheter in the aorta; celiac trunk is not visualized within the pancreatic mass (*red arrow*) and safe electrode positioning (*asterisk*) cannot be confirmed. (d) Catheter-based ceCT showing contrast in the celiac trunk (*red arrow*) within the pancreatic mass and the safe position of the electrode (*asterisk*) next to the celiac trunk

Adverse events associated with needle insertion (e.g., pneumothorax, hemorrhage, biliary tract injury) are more often encountered with IRE than with other ablation techniques, presumably due to the higher number of required insertions, the necessity for parallel probe placement in order to promote homogeneous energy delivery, and the fact that difficult-to-reach lesions are often centrally located and by definition surrounded by critical structures [26]. The recommended inter-electrode distance for each electrode-pair is 1.5–2.0 cm. Larger lesions require exponentially

more electrodes and overlapping ablations are usually necessary to obtain a complete ablation including a tumor-free margin [27]. The likelihood for adverse events as well as incomplete tumor coverage resulting in residual tumor increases with the number of electrodes [28].

To minimize the risk of per-procedural bleeding, coagulation abnormalities should be verified and corrected if necessary, aiming at an INR value of <1.20 and an APTT value of 25–40s.

### 7.3 Preventing Risks Associated with Pulsed Electrical Field Exposure

The application of multiple cycles of short and intense (up to 3000 Volt) electrical pulses presents several challenges in the anesthetic management that need to be anticipated and can lead to various site-specific complications (Table 7.1). These complications are discussed in detail in the concerning chapters.

In accordance to the working mechanism of IRE, vascular structures should theoretically remain intact [4–6]. However, vessel thrombosis and hemorrhage have

**Table 7.1** Site-specific AEs associated with IRE

Organ	Complication(s)	Incidence <sup>a</sup>	Severity
<i>Liver</i> [12]	Bile duct occlusion	Intermediate	Major
	Portal vein thrombosis/occlusion	Intermediate	Major
	Cholangitis	Low	Major
	Hemothorax	Low	Major
	Pneumothorax	High	Minor
	Pleural effusion	Intermediate	Minor
<i>Pancreas</i> [12, 36]	Portal vein thrombosis/occlusion	Intermediate	Major
	Pancreatitis	Intermediate	Minor – Major
	Bile leak	Low	Major
	Pancreaticoduodenal fistula	Low	Minor – Major
	Hematoma	Low	Minor
	Duodenal wall necrosis or leakage	Low	Major
<i>Kidney</i> [12]	Ureter obstruction	Low	Major
	Transient hematuria	High	Minor
	Adrenal ablation	Low	Minor
<i>Lung</i> [12]	Parenchymal hemorrhage	Intermediate	Major
	Pneumothorax	Very high	Minor
<i>Prostate</i> [36]	Transient potency loss	Intermediate	Minor
	Hematuria and/or debris	Intermediate	Minor
	Dysuria	Low	Minor
	Urinary tract infection	Low	Minor
	Urinary retention	Low	Minor
<i>Lesser pelvis</i> [37]	Neural function loss	High [38]	Major

<sup>a</sup>Classified as low-, intermediate-, high-, and very high risk if incidence <1%, ≥1 to <5%, ≥5 to <25%, and ≥25%, respectively

been reported post-IRE [29–31]. The most reported vessel-related complication post-IRE is thrombosis [11, 30]. The venous system might be more at risk for vascular damage than the arterial system, with the portal vein most often affected due to flow dynamics. Edema of the ablation zone following IRE may further stimulate progression of vessel thrombosis and obstruction due to compression [30]. In case of an acute vessel occlusion, arterial or portal vein stenting may be performed directly after IRE [24, 32]. For patients prone to a portal vein occlusion, based on a preexisting narrowed portal vein, the stenting procedure can be facilitated by inserting a catheter into the portal vein prior to the procedure, over which the stent can be easily deployed afterwards (Fig. 7.3).

Placement of a biliary endoprosthesis or PTC-drain prior to IRE is recommended in case of inadequate biliary drainage. Since an endoscopically placed biliary endoprosthesis (endoscopic retrograde cholangiopancreatography [ERCP]) allows for biliary drainage without the use of an indwelling external drain, this technique is considered the preferred treatment. In case of biliary

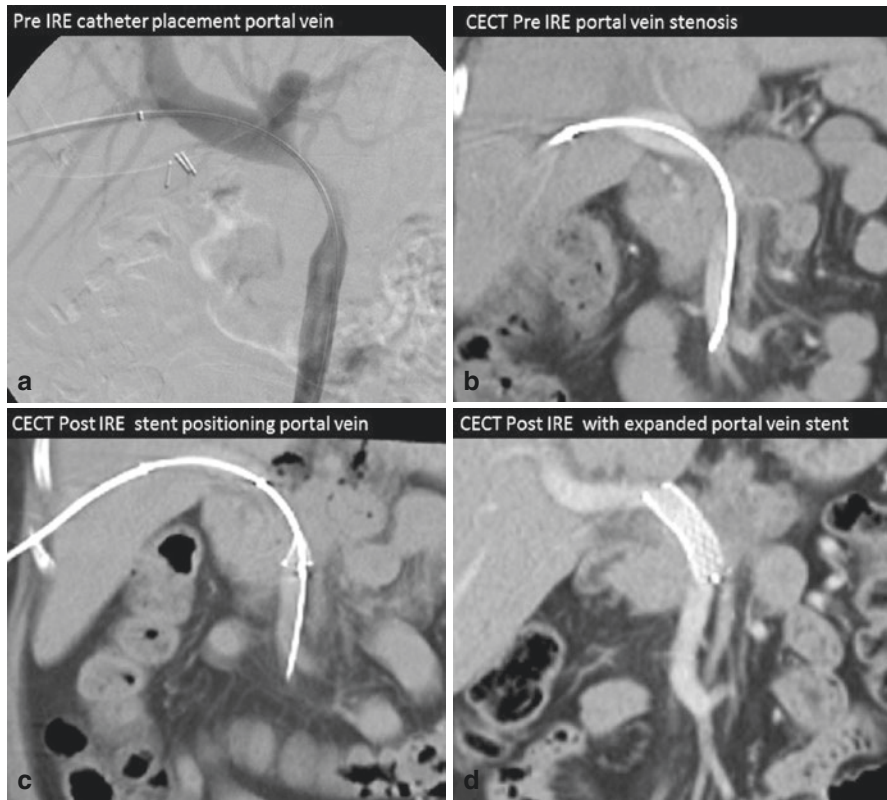


**Fig. 7.3** Portal vein stenting directly after IRE. (a) Catheter placement in the portal vein prior to IRE; (b) portal vein stenosis on ceCT prior to IRE; (c) stent positioning over the catheter after IRE; (d) expanded portal vein stent (Adapted from Vroomen et al. (submitted data))

obstruction in the weeks following IRE, placement of a biliary endoprosthesis through ERCP may be more difficult due to extensive swelling of the duodenal or ampullary area [24]. In the months following IRE, endoscopic placement may be hampered by IRE-induced fibrosis and remodeling of the ablated area. In these cases, percutaneous transhepatic bile duct drainage (PTCD) or rendez-vous techniques might be an option [33].

Direct contact between the active needle tip and vulnerable structures can cause thermal injury, as heat development of the electrodes during IRE has proven inevitable (see Chap. 9; *Thermal Effects of Irreversible Electroporation*) [10, 23, 34, 35]. Although a safety mechanism within the IRE system automatically turns off energy delivery in case of overcurrent (>50 Ampère), thermal injury cannot be completely excluded. To avoid potential thermal damage, the distance between the active tip of the electrode and heat-susceptible bile ducts or vessels should be at least 2 mm [12]. Voltage, pulse length, interelectrode distance, active tip length, and electrode configuration each have a strong effect on temperature development and distribution during IRE. Sequential pulsing may reduce the temperature rise and consequently the extent and volume of thermal damage [34]. Further research should demonstrate whether this is truly beneficial with respect to procedural safety and whether this does not compromise ablation zone size and oncologic efficacy.

---

## References

1. Date RS, Siriwardena AK. Radiofrequency ablation of the pancreas. II: intra-operative ablation of non-resectable pancreatic cancer. A description of technique and initial outcome. *JOP*. 2005;6(6):588–92.
2. Howard JH, et al. Radiofrequency ablation for unresectable tumors of the liver. *Am Surg*. 2008;74(7):594–600. discussion 600–1
3. Tanabe KK, et al. Radiofrequency ablation: the experts weigh in. *Cancer*. 2004;100(3):641–50.
4. Ahmed M, et al. Image-guided tumor ablation: standardization of terminology and reporting criteria—a 10-year update. *J Vasc Interv Radiol*. 2014;25(11):1691–705. e4
5. Bower M, et al. Irreversible electroporation of the pancreas: definitive local therapy without systemic effects. *J Surg Oncol*. 2011;104(1):22–8.
6. Golberg A, Yarmush ML. Nonthermal irreversible electroporation: fundamentals, applications, and challenges. *IEEE Trans Biomed Eng*. 2013;60(3):707–14.
7. Lee EW, et al. Advanced hepatic ablation technique for creating complete cell death: irreversible electroporation. *Radiology*. 2010;255(2):426–33.
8. Maor E, et al. The effect of irreversible electroporation on blood vessels. *Technol Cancer Res Treat*. 2007;6(4):307–12.
9. Cannon R, et al. Safety and early efficacy of irreversible electroporation for hepatic tumors in proximity to vital structures. *J Surg Oncol*. 2013;107(5):544–9.
10. Silk MT, et al. Percutaneous ablation of peribiliary tumors with irreversible electroporation. *J Vasc Interv Radiol*. 2014;25(1):112–8.
11. Martin RC 2nd, et al. Treatment of 200 locally advanced (stage III) pancreatic adenocarcinoma patients with irreversible electroporation: safety and efficacy. *Ann Surg*. 2015;262(3):486–94. discussion 492–4
12. Scheffer HJ, et al. Irreversible electroporation for nonthermal tumor ablation in the clinical setting: a systematic review of safety and efficacy. *J Vasc Interv Radiol*. 2014;25(7):997–1011. quiz 1011



13. Silk M, et al. The state of irreversible electroporation in interventional oncology. *Semin Intervent Radiol.* 2014;31(2):111–7.
14. Thomson KR, et al. Investigation of the safety of irreversible electroporation in humans. *J Vasc Interv Radiol.* 2011;22(5):611–21.
15. van den Bos W, et al. The safety and efficacy of irreversible electroporation for the ablation of prostate cancer: a multicentre prospective human in vivo pilot study protocol. *BMJ Open.* 2014;4(10):e006382.
16. Rampersaud YR, et al. Intraoperative adverse events and related postoperative complications in spine surgery: implications for enhancing patient safety founded on evidence-based protocols. *Spine (Phila Pa 1976).* 2006;31(13):1503–10.
17. Lencioni R, et al. Image-guided ablation of malignant liver tumors: recommendations for clinical validation of novel thermal and non-thermal technologies - a western perspective. *Liver Cancer.* 2015;4(4):208–14.
18. Holzheimer RG. Low-molecular-weight heparin (LMWH) in the treatment of thrombosis. *Eur J Med Res.* 2004;9(4):225–39.
19. Bergqvist D, et al. Duration of prophylaxis against venous thromboembolism with enoxaparin after surgery for cancer. *N Engl J Med.* 2002;346(13):975–80.
20. Sutcliffe JA, et al. Antibiotics in interventional radiology. *Clin Radiol.* 2015;70(3):223–34.
21. Venketasan AM, et al. Practice guideline for adult antibiotic prophylaxis during vascular and interventional radiology procedures. *J Vasc Interv Radiol.* 2010;21:1611–30.
22. Sawyer RJ, et al. Peripheral nerve injuries associated with anaesthesia. *Anaesthesia.* 2000;55(10):980–91.
23. Martin RC 2nd, et al. Irreversible electroporation therapy in the management of locally advanced pancreatic adenocarcinoma. *J Am Coll Surg.* 2012;215(3):361–9.
24. Scheffer HJ, et al. Ablation of locally advanced pancreatic cancer with percutaneous irreversible electroporation: results of the phase I/II PANFIRE study. *Radiology.* 2017;282(2):585–97.
25. van Tilborg AA, et al. Transcatheter CT arterial portography and CT hepatic arteriography for liver tumor visualization during percutaneous ablation. *J Vasc Interv Radiol.* 2014;25(7):1101–11. e4
26. Miklavcic D, et al. A validated model of in vivo electric field distribution in tissues for electrochemotherapy and for DNA electrotransfer for gene therapy. *Biochim Biophys Acta.* 2000;1523(1):73–83.
27. Ren H, et al. Treatment planning and image guidance for radiofrequency ablation of large tumors. *IEEE J Biomed Health Inform.* 2014;18(3):920–8.
28. Martin RC, et al. Irreversible electroporation of unresectable soft tissue tumors with vascular invasion: effective palliation. *BMC Cancer.* 2014;14:540.
29. Martin RC 2nd, et al. Irreversible electroporation in locally advanced pancreatic cancer: potential improved overall survival. *Ann Surg Oncol.* 2013;20(Suppl 3):S443–9.
30. Narayanan G, et al. Vessel patency post irreversible electroporation. *Cardiovasc Intervent Radiol.* 2014;37(6):1523–9.
31. Philips P, Hays D, Martin RC. Irreversible electroporation ablation (IRE) of unresectable soft tissue tumors: learning curve evaluation in the first 150 patients treated. *PLoS One.* 2013;8(11):e76260.
32. Ekici Y, et al. Arterial complication of irreversible electroporation procedure for locally advanced pancreatic cancer. *World J Gastrointest Oncol.* 2016;8(10):751–6.
33. Testoni PA, et al. Papillary cannulation and sphincterotomy techniques at ERCP: European Society of Gastrointestinal Endoscopy (ESGE) clinical guideline. *Endoscopy.* 2016;48(7):657–83.
34. van den Bos W, et al. Thermal energy during irreversible electroporation and the influence of different ablation parameters. *J Vasc Interv Radiol.* 2016;27(3):433–43.
35. Trueba-Arguinarena FJ, de Prado-Otero DS, Poves-Alvarez R. Pancreatic adenocarcinoma treated with irreversible electroporation case report: first experience and outcome. *Medicine (Baltimore).* 2015;94(26):e946.

36. Wagstaff PG, et al. Irreversible electroporation: state of the art. *Onco Targets Ther.* 2016;9:2437–46.
37. Niessen C, et al. Palliative treatment of presacral recurrence of endometrial cancer using irreversible electroporation: a case report. *J Med Case Rep.* 2013;7:128.
38. Vroomen, L., et al. Irreversible electroporation to treat malignant tumor recurrences within the pelvic cavity: a case series. *Cardiovasc Intervent Radiol.* 2017. [Epub ahead of print].

---

# Treatment Planning, Needle Insertion, Image Guidance, and Endpoint Assessment

# 8

Lukas Philipp Beyer and Philipp Wiggermann

---

## 8.1 Treatment Planning

For IRE in curative intent, the entire tumor with an appropriate safety margin must be covered by a sufficiently strong electrical field. The exact threshold depends on the tissue type and IRE parameters including pulse duration and pulse number [1], but generally electric fields higher than 600 V/cm are recommended [2]. To achieve this, exact placement of two up to six electrodes around and/or inside the tumor at precisely defined distances is necessary. For large tumors requiring more than six electrodes, they can be repositioned to perform overlapping ablations.

In contrast to thermal ablation modalities, IRE can be used to treat tumors in the immediate vicinity of large vascular structures and heat-sensitive structures such as nerves or bile ducts. The distribution of the electric field depends on the position of the electrodes and the conductivity of the tissue and is influenced by higher conductivity of blood vessels [3]. All electrodes should be placed as parallel as possible to each other to ensure homogenous energy fields.

This means that careful planning of the electrode placement is mandatory to achieve complete ablation [4]. The NanoKnife generator includes a simple graphical simulation of the ablation zone. The probes can be arranged on a grid by the user and the anticipated ablation zone is displayed. Specific ablation procedure parameters can be defined for each probe pair, and the changes are reflected in the graphical representation of the ablation zone. The configuration of the ablation zone should cover the entire tumor and a tumor-free margin [5]. Because the ablation area extends only a few millimeters outward of the electrodes, they should be placed neighboring to the tumor [6] to ensure adequate safety margin.

---

L.P. Beyer, MD, PhD • P. Wiggermann, MD, PhD (✉)  
Department of Radiology, University of Regensburg, Regensburg, Germany  
e-mail: [philipp.wiggermann@ukr.de](mailto:philipp.wiggermann@ukr.de)

However, the NanoKnife simulation does not consider the local electric field distribution, which is the most important factor for successful ablation with IRE. Therefore, software tools have been developed which allow patient-specific treatment planning including medical image segmentation and numerical optimization of the treatment parameters. They build a three-dimensional model of the target tissue from the CT or MRI images and use this model to optimize the treatment parameters.

The web-based GO-SMART environment for planning of minimal invasive cancer treatment was cofounded by the European Union [7]. It allows segmentation of the patient scan, the setup of the ablation parameters including electrode positions, and the numerical simulation of the ablation lesion. It also allows registration of the actual applicator positions from the CT data and re-running the simulation with the actual positions.

In clinical practice the use of software-based planning and simulation for IRE treatment is often waived because of time constraints. The electrodes are then placed freehand with a desired separation of 20 mm, which has been shown to be an effective treatment distance, e.g., for hepatic IRE [8].

---

## 8.2 Needle Insertion and Image Guidance

Depending on the tumor type and location, the IRE electrodes can be positioned either percutaneously under CT or ultrasound guidance or intraoperatively. While the electrode placement is like RFA or MWA, parallel placement of multiple electrodes with a maximum distance of 2.0 cm can be very challenging [9]. Limited stability of the 19 gauge IRE electrodes as compared to MW or RF needles makes it more difficult to correct a needle deviation. Therefore, ablation of deep-seated and hard-to-image lesions highly depends on the experience of the interventionalist and can be very time-consuming. For example, for CT-guided percutaneous ablation of liver tumors, the average duration for placement of the IRE electrodes was 87 min [10].

In case of ultrasound guidance for needle placement, electromagnetic tracking-based fusion imaging with computed tomography/magnetic resonance (CT/MR) images can be a valuable tool, especially for the liver and prostate [11] interventions. The fused CT or MR images show the same plane as the ultrasound image and are calculated in real time. For hard-to-visualize lesions in conventional b-mode, contrast-enhanced US (CEUS) can be fused to improve lesion detection.

Because CT enables multiplanar reconstruction and the surrounding structures, we prefer CT guidance for liver and pancreas ablations over ultrasound. CT fluoroscopy is a valuable tool to reduce intervention times. It is an acquisition mode that allows continuous image update using in-room table control. After the initial, often contrast-enhanced planning scan, the electrodes are placed using CT fluoroscopy for repeated checking of the needle position until all needles are placed in the required position. Additional spiral CT scans of the liver can be performed during the intervention to check probe positions.

One major drawback of CT-guided IRE is the bad visibility of the tumor and adjacent vessels, making safe probe placement difficult. Several techniques were suggested to enhance tumor and vessel delineation. To reduce the contrast dose “bolus chasing” or “low tube voltage,” CT protocols can be used subsequently enabling the repeated administration of contrast agent [12, 13]. For hepatic IRE, a catheter can be placed in the hepatic artery for the repeated administration of small doses to enable real-time repetitive CT fluoroscopy [14] of the tumor and the surrounding vessels. Similarly, for ablation of pancreatic lesions, the placement of a catheter in the proximal abdominal aorta has been suggested [15].

The development of numerous navigation systems for ablation brings the opportunity for higher accuracy and faster intervention times. Several different commercially available systems and techniques exist, all with different benefits and disadvantages [16].

The available navigation systems can generally be divided into two different classes: those which are fixed absolutely or relatively to the patient and use “robotic” movements for needle placement and those which use optical or electromagnetic tracking of the electrodes.

We are currently aware of two vendors in the first group. Both support planning of several parallel trajectories which makes them suitable for IRE electrode placement. The devices from PerfInt are registered on the floor at a fixed position and come with a stereotactic arm with a five-DOF axis. The iSys1 is attached to the treatment table and includes radiopaque markers on the device for semiautomatic registration in the CT scan. Its application in IRE is currently limited by its restricted range of motion; therefore several manual repositionings each followed by new registration scans might have to be performed for one ablation.

To ensure a sufficient target current, it is possible to apply test pulses between each electrode combination (usually ten pulses of 1,500 V/cm with a duration of 70  $\mu$ s). If the applied current lies outside the desired range (usually 20–50 A), the voltage settings can be manually adjusted. After adjustment, the remaining pulses can be administered. If the tumor is too large for the maximum exposure of 2 cm, one or multiple pullbacks of the electrodes with subsequent re-ablations can be performed.

---

### 8.3 Ablation Monitoring and Endpoint Assessment

Intraoperative monitoring and post-ablation imaging are key to control the success of ablation [17]. Awareness of post-IRE imaging findings is of the utmost importance to assess technical efficacy as well as to ensure long-term ablation success and for the early detection of local recurrence post ablation. Unfortunately, much is still unknown about the specific imaging findings after IRE.

For hepatic IRE, the practicability of real-time monitoring has been confirmed in human studies. Typically, a small area with gas forms around the tip of the probes, probably caused by electrolysis of water into hydrogen gas and oxygen, which appears as a small hyperechoic area in B-mode ultrasound. Depending on the electroporation protocol used, these small gas bubbles may also cover the entire ablation

zone. The ablation zone appears as a hypoechoic area immediately after ablation. During the next 15 min, this zone progressively becomes more isoechoic, and a peripheral hyperechoic rim starts to form 90–120 min after ablation. This peripheral rim was shown to best correlate with the pathologic findings [18] of necrosis/apoptosis in the ablation area. In addition, contrast-enhanced ultrasound may offer an additional advantage by improved delineation of the tumor, respectively, the ablation area.

For short- and long-term follow-up after IRE of hepatic tumors, contrast-enhanced CT (ceCT) and MRI (ceMRI) are the most commonly used imaging modalities. Animal studies investigating hepatic IRE showed that ablation area in histological specimen correlates well with the non-enhancing area in both ceCT and ceMRI [19, 20], making both imaging modalities suitable to ensure complete coverage of the tumor and assessment of the safety margin [21]. Like thermal ablation, a transient peripheral rim of contrast enhancement can be detected after IRE, reflecting reactive hyperemia [22, 23]. Gas formation can also be noted on CT. When evaluating ceCT or ceMRI after IRE of hypervascular liver tumors, care should be taken not to confuse this rim with residual tumor tissue [24].

MRI is particularly useful for assessing the outcome after IRE of non-enhancing liver tumors and if contrast media is not suitable. On T2-weighted sequences, most liver metastases appear hyperintense compared to the surrounding liver tissue. After IRE, the ablation area shows a hypointense central area, surrounded by a hyperintense reactive rim probably caused by edema. The hypointense area showed a high correlation with the pathologically confirmed ablation zone in an animal study in rodent liver. Therefore, native MRI with T2-weighted sequences can be a useful alternative to ceCT or ceMRI imaging for follow-up [20].

Routinely ceCT 1 day post ablation is performed to exclude complications, ceMRI for further follow-up after 6 weeks, and at regular intervals of 3 months to rule out local disease progression.

While PET-CT seems to be superior to CT or MRI alone regarding the detection of local progression after thermal ablation of colorectal liver metastases, no comparable data has been published for IRE [25]. Three days after IRE, an FDG-avid peripheral rim can be depicted, which may be due to an increasing metabolic activity at the periphery of the ablation zone. This peripheral increase of FDG uptake usually disappears 1 month after IRE. Therefore, exclusion of residual tumor tissue with PET-CT should either be performed within 24 h after IRE or after the initial inflammatory reaction has resolved [21].

Only few studies exist that describe the role of imaging after pancreatic IRE [26, 27]. Both ceMRI and ceCT revealed an ill-defined ablation zone with absent or decreased contrast enhancement. Diffusion-weighted imaging (DWI) signal intensity decreased after ablation, and a focal hyperintense spot in the b800 DWI might be an early predictor of local tumor recurrence. Imaging 6 weeks after IRE showed a volume increase of the ablation zone, followed by a decrease during further follow-up. Analogous to hepatic IRE, small gas pockets are visible in the ablation area, probably because of electrolysis. The role of FDG PET-CT in follow-up after pancreatic IRE has not been investigated to date.

Even less data is available on the imaging features after IRE in prostates. While gray-scale TRUS is unable to visualize IRE ablation effects, CEUS shows a homogenous, non-perfused ablation zone [28]. Similarly, in ceMRI the ablation zone is visible as an area of non-contrast enhancement. T2-weighted imaging showed heterogeneous signal intensity with hypointense margins in some cases. Both CEUS and T2-weighted MRI showed a strong correlation of the ablation volume in imaging and pathologic findings. A midterm follow-up study using CEUS showed a significant involution of the prostate gland during the first 3 months and a significant decrease of the ablation zone during the first 6 months after IRE [29].

---

## References

1. Qin Z, Jiang J, Long G, Lindgren B, Bischof JC. Irreversible electroporation: an in vivo study with dorsal skin fold chamber. *Ann Biomed Eng.* 2013;41(3):619–29.
2. Neal RE 2nd, Garcia PA, Kavnaudias H, Rosenfeldt F, McLean CA, Earl V, et al. In vivo irreversible electroporation kidney ablation: experimentally correlated numerical models. *IEEE Trans Biomed Eng.* 2015;62(2):561–9.
3. Marcan M, Kos B, Miklavcic D. Effect of blood vessel segmentation on the outcome of electroporation-based treatments of liver tumors. *PLoS One.* 2015;10(5):e0125591.
4. Kos B, Voigt P, Miklavcic D, Moche M. Careful treatment planning enables safe ablation of liver tumors adjacent to major blood vessels by percutaneous irreversible electroporation (IRE). *Radiol Oncol.* 2015;49(3):234–41.
5. Sofocleous CT, Sideras P, Petre EN. “How we do it” – a practical approach to hepatic metastases ablation techniques. *Tech Vasc Interv Radiol.* 2013;16(4):219–29.
6. Scheffer HJ, Nielsen K, van Tilborg AA, Vieveen JM, Bouwman RA, Kazemier G, et al. Ablation of colorectal liver metastases by irreversible electroporation: results of the COLDFIRE-I ablate-and-resect study. *Eur Radiol.* 2014;24(10):2467–75.
7. Voigt P FJ, Petersen TO, Flanagan R, Pollari M, Payne, Fütterer, J, Portugaller H, Fischer S, Zangos S, Kahn T, Kolesnik M, Moche M. The development of a simulation tool for the clinical use in image guided percutaneous tumor ablations – the Go-Smart project. 96 th German Röntgenkongress; Hamburg, Germany 2015.
8. Ball C, Thomson KR, Kavnaudias H. Irreversible electroporation: a new challenge in “out of operating theater” anesthesia. *Anesth Analg.* 2010;110(5):1305–9.
9. Lu DS, Kee ST, Lee EW. Irreversible electroporation: ready for prime time? *Tech Vasc Interv Radiol.* 2013;16(4):277–86.
10. Beyer LP, Pregler B, Michalik K, Niessen C, Dollinger M, Muller M, et al. Evaluation of a robotic system for irreversible electroporation (IRE) of malignant liver tumors: initial results. *Int J Comput Assist Radiol Surg.* 2017;12(5):803–09.
11. Lee MW. Fusion imaging of real-time ultrasonography with CT or MRI for hepatic intervention. *Ultrasonography.* 2014;33(4):227–39.
12. Auler MA, Heagy T, Aganovic L, Brothers R, Costello P, Schoepf UJ. Saline chasing technique with dual-syringe injector systems for multi-detector row computed tomographic angiography: rationale, indications, and protocols. *Curr Probl Diagn Radiol.* 2006;35(1):1–11.
13. Marin D, Nelson RC, Samei E, Paulson EK, Ho LM, Boll DT, et al. Hypervascular liver tumors: low tube voltage, high tube current multidetector CT during late hepatic arterial phase for detection – initial clinical experience. *Radiology.* 2009;251(3):771–9.
14. van Tilborg AA, Scheffer HJ, Nielsen K, van Waesberghe JH, Comans EF, van Kuijk C, et al. Transcatheter CT arterial portography and CT hepatic arteriography for liver tumor visualization during percutaneous ablation. *J Vasc Interv Radiol.* 2014;25(7):1101–11. e4

15. Scheffer HJ, Vroomen LG, de Jong MC, Melenhorst MC, Zonderhuis BM, Daams F, et al. Ablation of locally advanced pancreatic cancer with percutaneous irreversible electroporation: results of the phase I/II PANFIRE study. *Radiology*. 2017;282(2):585–97.
16. Wood BJ, Kruecker J, Abi-Jaoudeh N, Locklin JK, Levy E, Xu S, et al. Navigation systems for ablation. *J Vasc Interv Radiol*. 2010;21(8 Suppl):S257–63.
17. Appelbaum L, Mahgerefteh SY, Sosna J, Goldberg SN. Image-guided fusion and navigation: applications in tumor ablation. *Tech Vasc Interv Radiol*. 2013;16(4):287–95.
18. Appelbaum L, Ben-David E, Sosna J, Nissenbaum Y, Goldberg SN. US findings after irreversible electroporation ablation: radiologic-pathologic correlation. *Radiology*. 2012;262(1):117–25.
19. Lee YJ, Lu DS, Osuagwu F, Lassman C. Irreversible electroporation in porcine liver: acute computed tomography appearance of ablation zone with histopathologic correlation. *J Comput Assist Tomogr*. 2013;37(2):154–8.
20. Zhang Y, Guo Y, Ragin AB, Lewandowski RJ, Yang GY, Nijm GM, et al. MR imaging to assess immediate response to irreversible electroporation for targeted ablation of liver tissues: preclinical feasibility studies in a rodent model. *Radiology*. 2010;256(2):424–32.
21. Neal RE II, Cheung W, Kavnaudias H, Thomson KR. Spectrum of imaging and characteristics for liver tumors treated with irreversible electroporation. *J Biomed Sci Eng*. 2012;5:813–8.
22. Dollinger M, Jung EM, Beyer L, Niessen C, Scheer F, Muller-Wille R, et al. Irreversible electroporation ablation of malignant hepatic tumors: subacute and follow-up CT appearance of ablation zones. *J Vasc Interv Radiol*. 2014;25(10):1589–94.
23. Kim YS, Rhim H, Lim HK, Choi D, Lee MW, Park MJ. Coagulation necrosis induced by radio-frequency ablation in the liver: histopathologic and radiologic review of usual to extremely rare changes. *Radiographics*. 2011;31(2):377–90.
24. Kim SK, Lim HK, Kim YH, Lee WJ, Lee SJ, Kim SH, et al. Hepatocellular carcinoma treated with radio-frequency ablation: spectrum of imaging findings. *Radiographics*. 2003;23(1):107–21.
25. Nielsen K, van Tilborg AA, Scheffer HJ, Meijerink MR, de Lange-de Klerk ES, Meijer S, et al. PET-CT after radiofrequency ablation of colorectal liver metastases: suggestions for timing and image interpretation. *Eur J Radiol*. 2013;82(12):2169–75.
26. Akinwande O, Ahmad SS, Van Meter T, Schulz B, Martin RC. CT findings of patients treated with irreversible electroporation for locally advanced pancreatic cancer. *J Oncol*. 2015;2015:680319.
27. Vroomen LG, Scheffer HJ, Melenhorst MC, de Jong MC, van den Bergh JE, van Kuijk C, et al. MR and CT imaging characteristics and ablation zone volumetry of locally advanced pancreatic cancer treated with irreversible electroporation. *Eur Radiol*. 2017;27(6):2521–31.
28. van den Bos W, de Bruin DM, van Randen A, Engelbrecht MR, Postema AW, Muller BG, et al. MRI and contrast-enhanced ultrasound imaging for evaluation of focal irreversible electroporation treatment: results from a phase I-II study in patients undergoing IRE followed by radical prostatectomy. *Eur Radiol*. 2016;26(7):2252–60.
29. Beyer LP, Pregler B, Niessen C, Michalik K, Haimerl M, Stroszczyński C, et al. Percutaneous irreversible electroporation (IRE) of prostate cancer: contrast-enhanced ultrasound (CEUS) findings during follow up. *Clin Hemorheol Microcirc*. 2016;64(3):501–06.



---

# Thermal Effects of Irreversible Electroporation

# 9

Eran van Veldhuisen, J.A. Vogel, J.H. Klaessens,  
and R.M. Verdaasdonk

Although irreversible electroporation (IRE) is thought to be a nonthermal technique for the ablation of soft tissue, objective temperature measurements and mathematical models have shown that temperature increase during treatment can be significant. The nonthermal mechanism is thought to be caused by a disturbance in the cell's homeostasis through the formation of nanopores in the cell membrane, making it permeable for its contents. However, histologically, thermal damage is also observed. Therefore the mechanism of irreversible electroporation is presumed to be a combination of these effects. Thermal energy produced during treatment with IRE can both be a contributory factor to cell death and can potentially also be harmful in the presence of thermally vulnerable structures. Previous studies with purely thermal techniques in the pancreas and liver have shown potential severe morbidity such as bleedings and bile leakage.

Several IRE parameters, such as field strength and pulse durations, are linearly related to the production of thermal energy. This ought to be anticipated on by careful treatment planning. Moreover, tissue heterogeneities (both natural and artificial) such as vascular structures or metal stents can cause a redistribution of the electric field by an electric field sink effect. This can cause an inhomogeneous distribution of the electric field, which in turn can cause tumor recurrences. Further insight in these mechanisms is needed, in order to allow for optimization of treatment.

---

E. van Veldhuisen (✉) • J.A. Vogel  
Department of Surgery, Academic Medical Center,  
Amsterdam, The Netherlands  
e-mail: [e.vanveldhuisen@amc.uva.nl](mailto:e.vanveldhuisen@amc.uva.nl)

J.H. Klaessens • R.M. Verdaasdonk  
Department of Physics and Medical Technology, VU University Medical Center,  
Amsterdam, The Netherlands

## 9.1 Introduction

Irreversible electroporation (IRE) is an ablation technique that is supposedly not based on a thermal effect but which is rather based on high-voltage, low-frequency electrical pulses, damaging cell membranes by creating nanoscale pores, causing loss of homeostasis and cell death by both apoptosis and necrosis [18]. Hence the origin of the term “electroporation” suggests that pores are created in cell membranes with the use of electric energy. However, previously published experiments performing temperature measurements during ablation with IRE have shown that temperature increase through IRE can be significant in certain cases (e.g. high pulse numbers, durations, or number of electrodes) to cause thermal damage [8, 26]. Therefore, consensus on the mechanism of work of IRE has not been realized yet. It is presumed that, through this nonthermal mechanism, IRE can be used as an alternative for purely thermal-based ablation techniques such as radiofrequency ablation. These thermal techniques can be contraindicated for the treatment of a malignancy in case of near presence or involvement with thermally vulnerable structures such as the duodenum, bile ducts, or blood vessels. Moreover, treatment efficacy of these techniques can be hampered by a heat sink effect due to cooling down of the ablation zone through the relatively cool blood flow [24]. However, vital structures have shown to remain structurally unharmed while performing IRE on tissue with these structures traversing the ablation zones [10]. Yet the question remains whether all effects of IRE are of a nonthermal origin. Contrary to the belief that the production of heat is an unwanted side effect of IRE, a possible thermal effect could also be used to enhance tissue damage, thus increasing the efficacy of ablation. Besides heat sink, other factors such as inhomogeneities (both artificial and natural) may also affect the distribution of the ablation zone. However, a validated model for prediction of the ablation zone has not been realized yet, due to the limited insight in the mechanism of work of IRE and factors that contribute to an altered distribution of the ablation zone.

---

## 9.2 The Theoretical Mechanism

The exact mechanism of inducing cell death by irreversible electroporation remains unknown. The mechanism of permeabilization of cell membranes by electrical pulses is widely used in order to deliver larger structures into the cell cytoplasm, such as DNA in electrogene therapy and large medicine molecules in electrochemotherapy [20]. It is believed that IRE causes a disturbance in the cell’s homeostasis, either by permeabilization of the cell membrane through the formation of nanopores in the lipid bilayer, thermal damage to the cell, or, most expectedly, a combination of these effects [8, 18]. Likewise, tissue treated with IRE shows both characteristics of apoptosis and necrosis while performing histological evaluation [8]. Apoptosis often leads to regeneration of treated tissue, in contrast to necrosis, which leads to the formation of fibrotic scar tissue. Therefore cell death induced by apoptosis has

preference over necrosis. IRE is thought to cause relatively more apoptosis, compared to purely thermal techniques. This makes IRE a potentially beneficial technique in addition to contemporary focal therapy. Yet thermal damage is often seen while performing histological evaluation of IRE-treated tissue [8]. This can be explained by the Joule heating effect, where electric energy is converted to thermal energy while passing through a resistor [26]. However, the ratio between an IRE effect and a thermal effect remains under discussion.

### 9.3 The Nonthermal Spectrum of Pulsed Electrical Fields

The effect of electroporation through permeabilization of the cell membrane is caused by the appliance of electrical pulses across the cell [18]. Under normal conditions, the cell membrane is impermeable for free diffusion of cell contents. Electroporation causes the electrochemical potential around the cell membrane to change, therefore inducing instabilities in the polarized cell membrane lipid bilayer. The shape of the membrane is altered, forming aqueous pathways, so-called nanopores, which causes the cell's contents to diffuse freely through the cell membrane.

The presumable electroporation effect through permeabilization of the cell membrane is thought to be the result of an induced transmembrane potential through the appliance of an electric field:  $\Delta\phi m$ .

$\Delta\phi m$  can be quantitatively determined with the following equation:

$$\Delta\phi m = -1.5 E \times f(\sigma) \times r \times \cos\theta$$

- $\Delta\phi m$  Potential difference at a specific location of cell membrane
- $E$  Electric field strength in V/cm
- $r$  Cell radius
- $\theta$  Angle of the radial direction vector
- $f(\sigma)$  Resultant function of cell's electrical conductivity

As a result of the induced membrane potential, the cell's membrane becomes permeable for free diffusion of the cell's contents, which induces cell death through apoptosis [10].

Electroporation is previously determined by measurements of change in membrane impedance of cells subjected to an electric field. This effect can both be reversible and irreversible. Only irreversible electroporation causes cell death, whereas reversible electroporation is associated with cell survival. The difference in outcome between irreversible and reversible electroporation is based on the strength of the electric field and the duration of the applied pulses. Multiple studies have demonstrated the nonthermal effects of IRE, using freeze-fracture studies, mathematical models, tissue conductivity, and membrane impedance measurements during treatment with IRE. In these studies, a domain of electrical pulse parameters

was determined that can cause irreversible tissue damage, but with negligible thermal effects [3]. In general, thermal damage is assumed to be caused by temperatures exceeding 50 °C.

Edd and colleagues measured temperature increase during an *in vivo* experiment. Although the ablation zones near the edges of the electrodes showed histological signs of thermal damage, the majority of the treated region showed macroscopic changes that were likely of a nonthermal origin [7]. The estimated temperature increase in these zones was 2–3 °C, which is insufficient to cause thermal damage. Similar results have been reported by Edd and Davalos in comparable experiments where a temperature increase of approximately 1.15 °C was measured [6]. Hence the fact is that tissue damage cannot be attributed to thermal damage but as a direct result of IRE. These findings are supported by *in vitro* experiments with liver cancer cells demonstrating that complete cell death can be achieved without thermal effects [14].

In case of a nonthermal mechanism of work, one of the main advantages of IRE over contemporary ablation techniques would be the lack of thermal damage. As a result, vital structures such as blood vessels, bile ducts, and nerves would remain structurally unharmed [10]. Moreover, the effect of IRE would in theory also not be impaired by the heat sink effect, whereas relatively cool blood flow can reduce the efficacy of treatment in example of contemporary thermal focal ablation therapies [24]. Therefore irreversible electroporation can potentially be an asset in the treatment of unresectable tumors.

---

## 9.4 The Thermal Effects of IRE

Although IRE is thought to be a nonthermal ablation technique, previous experiments have shown that there is in fact a detectable temperature increase during treatment, with significant results of thermal damage proved by histological evaluation [5]. Thermal damage in tissue is characterized macroscopically by white zones of coagulation [8]. On pathological evaluation, the ablation zones show signs of streaming cytoplasm and condensation of cell nuclei, the latter being referred to as “pyknosis” [1]. This is often seen surrounding the electrodes, where the highest temperatures during treatment are realized.

Higher temperatures are measured closer to the probes and are also reliant on tip exposure as shown in Figs. 9.1 and 9.2.

The increase of thermal energy is associated with higher electric field strengths, active tip lengths, interelectrode distances, and/or increasing pulse numbers, as shown in Figs. 9.2, 9.7, 9.8, and 9.9.

When pulses are delivered sequentially instead of continuously, the temperature decreases during each break. In addition, by extending the pause between the pulse series, the resultant temperature increase can be lowered.

Two *in vitro* [25, 26] and four *in vivo* studies [5, 8, 27, Vogel et al. 2016 (preliminary data)], have demonstrated the presence of a temperature increase when performing IRE. In the *in vitro* studies, a temperature increase was demonstrated, which was higher with a larger number of pulses, larger pulse duration, or larger interelectrode distance. Two *in vivo* studies demonstrated that when settings used

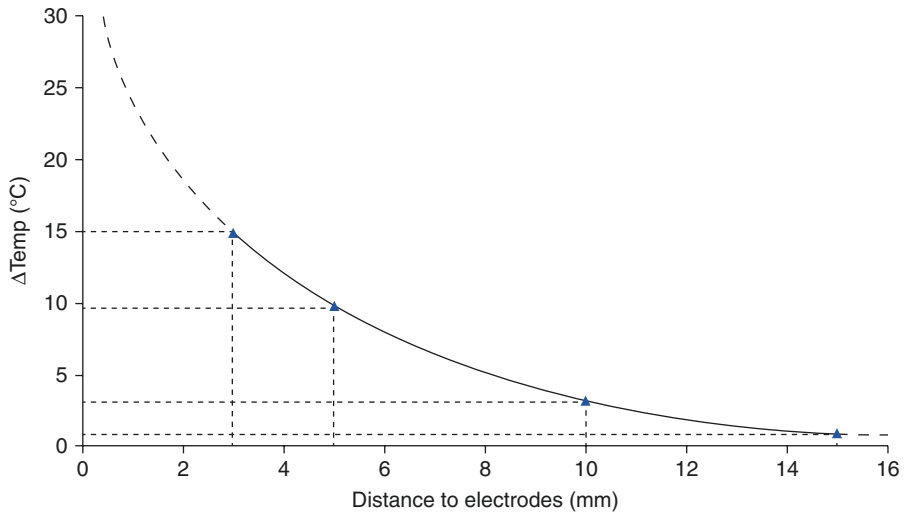


**Fig. 9.1** Exponential curve shows temperatures at different distance to the electrodes [26]

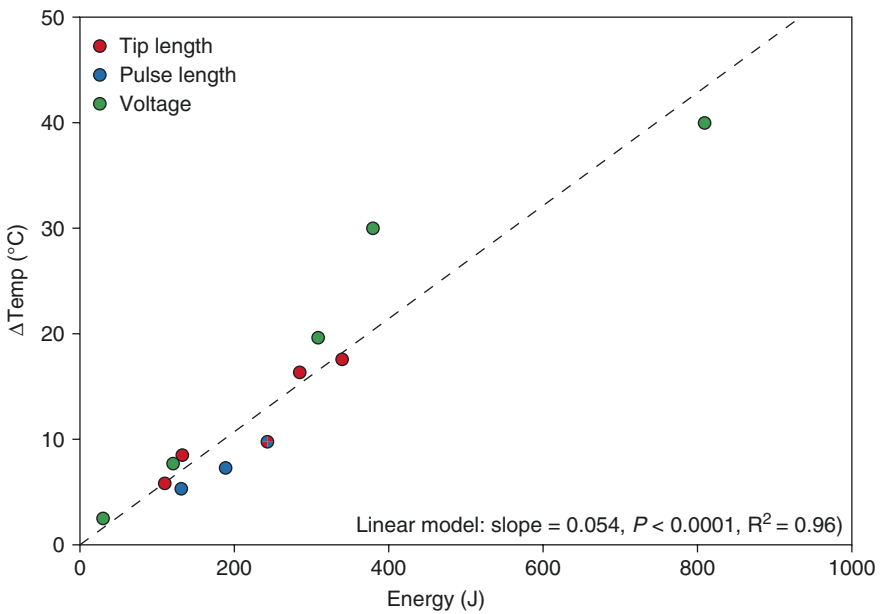


**Fig. 9.2** Linear fitting of all temperature measurements versus the total delivered energy for all conditions in which the distance between the electrodes was constant (15 mm) [26]

are within the advised range, no thermal damage is present. In one study, where IRE in the pancreas and liver of healthy pigs was performed, thermal damage was reported according to the previously mentioned characteristics. With the use of standard settings, no thermal damage was observed, while it appeared present when >270 pulses were used or a voltage of >2,000 V/cm and only in pancreatic tissue. In the second study, IRE was performed only in liver tissue, and thermal damage was defined as classic findings of gross and histopathologic coagulation necrosis and expression of heat-shock protein-70 (HSP-70). Thermal damage was most distinct when temperatures exceeded 60 °C, whereas purely IRE-based histological features were seen below 42 °C.

The other two *in vivo* studies [5, 27], performing IRE in healthy kidney, liver, and pancreas tissue, demonstrated a mean temperature increase of 21.5 °C, 13.6 °C, and 10.7 °C for the kidney, liver, and pancreas, respectively. This was accompanied by pathological damage in the study by Wagstaff et al. characterized as a pale region of discoloration, while the study by Vogel et al. did not report on pathology.

The temperature rise in a volume of tissue can be predicted with a simple model based on calorimetry. One calorie (= 4.2 J) is the amount of energy necessary to increase the temperature of a volume of 1 cm<sup>3</sup> water (= 1 g) with 1 °C. The temperature increase of a given volume can then be calculated according to the formula:

$$\Delta T = \frac{E}{v}$$

- $E$  energy in J
- $V$  volume in cm<sup>3</sup>

However, due to thermal conduction, the thermal energy produced during ablation will dissipate in a larger volume, and blood perfusion will therefore act as a heat sink. Depending on the time frame in which the energy is delivered, this cooling effect becomes more prominent.

An estimation of the maximum temperature increase during treatment with IRE can be made by assuming an ideal situation with a negligible effect of perfusion (no heat sink) and by assuming the tissue as virtually 100% water (which is ~80% in reality).

IRE pulses at 2,000 V, 20 A, with a duration of 90 μs will result in the production of ~2 J of energy.

The heated volume around two electrodes spaced 1 cm apart can be calculated by assuming the electrode tips as two cylinders of 2 cm in length and 1 cm in diameter (=4 cm<sup>3</sup>) (Fig. 9.3).

Pulses are delivered with a sequence of 90 pulses per minute, which results in the following equation:

$$P = I \times V \sim 4 \text{ J per pulse}$$

And thus  $90 \times 4 \text{ J} = 360 \text{ J}$  for 90 pulses.

**Fig. 9.3** Simplified model of IRE with an IED of 1 cm

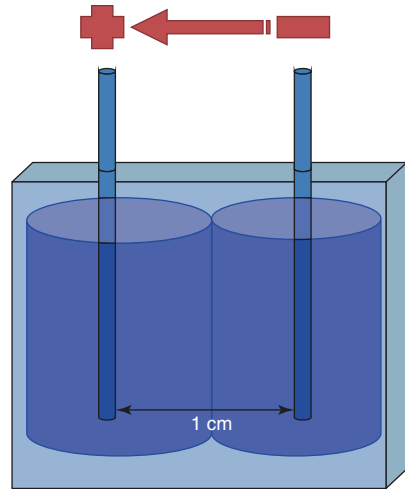
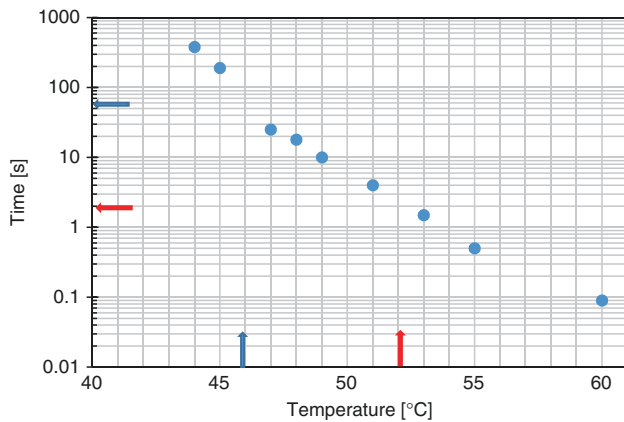


**Fig. 9.4** Time–temperature threshold curve for human skin constructed from Moritz [17]



The estimated maximum temperature rise depending on electrode distance is shown in Fig. 9.8. The resulting temperature will decrease slowly by heat dissipation or more quickly when there is blood perfusion.

Assuming the maximum temperature rise would only be half the calculated value, the temperature levels and time exposure of the tissue for over 60 s can easily result in permanent tissue damage as shown in the Arrhenius integral (Fig. 9.4). Although this is a straightforward and simplified model, this can be used as a rule of thumb to estimate the maximum temperature rise using an ablation technique that produces thermal energy in biological tissues. However, due to the perfusion of the viable tissue which results in a heat sink effect and the assumption that the treated tissue exists for a 100% out of water, the overall thermal energy produced during treatment with IRE is overestimated by definition according to this model.

## 9.5 Arrhenius Integral

Many articles have been published on thermal tissue damage related to the temperature increase over a time period [4, 11, 12, 16, 21, 22]. In basic the Arrhenius reaction rate (1889) and the Henriques–Moritz damage model (1947) describe the total thermal damage over time from  $t = 0$  to  $t = \tau$

$$\begin{aligned}\Omega(t) &= \int_0^{\tau} A e^{-\frac{E_a}{RT(t)}} dt \\ &= \ln \left\{ \frac{C(0)}{C(\tau)} \right\}\end{aligned}$$

- $c(t)$  Concentration of living cells at time  $t$
- $c(0)$  Initial concentration of living cells
- $R$  Universal gas constant
- $A$  “Frequency” factor for the kinetic expression ( $s^{-1}$ )
- $E_a$  Activation energy for the irreversible damage reaction ( $J \text{ mol}^{-1}$ )

The  $A$  and  $E_a$  are the Arrhenius coefficients that must be acquired experimentally, and for different tissues these are available in literature. With the Arrhenius integral and the Arrhenius coefficients, the tissue damage can be calculated for time–temperature exposures. In Fig. 9.4 the time–temperature damage thresholds for human skin are shown [17] from experimental findings. If we take, for example, a temperature increase of 10 °C, tissue damage will occur from 60 s or longer. And for a temperature increase of 15 °C, tissue damage will occur already after 2 s. Therefore we can predict that IRE causes thermal damage in certain cases.

---

## 9.6 The Influence of Electrical Field Inhomogeneities on the Distribution of Thermal Energy

### 9.6.1 Natural Inhomogeneities

The development of thermal energy is inherent to delivering a large electrical power to a tissue, which can be seen as a resistor. However, the amount of thermal energy differs with settings. Secondly, an increase could also differ in the presence of different tissue heterogeneities. For example, the presence of large vascular structures or vessel clusters could lead to redistribution of the generated thermal energy, thereby lowering the temperature increase [9]. This could hypothetically reduce treatment efficacy.

Secondly, the presence of heat sink effect was demonstrated, where temperature increase was much higher in ablations of tissue distant from large blood vessels, while temperature increased only barely in the proximity of large vessels, both in the pancreas and in liver tissue. However, the effects of this heat sink on pathological outcomes remain unknown.



As with heat sink, large vascular structures and vessel clusters can also cause heterogeneous distribution of electric field strength, known as electric field sink. Golberg et al. performed an observational study for electric field distribution in the presence of natural heterogeneities such as vascular structures [9]. The results of this experiment showed a relevant redirection of electric field strength in the presence of vascular structures. Histologically, cell survival was observed in regions with reduced field strength, whereas zones distant to vascular structures showed extensive hepatocyte cell death. Not merely a decrease in field intensity was measured; zones with increased field strength were also observed. This can be of significant importance during treatment, whereas the presence of natural heterogeneities and thus redistribution of the electric field can significantly reduce the effect of treatment and possibly lead to tumor survival.

### 9.6.2 Artificial Inhomogeneities

At last, the presence of metal parts in the ablation zone could lead to a redistribution of electrical and thermal energy [25].

However a case report was published by Mansson et al. where a patient with a metal bile duct stent was treated with IRE and died of a serious complication of duodenal and colon perforation and bleeding from a branch of the superior mesenteric artery, leading to great concerns of IRE around a metal stent [13]. The causality between the stent and the complication could not be established. Scheffer et al. demonstrated a higher temperature increase at the electrode tips when a metal stent was present in the ablation zone, without direct heating of the metal stent, but, contrarily, a remaining rim of vital tissue, immediately surrounding the stent [25]. Also Dunki-Jacobs et al. have demonstrated a difference in temperature increase when metal implants (stents and clips) are present in the ablation area; however, specific details on these experiments were not provided [5].

Moreover, Neal et al. performed experiments with expired radiotherapy seeds in ex and in vivo canine prostate and did not demonstrate a difference in the ablation. However, the lack of effect could be attributed to the small size of the seeds, while bigger implants could lead to a larger effect [19]. Ben-David and colleagues have demonstrated that grounded metal plates can result in pulling the electric field away from the positive electrode, towards the metal plate [2]. However, this effect should not be present in the case of ungrounded objects.

---

## 9.7 Thermal Energy as a Potentially Dangerous Side Effect

As in purely thermal-based ablation techniques such as radiofrequency ablation (RFA) or high-intensity focused ultrasound (HIFU), temperature increase during treatment with IRE can be of risk while performing treatment near structures that are vulnerable to thermal damage. As previously reported in experiments with RFA, thermal injury to traversing vital structures may cause a potential risk of bleeding (up to 22%), pancreatic fistulae (14%), or bile leaks in the pancreas (14%) [15]. The

increase in temperature caused by IRE cannot be neglected and can be of serious threat to these structures. Therefore careful treatment planning is crucial. On the other hand, structures such as blood vessels and bile ducts induce a heat sink effect, making these vital structures less prone to the potential thermal effects of irreversible electroporation [8].

## 9.8 Thermal Energy as a Contributory Element of IRE

Although thermal damage caused by IRE is often seen as an unwanted side effect, this feature could also be used as an enhancement of irreversible electroporation. Thermal damage is only seen surrounding the electrodes (Fig. 9.5), whereas the temperature during treatment decreases with distance to the electrodes. Therefore, the periphery of the ablation zone is less prone to thermal damage and cell death by means of necrosis. Vital structures can be avoided by careful treatment planning and placement of the electrodes. Moreover, by placing the electrodes centrally in and around the tumor, thermal damage could potentially enhance treatment efficacy as contributory factor to cell death.

Yet due to the fact that IRE is a relatively new technique and its mechanism of work has not fully been understood yet, not all parameters for homogeneous distribution of the ablation zone and optimal treatment settings can be predicted. As a result, inhomogeneous distribution of the ablation zone can lead to incomplete ablations [9], which, in turn, can cause tumor recurrences. This can be objectified by the multi-institutional, prospective study performed by Philips et al. from 2009 through 2012, where a total of 150 patients were treated primarily for liver and pancreatic tumors [23]. In total, after a median follow-up of 18 months, 31% tumor recurrences were reported. Therefore, better understanding of the distribution of the electric field and the influence of heterogeneities is needed, in order for better treatment planning and clinical outcomes.

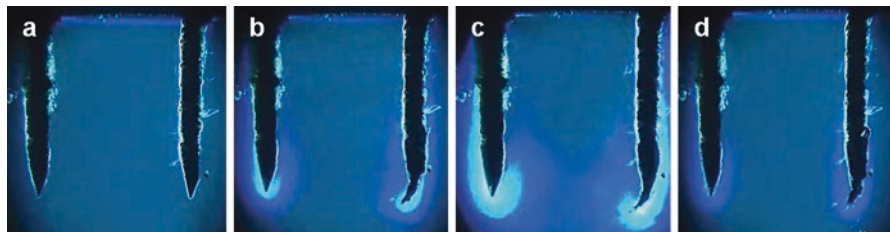
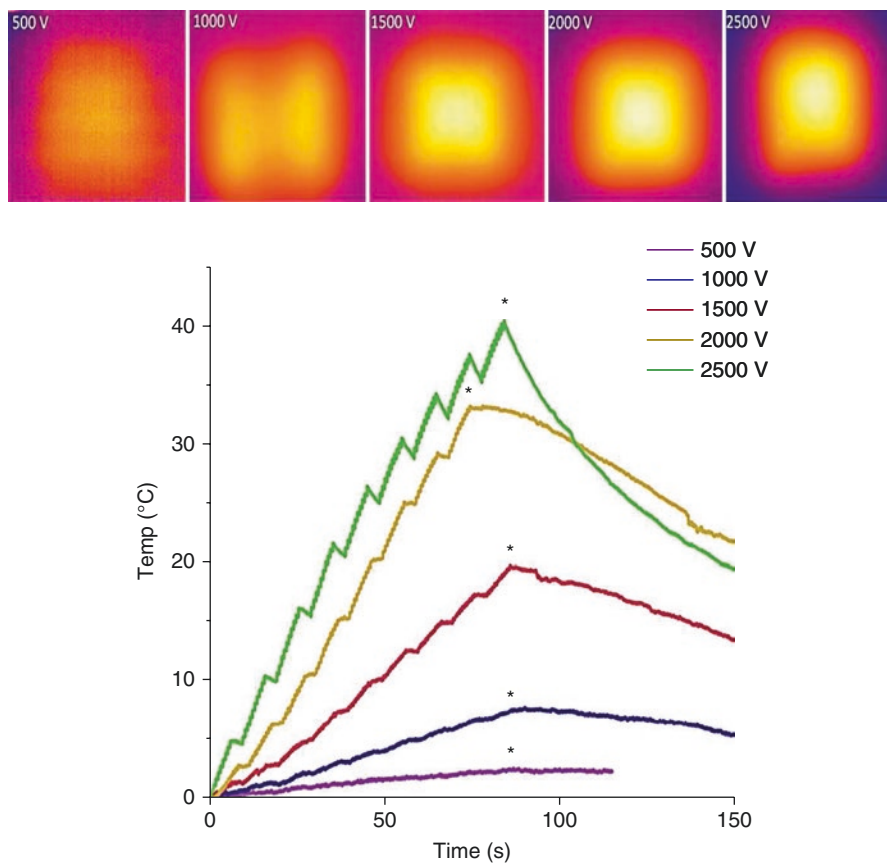


**Fig. 9.5** High-speed color schlieren images show the temperature gradient distribution during (a–c) an IRE pulse train of ten pulses and (d) the subsequent relaxation using default settings (15-mm interelectrode distance, 15-mm active tip length, delivering  $1 \times 90$  pulses with a pulse length of 90 ms, 90 pulses per minute, and pulse intensity of 1,000 V/cm) [26]



	Voltage (V/cm)	Energy (J)	$\Delta I$ (A)	$T_{\max}$ (°C)	$\Delta T$ (°C)	Error on $\Delta T$ (%)
—	500	30	1	13.7	2.5	$\pm 3$
—	1000	122	2	17.6	7.7	$\pm 4$
—	1500	310	11	30.5	19.6	$\pm 3$
—	2000	381	20	41.1	30.1	$\pm 2$
—	2500	810	17	59.7	40.4	$\pm 2$

**Fig. 9.6** Temperature increase ( $T$ ) and current development ( $A$ ) over time of various voltages and resultant dissipated energy in a gel experiment investigated with a thermal camera. *Asterisk* represents the end of pulse delivery [26]

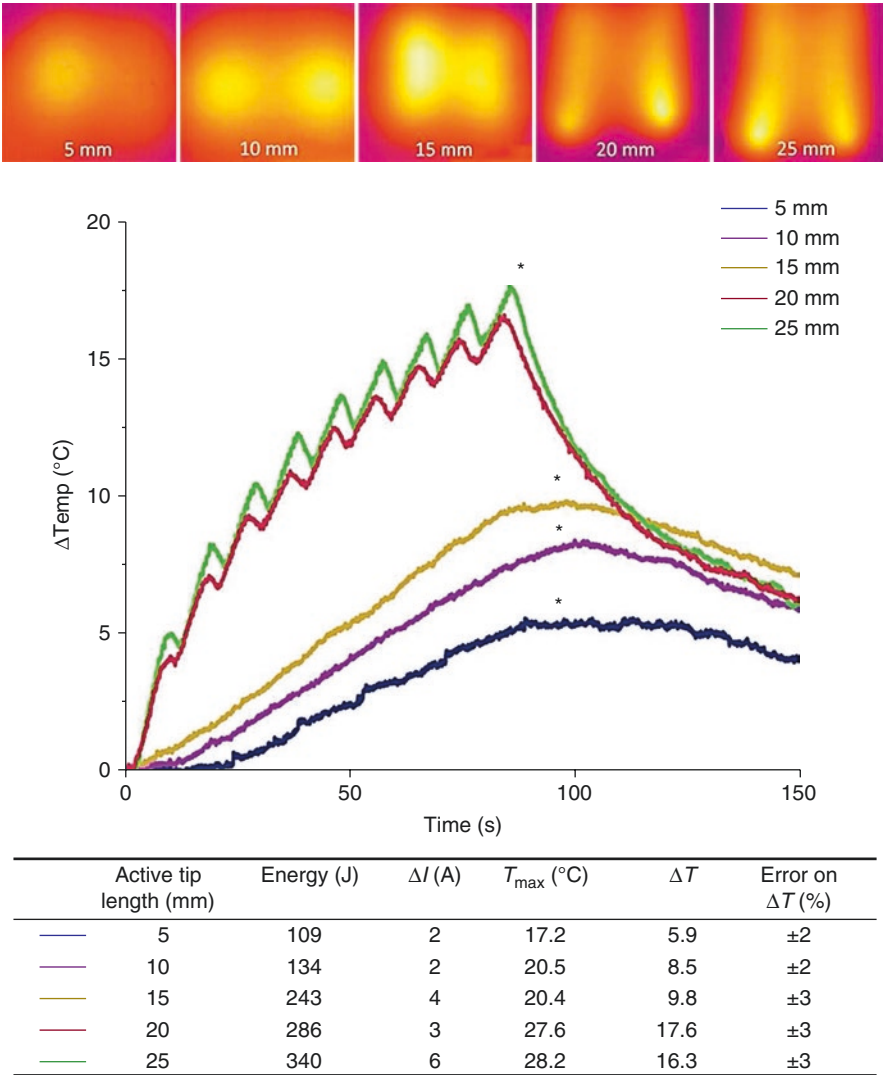
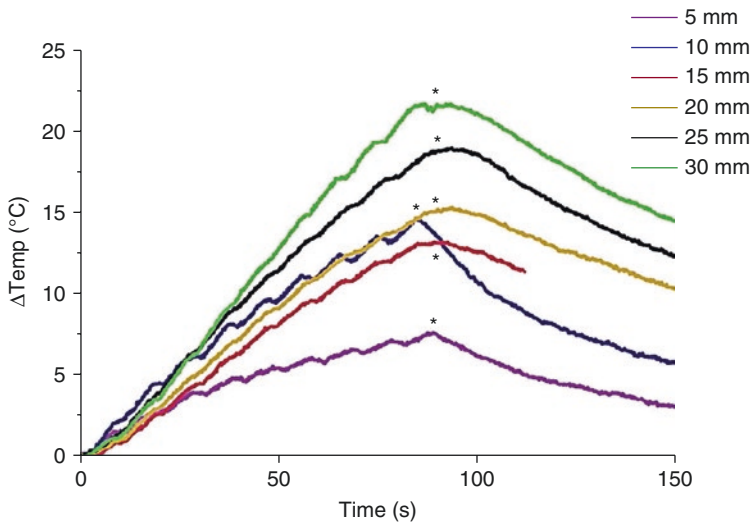
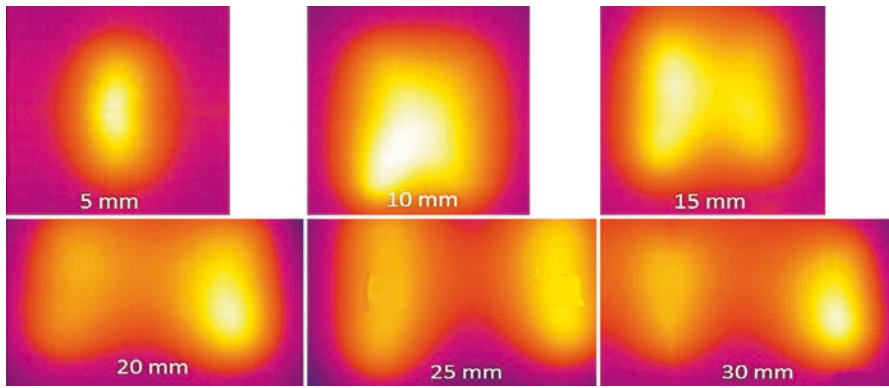
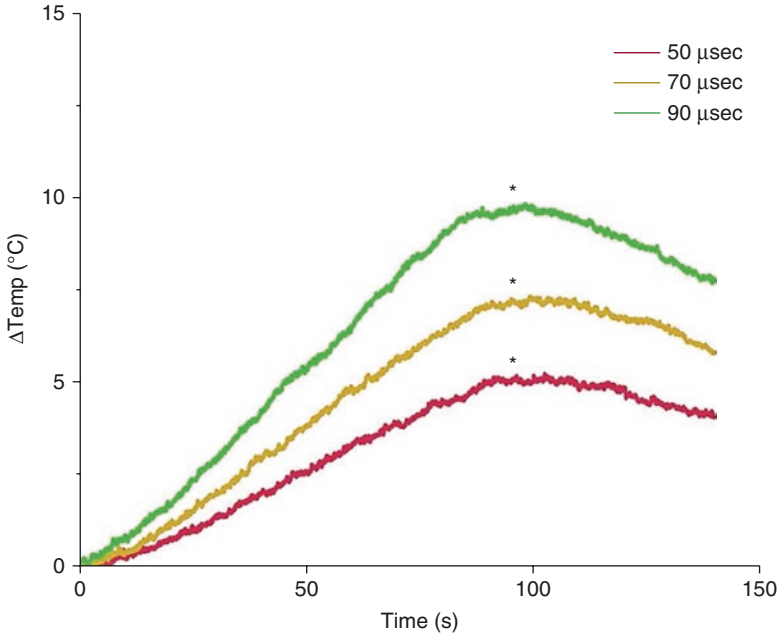


**Fig. 9.7** Temperature ( $T$ ) and current development ( $A$ ) over time for various active tip lengths and resultant total dissipated energy in a gel experiment investigated with a thermal camera. Asterisk represents the end of pulse delivery [26]



	Interelectrode distance (mm)	Energy (J)	$\Delta I$ (A)	$T_{max}$ (°C)	$\Delta T$	Error on $\Delta T$ (%)
—	5	57	2	17.7	7.6	$\pm 3$
—	10	122	2	25.1	14.6	$\pm 3$
—	15	243	4	24.2	13.4	$\pm 3$
—	20	413	7	25.3	15.1	$\pm 2$
—	25	608	10	31.6	18.9	$\pm 2$
—	30	899	10	36.5	21.5	$\pm 2$

**Fig. 9.8** Temperature ( $T$ ) and current development ( $A$ ) over time for various interelectrode distances with 1,000 V/cm and resultant total dissipated energy in a gel experiment investigated with a thermal camera. Asterisk represents the end of pulse delivery [26]



	Pulse length ( $\mu\text{s}$ )	Energy (J)	$\Delta I$ (A)	$T_{\text{max}}$ ( $^{\circ}\text{C}$ )	$\Delta T$	Error on $\Delta T$ (%)
—	50	132	3	17.3	5.3	$\pm 4$
—	70	189	4	19.3	7.3	$\pm 4$
—	90	243	4	20.4	9.8	$\pm 3$

**Fig. 9.9** Temperature ( $T$ ) and current development ( $A$ ) over time of various pulse lengths and dissipated energy in a gel experiment investigated with a thermal camera. Asterisk represents the end of pulse delivery [26]

## Conclusion

Although the effect of IRE is supposed to be of a nonthermal origin, several experiments have objectified the increase in thermal energy during ablation. This is not merely an unwanted side effect, but may also contribute to cell death. However, damage to structures that are vulnerable to temperature increase can cause severe morbidity during treatment. This ought to be anticipated on by careful treatment planning. Moreover, tissue heterogeneities may cause inhomogeneous distribution of the electric field, which may lead to incomplete ablations and thus tumor recurrence. Therefore, more insight is needed in the mechanism of work of irreversible electroporation to allow for clinical optimization.

## References

1. Appelbaum L, Ben-David E, Sosna J, Nissenbaum Y, Goldberg SN. US findings after irreversible electroporation ablation: radiologic-pathologic correlation. *Radiology*. 2012;262(1):117–25.
2. Ben-David E, Ahmed M, Faroja M, Moussa M, Wandel A, Sosna J, Appelbaum L, Nissenbaum I, Goldberg SN. Irreversible electroporation: treatment effect is susceptible to local environment and tissue properties. *Radiology*. 2013;269(3):738–47.
3. Davalos RV, Rubinsky B, Mir LM. Theoretical analysis of the thermal effects during in vivo tissue electroporation. *Bioelectrochemistry*. 2003;61(1–2):99–107.
4. Dewhirst MW, Viglianti BL, Lora-Michiels M, Hoopes PJ, Hanson M. Thermal dose requirement for tissue effect: experimental and clinical findings. *Proc SPIE Int Soc Opt Eng*. 2003;4954:37.
5. Dunki-Jacobs EM, Philips P, Martin RC 2nd. Evaluation of thermal injury to liver, pancreas and kidney during irreversible electroporation in an in vivo experimental model. *Br J Surg*. 2014;101(9):1113–21.
6. Edd JF, Davalos RV. Mathematical modeling of irreversible electroporation for treatment planning. *Technol Cancer Res Treat*. 2007;6(4):275–86.
7. Edd JF, Horowitz L, Davalos RV, Mir LM, Rubinsky B. In vivo results of a new focal tissue ablation technique: irreversible electroporation. *IEEE Trans Biomed Eng*. 2006;53(7):1409–15.
8. Faroja M, Ahmed M, Appelbaum L, Ben-David E, Moussa M, Sosna J, Nissenbaum I, Goldberg SN. Irreversible electroporation ablation: is all the damage nonthermal? *Radiology*. 2013;266(2):462–70.
9. Golberg A, Bruinsma BG, Uygun BE, Yarmush ML. Tissue heterogeneity in structure and conductivity contribute to cell survival during irreversible electroporation ablation by “electric field sinks”. *Sci Rep*. 2015;5:8485.
10. Golberg A, Yarmush ML. Nonthermal irreversible electroporation: fundamentals, applications, and challenges. *IEEE Trans Biomed Eng*. 2013;60(3):707–14.
11. Henriques FC Jr. Studies of thermal injury; the predictability and the significance of thermally induced rate processes leading to irreversible epidermal injury. *Arch Pathol (Chic)*. 1947;43(5):489–502.
12. Henriques FC, Moritz AR. Studies of thermal injury: I. The conduction of heat to and through skin and the temperatures attained therein. A theoretical and an experimental investigation. *Am J Pathol*. 1947;23(4):530–49.
13. Mansson C, Nilsson A, Karlsson BM. Severe complications with irreversible electroporation of the pancreas in the presence of a metallic stent: a warning of a procedure that never should be performed. *Acta Radiol Short Rep*. 2014;3(11):2047981614556409.
14. Miller L, Leor J, Rubinsky B. Cancer cells ablation with irreversible electroporation. *Technol Cancer Res Treat*. 2005;4(6):699–705.
15. Moir J, White SA, French JJ, Littler P, Manas DM. Systematic review of irreversible electroporation in the treatment of advanced pancreatic cancer. *Eur J Surg Oncol*. 2014;40(12):1598–604.
16. Moritz AR. Studies of thermal injury: III. The pathology and pathogenesis of cutaneous burns. An experimental study. *Am J Pathol*. 1947;23(6):915–41.
17. Moritz AR, Henriques FC. Studies of thermal injury: II. The relative importance of time and surface temperature in the causation of cutaneous burns. *Am J Pathol*. 1947;23(5):695–720.
18. Neal RE 2nd, Davalos RV. The feasibility of irreversible electroporation for the treatment of breast cancer and other heterogeneous systems. *Ann Biomed Eng*. 2009;37(12):2615–25.
19. Neal RE 2nd, Smith RL, Kavnoudias H, Rosenfeldt F, Ou R, McLean CA, Davalos RV, Thomson KR. The effects of metallic implants on electroporation therapies: feasibility of irreversible electroporation for brachytherapy salvage. *Cardiovasc Intervent Radiol*. 2013;36(6):1638–45.
20. Neumann E, Schaefer-Ridder M, Wang Y, Hofschneider PH. Gene transfer into mouse lyoma cells by electroporation in high electric fields. *EMBO J*. 1982;1(7):841–5.
21. Pearce JA. Models for thermal damage in tissues: processes and applications. *Crit Rev Biomed Eng*. 2010;38(1):1–20.

22. Pearce JA. Comparative analysis of mathematical models of cell death and thermal damage processes. *Int J Hyperth.* 2013;29(4):262–80.
23. Philips P, Hays D, Martin RC. Irreversible electroporation ablation (IRE) of unresectable soft tissue tumors: learning curve evaluation in the first 150 patients treated. *PLoS One.* 2013;8(11):e76260.
24. Pillai K, Akhter J, Chua TC, Shehata M, Alzahrani N, Al-Alem I, Morris DL. Heat sink effect on tumor ablation characteristics as observed in monopolar radiofrequency, bipolar radiofrequency, and microwave, using ex vivo calf liver model. *Medicine (Baltimore).* 2015;94(9):e580.
25. Scheffer HJ, Vogel JA, van den Bos W, Neal RE 2nd, van Lienden KP, Besselink MG, van Gemert MJ, van der Geld CW, Meijerink MR, Klaessens JH, Verdaasdonk RM. The influence of a metal stent on the distribution of thermal energy during irreversible electroporation. *PLoS One.* 2016;11(2):e0148457.
26. van den Bos W, Scheffer HJ, Vogel JA, Wagstaff PG, de Bruin DM, de Jong MC, van Gemert MJ, de la Rosette JJ, Meijerink MR, Klaessens JH, Verdaasdonk RM. Thermal energy during irreversible electroporation and the influence of different ablation parameters. *J Vasc Interv Radiol.* 2016;27(3):433–43.
27. Wagstaff PG, de Bruin DM, van den Bos W, Ingels A, van Gemert MJ, Zondervan PJ, Verdaasdonk RM, van Lienden KP, van Leeuwen TG, de la Rosette JJ, Laguna Pes MP. Irreversible electroporation of the porcine kidney: temperature development and distribution. *Urol Oncol.* 2015;33(4):168 e161–7.



---

## **Part IV**

# **Clinical Practice**

Karin Nielsen, Hester J. Scheffer, M. Petrousjka van den Tol,  
and Anders Nilsson

---

## 10.1 Introduction

The liver is a well-known site for tumors of benign as well as malignant origin. In the Western world, the most frequent hepatic malignancies encountered are liver metastases, especially but not solely from colorectal origin. Primary liver tumors, or the hepatocellular carcinoma (HCC), more frequently develop in people from Asian and Mediterranean countries. Although treatment of various solid tumors can be very different, they all have one thing in common. The only treatment option with curative intent is local treatment. Because nowadays several treatment modalities are available, diagnosis and treatment evaluation should be done by a specialized multidisciplinary (oncologic) liver team including a dedicated surgeon, an interventional and a diagnostic radiologist, a medical oncologist, a hepatologist, a radiation oncologist, a pathologist, and a nuclear medicine physician.

Historically, surgical resection is considered the gold standard for potentially curative treatment. However, site, size, and number of the tumor(s) can prohibit possibilities for a complete resection. Fortunately, the search for alternatives to achieve complete tumor eradication in a part of this patient population has already been started in the 1980s and is still continuing. Local tumor ablation has emerged as a popular alternative to broaden the therapeutic possibilities for a selection of these patients. The most well-known ablation technique for liver tumors is radiofrequency

---

K. Nielsen • M.P. van den Tol  
Department of Surgery, VU University Medical Center,  
de Boelelaan 1117, 1081 HV Amsterdam, The Netherlands

H.J. Scheffer (✉)  
Department of Radiology and Nuclear Medicine, VU University Medical Center,  
de Boelelaan 1117, 1081 HV Amsterdam, The Netherlands  
e-mail: [hj.scheffer@vumc.nl](mailto:hj.scheffer@vumc.nl)

A. Nilsson  
Department of Radiology, Uppsala University Hospital, 751 85 Uppsala, Sweden

ablation (RFA) and microwave ablation (MWA). Although very effective in selected cases, it is not suitable for all liver tumors. To overcome two limitations of thermal ablation, the heat sink effect and the risk for collateral damage to surrounding structures, the search for alternatives is ongoing. Irreversible electroporation has presented itself as a less thermal ablation technique that can offer a solution for tumors located in the hilum of the liver near large bile ducts and portal veins.

IRE is based on the pulsatile application of a strong electric field (1,000–1,500 V/cm) between electrodes inserted around the tumor. These electrical pulses alter the existing transmembrane potential. As a consequence, nanoscale defects appear in the lipid bilayer of the cell membrane. Depending on the amplitude and duration of the pulses, the permeability of the cell membrane is reversible after which the cell survives or irreversible after which the cell dies through loss of homeostasis [1]. Although IRE is believed to effectively destroy all cells within the ablation zone, the less thermal nature of IRE results in relative preservation of the extracellular matrix. Preclinical studies show that, as a result, the structural integrity of inlaying and adjacent tissue structures like blood vessels, bile ducts, nerves, and other vital structures is largely preserved [2–4]. Therefore, the technique possibly provides a solution for treatment of tumors located in the hilum of the liver.

---

## 10.2 Physiological and Anatomical Considerations

### 10.2.1 Segments

The liver, being the second largest organ in the human body, weighs about 1,200–1,800 g and is divided in the small left lobe (15% of the total weight) and the right lobe by the falciform ligament and the dorsal umbilical fissure.

The internal structure of the liver is preferably described by its functional anatomy rather than its morphological anatomy. Although on the outer surface of the liver there is an absence of visible anatomical boundaries, the liver is composed of eight different segments that are hemodynamically autonomous. The French surgeon and anatomist Claude Couinaud was the first to describe these functionally independent segments, allowing partial liver resections without damaging other segments. The current system to describe the internal anatomy was named after him (Fig. 10.1).

The first division is formed by the first bifurcation of the portal vein, dividing the liver into the left and right half. The second bifurcation of the left and right portal vein divides both halves in four portal sectors: right posterior, right anterior, left medial, and left anterior. These four sectors are separated by the left-middle and right hepatic veins. The plane in which the middle hepatic vein is located, which runs from the gallbladder to inferior caval vein, divides the left 1/3 and the right 2/3 hemiliver.

After a third bifurcation of the portal vein, all but one of the four sectors is divided in two autonomic segments with their own portal pedicle containing a bile duct, a portal vein branch, and an artery. Only the left anterior sector consists of one segment (segment II), which contains the left hepatic vein.

Segment I, or the caudate lobe, receives portal triads from both liver halves and has veins that drain directly into the vena cava. It lies on the left side of the vena

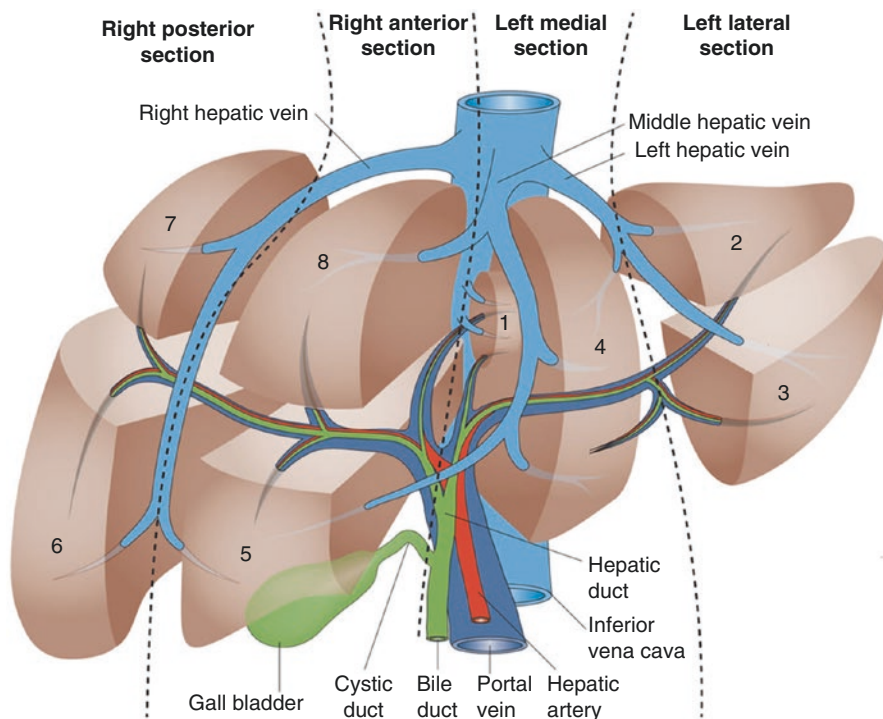


**Fig. 10.1** Claude Couinaud's segmental liver anatomy

cava somewhat hidden by the lesser omentum on the dorsal side of the liver. The caudate lobe is connected to the right liver half by the caudate process ventral of the vena cava and by the ligamentum vena cava on the dorsal side of the caval vein. Segments II, VII, and VIII have a close relation with the diaphragm; segment II lies especially close to the heart.

The location of the lobus caudatus, or segment I, has been described above. The remaining individual segments are numbered in a clockwise fashion starting superiorly in the left hemiliver. Segments II and III lie lateral to the left hepatic vein and falciform ligament with II superior and III inferior to the portal plane. Segment IV lies medial to the falciform ligament, between the left and middle hepatic veins. It is subdivided into IVa (superior) and IVb (inferior) subsegments. Segments V to VIII make up the right hemiliver. Segment V is located below the portal plane between the middle and right hepatic veins in close relation with the gallbladder. Segment VI is located below the portal plane lateral to the right hepatic vein and is related with the right kidney and the hepatic flexure of the colon. Segment VII is located above the portal plane lateral to the right hepatic vein and is mainly located retroperitoneal. Segment VIII is located above the portal plane between the middle and right hepatic veins and is closely related to the vena cava and the diaphragm.

### 10.2.2 Portal Triad

The portal triad consists of three main structures: arterial blood supply, branches of the portal venous system, and bile ducts.

The arterial blood supply is responsible for 25% of the total blood volume and 50% of oxygen supply. The proper hepatic artery originates from the celiac trunk. At the hepatoduodenal ligament, the proper hepatic artery divides in the right hepatic artery and the left hepatic artery. The intrahepatic course of the arterial blood flow follows the portal branches and bile ducts to the different segments, although the right hepatic artery often supplies segment IV. Ligation of the proper hepatic artery often leads to necrosis of the liver, depending on collateral circulation. Ligation of the left or right hepatic artery does not lead to necrosis because small intersegmental arteries between the left and right lobe will open within 24 h after ligation. Anatomical variation is as frequent as 40%.

The intrahepatic bile ducts follow the portal triads toward the hilum, where the right and left hepatic ducts unite to form the common hepatic duct. The right hepatic duct stretching only 1 cm is very short. In over 15% of the patients, there are anatomical variants. Sometimes bile ducts from segments V/VIII and VI/VII drain separately in the left hepatic duct, and occasionally segment VII/VIII has their own bile duct that terminates in the common bile duct.

The gallbladder is attached to liver segments IV and V. Depending on the localization of the tumor, a cholecystectomy prior to ablation can be mandatory.

The portal vein is responsible for 75% of hepatic blood flow and 50% of its oxygen supply. The superior mesenteric and splenic veins, together with the left and right gastric veins, compose the portal vein. It traverses the hepatoduodenal ligament, and at the hilum, there is a bifurcation in a short right and a longer left extrahepatic branch. The intrahepatic bifurcations are described above (“Segments”). Intrahepatic anastomoses between the portal system do not occur.

### 10.2.3 Venous Drainage

The venous drainage of the liver consists of three hepatic veins, although accessory veins exist in 15% of the patients. The right hepatic vein drains segment VI/VII and a part of V/VIII. The middle hepatic vein drains segment IVb completely and a part of segment IVa/V/VIII. The left hepatic vein drains segment II/III and part of IVa.

All three veins drain on the suprahepatic vena cava. The middle and the left veins often share a short common tract that enters the vena cava. This common vein has a longer extrahepatic course than the right vein. Segment I drains directly into the vena cava with multiple smaller veins.

---

## 10.3 Organ-Specific Disease: Solid Hepatic Tumors

Many different tumors from different origin can manifest in the liver parenchyma. The indication for IRE of nonsolid lesions has not yet been established and is therefore beyond the scope of this chapter.

### 10.3.1 Benign

#### 10.3.1.1 Hepatocellular Adenoma

Hepatocellular adenoma (HCA) is a relative uncommon benign tumor of the liver that occurs more frequently in women than in men. The female/male ratio ranges between 3.9:1 and 11:1 [5]. Over the years an association between oral contraceptives and hepatocellular adenoma emerged and was first described in the 1970s [6]. The relative risk ratios for HCA of women that had used contraceptives for more than 9 years were 25 compared to women that had used oral contraceptives for less than 1 year. Although uncommon in men, adenomas are associated with the use of anabolic steroids [7]. Other conditions associated with adenomas are androgenic steroids, beta-thalassemia, tyrosinemia, type 1 diabetes mellitus, hemochromatosis, barbiturate usage, and clomiphene intake.

Spontaneous development of an HCA into hepatocellular carcinoma is rare but possible in larger lesions. In addition, these larger adenomas have the potential for spontaneous rupture and bleeding, possibly leading to shock. Therefore, when over 5 cm in diameter, local treatment of an HCA such as surgical resection, RFA, or embolization should be considered. During pregnancy, hormone-induced growth of a preexisting HCA can lead to spontaneous hemorrhage or rupture that may threaten the life of both mother and child. Hence, female patients with large (>5 cm) or hormone-sensitive adenomas are advised either to avoid pregnancy or to undergo invasive treatment prior to pregnancy [8–10]. When an adenoma occurs in the presence of a glycogen storage disease (types 1 and 3), it can also be a precursor of a hepatocellular carcinoma [11].

#### 10.3.1.2 Focal Nodular Hyperplasia (FNH)

This benign lesion of the liver is typically an incidental finding in women in their reproductive years. The origin of FNH is thought to be due to hyperplastic growth of normal hepatocytes with a malformed biliary draining system. It is also thought to be in response to a preexistent arteriovenous malformation [12]. When the diagnosis is certain, treatment is rarely indicated. Only large (>5 cm) lesions may be the cause of abdominal complaints, especially when located in the left liver lobe. The arterial supply is derived from the hepatic artery, whereas the venous drainage is into the hepatic veins. FNH does not contain portal venous supply. This makes this lesion especially vulnerable to arterial embolization.

#### 10.3.1.3 (Giant) Hemangioma

Hepatic hemangioma is a benign, nonneoplastic hypervascular lesion, also known as a venous malformation. Its exact etiology is unknown; however, there might be a genetic component to its origin. Hemangiomas are the most frequently encountered benign liver tumors. Lesions over 5 cm are referred to as giant hemangiomas [13]. Although most hemangiomas are asymptomatic, larger lesions may produce a variety of symptoms including pain, fullness, nausea, vomiting, and fever. For patients with invalidating symptoms, the most renowned treatment is surgical resection. Unfortunately, surgical resection is associated with morbidity up to 27% and even a small risk of mortality [13–15]. Although mainly based on small case series and

case reports, radiofrequency ablation (RFA) has shown promising results in the recent literature for the less-invasive treatment of relatively small GCH with only minor complications documented [16, 17]. Recently bipolar RFA was suggested as a successful alternative for surgery in a small study population [18]. A remarkable volume reduction (58–92%) coincided with complete (two out of four patients) or considerable (two out of four patients) symptom relief. However, complications like acute kidney failure have been described [19].

### 10.3.2 Malignant

Most malignant hepatic tumors in the Western world are metastases from different primary tumors, most often from colorectal origin. In Mediterranean, African, and Asian countries, hepatocellular carcinoma is more frequent.

#### 10.3.2.1 Liver Metastases

A large number of primary malignancies have the ability to metastasize to the liver. There is general consensus that treatment of metastases from colorectal origin can be curative, and therefore local treatment should be initiated when tumor burden allows for complete eradication. Although small bowel tumor metastases are rare, general consensus considers workup and treatment similar to metastases from colorectal origin. There is no consensus for treatment of metastases other than from intestinal origin. When oligometastases from different primary tumors are present (e.g., breast, lung, or melanoma), the indication for treatment should always be discussed in a multidisciplinary team.

Colorectal carcinoma is currently the third most common cause of cancer-related death in the Western world. The main area of concern for these patients is the development of hematogenous metastases in 40–60% of these patients, 50% of which have metastases present at time of diagnosis of the primary tumor [20]. Liver metastases are an important determinant of their prognosis; 5-year survival of patients without distant metastases at time of diagnosis is 60–95%; this drops dramatically to 8% when synchronous liver metastases are present [20].

Historically, surgical resection was considered the gold standard for potentially curative treatment. When all metastases can be resected, cure is possible resulting in a 5-year overall survival rate between 25% and 60% [21–23]. Nowadays, the only criteria for surgical resection are that the future remnant liver should exceed 25% in a healthy liver, and 30% after systemic chemotherapy or underlying liver disease, with adequate vascular in- and outflow and biliary drainage and at least two contiguous liver segments [24]. Despite broadening of the criteria for resectability, a large proportion (70–80%) of patients with CRLM are deemed unresectable owing to an insufficient future remnant liver volume, even after conversion chemotherapy. New surgical techniques have been developed to overcome this problem. Preoperative portal vein embolization (PVE) induces atrophy of the embolized, tumor-bearing liver segments, while compensatory hypertrophy occurs in the non-embolized lobe. This increases the future remnant liver volume and, supposedly, its function,

enabling surgical resection of the tumors. Although this technique converts unresectable to resectable disease in selected patients, tumor progression has been described in the interval between embolization and resection, causing 6.4–33% of the metastases to be unresectable at time of surgery [25]. PVE is often used in a two-stage hepatectomy. In a two-stage strategy, compensatory liver regeneration after a first noncurative hepatectomy may enable a second curative resection. Seventy percent of the patients that were initially deemed eligible for this strategy have shown to undergo both operations.

The search for alternatives to achieve complete tumor eradication without the need for surgical resection already started in the 1980s and is still continuing. Local tumor ablation has emerged as a popular alternative to broaden the therapeutic possibilities for a selection of these patients, with radiofrequency ablation (RFA) as the clinically most relevant ablation technique up to date.

The principle of RFA is based on generation of a high-frequency alternating current, which causes heat with subsequent evaporation of intracellular water which leads to irreversible cellular changes, including intracellular protein denaturation, melting of membrane lipid bilayers, and coagulative necrosis of individual tumor cells and all other cells within the ablation zone. This effect is reached by using electromagnetic waves with frequencies less than 30 MHz (usually between 375 and 500 kHz). This causes agitation of ions, which creates frictional heat that extends into the tissue by conduction. A probe is inserted into the center of a tumor either percutaneously using CT guidance or surgically using intraoperative ultrasound. The latter can be performed by an open or laparoscopic approach. After insertion of the needle, a little “umbrella” is unfolded to increase the ablation zone, so that a maximal diameter of 3–3.5 cm is covered. Larger tumors need multiple ablations.

Recent literature shows that RFA can result in complete tumor clearance and an increased life expectancy. Median and 5-year survival rates of patients with solitary colorectal hepatic metastases are reported up to 40 months and 46.5%, respectively [26]. This technique is especially developed for patients with metastases that are not eligible for surgical resection and usually have more than one lesion. This makes the comparison to both techniques unreliable. However, when treating a mean of three lesions per patient with RFA, a 5-year survival of 18–43% can be achieved [27–29], which seems comparable to survival rates following resection of  $\geq 3$  lesions of 22–38% [30, 31]. The only prospective study comparing resection with percutaneous RFA in CRLM amenable to surgery was by Otto et al. Although patients with lesions up to 5 cm were included, the results are consistent with those of other studies regarding RFA: a higher rate of local tumor recurrence and shorter progression-free survival after RFA but with comparable overall survival [32]. Ruers et al. compared RFA combined with chemotherapy and chemotherapy alone in an EORTC study and found a significantly prolonged DFS and even a significant improved OS (median 45.6 vs 40.5 months,  $p = 0.01$ ) [33].

Morbidity and mortality of RFA are low compared to other ablative techniques, 6–9% and 0–2%, respectively [34]. The possibility of a minimally invasive, percutaneous approach is a benefit over surgical resection, especially in patients with extended comorbidity precluding major surgery.



An important advantage of target-focused treatment like RFA over surgery includes the localized destruction of target tissue alone and preservation of surrounding viable liver tissue, thereby making it possible to treat multiple, bilobar, lesions (>10) in one session.

The main disadvantage of RFA is the risk of a local site recurrence, which indeed occurs more frequently than after resection. This is in fact a matter of concern, with local recurrence rates reported between 3.6% and 40%, compared to 2–5% after resection, depending on the size and location of the lesion [28, 34]. This risk is increased for larger lesions and for tumors located near large blood vessels, since heat can be lost to the flowing blood: the so-called “heat sink” effect. Lesions <2 cm are hardly susceptible for this problem, but with 40% the recurrence rate after RFA of lesions >5 cm is high. Therefore, microwave ablation was developed. MWA utilizes dielectric hysteresis with active tissue heating and does not rely on the passive conduction of heat. For this reason MWA is often preferred over RFA for perivascular CRLM. However, microwave systems also face several limitations including underpowered generators, shaft heating, large-diameter probes, long and relatively thin ablation zones, less predictable ablation zones, and higher peak temperatures with the potential hazard to occlude important vessels or damage vital structures such as the major bile ducts [35].

Historically, conventional external beam radiation therapy (EBRT) has had a limited role in the treatment of liver metastases. EBRT uses large radiation fields that inevitably deliver a high percentage of the radiation dose to surrounding critical structures. The low tolerance of liver tissue to radiation raises the risk of radiation-induced liver disease (RILD). RILD syndrome is characterized by anicteric ascites with elevation of alkaline phosphatase and liver transaminases, which occurs 2 weeks to 4 months after radiotherapy and can result in liver failure and death [36]. In an attempt to maximize radiation efficacy and minimize toxicity, studies investigated other radiation delivery modalities. A recent advancement in radiation therapy is stereotactic ablative body radiotherapy (SABR or SBRT). Unlike standard radiotherapy, which delivers conventional fractions (ranging from 1.5 to 3 Gy) to a larger volume, SABR entails the precise delivery of high-dose in a single or a few fractions (one to six fractions [37, 38]). This limits the dose delivered to healthy liver tissue, resulting in decreased toxicity and dose escalation to the tumor. Treatment planning is based on four-dimensional diagnostic imaging, taking into account target motion associated with breathing, by either respiratory gating or tracking.

SABR has proven to be of value in tumors located centrally around the portal triad. However, the technique is precluded when other organs are located within 8 mm from the radiation area, like the stomach or duodenum. With multiple (>3) lesions or lesions >6 cm in diameter, there is still an increased risk of RILD or other toxicities [39]. Therefore, SABR seems most suitable in oligometastases that are unsuitable for surgical resection or RFA, similar to IRE. Local control, and not survival, is currently the most important endpoint in studies concerning SABR, due to the large variation in cancer stage and patient population. In studies evaluating the

use of SABR in patients with unresectable CRLM, the reported 2-year lesion-based local control varies from 72% to 90% [40, 41].

### 10.3.2.2 Hepatocellular Carcinoma

Hepatocellular carcinoma (HCC) is the most common type of liver cancer and one of the most common tumors worldwide. It is a relatively rare disease in developed countries but its incidence rapidly increases in areas where hepatitis B infections are common. It can present itself by icterus, ascites, coagulation disorders, weight loss, and pain in the right upper quadrant of the abdomen.

The most important risk factors vary widely from country to country and include alcoholism, hepatitis B, hepatitis C (25% of causes globally), aflatoxin, liver cirrhosis, hemochromatosis, alpha-1 antitrypsin deficiency, type 2 diabetes (probably aided by obesity), and hemophilia [42–44]. In countries like China where hepatitis B is endemic, it is the predominant cause of HCC, whereas in developed countries with low incidence of hepatitis B because of high vaccination rates, the major cause of HCC is cirrhosis (often secondary to hepatitis C, obesity, or alcohol abuse).

As a result of technological improvements, the number of therapeutic modalities available for HCC has increased dramatically. Theoretically, the best treatment for small HCC is liver transplantation, but the scarcity of donor organs and high costs constrain the use of this treatment. In addition to the traditional surgical resection and liver transplantation, other therapies, such as transcatheter arterial chemoembolization (TACE), RFA, percutaneous ethanol injection (PEI), and percutaneous microwave ablation (MWA), have also been used. SABR does not currently play a primary role in the treatment of HCC and is still considered experimental or a bridge to transplantation.

Despite all these treatment options, HCC still has the second highest cancer-related mortality worldwide because most patients are diagnosed in an advanced stage.

The choice of treatment of HCC is based on the Barcelona criteria [45]. This classification uses variables related to tumor stage, liver functional status, performance status, and cancer-related symptoms and links the stages described to a treatment algorithm. Stage 0-A-B can be treated with surgical resection, intra-arterial therapies, or liver transplantation. Patients with stage C-D disease have to rely on (palliative) systemic treatment using sorafenib, phase II trial agents, or symptomatic relief. For a patient to be suitable for liver transplantation, one needs to meet the Milan criteria: single tumor with diameter  $\leq 5$  cm or up to three tumors each with a diameter  $\leq 3$  cm, no extrahepatic involvement, and no major vessel involvement [46]. Therefore, the demand for novel treatment strategies for small HCCs has been raised in both surgical resection and nonsurgical resection cases [47].

The 5-year overall survival of all patients with HCC is 14% but highly dependent on the stage of the disease. Stages 0 and A have a good 5-year survival after surgery (transplantation or resection) with 80–90% and 70–80%, respectively. Median survival of patients with stage B after intra-arterial therapy is 36–45 months. Overall survival decreases to 9–10 months in stage C treated with sorafenib to 3–4 months in end-stage HCC [48].

## 10.4 Current and Future Indications of IRE

### 10.4.1 Benign

Currently IRE is not commonly applied for benign liver lesions. The literature describes only one case in which a large, centrally located hepatocellular adenoma was treated with IRE in a woman with a strong pregnancy wish [49]. Due to the central location, the lesion was considered unsuitable for surgical resection and thermal ablation. Embolization had also proven unsuccessful due to the tumor's extensive arterial blood supply. Percutaneous IRE treatment was performed without complications. However, the ablation zone was much larger than anticipated. Local surroundings and tissue-specific conductivity both have an effect on size and shape of the ablation zone [50]. Hypothetically, the increased ablation zone size could suggest that the conductivity of adenoma tissue is higher than that of normal liver parenchyma, resulting in a lower electric field threshold for IRE. Future work should correlate ablation volumes with numerical simulations to determine an effective electric field threshold for each particular tumor to guide future ablations.

Besides the rare occurrence of centrally located HCAs with absolute treatment indication, there is currently no other indication for the use of IRE in benign liver tumors.

### 10.4.2 Malignant

IRE is particularly indicated for malignant liver lesions that are strictly unsuitable for surgical resection or thermal ablation due to their anatomic location. Currently the indication lies with colorectal liver metastases, HCC, and liver metastases from other primary origin. IRE for unresectable perihilar cholangiocarcinoma is currently under investigation (see chapter 12). The indication for local tumor ablation, and thus for IRE, should always be made following multidisciplinary deliberation. Similar to surgical resection, the general criterion for image-guided ablation is that it is performed with curative intent, which means that all tumors must be suitable for some kind of local treatment. Concurrent treatment of additional tumors in the same treatment session, by, for example, resection or thermal ablation, is therefore not uncommon. IRE is repeatable and can be used to treat residual disease as well as new lesions [51].

Although there are no strict size criteria, similar to radiofrequency ablation, IRE appears to be most effective for tumors  $\leq 3$  cm in diameter; beyond this size treatment efficacy quickly decreases and may require staged therapy with multiple ablation sessions [52]. Similarly, there is no absolute number of tumor eligibility [53]. Besides size and number of the lesions, factors such as age, performance status, comorbidity, and previous oncologic treatment play part in the assessment of a patient's suitability for local treatment. Given the versatility in local tumor ablation, the indication for IRE should be discussed in a multidisciplinary liver tumor board.

In our institution, unsuitability for thermal ablation is defined as follows; in order to preserve liver function, at least one hepatic vein and one portal vein must remain

patent. Lesions that are located within 5 mm from a major vessel are considered unsuitable for radiofrequency ablation due to the risk of incomplete ablation caused by the heat sink effect. This risk does not account for microwave ablation. However, due to higher temperatures achieved with MWA and more unpredictable size of the ablation zone, these vessels are at risk for occlusion. Therefore, if after previous liver surgery only two portal veins or hepatic veins remain, and subsequently a lesion develops within the fork of one of these veins, MWA is contraindicated due to the risk of vessel occlusion and liver perfusion shutdown. Similarly, if only one portal vein or hepatic vein remains patent after previous surgical procedures, MWA in the vicinity of this vein is too dangerous. In these cases, IRE can be a suitable treatment option. Due to the risk for thermal damage, lesions that are located less than 5 mm from the right, left, or common bile duct are also considered unsuitable for RFA or MWA due to the risk of thermal damage to the bile duct.

---

## 10.5 Contraindications

Patient-related contraindications include ASA >3, including patients that are considered unfit to undergo general anesthesia, and ventricular cardiac arrhythmias. Epilepsy can be considered a relative contraindication [54]. Coagulation abnormalities should be corrected (INR <1.2, APTT 25–40 and platelet count >150,000/mcL) (see chapter 6).

Tumors infiltrating the portal triad are non-eligible for IRE. The distance between the ablation zone and the portal triad including a 0.5–1-cm tumor-free margin should be at least 2 mm. The increase in temperature close to the probes can cause damage to these vital structures with the risk of hemorrhage or biloma.

Special care is warranted when a metallic stent is present in the bile ducts, since the redistribution of the electric field and the development of heat in the presence of metal objects are unpredictable and not well understood (see also chapter 9) [55]. Recent preclinical work has shown that IRE in the vicinity of a metal stent does not cause notable increased heating of the metal stent, but results in higher temperatures around the electrodes, which could in theory lead to thermal injury. In vivo, a remnant viable tissue region immediately adjacent to the stent was observed. These findings reinforce the appeal to either place plastic biliary endoprotheses or to remove metal stents prior to IRE whenever possible [56]. The influence of metallic objects on the electric field distribution and subsequent ablation zone should be further explored.

---

## 10.6 Patient Workup and Treatment Planning

The need for multidisciplinary decision-making cannot be emphasized enough. In this way, all possible options can be discussed. The patient should be aware of the preliminary phase that IRE is in and should be informed about all other possible treatment options.

Diagnosis of can often rely on pre-procedural imaging using ultrasound, four-phase liver CT and/or a contrast-enhanced MRI or  $^{18}\text{F}$ -fluorine deoxyglucose positron emission tomography ( $^{18}\text{F}$ -FDG PET)-CT (for CRLM), combined with the medical history of the patient. Blood tests are used for specific tumor markers such as carcinoembryonic antigen (CEA) for CRLM and alpha-fetoprotein (AFP) for HCC. In the case of HCC or metastatic disease other than from colorectal origin, histology is preferred using thick needle biopsy.

Safety precautions taken before and during the procedure start with adherence to the absolute contraindications mentioned above. All patients should have been fasting for 4–6 h prior to the procedure. All procedures (open and percutaneous) require general anesthesia including complete muscle relaxation to prevent muscle contractions expressed as a train of four of 0 (see chapter “Anesthesiology”). Before commencing the procedure, accurate R wave detection is confirmed by applying a three-lead ECG attached to the IRE device. In the beginning, we would use defibrillator pads as a precaution. In the absence of major arrhythmias or cardiac complications, we stopped using them.

---

## 10.7 Tips and Tricks on the General Technique, Approach, and Image Guidance

With IRE, the important thing is that the needles can be placed in a predetermined pattern, at a known distance from each other, more or less parallel and, most users would agree, at least a few millimeters away from structures that might otherwise be damaged by the small amount of heat that may surround the needles. The needles can thus be placed intraoperatively, laparoscopically, or percutaneously. The guiding techniques can be palpation (if intraoperative), CT, or ultrasound. Furthermore, both CT and ultrasound can be performed “freehand”, guided by a needle guidance device or by more advanced computer-based robotic techniques. It has been suggested that using robotic guidance saves time which is important as the IRE needle placement can be quite time consuming, especially when up to six needles are being used [57, 58]. However, there is so far no evidence that one technique, or combination of techniques, is superior when it comes to the ablation results, either in respect to initial ablation zone or later local recurrence. The approach must then be based upon things like the location of the tumor, the available resources, and the individual skill set of the person performing the ablation. A percutaneous approach is, obviously, less invasive but also dependent on adequate imaging. For example, a small tumor in a large patient, difficult to visualize on CEUS or CT, might be done using an intraoperative approach, whereas a tumor clearly seen on imaging may be done percutaneously using guidance by CT (large patient) or ultrasound (slim patient). Any combination of the above can of course be used, i.e., intraoperative ultrasound, placing the needles with ultrasound and checking the position with CT. The important thing is that those involved are comfortable with the chosen method(s) and can place the needles adequately as this is vital for a successful result [50, 59]. As with all intervention, seeing one procedure

done by someone else (preferably in the same way as one plans to do it) helps overcome the learning curve that does exist as with all new procedures [60], and tips and tricks can be picked up. Even though the needles are sharp enough to penetrate the skin, a small incision is commonly used to ensure a smooth passage of the needle, and when using ultrasound for guidance, this has the added advantage that the experienced interventional ultrasonographer will “feel” the tissue planes as the needle crosses them without the skin “snagging” around the needle shaft. On the other hand, clotted blood from the incisions will eventually interfere with the ultrasound quality in an extended needle placement.

As with all IRE treatments, general anesthesia is mandatory with a deep muscle relaxation in order to avoid muscle contraction in the patient when the electrical treatment pulses are given. At best, excessive movement is disturbing; at worst, it may cause dislocation of the needles giving an inadequate treatment result or even damage to sensitive structures close to the needle tip. Most patients are treated in a supine position as it is the most common examination position both for CT and ultrasound and also makes it easier for the anesthetist. However, supine or even prone positions may be used to ensure a safe needle passage from the skin to the tumor area. Even though IRE is a safe method [52], we still insert needles capable of causing damage to blood vessels, bowel structures, etc., and care must be taken both with the patient position and tricks like hydrodissection to achieve the best needle paths possible.

The actual treatment in an IRE ablation, i.e., the electrical pulses as opposed to heat or cold in a thermal ablation, is comparatively safe as indicated by the fact that the complication rate has not been seen to go up when larger tumors in more difficult positions are treated [60]. The electrical pulses may, however, cause a vessel spasm seen as a narrowing of both arteries and veins. In most cases this will resolve in a short space of time but remaining vessel and bile duct stenosis has been seen [61, 62]. Complications that may arise from damage caused by the needles are of course mainly localized hematomas or, worse, a diffuse bleeding. When ablating in the liver using an intercostal approach, the needle path may cross the pleural space. Pneumothorax has been reported but not so far clinically significant. As with all ablations in the liver, care should be taken when performing an ablation in a patient who has had a papillotomy or a choledochojunostomy. Prophylactic antibiotics should be considered as there is a risk of abscess formation [63, 64]. In vivo studies have shown a slight increase in temperature around the needles, and this needs to be remembered when placing needles even though no complications have been attributed to this so far [55]. However, this effect was shown to be more pronounced when a metallic stent was placed in the ablation zone even though the stent itself did not get hot. Also, after the ablation, viable tissue could be found adjacent to the stent that may act as a Faraday’s cage preventing an adequate treatment. The treatment in itself, as we ablate liver tissue, will cause an increase of liver function tests but not more so than with other ablation techniques and should not be seen as an indication of excessive liver damage [65].

As the whole purpose of using IRE as an ablation method is to preserve vulnerable structures like vessels, the ablation zone, contrary to a thermal ablation,

will still have perfusion albeit decreased. This is important to remember when doing follow-up imaging. Many methods have been used and the findings of decreased perfusion can be seen on all contrast-enhanced images. CT should be done in the portal phase and a 3D analysis may be helpful [66, 67]. B-mode ultrasound will show a hypochoic area just after the ablation and this can be used as an indication of the ablation zone but not for absolute size. CEUS however will give an accurate estimation of the ablation [68]. When using MRI for follow-up, it is important to be familiar with the post-IRE changes as many imaging parameters will be altered [69].

### 10.7.1 Optimizing Target Visibility

Tumor tissue and ablation zones are often barely visible on unenhanced CT especially when they have been pretreated with chemotherapy. During CT-guided IRE, the delineation of tumor and surrounding vessels and the induced coagulation zone are often limited to a time window after administration of intravenous contrast material. Consequently, if the maximum dose of the contrast agent is reached after one or two injections required for treatment planning before the procedure, repetitive intraprocedural monitoring is restricted. This is a major drawback because dynamic and real-time tumor and vessel delineation are key to safe and precise probe placement. A method to reduce the contrast dose is bolus chasing. This allows preablation and postablation contrast imaging for all ablative modalities [70]. To further improve intraprocedural lesion and vessel conspicuity, we recently demonstrated the feasibility of transcatheter CT hepatic angiography (CTHA) with percutaneous liver tumor ablation [71]. The injection of a contrast agent directly into the proper hepatic artery enables repeated contrast-enhanced imaging and real-time CT fluoroscopy, which improves lesion conspicuity and also provides real-time information on the vicinity of blood vessels. Immediately after IRE, the ablated area is clearly delineated, with the typical appearance of the avascular ablation zone surrounded by a hypervascular rim (Figs. 10.2, 10.3, and 10.4).

---

## 10.8 Complications

A systematic review of the literature evaluated the safety of hepatic IRE in 129 patients (227 tumors). Overall complication rate was 16% (21/129), and these were all minor complications [52]. The electric fields applied in IRE can cause cardiac arrhythmias, but synchronized pulsing with the heart rhythm greatly reduces this risk (see chapter “Anesthesiology”). The systematic review showed that with cardiac gating, only minor arrhythmias occurred (incidence = 2.2%). Even when hepatic lesions are located close to the heart, IRE can be safely applied when pulses are delivered in synchrony with the R wave [73].

When using the open approach, all complications that apply for hepatic surgery should be taken into account, especially when IRE is combined with surgical

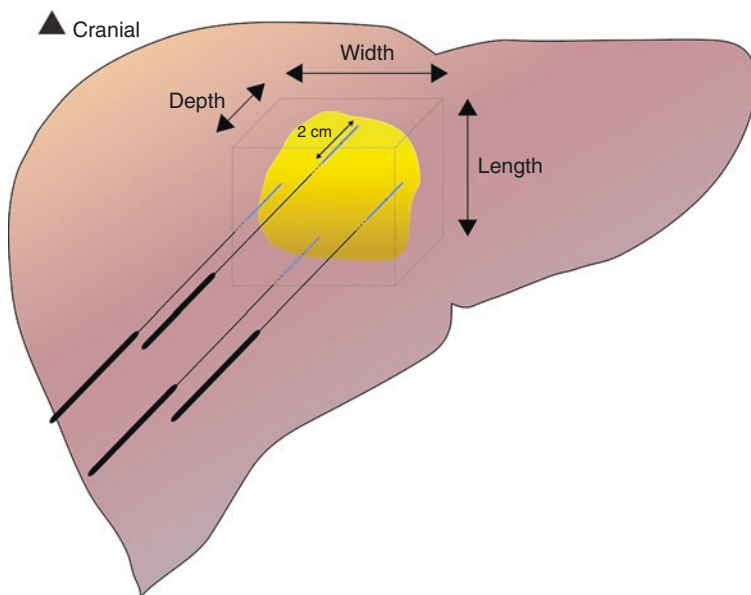


**Fig. 10.2** Adapted from Scheffer et al. Definition of depth, length, and width of the treatment zone in relation to the electrode application [72]

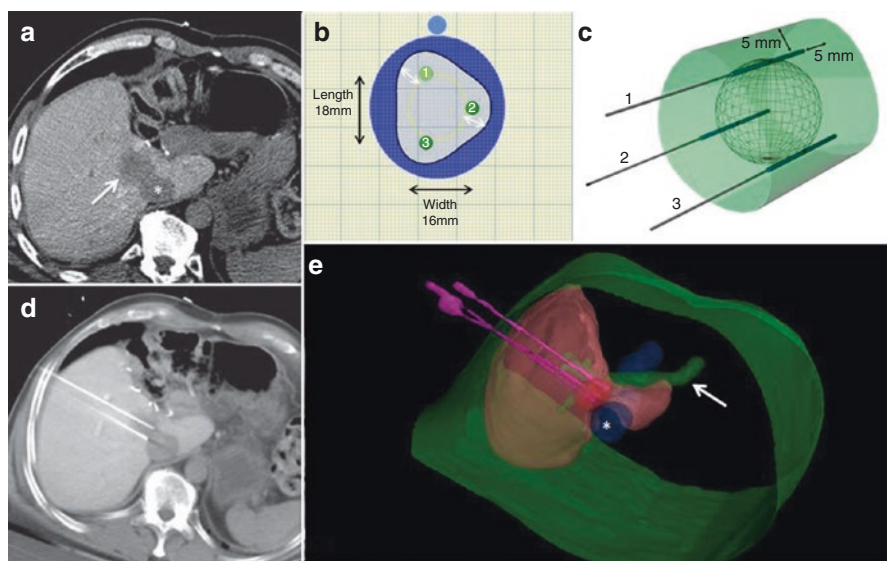


**Fig. 10.3** Adapted from Scheffer et al. (a) CT pre-IRE shows a central hypoattenuating CRLM (arrow). The asterisk represents the inferior vena cava. (b) Planning of electrode configuration, with the yellow circle representing the tumor (18-mm length and 16-mm width) and the white arrows representing the expected tumor-free margin. (c) Calculated ablation zone extending 5 mm outward from each electrode in all directions. (d) CT fluoroscopy showing two of three electrodes placed in the periphery of the tumor. (e) Three-dimensional reconstruction of the electrodes positioned in the periphery of the tumor and the close proximity of the tumor to the inferior vena cava (asterisk) and the common bile duct (arrow) [72]



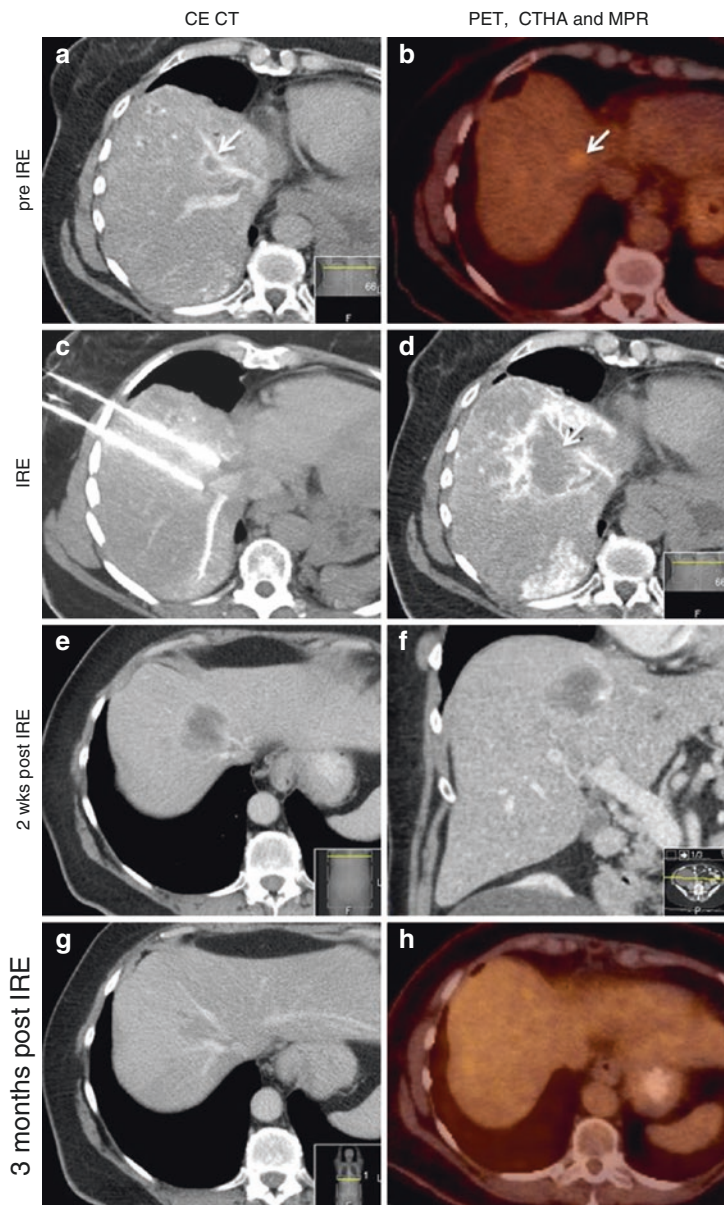


**Fig. 10.4** Adapted from Scheffer et al. (a) Transcatheter ceCT (CTHA) showing a small nonattenuating CRLM (*arrow*) adjacent to the middle hepatic vein. (b) PET-CT pre-IRE showing the FDG-avid lesion (*arrow*). (c) CT fluoroscopy with two electrodes in situ. (d) CTHA immediately post-IRE showing a large nonenhancing ablation zone surrounding the lesion (*arrow*) with peripheral hyperattenuating rim. (e) ceCT 2 weeks post-IRE showing shrinkage of the hypodense ablation zone. (f) Coronal MPR of ceCT 2 weeks post-IRE. (g) ceCT 3 months post-IRE demonstrating further shrinkage of the nonenhancing ablation zone. (h) PET-CT 3 months post-IRE showing absence of tracer uptake of the treated lesion. CTHA CT hepatic angiography [72]

resection. Some complications are directly related to the surgical trauma: hemorrhage, wound infection, hernia cicatricialis, biloma, or (intra-abdominal) abscess formation. Other complications are related to postoperative pain and inactivity: ileus, urinary tract infection, pneumonia, and thromboembolic complications.

Adverse events of the percutaneous approach can be posture-related. When the patient is under general anesthesia with the arms positioned over the head, which is the required position during CT-guided procedures, there is a significant risk of neuropraxia of the brachial plexus [4].

Puncture-related complications such as pneumothorax and hemorrhage are infrequently encountered and are comparable to other needle-guided liver interventions [72].

The lesions included in the systematic review were mostly located close to portal vessels and bile ducts. Stenosis or occlusion of these structures was reported in 8/129 treated patients (6%), of which two were probably related to tumor progression [74]. Although IRE is believed to be primarily nonthermal, heat development immediately adjacent to the electrodes has been described [75], which may have caused thermal coagulation and subsequent occlusion of a bile duct that was in direct contact with one of the needles [74]. To prevent unintended damage when ablating near thermally sensitive critical structures, we therefore recommend avoiding placement of the electrodes less than 2 mm to the central bile ducts or large blood vessels. Overall, considering that IRE was mostly performed on tumors near or around portal pedicles, vascular and biliary structures, the preservation of these structures seems probable. This suggests that IRE may be a safer option than thermal ablation in this area. Further studies with longer follow-up times are still needed to confirm these results.

Retrospective comparison of postprocedural pain after hepatic IRE and RFA showed similar moderate pain intensity with comparable amounts of self-administered pain medication [76].

Traversing the intestines during needle placement should be avoided when possible. In open IRE this is usually not an issue. During percutaneous IRE pneumo-, hydro-, or balloon dissection can be an option to increase the distance between different vital structures (see chapter “Safety-Enhancing Procedures”). This can also be useful when a target lesion is located in close proximity to the intestinal tract, like the duodenum or stomach. If contact with the intestines cannot be avoided, supplementary antibiotic prophylaxis is recommended.

---

## 10.9 Follow-Up and Response Evaluation

A recently published systematic review on hepatic IRE reported rapid elevations within 24 h after IRE of liver transaminases ALT and AST, which signals hepatocellular injury [69]. In this study, the transaminases returned to baseline following 1 or 2 months. Serum bilirubin also rose to peak level on day 1 and normalized 2 months later. The peak values of elevation were consistent with those of other ablation modalities. During follow-up, tumor markers carcinoembryonic antigen (CEA) for

CRLM and alpha-fetoprotein (AFP) for HCC should be monitored preferably 3 monthly. Bilirubin levels should also be monitored; rising bilirubin can signal bile duct occlusion or stenosis as a late complication of IRE treatment or tumor progression.

CT and magnetic resonance imaging (MRI) are the most commonly used imaging methods to monitor postablative lesions for remnant or recurrent disease after hepatic radiofrequency ablation and microwave ablation. Several studies have shown the superiority of PET-CT over morphologic imaging alone in the follow-up after thermal ablation of CRLM with a sensitivity and specificity of PET-CT (92% and 100%) compared with that of ceCT (83% and 100%) regarding the detection of local tumor progression [77]. Much is still unknown about the imaging characteristics of liver lesions treated with IRE. As a consequence, standardized follow-up regimens are lacking. To investigate the typical appearance of electroporated CRLM, in our institution we have performed regular ceCT, PET-CT, and MRI during follow-up.

### 10.9.1 Computed Tomography

Post-IRE ceCT is used to ensure that the realm of ablation encompasses the originally targeted volume with a good margin and to exclude complications. Immediately after IRE, the ablation zone appears hypodense and can show an enhancing peripheral rim. Follow-up CT imaging at 4–6 weeks is performed to exclude new sites of disease and local disease progression. Realistically, it is difficult to exclude local progression this early after IRE on CT as CRLM typically do not enhance unless there are additional sites of involvement or significant increase in the size of the postablation hypodense lesions. In the months after ablation, the ablation zone slowly decreases in size and should not show uptake of the contrast agent (Fig. 10.4g).

### 10.9.2 Positron Emission Tomography

PET scans show a dynamic response to the IRE ablation. Three days following IRE, an FDG-avid peripheral zone surrounding the ablated region appears. This initial increase in tracer uptake at the periphery of the IRE region may be explained by an inflammatory response, increasing metabolic activity at the targeted region as the cellular debris are removed from the targeted site [78]. For PET-avid lesions, we have found PET-CT obtained within 24 h after IRE useful to assess completeness of ablation, which at this point in time must show absence of tracer uptake within the ablated region. In our experience, the inflammatory response visible as increased rim-like tracer uptake at the periphery of the lesion can persist for several months, which renders evaluation of the ablation zone difficult. However, ablated lesions, which show focal uptake rather than rim-like uptake in the periphery, are considered suspect for local recurrence.

### 10.9.3 Magnetic Resonance Imaging

Prior to IRE, the lesion appears hypointense on T1-weighted imaging (Fig. 10.5a) and hyperintense on T2-weighted imaging compared to the normal liver parenchyma (Fig. 10.5b). One day post-IRE, T1-weighted contrast-enhanced MRI demonstrates a nonenhancing hypointense center and a slightly enhancing peripheral rim (Fig. 10.5d). One day post-IRE, T1-weighted contrast-enhanced MRI demonstrates a nonenhancing hypointense center and a slightly enhancing peripheral rim (Fig. 10.5d). One day post-IRE, T2-weighted MRI demonstrates a hypointense center and a hyperintense rim (Fig. 10.5e). One day post-IRE, DWI demonstrates diffusion restriction of the ablated area especially at the periphery and reduced diffusion restriction of the ablated lesion (arrow) (Fig. 10.5f). Two weeks post-IRE, CE T1, T2, and DWI images demonstrate resolution of the ablated area (Fig. 10.5g-i). Three months post-IRE, CE T1, T2, and DWI images demonstrate resolution of the ablated area (Fig. 10.5j-l).

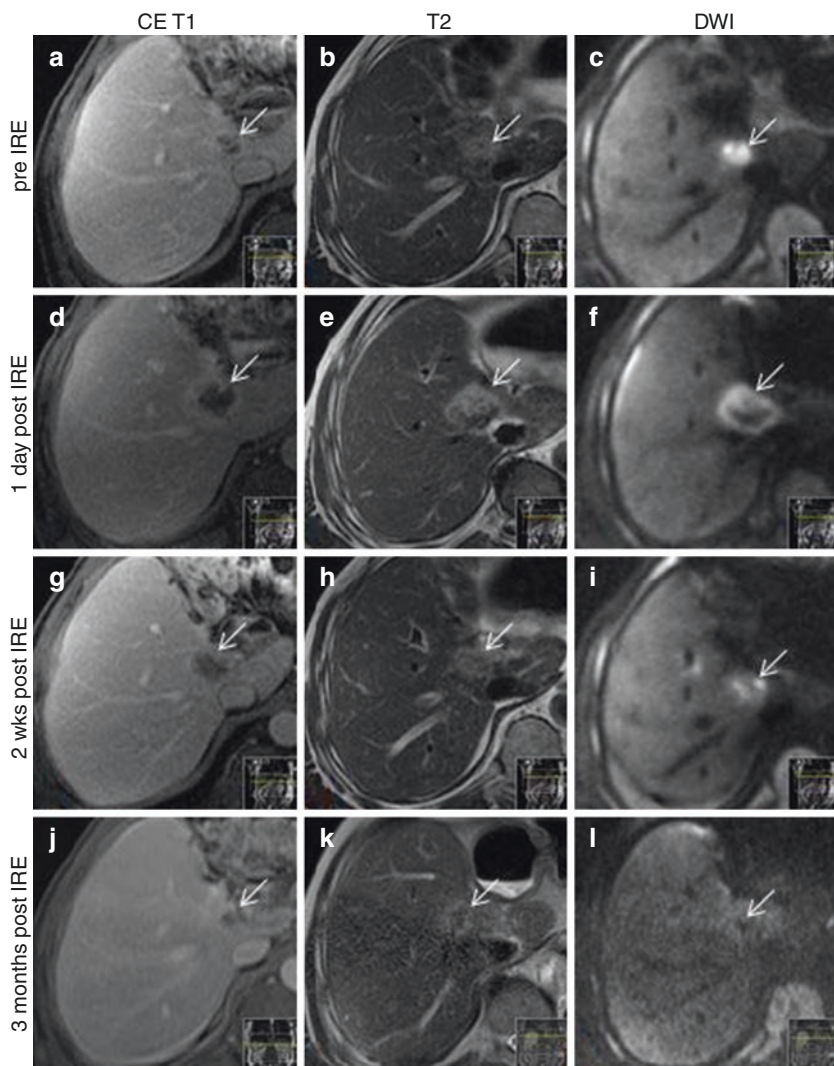


**Fig. 10.5** Adapted from Scheffer et al. MR images of a central CRLM treated with IRE. (a–c) CE T1-weighted, T2-weighted, and DWI image of a lesion before IRE. (d, e) MRI 1 day post-IRE demonstrating a hypointense ablation zone with hyperintense rim on T2 and an enhancing rim on CE T1. (f) DWI 1 day post-IRE with diffusion restriction of the ablated area especially at the periphery and reduced diffusion restriction of the ablated lesion (arrow). (g–i) CE T1, T2, and DWI images 2 weeks and 3 months post-IRE demonstrating resolution of the ablated area [72]

T2-weighted MRI of the ablated region typically shows a hypointense center, surrounded by a hyperintense reactive rim, probably caused by cytotoxic edema due to the ion leakage (Fig. 10.5e). Diffusion-weighted imaging b800 shows a similar appearance (Fig. 10.5f).

Comparable findings were reported by Barabasch et al. who prospectively investigated the MR imaging characteristic after hepatic IRE in 27 patients with 37 hepatic metastases. In their study, the hyperintense rim and its enhancement resolved within 3 months after IRE in 95% of cases [79]. The ablation zones resolved completely in just over half of the cases (57%, 21/37), by an average of 14 weeks after IRE. As for CT and PET, when evaluating immediate post-IRE outcome, care should be taken that the hyperemic rim is not confused with regions of residual tumor, which would demonstrate focal and irregular peripheral enhancement [78].

---

## 10.10 Disease Recurrence

The main concern following tumor ablation is the risk of developing local tumor progression (LTP). On four-phase liver CT, LTP is defined as a growing (>20%, longest diameter, axial plane) hypodense lesion within 1 cm of the ablation zone. On <sup>18</sup>F-FDG PET-CT, focally increased FDG uptake within 1 cm of the ablation region is considered an LTP [77]. Early diagnosis of LTP is imperative because repeated treatment can still effectuate complete tumor clearance, especially for smaller recurrences.

A major challenge in reporting results on IRE for CRLM and HCC is the lack of uniform response criteria that can fully capture the efficacy of the procedure. Specific periprocedural imaging guidelines are needed to reassure the interventional radiologist when complete tumor ablation has occurred. A new response assessment system specific for CRLM was recently proposed, which can also be applied to ablative and transarterial modalities: the Metabolic Imaging And Marker Integration (MIAMI) criteria [51] (Table 10.1).

The value of these criteria lies in the combination of anatomical response parameters using the Response Evaluation Criteria In Solid Tumors (RECIST) criteria and two functional parameters: PET activity and carcinoembryonic antigen levels. The application of the MIAMI criteria stratifies patients into two groups: those who have clinical benefit (complete response, partial response, and stable disease) and those who have no clinical benefit (progressive disease). The efficacy of IRE for CRLM was investigated in this study, and when the MIAMI criteria were applied, patients who showed clinical benefit exhibited significantly longer survival than patients who did not show clinical benefit ( $P = 0.018$ ). Clearly, these criteria need validation in larger studies before they can be recommended for clinical application.

Barabasch et al. found that in three patients, in whom the hyperintense rim depicted on the MRI study performed within 24 h after was incomplete and did not include the full volume of the target lesions, follow-up imaging confirmed that the ablation had been incomplete [79]. Accordingly, they suggested that if doubt exists

**Table 10.1** Proposed Miami criteria

Detail	MIAMI criteria			
	Complete response	Partial response	Stable disease	Progressive disease
Sum of longest dimensions on CT (RECIST)	Any decrease or <20% increase in target lesion(s)	Any decrease or <20% increase	Any decrease or <20% increase	≥20% increase or any new lesions
SUV <sub>max</sub> on PET/CT scan (PERCIST)	Resolution of FDG uptake in target lesion(s)	≥30% decrease	No new lesions with ±30% change in SUV <sub>max</sub>	New abnormal FDG-avid lesions
CEA level after therapy	Normalization of CEA level	≥50% decrease	–	–
Criteria required <sup>a</sup>	RECIST plus either PERCIST or CEA	RECIST plus either PERCIST or CEA	One of two	One of two

<sup>a</sup>If CT is the only evaluation modality available, the MIAMI response will be the same as the RECIST response. If all three modalities are available and there is discordance, the RECIST and PERCIST response takes precedence over the CEA response. CEA carcinoembryonic antigen, PERCIST positron emission tomography response criteria in solid tumors, RECIST response evaluation criteria in solid tumors, SUV<sub>max</sub> maximum standardized uptake value

with regard to the local completeness of the procedure after CT-guided IRE, MRI on the day after IRE is useful. For the long-term follow-up, they also suggested to start at 3 months after the procedure because by that time, signs of inflammation (hyperintense rim and strong contrast enhancement), at least in non-cirrhotic liver, should have subsided [80]. The radiologic ablation zone measurements show a high correlation with the histologically confirmed ablation zone in a study on IRE in rodent liver ( $P = 0.001$  for both T1- and T2-weighted measurements) and could therefore also be useful as an indicator for complete or incomplete ablation and for follow-up evaluation of clinical outcome [81].

## 10.11 Results from Literature

New cancer treatments are typically best defined from phase III randomized trials comparing the new therapy with the current standard. However, in the field of local tumor ablation, this has proven difficult since its introduction decades ago, the number of randomized trials remains very limited. Most of the clinical data on IRE originate from case series and case reports with level 4 evidence and are subject to several limitations, such as short follow-up period, low patient number, heterogeneous study design and patient selection, retrospective study design, and variable imaging modalities [82]. These limitations should be taken in mind when interpreting the current data.

**Table 10.2** Overview of clinical studies investigating efficacy of IRE for hepatic tumors

Study	Year	Patients (lesions)	Size (cm), median (range)	Approach	Tumor type, per patient	Efficacy
Cannon et al. [83]	2012	44 (48)	2.5 (1.1–5.0)	Open (14)	HCC (14)	3 months 97%
				Percutaneous (28)	CRLM (20)	6 months 95%
				Lap (2)	Other (10)	
Cheung et al. [86]	2013	11 (18)	1.9 (1–6.1)	Percutaneous	HCC (11)	3 months 67% 12 months 72%
Hosein et al. [51]	2014	29 (58)	2.7 (1.2–7.0)	Percutaneous	CRLM	11 months 79%
Kingham et al. [84]	2012	28 (54)	1.0 (0.5–5.0)	Open (22)	HCC (2)	3 months 96%
				Percutaneous (6)	CRLM (21)	6 months 93%
					Other (5)	
Niessen et al. [64]	2016	34 (65)	2.4 (0.2–7.1)	Percutaneous	HCC (33)	3 months 87.4%
					CRLM (22)	6 months 79.8%
					Other (10)	12 months 74.8%
						Median TTP 15.6 months
Silk et al. [74]	2014	9 (19)	3.0 (1.0–4.7)	Percutaneous	CRLM (8)	9 months 55%
					Other (1)	
Thomson et al. [4]	2011	13 (45)	2.8 (1.0–8.8)	Percutaneous	CRLM (6)	3 months 67%
					Other (7)	

IRE is, at this time, only used as “last-resort” curative treatment in patients that would otherwise receive chemotherapy with palliative intent [83–85]. Early efficacy ranges widely between 55% and 95% in the published studies (Table 10.2). Several studies have reported an increased recurrence risk for larger tumors [4, 74, 84, 86]. For tumors <3 cm, efficacy is significantly better: Cheung et al. [86] achieved 93% ablation success for tumors <3 cm and 100% for tumors <2 cm at 18 months ( $P = .003$ ), and Cannon et al. [83] reported 98% efficacy for tumors <3 cm at 12 months. Silk et al. [74] described local tumor recurrence in five of nine patients, with a median tumor size of 3.0 cm. A likely solution would be to increase either the number of probes required to treat larger lesions or the number of probe repositionings. For example, a four-probe array with an interprobe distance of 2 cm creates a 3-cm ablation zone. Considering a 1-cm tumor-free margin, this would imply a maximum lesion size of 1 cm for this four-probe array. Misplacement of the probes by a margin of millimeters can result in residual tumor, so accurate imaging during the procedure is essential. Presumably, precise placement of larger probe arrays is more difficult, especially because probe placement through vulnerable structures should be avoided.

Notably, of the tumors treated by Kingham et al. 44% were located <0.5 cm from a major portal vein, and 14% were located 0.6–1 cm from a major portal vein, which implied a relative contraindication for RF ablation owing to the probability of heat sink-induced recurrence [84]. Efficacy at 6 months was 93%. Similarly, IRE near

the right portal vein ( $n = 2$ ) and the middle hepatic vein ( $n = 1$ ) was successful for two of three HCCs treated by Cheung et al. The tumor that showed residual disease measured 6.1 cm. This suggests that the cellular destruction mechanism is indeed not impeded by heat sink.

Current local control rates of IRE are still inferior to thermal ablation and surgical resection, especially for larger lesions. Several aspects could lead to improved efficacy. For example, animal studies have shown that the changes in electric conductivity of the ablated tissue—among others—determine ablation success. These changes could provide real-time feedback on treatment outcome [87–89]. However, organ-specific and tumor-specific electric field dose-response studies are lacking, and much remains unknown about the clinical possibilities to destroy malignant tissues with irregular geometries and heterogeneous properties. Knowledge of the electric and thermal properties of different tissue types should allow for the identification of an optimal electric field—strong enough for maximized tissue ablation but weak enough to avoid excessive thermal effects [90]. Hopefully increasing knowledge will lead to improved treatment efficacy in the future. The value of IRE compared to SABR for hepatic lesions has not been investigated and will be the focus of a future trial (COLDFIRE-3, study in preparation).

---

### Conclusion

At this time, IRE should be reserved for well-selected patients with relatively small HCC and (colorectal) liver metastases that are truly unsuitable for resection and thermal ablation. In general this means tumors abutting the portal triad or the hepatic venous pedicle, where thermal ablation is considered unsafe and less effective. Technical improvements of the ablation device and increasing knowledge about tissue-specific electrical properties may result in improved efficacy in the future.

---

### References

1. Lee EW, Thai S, Kee ST. Irreversible electroporation: a novel image-guided cancer therapy. *Gut Liver*. 2010;4(Suppl 1):S99–S104.
2. Edd JF, Horowitz L, Davalos RV, Mir LM, Rubinsky B. In vivo results of a new focal tissue ablation technique: irreversible electroporation. *IEEE Trans Biomed Eng*. 2006;53(7):1409–15.
3. Maor E, Ivorra A, Leor J, Rubinsky B. The effect of irreversible electroporation on blood vessels. *Technol Cancer Res Treat*. 2007;6(4):307–12.
4. Thomson KR, Cheung W, Ellis SJ, Federman D, Kavnoudias H, Loader-Oliver D, et al. Investigation of the safety of irreversible electroporation in humans. *J Vasc Interv Radiol*. 2011;22(5):611–21.
5. Reddy KR, Kligerman S, Levi J, Livingstone A, Molina E, Franceschi D, et al. Benign and solid tumors of the liver: relationship to sex, age, size of tumors, and outcome. *Am Surg*. 2001;67(2):173–8.
6. Baum JK, Bookstein JJ, Holtz F, Klein EW. Possible association between benign hepatomas and oral contraceptives. *Lancet*. 1973;2(7835):926–9.
7. Martin NM, Abu Dayyeh BK, Chung RT. Anabolic steroid abuse causing recurrent hepatic adenomas and hemorrhage. *World J Gastroenterol*. 2008;14(28):4573–5.
8. Agrawal S, Agarwal S, Arnason T, Saini S, Belghiti J. Management of hepatocellular adenoma: recent advances. *Clin Gastroenterol Hepatol*. 2015;13(7):1221–30.



9. Almashhrawi AA, Ahmed KT, Rahman RN, Hammoud GM, Ibdah JA. Liver diseases in pregnancy: diseases not unique to pregnancy. *World J Gastroenterol.* 2013;19(43):7630–8.
10. Broker ME, Ijzermans JN, van Aalten SM, de Man RA, Terkivatan T. The management of pregnancy in women with hepatocellular adenoma: a plea for an individualized approach. *Int J Hepatol.* 2012;2012:725735.
11. Kudo M. Hepatocellular adenoma in type Ia glycogen storage disease. *J Gastroenterol.* 2001;36(1):65–6.
12. Grazioli L, Morana G, Kirchin MA, Schneider G. Accurate differentiation of focal nodular hyperplasia from hepatic adenoma at gadobenate dimeglumine-enhanced MR imaging: prospective study. *Radiology.* 2005;236(1):166–77.
13. Lerner SM, Hiatt JR, Salamandra J, Chen PW, Farmer DG, Ghobrial RM, et al. Giant cavernous liver hemangiomas: effect of operative approach on outcome. *Arch Surg.* 2004;139(8):818–21. discussion 21–3.
14. Clarke DL, Currie EJ, Madhavan KK, Parks RW, Garden OJ. Hepatic resection for benign non-cystic liver lesions. *HPB (Oxford).* 2004;6(2):115–9.
15. Hoekstra LT, Bieze M, Erdogan D, Roelofs JJ, Beuers UH, van Gulik TM. Management of giant liver hemangiomas: an update. *Expert Rev Gastroenterol Hepatol.* 2013;7(3):263–8.
16. Fan RF, Chai FL, He GX, Wei LX, Li RZ, Wan WX, et al. Laparoscopic radiofrequency ablation of hepatic cavernous hemangioma. A preliminary experience with 27 patients. *Surg Endosc.* 2006;20(2):281–5.
17. Sharpe EE 3rd, Dodd GD 3rd. Percutaneous radiofrequency ablation of symptomatic giant hepatic cavernous hemangiomas: report of two cases and review of literature. *J Vasc Interv Radiol.* 2012;23(7):971–5.
18. Meijerink MR, van den Tol P, van Tilborg AA, van Waesberghe JH, Meijer S, van Kuijk C. Radiofrequency ablation of large size liver tumours using novel plan-parallel expandable bipolar electrodes: initial clinical experience. *Eur J Radiol.* 2011;77(1):167–71.
19. van Tilborg AA, Dresselaars HF, Scheffer HJ, Nielsen K, Sietses C, van den Tol PM, et al. RF ablation of giant hemangiomas inducing acute renal failure: a report of two cases. *Cardiovasc Intervent Radiol.* 2016;39(11):1644–8.
20. Leporrier J, Maurel J, Chiche L, Bara S, Segol P, Launoy G. A population-based study of the incidence, management and prognosis of hepatic metastases from colorectal cancer. *Br J Surg.* 2006;93(4):465–74.
21. Abdalla EK, Vauthey JN, Ellis LM, Ellis V, Pollock R, Broglio KR, et al. Recurrence and outcomes following hepatic resection, radiofrequency ablation, and combined resection/ablation for colorectal liver metastases. *Ann Surg.* 2004;239(6):818–25. discussion 25–7.
22. Koopman M, Antonini NF, Douma J, Wals J, Honkoop AH, Erdkamp FL, et al. Sequential versus combination chemotherapy with capecitabine, irinotecan, and oxaliplatin in advanced colorectal cancer (CAIRO): a phase III randomised controlled trial. *Lancet.* 2007;370(9582):135–42.
23. Wei AC, Greig PD, Grant D, Taylor B, Langer B, Gallinger S. Survival after hepatic resection for colorectal metastases: a 10-year experience. *Ann Surg Oncol.* 2006;13(5):668–76.
24. Clavien PA, Petrowsky H, DeOliveira ML, Graf R. Strategies for safer liver surgery and partial liver transplantation. *N Engl J Med.* 2007;356(15):1545–59.
25. de Graaf W, van den Esschert JW, van Lienden KP, van Gulik TM. Induction of tumor growth after preoperative portal vein embolization: is it a real problem? *Ann Surg Oncol.* 2009;16(2):423–30.
26. Wu YZ, Li B, Wang T, Wang SJ, Zhou YM. Radiofrequency ablation vs hepatic resection for solitary colorectal liver metastasis: a meta-analysis. *World J Gastroenterol.* 2011;17(36):4143–8.
27. Evrard S, Rivoire M, Arnaud J, Lermite E, Bellera C, Fonck M, et al. Unresectable colorectal cancer liver metastases treated by intraoperative radiofrequency ablation with or without resection. *Br J Surg.* 2012;99(4):558–65.
28. Nielsen K, van Tilborg AA, Meijerink MR, Macintosh MO, Zonderhuis BM, de Lange ES, et al. Incidence and treatment of local site recurrences following RFA of colorectal liver metastases. *World J Surg.* 2013;37(6):1340–7.

29. Siperstein AE, Berber E, Ballem N, Parikh RT. Survival after radiofrequency ablation of colorectal liver metastases: 10-year experience. *Ann Surg.* 2007;246(4):559–65. discussion 65–7.
30. Al-Asfoor A, Fedorowicz Z, Lodge M. Resection versus no intervention or other surgical interventions for colorectal cancer liver metastases. *Cochrane Database Syst Rev.* 2008;2:CD006039.
31. Muratore A, Ribero D, Zimmitti G, Mellano A, Langella S, Capussotti L. Resection margin and recurrence-free survival after liver resection of colorectal metastases. *Ann Surg Oncol.* 2010;17(5):1324–9.
32. Otto G, Duber C, Hoppe-Lotichius M, Konig J, Heise M, Pitton MB. Radiofrequency ablation as first-line treatment in patients with early colorectal liver metastases amenable to surgery. *Ann Surg.* 2010;251(5):796–803.
33. Ruers T, Punt C, Van Coevorden F, Pierie JP, Borel-Rinkes I, Ledermann JA, et al. Radiofrequency ablation combined with systemic treatment versus systemic treatment alone in patients with non-resectable colorectal liver metastases: a randomized EORTC intergroup phase II study (EORTC 40004). *Ann Oncol.* 2012;23(10):2619–26.
34. Wong SL, Mangu PB, Choti MA, Crocenzi TS, Dodd GD 3rd, Dorfman GS, et al. American Society of Clinical Oncology 2009 clinical evidence review on radiofrequency ablation of hepatic metastases from colorectal cancer. *J Clin Oncol.* 2010;28(3):493–508.
35. van Tilborg AA, Scheffer HJ, de Jong MC, Vroomen LG, Nielsen K, van Kuijk C, et al. MWA versus RFA for perivascular and peribiliary CRLM: a retrospective patient- and lesion-based analysis of two historical cohorts. *Cardiovasc Intervent Radiol.* 2016;39(10):1438–46.
36. Dawson LA, Normolle D, Balter JM, McGinn CJ, Lawrence TS, Ten Haken RK. Analysis of radiation-induced liver disease using the Lyman NTCP model. *Int J Radiat Oncol Biol Phys.* 2002;53(4):810–21.
37. Potters L, Kavanagh B, Galvin JM, Hevezi JM, Janjan NA, Larson DA, et al. American Society for Therapeutic Radiology and Oncology (ASTRO) and American College of Radiology (ACR) practice guideline for the performance of stereotactic body radiation therapy. *Int J Radiat Oncol Biol Phys.* 2010;76(2):326–32.
38. Seung SK, Larson DA, Galvin JM, Mehta MP, Potters L, Schultz CJ, et al. American College of Radiology (ACR) and American Society for Radiation Oncology (ASTRO) practice guideline for the performance of Stereotactic Radiosurgery (SRS). *Am J Clin Oncol.* 2013;36(3):310–5.
39. Comito T, Clerici E, Tozzi A, D'Agostino G. Liver metastases and SBRT: a new paradigm? *Rep Pract Oncol Radiother.* 2015;20(6):464–71.
40. Kirichenko A, Gayou O, Parda D, Kudithipudi V, Tom K, Khan A, et al. Stereotactic body radiotherapy (SBRT) with or without surgery for primary and metastatic liver tumors. *HPB (Oxford).* 2016;18(1):88–97.
41. Scorsetti M, Clerici E, Comito T. Stereotactic body radiation therapy for liver metastases. *J Gastrointest Oncol.* 2014;5(3):190–7.
42. Alter MJ. Epidemiology of hepatitis C virus infection. *World J Gastroenterol.* 2007;13(17):2436–41.
43. El-Serag HB, Hampel H, Javadi F. The association between diabetes and hepatocellular carcinoma: a systematic review of epidemiologic evidence. *Clin Gastroenterol Hepatol.* 2006;4(3):369–80.
44. White DL, Kanwal F, El-Serag HB. Association between nonalcoholic fatty liver disease and risk for hepatocellular cancer, based on systematic review. *Clin Gastroenterol Hepatol.* 2012;10(12):1342–59 e2.
45. Llovet JM, Fuster J, Bruix J, Barcelona-Clinic Liver Cancer G. The Barcelona approach: diagnosis, staging, and treatment of hepatocellular carcinoma. *Liver Transpl.* 2004;10(2 Suppl 1):S115–20.
46. Mazzaferro V, Regalia E, Doci R, Andreola S, Pulvirenti A, Bozzetti F, et al. Liver transplantation for the treatment of small hepatocellular carcinomas in patients with cirrhosis. *N Engl J Med.* 1996;334(11):693–9.
47. Dong W, Zhang T, Wang ZG, Liu H. Clinical outcome of small hepatocellular carcinoma after different treatments: a meta-analysis. *World J Gastroenterol.* 2014;20(29):10174–82.

48. European Association For The Study Of The L, European Organisation For R, Treatment Of C. EASL-EORTC clinical practice guidelines: management of hepatocellular carcinoma. *J Hepatol.* 2012;56(4):908–43.
49. Scheffer HJ, Melenhorst MC, van Tilborg AA, Nielsen K, van Nieuwkerk KM, de Vries RA, et al. Percutaneous irreversible electroporation of a large centrally located hepatocellular adenoma in a woman with a pregnancy wish. *Cardiovasc Intervent Radiol.* 2015;38(4):1031–5.
50. Ben-David E, Ahmed M, Faroja M, Moussa M, Wandel A, Sosna J, et al. Irreversible electroporation: treatment effect is susceptible to local environment and tissue properties. *Radiology.* 2013;269(3):738–47.
51. Hosein PJ, Echenique A, Loaiza-Bonilla A, Froud T, Barbery K, Rocha Lima CM, et al. Percutaneous irreversible electroporation for the treatment of colorectal cancer liver metastases with a proposal for a new response evaluation system. *J Vasc Interv Radiol.* 2014;25(8):1233–9. e2.
52. Scheffer HJ, Nielsen K, de Jong MC, van Tilborg AA, Vieveen JM, Bouwman AR, et al. Irreversible electroporation for nonthermal tumor ablation in the clinical setting: a systematic review of safety and efficacy. *J Vasc Interv Radiol.* 2014;25(7):997–1011. quiz.
53. Sofocleous CT, Sideras P, Petre EN. “How we do it” – a practical approach to hepatic metastases ablation techniques. *Tech Vasc Interv Radiol.* 2013;16(4):219–29.
54. Nielsen K, Scheffer HJ, Vieveen JM, van Tilborg AA, Meijer S, van Kuijk C, et al. Anaesthetic management during open and percutaneous irreversible electroporation. *Br J Anaesth.* 2014;113(6):985–92.
55. Dunki-Jacobs EM, Philips P, Martin RC 2nd. Evaluation of thermal injury to liver, pancreas and kidney during irreversible electroporation in an in vivo experimental model. *Br J Surg.* 2014;101(9):1113–21.
56. Scheffer HJ, Vogel JA, van den Bos W, Neal RE 2nd, van Lienden KP, Besselink MG, et al. The influence of a metal stent on the distribution of thermal energy during irreversible electroporation. *PLoS One.* 2016;11(2):e0148457.
57. Beyer LP, Pregler B, Michalik K, Niessen C, Dollinger M, Muller M, et al. Evaluation of a robotic system for irreversible electroporation (IRE) of malignant liver tumors: initial results. *Int J Comput Assist Radiol Surg.* 2017;12(5):803–9.
58. Beyer LP, Pregler B, Niessen C, Schicho A, Haimerl M, Jung EM, et al. Stereotactically-navigated percutaneous Irreversible Electroporation (IRE) compared to conventional IRE: a prospective trial. *Peer J.* 2016;4:e2277.
59. Golberg A, Bruinsma BG, Uygun BE, Yarmush ML. Tissue heterogeneity in structure and conductivity contribute to cell survival during irreversible electroporation ablation by “electric field sinks”. *Sci Rep.* 2015;5:8485.
60. Philips P, Hays D, Martin RC. Irreversible electroporation ablation (IRE) of unresectable soft tissue tumors: learning curve evaluation in the first 150 patients treated. *PLoS One.* 2013;8(11):e76260.
61. Lee YJ, Lu DS, Osuagwu F, Lassman C. Irreversible electroporation in porcine liver: short- and long-term effect on the hepatic veins and adjacent tissue by CT with pathological correlation. *Investig Radiol.* 2012;47(11):671–5.
62. Narayanan G, Bhatia S, Echenique A, Suthar R, Barbery K, Yrizarry J. Vessel patency post irreversible electroporation. *Cardiovasc Intervent Radiol.* 2014;37(6):1523–9.
63. Dollinger M, Beyer LP, Haimerl M, Niessen C, Jung EM, Zeman F, et al. Adverse effects of irreversible electroporation of malignant liver tumors under CT fluoroscopic guidance: a single-center experience. *Diagn Interv Radiol.* 2015;21(6):471–5.
64. Niessen C, Beyer LP, Pregler B, Dollinger M, Trabold B, Schlitt HJ, et al. Percutaneous ablation of hepatic tumors using irreversible electroporation: a prospective safety and midterm efficacy study in 34 patients. *J Vasc Interv Radiol.* 2016;27(4):480–6.
65. Froud T, Venkat SR, Barbery KJ, Gunjan A, Narayanan G. Liver function tests following irreversible electroporation of liver tumors: experience in 174 procedures. *Tech Vasc Interv Radiol.* 2015;18(3):140–6.

66. Lee YJ, Lu DS, Osuagwu F, Lassman C. Irreversible electroporation in porcine liver: acute computed tomography appearance of ablation zone with histopathologic correlation. *J Comput Assist Tomogr.* 2013;37(2):154–8.
67. Vollherbst D, Fritz S, Zelzer S, Wachter MF, Wolf MB, Stampfl U, et al. Specific CT 3D rendering of the treatment zone after Irreversible Electroporation (IRE) in a pig liver model: the “Chebyshev Center Concept” to define the maximum treatable tumor size. *BMC Med Imaging.* 2014;14:2.
68. Sugimoto K, Moriyasu F, Kobayashi Y, Kasuya K, Nagakawa Y, Tsuchida A, et al. Assessment of various types of US findings after irreversible electroporation in porcine liver: comparison with radiofrequency ablation. *J Vasc Interv Radiol.* 2015;26(2):279–87 e3.
69. Guo Y, Zhang Y, Nijm GM, Sahakian AV, Yang GY, Omary RA, et al. Irreversible electroporation in the liver: contrast-enhanced inversion-recovery MR imaging approaches to differentiate reversibly electroporated penumbra from irreversibly electroporated ablation zones. *Radiology.* 2011;258(2):461–8.
70. Auler MA, Heagy T, Aganovic L, Brothers R, Costello P, Schoepf UJ. Saline chasing technique with dual-syringe injector systems for multi-detector row computed tomographic angiography: rationale, indications, and protocols. *Curr Probl Diagn Radiol.* 2006;35(1):1–11.
71. van Tilborg AA, Scheffer HJ, Nielsen K, van Waesberghe JH, Comans EF, van Kuijk C, et al. Transcatheter CT arterial portography and CT hepatic arteriography for liver tumor visualization during percutaneous ablation. *J Vasc Interv Radiol.* 2014;25(7):1101–11 e4.
72. Scheffer HJ, Melenhorst MC, Echenique AM, Nielsen K, van Tilborg AA, van den Bos W, et al. Irreversible electroporation for colorectal liver metastases. *Tech Vasc Interv Radiol.* 2015;18(3):159–69.
73. Deodhar A, Dickfeld T, Single GW, Hamilton WC Jr, Thornton RH, Sofocleous CT, et al. Irreversible electroporation near the heart: ventricular arrhythmias can be prevented with ECG synchronization. *AJR Am J Roentgenol.* 2011;196(3):W330–5.
74. Silk MT, Wimmer T, Lee KS, Srimathveeravalli G, Brown KT, Kingham PT, et al. Percutaneous ablation of peribiliary tumors with irreversible electroporation. *J Vasc Interv Radiol.* 2014;25(1):112–8.
75. Faroja M, Ahmed M, Appelbaum L, Ben-David E, Moussa M, Sosna J, et al. Irreversible electroporation ablation: is all the damage nonthermal? *Radiology.* 2013;266(2):462–70.
76. Narayanan G, Froud T, Lo K, Barbary KJ, Perez-Rojas E, Yrizarry J. Pain analysis in patients with hepatocellular carcinoma: irreversible electroporation versus radiofrequency ablation—initial observations. *Cardiovasc Intervent Radiol.* 2013;36(1):176–82.
77. Nielsen K, van Tilborg AA, Scheffer HJ, Meijerink MR, de Lange-de Klerk ES, Meijer S, et al. PET-CT after radiofrequency ablation of colorectal liver metastases: suggestions for timing and image interpretation. *Eur J Radiol.* 2013;82(12):2169–75.
78. Neal RE, Cheung W, Kavnaudias H, Thomson KR. Spectrum of imaging and characteristics for liver tumors treated with irreversible electroporation. *J Biomed Sci Eng.* 2012;5(12A):5.
79. Barabasch A, Distelmaier M, Heil P, Kramer NA, Kuhl CK, Bruners P. Magnetic resonance imaging findings after percutaneous irreversible electroporation of liver metastases: a systematic longitudinal study. *Investig Radiol.* 2017;52(1):23–9.
80. Padia SA, Johnson GE, Yeung RS, Park JO, Hippe DS, Kogut MJ. Irreversible electroporation in patients with hepatocellular carcinoma: immediate versus delayed findings at MR imaging. *Radiology.* 2016;278(1):285–94.
81. Zhang Y, Guo Y, Ragin AB, Lewandowski RJ, Yang GY, Nijm GM, et al. MR imaging to assess immediate response to irreversible electroporation for targeted ablation of liver tissues: preclinical feasibility studies in a rodent model. *Radiology.* 2010;256(2):424–32.
82. Centre for Evidence-Based Medicine (CEBM). Levels of evidence [cited 2016 April 11]. n.d. Available from: [http://www.cebm.net/levels\\_of\\_evidence](http://www.cebm.net/levels_of_evidence).
83. Cannon R, Ellis S, Hayes D, Narayanan G, Martin RC 2nd. Safety and early efficacy of irreversible electroporation for hepatic tumors in proximity to vital structures. *J Surg Oncol.* 2013;107(5):544–9.

84. Kingham TP, Karkar AM, D'Angelica MI, Allen PJ, Dematteo RP, Getrajdman GI, et al. Ablation of perivascular hepatic malignant tumors with irreversible electroporation. *J Am Coll Surg*. 2012;215(3):379–87.
85. Eller A, Schmid A, Schmidt J, May M, Brand M, Saake M, Uder M, Lell M. Local control of perivascular malignant liver lesions using percutaneous irreversible electroporation: initial experiences. *Cardiovasc Intervent Radiol*. 2015;38(1):8.
86. Cheung W, Kavnoudias H, Roberts S, Szkandera B, Kemp W, Thomson KR. Irreversible electroporation for unresectable hepatocellular carcinoma: initial experience and review of safety and outcomes. *Technol Cancer Res Treat*. 2013;12(3):233–41.
87. Glahder J, Norrild B, Persson MB, Persson BR. Transfection of HeLa-cells with pEGFP plasmid by impedance power-assisted electroporation. *Biotechnol Bioeng*. 2005;92(3):267–76.
88. Ivorra A, Al-Sakere B, Rubinsky B, Mir LM. In vivo electrical conductivity measurements during and after tumor electroporation: conductivity changes reflect the treatment outcome. *Phys Med Biol*. 2009;54(19):5949–63.
89. Pavlin M, Kanduser M, Rebersek M, Pucihar G, Hart FX, Magjarevic R, et al. Effect of cell electroporation on the conductivity of a cell suspension. *Biophys J*. 2005;88(6):4378–90.
90. Neal RE 2nd, Kavnoudias H, Cheung W, Golebiowski B, McLean CA, Thomson KR. Hepatic epithelioid hemangioendothelioma treated with irreversible electroporation and antibiotics. *J Clin Oncol*. 2013;31(27):e422–6.

Martijn R. Meijerink, Anders Nilsson,  
Govindarajan Narayanan, and Robert Martin

---

## 11.1 Introduction

Over 95% of pancreatic cancers are exocrine tumors that bare a dismal prognosis. Although oncological outcome is best for patients presenting with nonmetastatic resectable disease, cure is rarely achieved [1]. Up to 40% of patients present with nonmetastatic disease that is considered unresectable due to vascular encasement (locally advanced pancreatic carcinoma or LAPC) [1, 2]. These patients are nowadays routinely offered systemic chemotherapy with or without radiotherapy. Irreversible electroporation (IRE) represents a promising new method for focal destruction of pancreatic tumors. Evidence to support its effectiveness is gradually surfacing.

Over the last years, image-guided pancreatic tumor ablation has gained increased interest when surgical options are excluded. However, thermal ablation techniques such as radiofrequency ablation (RFA) and microwave ablation (MWA) are associated with substantial morbidity and mortality, due to the proximity of large vessels, the pancreatic and common bile duct, and the gastroduodenal wall [3]. Another major downside of thermal ablation techniques is the so-called “heat-sink” effect, when heat is lost to the flowing blood, which can hinder complete ablation [4].

One of the most promising new tumor ablation techniques, with distinct theoretical advantages over thermal ablative therapies, is irreversible electroporation (IRE). Since

---

M.R. Meijerink (✉)

Department of Radiology and Nuclear Medicine, VU University Medical Center,  
de Boelelaan 1117, 1081 HV Amsterdam, The Netherlands  
e-mail: [mr.meijerink@vumc.nl](mailto:mr.meijerink@vumc.nl)

A. Nilsson

Department of Radiology and Nuclear Medicine, Uppsala, Sweden

G. Narayanan

Department of Radiology and Nuclear Medicine, Miami, FL, USA

R. Martin

Department of Surgery, Louisville, KY, USA

IRE is thought to leave the integrity of inlying and adjacent vulnerable structures like large blood vessels, bile ducts, and intestines intact, IRE in theory represents a safe and feasible method to destroy pancreatic tumors that are considered unsuitable for surgical resection. Supporting evidence is gradually surfacing.

---

## 11.2 Anatomical and Physiological Considerations

The pancreas lies behind the peritoneum of the posterior abdominal wall and is covered by connective tissue, although it does not have a true capsule [5]. The second and third duodenum curvatures lie around the head of the pancreas. The anterior surface of the head of the pancreas is adjacent to the pylorus, the first part of the duodenum, and the transverse colon. The posterior surface adjoins the hilum and medial border of the right kidney, the inferior caval vein, the renal vasculature, the right gonadal vein, and the right muscular crus of the diaphragm. The uncinata process is an extension of the pancreatic tissue of variable shape off the lower part of the head of the pancreas, extending to the left and upward. The neck of the pancreas is a constricted part of the gland extending from the head of the pancreas toward the left, joining the head with the body of the pancreas. The neck extends to the right as far as the anterior superior pancreaticoduodenal artery from the gastroduodenal artery and lies anterior to the confluence of the superior mesenteric and splenic veins to form the portal vein. It is partly covered by the pylorus and the peritoneum of the minor omentum. The anterior surface of the pancreatic body is covered by the peritoneum of the omental bursa that separates the stomach from the pancreas. The stomach and the transverse mesocolon abut the body anteriorly. Posterior to the body of the pancreas are the aorta, the origin of the superior mesenteric artery, the left crus of the diaphragm, the left kidney and adrenal gland, and the splenic vein. The midline part of the body lies over the lumbar vertebrae, which makes this area of the pancreas most at risk to abdominal trauma. The body passes laterally and merges with the tail of the pancreas without a marked junction point. The relatively mobile tail is located in the anterior pararenal space. Its tip usually reaches the hilum of the spleen. With the splenic artery and vein, the tail is enclosed between the two layers of the splenorenal ligament.

The common bile duct is located in the posterior wall of the duodenum to the right of the gastroduodenal artery. The bile duct passes through the pancreatic head, to join with the main pancreatic duct before reaching the major duodenal papilla. The main pancreatic duct (of Wirsung) is formed by ductules that drain the lobules of the gland. At the level of the major papilla, the duct joins the common bile duct. In adults the length of the common channel averages 5 mm. The accessory pancreatic duct of Santorini, present in more than two thirds of patients, usually communicates with the main duct. The accessory duct lies anterior to the bile duct and usually drains into the minor papilla, which lies proximal to the ampulla of Vater.

The pancreas derives blood from several branches of the celiac and superior mesenteric arteries [6]. The descending part of the duodenum and the head of the pancreas are supplied by two pancreaticoduodenal arterial arcades. They are formed by the anterior and posterior superior pancreaticoduodenal arteries from the

gastroduodenal artery that arises off the common hepatic branch of the celiac artery to join a second pair of anterior and posterior inferior pancreaticoduodenal arteries. The anterior inferior pancreaticoduodenal artery arises from the superior mesenteric artery by the inferior margin of the pancreatic neck. The posterior inferior pancreaticoduodenal artery originates from the gastroduodenal artery. Its course is visible on the posterior surface of the pancreas, and branches may join the dorsal pancreatic artery. The dorsal pancreatic artery frequently arises from the splenic artery at the pancreatic neck. A right branch supplies the head and joins the posterior arcade. One or two left branches pass through the body and tail of the pancreas. The course of the splenic artery is posterior to the body and tail and loops above and below the superior margin of the pancreas. It gives off the great pancreatic artery, which usually joins one of the posterior superior arcades after giving off the inferior pancreatic artery. The caudal pancreatic artery arises from the left gastroepiploic artery or from a splenic branch at the spleen. It joins branches of the splenic and great pancreatic arteries.

In general, the venous drainage of the pancreas parallels the arterial blood supply. It flows into the portal vein, which is formed by the joining of the superior mesenteric and splenic veins at the confluence behind the neck of the pancreas. The portal vein lies behind the pancreas, with the common bile duct to the right and the hepatic artery to the left. The pancreatic veins that drain the neck, body, and tail of the pancreas join the splenic vein. The pancreaticoduodenal veins lie close to their corresponding arteries and empty into the splenic or portal veins. Because of the close anatomic relationship of the portal vein with the pancreas, inflammatory or neoplastic diseases involving the pancreatic body and tail can lead to portal vein occlusion. This in turn can result in retrograde venous drainage toward the splenic hilum and the short gastric and left gastroepiploic veins which may result in gastric varices.

The superior and inferior lymphatic vessels run along the border of the pancreas, respectively, with the splenic blood vessels and the inferior pancreatic artery [7, 8]. Those on the left side of the body and tail empty into nodes in the splenic hilum. Those on the right side of the body and the pancreatic neck empty into nodes near the upper border of the head. Lymphatic vessel drainage of the pancreatic head is composed of an anterior system and a posterior system. These vessels generally occupy the grooves between the head of the pancreas and the duodenum, near the pancreaticoduodenal blood vessels. The lymphatic drainage of the head of the pancreas and duodenum eventually flows into the celiac and superior mesenteric groups of pancreatic nodes and into the cisterna chyli. The lymphatics of the body pass to the pancreaticosplenic nodes lying along the superior border, which drain into celiac nodes. The lymphatics of the tail drain into splenic hilar nodes.

The celiac plexus, the largest of the three sympathetic plexuses, is situated at the level of the upper part of the first lumbar vertebra and is composed of two large ganglia, the celiac ganglia, and a dense network of nerve fibers uniting them together [9]. It surrounds the celiac artery and the root of the superior mesenteric artery. It lies behind the stomach and the omental bursa, in front of the crus of the diaphragm and the commencement of the abdominal aorta, and between the suprarenal glands.



The plexus and the ganglia receive the greater and lesser splanchnic nerves of both sides and some filaments from the right vagus and give off numerous secondary plexuses along the neighboring arteries. The celiac ganglia (semilunar ganglia) are two large irregularly shaped masses having the appearance of lymph glands and placed one on either side of the middle line in front of the crura of the diaphragm close to the suprarenal glands, that on the right side being placed behind the inferior vena cava. The upper part of each ganglion is joined by the greater splanchnic nerve, while the lower part, which is segmented off and named the aorticorenal ganglion, receives the lesser splanchnic nerve and gives off the greater part of the renal plexus. The greater splanchnic nerves modulate the activity of the enteric nervous system of the foregut. They also provide the sympathetic innervation to the adrenal medulla, stimulating catecholamine release. The lesser splanchnic nerves modulate the activity of the enteric nervous system of the midgut. The nerves that enter the pancreas include sympathetic, parasympathetic, and afferent components. The exact relationships of these fibers to the celiac ganglia and their distribution within the gland are not fully understood.

The pancreas is two glands intimately mixed together into one organ. The bulk of the pancreas is composed of exocrine cells that produce digestive enzymes. The endocrine pancreas, composed of small islands of cells (islets of Langerhans), constitutes approximately 4.5% of the pancreas volume and receives 10–15% of its blood flow [10]. It releases hormones such as insulin, glucagon, pancreatic polypeptide, preproinsulin, proglucagon, somatostatin, vasoactive intestinal peptide, growth hormone-releasing hormone, and gastrin. For these reasons, weight loss and new-onset diabetes mellitus often precede the clinical diagnosis of pancreatic carcinoma [11].

---

## 11.3 Pancreatic Malignancies

### 11.3.1 Pancreatic Adenocarcinoma

Pancreatic adenocarcinoma is among the most aggressive of all cancers. The overall 2-year survival rate is less than 10% and has barely improved over the past decades [12]. Tumors are often diagnosed at an advanced stage and as a consequence only 15–20% of patients are eligible for surgical resection. About 30–40% of patients present with locally advanced pancreatic cancer (LAPC, AJCC stage III), for whom median overall survival is approximately 1 year [13].

The clinical presentation of pancreatic malignancies depends on the size and location of the tumor as well as its metastases. Jaundice, pain, and weight loss are classic symptoms of pancreatic cancer [14]. Nonspecific early symptoms often are unrecognized; therefore, most pancreatic cancers are advanced at diagnosis. More than two thirds of pancreatic cancers occur in the head of the pancreas and usually present as steadily increasing jaundice caused by biliary duct obstruction. Painless obstructive jaundice traditionally is associated with surgically resectable cancers. Obstruction of the bile duct causes jaundice with disproportionately increased levels of conjugated bilirubin and alkaline phosphatase in the blood. The urine is dark

because of the high level of conjugated bilirubin and the absence of urobilinogen. The stool is pale because of the lack of stercobilinogen in the bowel. In addition to jaundice, rising bilirubin levels can cause severe pruritus. Patients with tumors in the body and tail of the pancreas generally present with nonspecific pain and weight loss. Body and tail tumors are much less likely to cause obstructive signs and symptoms. Patients may have pain in the epigastrium or back ranging from a dull ache to a severe pain. Tumors in the body and tail usually do not cause symptoms until they are large, and most present as locally advanced disease extending to the peritoneum and spleen.

### 11.3.2 Pancreatic Malignant Islet Cell Tumors

Islet cell tumors of the pancreas are rare tumors that are also called pancreatic neuroendocrine tumors. These tumors stem from neuroendocrine cells and tend to be slow-growing lesions that are often well treatable even after they have metastasized. Islet cell tumors can produce symptoms since up to half of these tumors may secrete hormones that produce side effects due to excessive secretion of the hormones such as insulin (insulinoma), gastrin (gastrinoma), glucagon (glucagonoma), VIP (VIPoma), and somatostatin (somatostatinoma).

---

## 11.4 Treatment of Pancreatic Malignancies

While surgical resection remains the only curative option, the majority of patients present with unresectable disease [15]. Even among those who undergo resection for AJCC stage I (tumor confined to the pancreas) and II (tumor growing outside the pancreas or pathology proven nodal metastases) disease, the reported median survival is 15–23 months, with a 5-year survival rate of approximately 20% [16]. Disappointingly, over the past decades, only modest improvements in survival have been realized despite improvements in diagnostic imaging, surgical technique, and chemotherapeutic options. Nevertheless, it remains clear that surgical resection is a prerequisite to achieve long-term survival. The prognosis for patients undergoing surgical resection for pancreatic ductal adenocarcinoma is highly dependent on margin status, with total gross excision and histologically negative margins (R0 resection) being associated with the best outcomes. Survival for patients who undergo total gross excision but have histologically positive margins (R1 resection) is reduced according to most series [17]. There is now emerging consensus that a subgroup of patients, previously considered poor candidates for resection because of the relationship of their primary tumor to surrounding vasculature, may benefit from resection, particularly when preceded by neoadjuvant therapy [18]. In these patients, an interface exists between the tumor and the superior mesenteric or portal vein measuring  $180^\circ$  or greater of the vessel wall circumference or between the tumor and the celiac trunk or superior mesenteric artery measuring less than  $180^\circ$  of the vessel wall circumference. Short-segment occlusion of the superior mesenteric/portal vein or hepatic artery is allowed if considered

reconstructable. For patients with unresectable stage III pancreatic cancer, systemic therapy with or without radiation has been the standard of care for decades. Relatively new chemotherapy regimens such as FOLFIRINOX (5-fluorouracil, leucovorin, irinotecan, and oxaliplatin) and the addition of nab-paclitaxel to gemcitabine have recently shown to significantly improve survival for patients with metastatic pancreatic adenocarcinoma. Nevertheless, the prognosis remains dismal [5, 6].

#### 11.4.1 Chemotherapy for LAPC

Several randomized studies have demonstrated a median overall survival of 9.2–11.7 months for patients with LAPC treated with gemcitabine alone [19, 20]. Although newer, potentially more effective, chemotherapy regimens have become available, most of these studies focused on patients with metastatic disease. One major advancement in systemic chemotherapy for pancreatic cancer is FOLFIRINOX (fluorouracil, folinic acid, oxaliplatin, and irinotecan), which resulted in a significant improvement in progression-free and overall survival of patients with metastatic disease in a phase III European study [21]. There is much interest to incorporate FOLFIRINOX into the multimodality treatment of LAPC, as several retrospective observational cohorts also suggest a survival benefit for patients with stage III pancreatic cancer. Nevertheless, no randomized controlled trials have so far evaluated the effect of FOLFIRINOX as a stand-alone therapy for LAPC. Several observational series have reported median overall survival results ranging 11.2–18.4 months for first-line FOLFIRINOX with or without radiotherapy [22–28]. Although complications such as neutropenia, neutropenic fever, anemia, thrombocytopenia, fatigue, anorexia, mucositis, nausea, vomiting, diarrhea, peripheral neuropathy, and alopecia are often encountered, the incorporation of specific dose reductions has decreased the number of patients having to stop treatment prior to having reached progression [29].

#### 11.4.2 Radiotherapy for LAPC

The role of concurrent radiotherapy for LAPC remains controversial as the results of randomized controlled trials are in conflict [30]. Traditionally, trials using radiotherapy include the use of conventional external beam radiation (EBR). This technique uses large radiation fields that inevitably deliver a high percentage of the radiation dose into critical surrounding structures. When irradiating abdominal tumors with conventional external beam radiation, strict adherence to normal structure dose constraints may limit the delivery of the intended radiation dose to the tumor and potentially result in premature local failure and death. Conversely, delivering high doses of radiation to adjacent critical structures without strict dose constraints increases the risk of late radiation-induced complications [31]. A recent advancement in radiation therapy is stereotactic ablative body radiotherapy (SABR). SABR can deliver higher doses of radiation more precisely to the tumor and a small margin (usually 2–3 mm) because of the rapid dose falloff beyond the treated volumes. This limits the dose delivered to normal bowel,

resulting in decreased toxicity and dose escalation to the tumor. Several studies investigated the effects of SABR for patients with LAPC. The reported median overall survival ranges from 6.2 to 24 months [32–35]. Complications include gastroparesis, gastrointestinal (duodenal) bleeding, duodenal or gastric ulcer, anorexia, nausea/vomiting, and thrombosis of the superior mesenteric vein or inferior vena cava.

### 11.4.3 New Local Ablative Therapies for LAPC

Due to poor efficacy results of currently used treatments, researchers are continuously investigating novel and modified treatment strategies to improve survival. Whereas two decades ago, image-guided tumor ablation techniques were still in its infancy, nowadays many different ablation techniques have substantially improved curative treatment possibilities for numerous types of localized cancer in many different organs. Different nonsurgical thermal ablation techniques (cryoablation, radiofrequency ablation (RFA), high-intensity focused ultrasound (HIFU), laser ablation, and microwave ablation (MWA)) have been investigated in order to improve survival for patients with LAPC. However, ablative therapies are limited due to the risk of thermal damage to nearby vital structures, associated with high complication rate (28–40%) and high mortality rate (7.5%) [36]. Also, the so-called “heat-sink” effect, in which tumor cells near to large vessels are prevented from adequate heating due to flowing blood cooling adjacent tissue, can lead to incomplete ablation. This effect is another drawback in the performance of thermal ablation in LAPC, since the tumor is typically surrounded by major vessels.

Irreversible electroporation (IRE) is a new, image-guided tumor ablation technique that takes advantage of the electric potential gradient that exists across cell membranes. The application of an electric field across a cell alters the cellular transmembrane potential. By reaching a sufficiently high voltage, the phospholipid bilayer structure of the cell membrane is permanently disrupted, inducing apoptosis and cell death [37]. Tumors in contact with vessels can be treated with IRE without compromising the vessels or resulting in heat-sink since its effectiveness relies on electrical energy. Because of its vessel-sparing mechanism of action, IRE is hypothesized to have wider indications than the thermal ablation technologies. This makes IRE a very attractive option in patients with LAPC, as the reason for unresectability is usually vascular encasement.

---

## 11.5 Patient Selection, Indications, and Contraindications

Because of the relatively high morbidity involved in the radical ablative treatment of pancreatic tumors, patient selection is fundamental. Patients must be motivated and understand that recovery may be prolonged, and that quality of life and daily functioning may be compromised, even following a successful procedure. Physicians should take patient comorbidities and overall performance status into account. Patients with poor functional reserve at baseline are not good candidates. Patients

should be evaluated with detailed and appropriate pre-procedural workup, including medical, cardiac, and pulmonary clearance, and optimized prior to the intervention. The treatment plan should ideally be made by a multidisciplinary team that includes interventional radiologists, surgeons, medical and radiation oncologists, abdominal diagnostic radiologists, and gastroenterologists.

Neoadjuvant systemic chemotherapy should be favored for patients with LAPC for several reasons. Firstly, to exclude patients with aggressive subtypes that will progress and/or metastasize during the induction period and who will presumably not benefit from an IRE procedure. Secondly, because a considerable percentage of patients will be downstaged to resectable disease and, given the promising percentage of R0 resections in this specific group, resection should be considered favorable over focal tumor ablation. Lastly, with a decrease in volumetric tumor size, the IRE procedure presumably becomes a safer and more efficacious treatment option.

Adult patients with non-metastasized histopathologically proven pancreatic adenocarcinoma are considered eligible for irreversible electroporation if the tumor is truly unresectable based on at least a dedicated contrast-enhanced pancreatic CT. The authors consider a tumor diameter of 5 cm the upper limit for IRE. In case of biliary obstruction, adequate biliary drainage prior to the procedure should be guaranteed either by placing a (nonmetal) biliary endoprosthesis prior to a percutaneous procedure or by creating a surgical biliodigestive anastomosis prior to an open procedure.

Transmucosal tumor invasion into surrounding intestines or extensive involvement (complete encasement) of the duodenum, a history of ventricular arrhythmias, congestive heart failure (>NYHA class 2), uncontrolled hypertension, and any implanted cardiac stimulation devices are considered absolute contraindications. Coronary artery disease (defined as myocardial infarction within 6 months prior to screening); atrial fibrillation; the presence of metallic foreign objects, such as non-removable self-expanding metal biliary stent (SEMS), in the ablation zone; and having received chemo- or immunotherapy maximum 4 weeks prior to the procedure are considered relative contraindications. Patients with a compromised liver function (e.g., signs of portal hypertension, INR > 1,5 without use of anticoagulants, ascites) or patients suffering uncontrolled infections are not good candidates. If the anatomical location of the tumor would necessitate advancing needles through the small bowel or colon safety-enhancing procedures such as pneumo-, hydro-, or balloon dissections or laparoscopic surgical assistance may be considered as well as a dorsal percutaneous approach [38]. For such procedures, extensive experience with percutaneous image-guided tumor ablation is mandatory.

---

## 11.6 Patient Workup and Treatment Planning

Eligible patients should be suitable for general anesthesia by anesthetic review with special attention to cardiac history and include electrocardiography (ECG). Routine blood samples should include electrolyte and creatinine testing, complete

blood count, and coagulation studies. For patients taking anticoagulant or antiplatelet drugs, the risk of stopping the medication must be balanced against the risk of harm if treatment is stopped. For low-risk procedures, aspirin can be continued. Clopidogrel and warfarin should be stopped although this may require bridging anticoagulation with unfractionated or low molecular weight heparin. Consultation with a cardiologist is particularly recommended for patients with coronary artery stents.

Prophylactic biliary protection is recommended for tumors adjacent to the biliary tree in order to prevent biliary obstruction caused by the IRE procedure. Placement of a plastic biliary endoprosthesis is much more challenging in the initial days following IRE due to extensive swelling of the ampullary area.

The treatment plan should be based on a dedicated contrast-enhanced abdominal CT (with the upper abdomen scanned according to a dedicated 3-mm-slice-multiphase-pancreatic tumor protocol). The size and shape of the tumor should determine the number and configuration of the needle electrodes aiming at an interelectrode distance of approximately 2 cm and a tumor-free margin of 0.5 cm.

---

## 11.7 Approach, Image Guidance, and Technique

The preferred line of attack for pancreatic IRE will be the topic of widespread debate for many years to come. Although, in general, pancreatic surgeons promote the open approach, most interventional radiologists prefer the percutaneous route. At this moment, advocating superiority of one over the other approach is ungrounded since no direct comparison has ever been performed. Both approaches have distinct advantages and disadvantages. The chapter authors each have their own preferences, which will be debated in the following sections. As there is currently no proof that one method is superior to the other, it can be said that the method of choice is the method that works best for the person about to perform the treatment. Procedures are always performed under general endotracheal anesthesia with deep paralysis, defined as zero twitches before IRE delivery as per a standard anesthesia twitch monitor. Using the only commercially available system currently out there (NanoKnife, AngioDynamics Inc., Queensbury, NY), at least 90 pulses of 1,000–1,500 V/cm with a 90-ms pulse length are delivered for each electrode pair, including 10 or 20 test pulses. An ECG-gating device is connected to a 5-lead ECG to allow IRE pulses to be synchronized with the refractory period of the heart to avoid arrhythmias. When necessary, additional doses to block the neuromuscular cascade can be administered by the anesthesiology team. Prior to the procedure, two defibrillation pads are placed and connected to a defibrillator as a precautionary measure. Given the high conductivity of pancreatic cancerous tissue and hence the higher risk to induce overcurrent, the active working length is routinely set at 1.5 cm by most physicians (Table 11.1).

**Table 11.1** The open versus the percutaneous approach for pancreatic IRE

	Open	Percutaneous
<b>Invasiveness</b>		
Length of hospital stay	Long	Short
Impact on quality of life	Major	Moderate
Pain assessment post-IRE	Moderate–high	Low–moderate
<b>Mortality</b>		
Related to IRE	4%	0%
Related to general procedure	2%	0%
	2%	0%
<b>Safety</b>		
Complications related to probe insertion	Less likely due to manual segregation of surrounding structures from the pancreas	Crossing the stomach or liver often inevitable. Traversing major blood vessels, the duodenum or colon should be avoided
Complications related to the delivery of pulsed electrical fields	Collateral damage to surrounding intestines less likely	Collateral damage to surrounding intestines possible
Complications caused by the general procedure	Complications caused by the laparotomy such as infection, bleeding, bile or pancreatic fluid leakage, fistula formation, and pancreatitis are common, as are pneumonia, pleural effusion, and deep vein thrombosis can occur	Complications such as pneumonia and deep vein thrombosis are rare
<b>Outcome</b>		
Progression-free survival	8.0–13.0 months	8.0–11.0 months
Overall survival	16.0–23.2 months	17.0–27.0 months

### 11.7.1 The Open Approach (R. Martin)

Access for open IRE is performed through a superior midline incision [39]. A superior midline incision is utilized based on the planned needle placement performed most commonly and in a safer manner through a caudal-to-cranial approach. In turn, the caudal-to-cranial approach is more easily facilitated through a midline laparotomy than through a bilateral subcostal laparotomy. The abdomen is thoroughly examined to rule out any type of occult solid organ liver metastases as well as peritoneal or mesenteric metastases. Intraoperative ultrasound of the liver is also performed to rule out any type of non-palpable liver metastases that may have been missed on dynamic CT scan. Only after no evidence of metastatic disease is confirmed is intraoperative ultrasound then turned to the operative assessment of the tumor. Given the lack of definitive accuracy as well as positive predictive value of CT scan alone because of volume averaging, it is important to ensure that the patient truly has greater than 180° encasement of the SMA before deciding on in situ IRE therapy vs. pancreaticoduodenectomy with margin accentuation with IRE along the

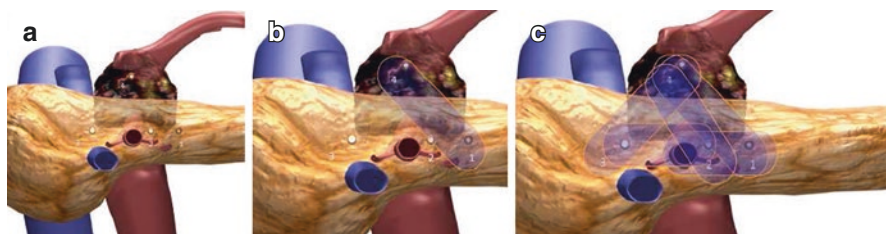


**Fig. 11.1** Axial plane with a triangle probe technique for locally advanced pancreatic tumor with a broader base in the axial plane requiring a three-probe posterior placement technique with either one probe (or two probes) on top to create the triangle. The probe pair with the longest distance (maximum 2.3 cm) is then treated first, followed by other probe pairs to ensure a complete irreversible electroporation utilizing all probe pairs that are active. Note – probe pair 1–3 is not active since the distance between them is more than 2.3-cm spacing [39]

SMA. Our optimal ultrasound technique is transgastric and is performed with placing the ultrasound probe on top of the gastric body closer to the pylorus. We recommend imaging with minimal amount of mobilization and avoiding the mobilization into the lesser sac, which further impedes optimal intraoperative imaging since this will disrupt the tissue planes with air and lead to a greater artifact. The reason for performing through a transgastric approach is that the stomach serosa allows for a complete and clean apposition of the ultrasound crystals and provides minimal to no artifact to truly image a pancreatic head lesion and subsequent portal vein as well as superior mesenteric vein. Thus, intraoperative ultrasound imaging has become our gold standard for elucidating whether a patient has a true locally advanced tumor or a borderline resectable tumor. In short, two monopolar probes with 2-cm spacing will deliver an electroporation defect of approximately axial 3.5 cm, anterior-posterior 2.5 cm, and cranial-caudal of 2.5 cm. This electroporation defect is achieved through a maximum of 1.5-cm exposure, 1,500 V/cm, with 100  $\mu$ s wavelength. Preoperative narcotic management was normalized to fentanyl dosages because that was the predominant narcotic used, with additional wide ranges of other narcotics being used. A jejunal feeding tube was used at the surgeon's discretion but was placed in most cases secondary to a conservative approach and to avoid a prolongation of hospital stay related to delayed gastric emptying. A prophylactic gastrojejunostomy, J-tube, or hepaticojejunostomy should be considered at surgeon's discretion (Fig. 11.1).

### 11.7.2 The Percutaneous US-Guided Approach (A. Nilsson)

When using ultrasound guidance, it is strongly recommended to plan the procedure by doing a contrast-enhanced ultrasound on the day before the ablation taking note of tumor delineation, projected needle paths, and possible vascular occlusions. Ultrasound, as in all types of image-guided intervention, has the advantage of being cheap and readily available in most departments. It offers a real-time image with a good delineation of vascular structures and spatial resolution, these traits being



important when a needle is to be placed very close to critical structures, which is most often the case with IRE. On the other hand, when using ultrasound, compared to CT, it is more difficult to measure the distance between the needles with absolute accuracy and also to know that the needles are parallel. To overcome these shortcomings, it is important to take special care about the positions of the needle insertions making the distances between the needles correct on the skin, maybe even with the use of a spacing device (image). Also, as we may not know the exact distance between needles, starting the treatment with ten pulses of a slightly lower V/cm than recommended enables the user to deliver some pulses (typically 10–20), check the resulting current (graph produced by the machine), and then adjust the V/cm according to the initial resulting amperes. Another drawback, it has to be admitted, is that needle placement under ultrasound guidance is not possible in all patients due to factors like obesity and/or overlying bowel gas so that the pancreas cannot be visualized. In most cases, though, the pancreas can be seen and the tip of the IRE needle is clearly visible on ultrasound. Another slightly weaker echo is also seen at the beginning of the active needle. This makes it easier to estimate if a pullback is needed or not. When the needles are in place the treatment, of course, follows the same guidelines as with CT guidance, see below.

### **11.7.3 The Percutaneous CT-Guided Approach (M. Meijerink)**

For optimal CT image quality, the arms should be elevated above the patient's head. To define the three-dimensional measurements of the tumor and its vicinity to vital structures, a contrast-enhanced (ce)CT or cone-beam CT scan should be performed prior to the ablation, preferably using multiplanar image reconstruction to verify and if necessary adjust the treatment plan. Needle electrodes will be advanced in and around the tumor under CT fluoroscopy guidance, aiming at an interelectrode distance of 15–24 mm. For spherical tumors <3 cm, placing three to five needles in the edge of the tumor should allow for a complete ablation. For lesions  $\geq 3$  cm, it is recommended to place one needle electrode in the center of the tumor and, depending on lesion size, at least four additional needles aiming at the outer margins. To avoid having to traverse the colon or other crucial structures, it is often necessary to use an angulated approach. For this reason, either gantry tilt, virtual gantry tilt, or CT to ultrasound real-time image registration and fusion software is crucial. Similar to percutaneous CT-guided thermal ablation, we advise to use pneumo- or hydrodissections whenever considered necessary. The order in which the electrodes are placed depends on the position of the patient with regard to the gantry (feet or head first) and the position of the physician (right or left side of the patient). To avoid blocking your view and to preserve all degrees of freedom with respect to the needle trajectory, we advise to begin with the electrode furthest away from the operator within the gantry. For larger tumors that need pullback ablations for complete coverage, we advise to start with the deep (dorsal) part of the tumor and work your way upward to the more superficial part. After having placed all electrodes, a ceCT scan is made to verify the exact needle locations and the interelectrode distances in a plane perpendicular to the needle electrodes, again

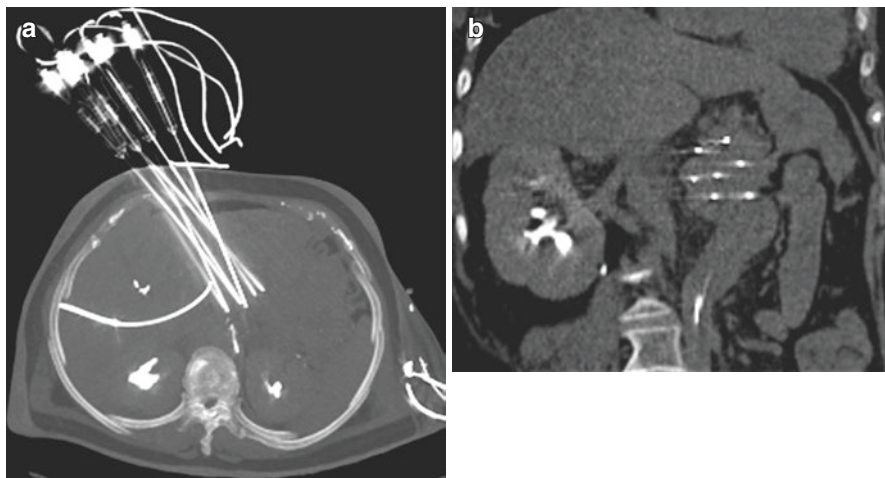


**Fig. 11.2** Example of a percutaneous CT-guided IRE procedure of the pancreas. Using transcatheter aortography (with a catheter in the aorta, we can repeatedly visualize the arteries and veins, while advancing the needles, with just 20 cc of contrast material [diluted 1:1 with saline])-guided CT fluoroscopy, one needle is placed in the center and six in the margins of the lesion. In this case, a total number of 12 electrode pairs (six connecting the outer electrodes and six connecting the central electrode with the outer electrodes)

using multiplanar image reconstruction. Immediately after the procedure, a third ceCT scan will assess the ablation zone and detect crucial early complications such as an active perilesional hemorrhage and/or iatrogenic vascular occlusions such as acute portal vein thrombosis (Fig. 11.2).

## 11.8 Complications

IRE-related hazards can be divided into three types: (1) risks associated with the general procedure, (2) risks associated with probe insertion, and (3) risks associated with exposing patients to pulsed electrical fields. Although an early systematic review describes a low overall complication rate for pancreatic IRE of 19% (8–42) and a major complication rate of 7% (3–42) [37], in the more recently published prospective PANFIRE trial, 10 out of 25 patients developed 23 adverse events (40%) [40].

Expected adverse events associated with the delivery of strong electric pulses are cardiac arrhythmias and severe muscle contractions. To prevent these events, pulses are generally delivered in the refractory period of the heart and with deep muscle paralysis. Scheffer et al. reported eight arrhythmias (CTCAE grade I–II), corresponding to a total incidence of 4% (8–194) [37]. Without synchronized pulsing, ventricular arrhythmias occurred four times (transient ventricular tachycardia) and immediately resolved after pulse delivery was aborted. With the use of cardiac synchronization, only atrial arrhythmias occurred, which resolved spontaneously or within 24 h after therapy. With the administration of muscle relaxants, no uncontrolled muscle contractions were reported. Only Thomson et al. reported a

transient increase in systolic blood pressure in all patients directly after IRE (20–30 mmHg), which normalized spontaneously [41].

Complications associated with probe insertion were spontaneous pneumothorax during anesthesia requiring chest drainage and small subcutaneous hematoma [37, 42].

On follow-up, five site-specific complications occurred. Two were portal vein thrombosis after open IRE; one required paracentesis and aldactone, and one was fatal [37, 43]. Two cases of bile leak (CTCAE grade III–IV) were reported after open IRE [44]. One patient had undergone concurrent duodenal stent removal via duodenotomy; in the other patient, the electrodes were placed transduodenally. Both complications required percutaneous drainage after which they resolved. Scheffer et al. reported pancreatitis only once in 42 procedures which resolved spontaneously (CTCAE grade II) [37]. Martin et al. reported elevated amylase and lipase in all 27 patients, without clinical signs of pancreatitis [45]. Abdominal pain grade I was reported in all patients (15 of 15) after percutaneous pancreatic ablation [42]. Pain was always easily manageable with oral or intravenous analgesics and did not lead to prolonged hospitalization. In the recently published prospective PANFIRE trial (percutaneous IRE), 10 out of 25 patients (40%) developed 23 adverse events (two CTCAE grade IV) [40]. One patient developed an edematous pancreatitis (Balthazar E; CT severity index [CTSI] 4) with bile leakage and hemodynamic instability requiring intravenous antibiotics, fluid resuscitation, and percutaneous drainage. Another patient presented with massive hematemesis 3 days after discharge caused by a duodenal wall ulcer directly adjacent to the ablation zone and was treated with blood transfusion and proton pump inhibitors. Three patients developed de novo biliary obstruction requiring biliary drainage within 90 days post-IRE (grade III). Two out of three endoscopic retrograde cholangiopancreatography (ERCP) revealed swelling of the ampullary area. In these cases, placement of a plastic biliary endoprosthesis was challenging, but eventually successful (Fig. 11.3).

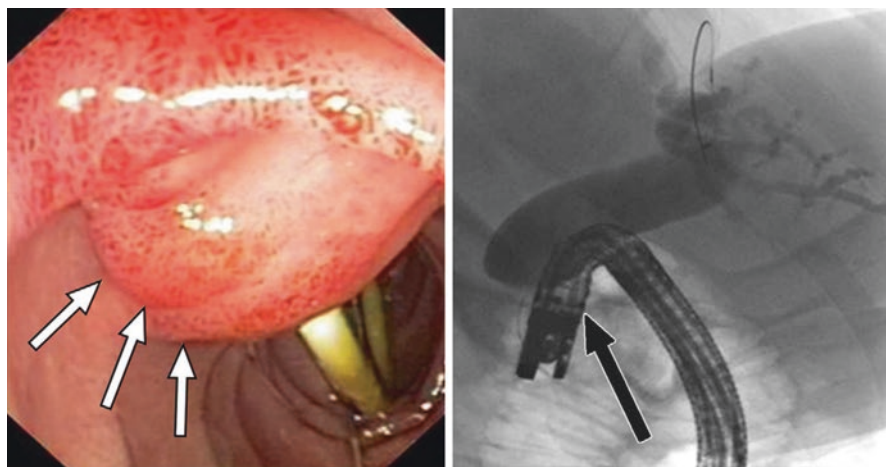


**Fig. 11.3** Adapted from Scheffer et al. (a) Image from endoscopic retrograde cholangiopancreatography performed 6 weeks after IRE shows erythematous swelling of the ampullary area, with major papilla turned backward. (b) Fluoroscopy image shows cannulation of major papilla by positioning duodenoscope in “long position” [40]

Another patient presented with cholangitis and an infected biloma, requiring percutaneous drainage and placement of a percutaneous transhepatic cholangiography drain (PTCD). In one patient, a near occlusion of the – previously slightly narrowed – superior mesenteric artery (SMA) was visible on ceCT 6 weeks post-IRE, with no other signs for local site recurrence. Because she also experienced postprandial abdominal cramps, a vascular stent was placed for symptom relief and to prevent mesenteric ischemia. Further, 12 gastrointestinal complications such as nausea, vomiting, diarrhea, delayed gastric emptying, abdominal pain, loss of appetite, and reduced intake were observed ( $n = 6$ ). Two patients required temporary nasogastric drainage and placement of a nasojejunal feeding tube. Diarrhea and abdominal pain were treated with loperamide and by adjusting the amount of pancreatic enzyme supplementation. There was a significant increase in amylase and lipase 1 day post-IRE compared to pre-IRE values ( $p = 0.009$  and  $p = 0.001$ ). After 2 weeks, amylase and lipase had returned to pre-IRE values ( $p = 0.26$  and  $p = 0.12$ ). Three patients developed clinical signs of pancreatitis (Table 11.2 and Fig. 11.4).

**Table 11.2** Adverse events of pancreatic IRE

Risks associated with the general procedure	Risks associated with probe insertion	Site-specific complications
Cardiac arrhythmias	Hemorrhage	Portal vein thrombosis, arterial stenosis
Transient hypertension	Pancreatic fistula	Pancreatitis, abdominal pain
		Hemorrhagic duodenal wall ulcer
		Biliary obstruction, pancreatitis
		Nausea, vomiting, diarrhea
		Delayed gastric emptying, loss of appetite, and reduced intake

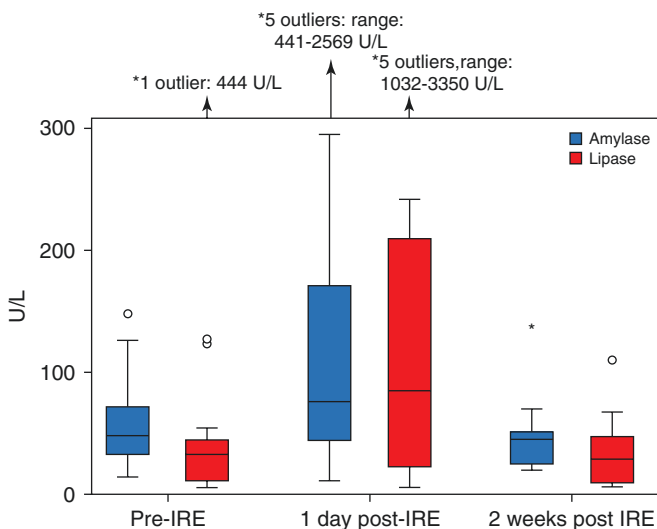


**Fig. 11.4** Adapted from Scheffer et al. Box-and-whisker plot shows amylase and lipase values before and after IRE [40]

## 11.9 Follow-Up and Response Evaluation

Knowledge of postinterventional MR and CT findings is essential for accurate interpretation of the ablated area [46]. Familiarity with these characteristics prevents confusion between normal or less typical postablational changes and residual or recurrent disease. In addition, timely recognition of IRE-related complications and vital tumor allows for expedited management and possible retreatment. The World Health Organization (WHO) and RECIST criteria depend on decrease in tumor size. However, decrease in viable cell mass is not always reflected by changes in tumor size. Exclusive reliance on tumor size does therefore not provide a complete assessment of tumor response and may lead to inaccurate conclusions. A preferable method of post-IRE treatment evaluation is to combine tumor and ablation zone sizes with functional information such as alterations in enhancement and diffusion.

Since little healthy pancreatic parenchyma surrounds the pancreatic tumor, the ablation zone is often ill-defined on MRI and especially on CT. Also, the presence of edema within the ablation zone impedes precise ablation zone delineation. A reasonable explanation for the observed hyperintense rim surrounding the ablation zone post-IRE is reactive hyperemia of edematous inflammatory origin. However, it cannot be excluded that this rim still contains residual disease and longer follow-up is needed to explore the exact significance. The remarkable hypointense rim that we found on T2 at 2 weeks suggests hemosiderin deposition resulting from degradation of the extravagated erythrocytes in the periphery of the ablation zone [46]. Post-IRE, arterial and portal venous phase CT attenuation decreased in nearly all patients. This decline in enhancement is in line with the observed postcontrast MRI findings which may be indicative for accurate tumor therapy response. The observed intralesional gas pockets may be caused by electrolysis of water into hydrogen and oxygen caused by the electric pulses or by vaporization due to heat development or by a combination of these mechanisms.

Initial post-IRE examinations reveal a notable volume increase on ceCT and ceMRI, followed by a decrease during follow-up. The calculated volumes varied widely between the two modalities, which is caused by the difficult ablation zone delineation from surrounding structures. Studies investigating the size and shape of the IRE ablation zone have predominantly correlated imaging findings to histology in animal studies. Overall, the radiological ablation zone size as measured on CT and MRI-DWI correlates well with the histologic ablation zone. In addition, studies suggested that ablation zone size and shape depend on the IRE parameters used and on the type of tissue ablated. There is clear concordance between our findings and preclinical and early clinical studies that describe a reduction of the size of the ablated area over several weeks, resulting from the clearance of cellular debris aided by the preservation of larger vessels.

Vroomen et al. all describe DWI-b800 hyperintensity and low ADC values at 6 weeks to predict tumor residue or early recurrence [46]. Hence, DWI-b800 and ADC may be useful to predict early recurrence or incomplete ablation, similar to imaging after hepatic ablation. This may allow for earlier retreatment. 18F-fluorodeoxyglucose positron emission tomography (18F-FDG PET) CT has demonstrated better diagnostic accuracy compared with ceCT and even MRI (without DWI-b800) in the diagnosis of pancreatic cancer. Also, 18F-FDG PET is increasingly used to assess tissue response to

chemoradiation for LAPC. One recent study showed the difference in maximum standardized uptake value (SUVmax) pre- and post-chemoradiation for LAPC was an independent predictor of clinical outcome [46] (Figs. 11.5 and 11.6).

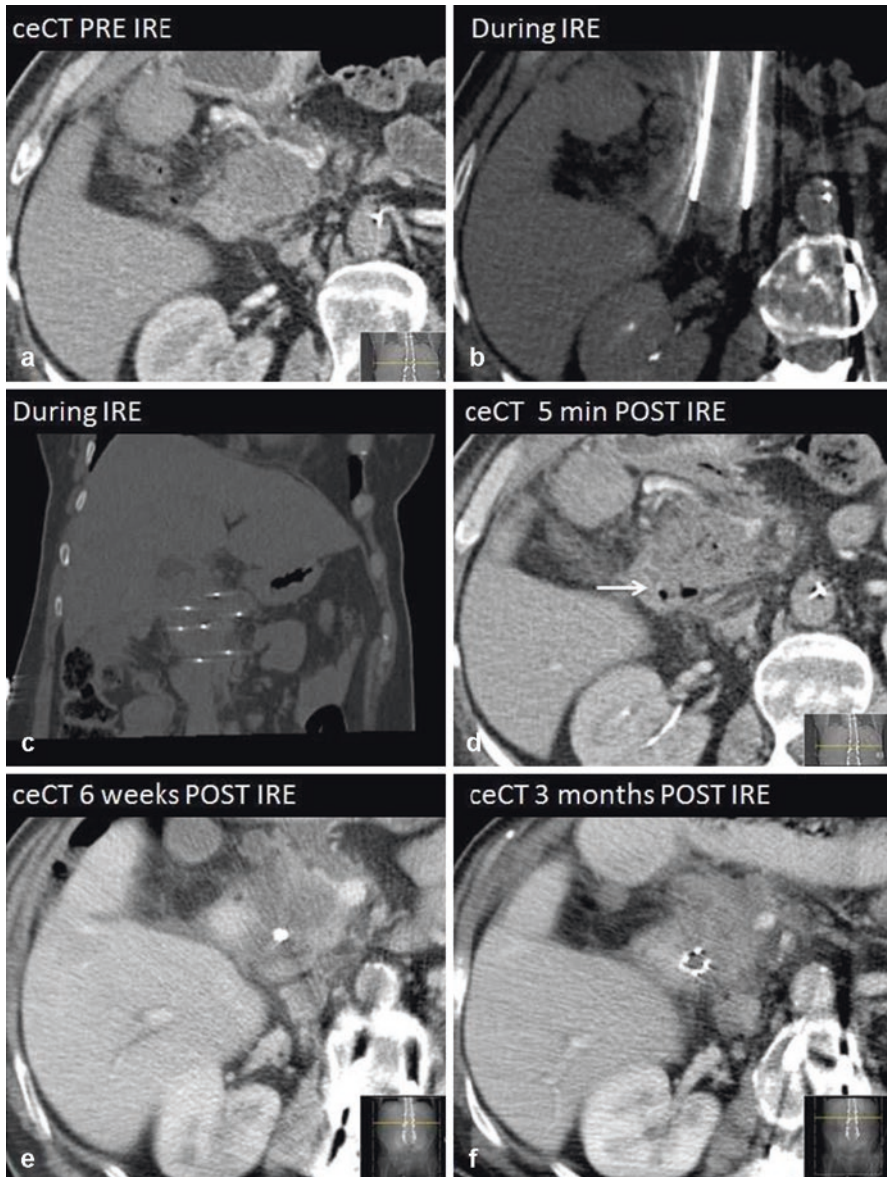


**Fig. 11.5** Adapted from Vroomen et al. Imaging findings during follow-up on ceCT (a) Isoattenuating tumor on ceCT pre-IRE (b) CT-guided placement of electrodes around the outer border of the tumor (c) Confirmation of correct electrode configuration according to the treatment plan with a nonenhanced CT scan (d) Hypoattenuating IRE ablation zone with intralesional gas pockets immediately after IRE (e) Hypoattenuating IRE ablation zone at 6 weeks follow-up (f) Hypoattenuating IRE ablation zone at 3 months follow-up [46]

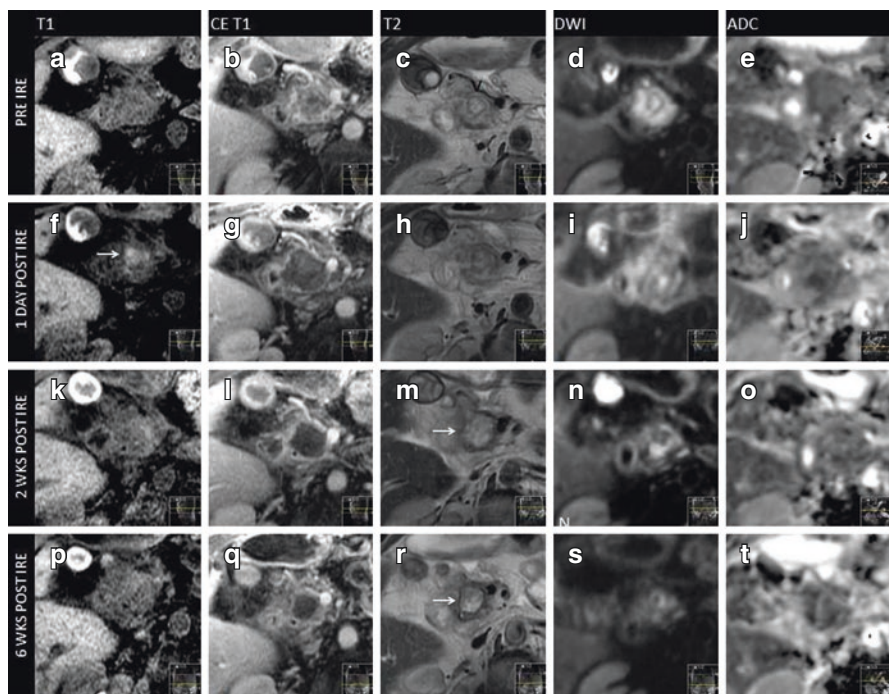


**Fig. 11.6** Adapted from Vroomen et al. Prior to IRE: (a) Isointense tumor on T1 sequence (b) Hypointense tumor on T1 sequence (portal venous phase) (c) Hyperintense tumor on T2 sequence (d) Hyperintense tumor on DWI-b800 sequence (e) Hypointense tumor on ADC map. 1 day post-IRE: (f) Isointense IRE ablation zone with small hyperintense blood residues on T1 sequence (g) Hypointense IRE ablation zone plus rim enhancement surrounding the treated area on T1 sequence (portal venous phase) (h) Hyperintense (+) IRE ablation zone on T2 sequence (i) Hyperintense (+) IRE ablation zone on DWI-b800 sequence (j) Isointense IRE ablation zone on ADC map. 2 weeks post-IRE: (k) Isointense IRE ablation zone on T1 sequence (l) Hypointense IRE ablation zone plus rim-enhancement surrounding the treated area on T1 sequence (portal venous phase) (m) Hyperintense (+) IRE ablation zone plus hypointense rim enhancement surrounding the treated area on T2 sequence (n) Hyperintense (+) IRE ablation zone on DWI-b800 sequence (o) Isointense IRE ablation zone on ADC map. 6 weeks post-IRE: (p) Isointense IRE ablation zone on T1 sequence (q) Hypointense IRE ablation zone on T1 sequence (portal venous phase) (r) Hyperintense (+) IRE ablation zone plus hypointense rim enhancement surrounding the treated area on T2 sequence (s) Hyperintense (+) IRE ablation zone on DWI-b800 (t) Isointense IRE ablation zone on ADC map [46]

## 11.10 Disease Recurrence

### 11.10.1 Local Recurrence After Pancreaticoduodenectomy

Regarding the role of repeat surgery after pancreaticoduodenectomy for pancreatic ductal adenocarcinoma, there is conflicting data in the literature. Kleef et al. included 30 patients with recurrent disease, 15 underwent repeat curative intent surgery and 15 did not [47]. The median survival was 17 months in the group that was resected versus 9.4 months in those who were not, with statistically significant survival improvement

in those patients who were resected after a disease-free interval of greater than 9 months. A second, larger study evaluated a series of 97 patients with pancreatic cancer recurrence. Of these, 57 had an isolated local recurrence and 41 were found to be resectable [48]. Again there was a significant survival advantage in those undergoing repeat resection with a median survival of 16.4 versus 9.4 months in those that were resectable or unresectable, respectively. The most recent study by Miyazaki et al. examined 170 patients with recurrent pancreatic cancer [49]. Sixty-seven of these had isolated recurrences within the pancreatic remnant and 11 ultimately underwent re-resection. Consistent with the previous reports, they found improved median survival of 25 months with repeat resection versus 9.3 months in those not resected. Although these three studies show similar results, with improved median survival in resectable cases of recurrent pancreatic cancer, a study from MD Anderson Cancer Center looked at the results of selective operation for locally recurrent or metastatic pancreatic cancer [50]. This study showed little benefit in resecting local recurrences in the pancreas even after a disease-free interval on over 20 months. Given the advances of systemic chemotherapy and stereotactic body radiation therapy, controversy regarding the specific sequencing of therapy for patients who develop recurrent disease within the pancreatic gland remnant remains. No clear guidelines regarding retreatment of pancreatic remnant carcinoma exist. Although feasible, the exact role for IRE to treat local site recurrences after resection remains unclear.

### 11.10.2 Local Recurrence After IRE

Although patients with local tumor residue after IRE should be considered suitable for retreatment, it may prove difficult to differentiate vital tumor tissue from fibrotic scar tissue based on early cross-sectional imaging findings. However, local site recurrence, detected at least 6 months after the initial procedure, in the absence of distant disease progression retreatment should be considered. Local recurrence (LR) is defined as a focal or diffuse growing mass (>20% solid lesion increase in longest diameter on the axial plane) within 1 cm of the ablated region compared to the new baseline scan at 4–12 weeks post-IRE. Although the median time to local progression was 13 months in the PANFIRE trial (percutaneous IRE) and 14 months in Martin's registry (open IRE), the number of patients eventually suitable for repeat ablation was low (3/25 in the PANFIRE trial), primarily because of coexisting extra-pancreatic disease or a multidirectional growth pattern of the recurring tumor tissue [40, 44] (Fig. 11.7).

---

## 11.11 Results from Literature

### 11.11.1 Quality of Life

The most relevant and attainable goal in management of LAPC is good symptom palliation. Therefore, quality of life (QoL) outcomes should be carefully weighed against survival benefit and treatment-related complications. In the PANFIRE trial, no significant decrease in QoL or pain perception was described in the early months after IRE, and the deterioration hereafter conceivably reflects disease progression [40].



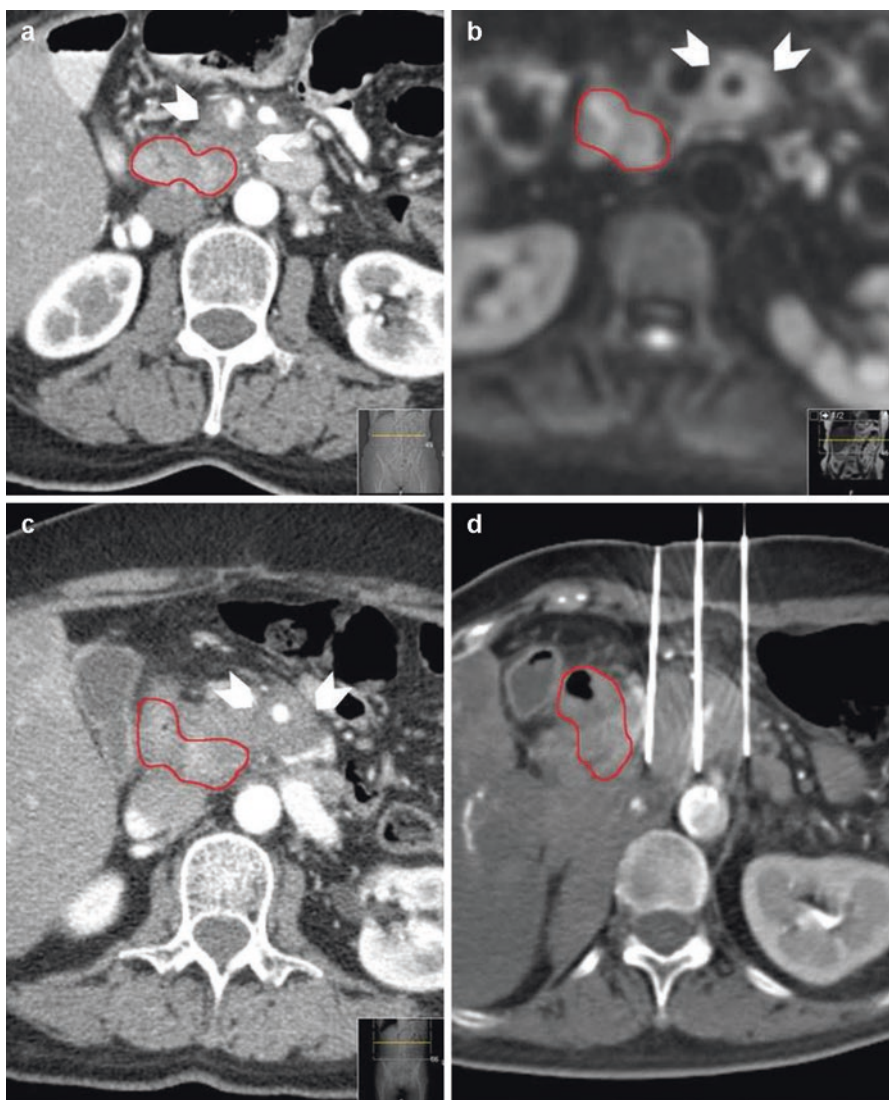


**Fig. 11.7** Adapted from Scheffer et al. and Vroomen et al. The development of a local recurrence. *Red line*, duodenum. (a) CeCT pre-IRE showing the initial tumor (*white arrowheads*) that was treated with IRE (b) MR DWI-b800 6 weeks post-IRE showing new hyperintensity around the superior mesenteric artery (*white arrowheads*) (c) CeCT 4 months post-IRE showing evident local recurrence (*white arrowhead*) (d) re-IRE of the local recurrence [40, 46]

### 11.11.2 Overall and Progression-Free Survival

Ten studies (excluding case reports) reported survival results: six retrospective series, two prospective cohorts, and two prospective controlled clinical trials [40, 42, 44, 51–56]. The chemotherapeutic regimens in these series were heterogeneous

(Table 11.1). Chemotherapy was administered as palliative therapy, as neoadjuvant or induction therapy prior to IRE, or as adjuvant regimen after IRE, which makes overall survival results from IRE difficult to interpret. For the open approach, we could extract 281 patients with a mean median OS of 15.2 months from IRE and 22.9 months from date of diagnosis (range 16–23.2 months). For the percutaneous group, we included 138 patients with a mean median OS from date of diagnosis of 22.3 months from the date of diagnosis (range 17–27 months). These heterogeneous results are probably caused by differences in selection criteria and referral bias, and hence it remains erratic to compare these results and jump to conclusions regarding the superior approach or the best (neo)adjuvant chemotherapeutic regimen.

---

## 11.12 Ongoing and Future Clinical Trials

There is no standard of care for patients with locally advanced pancreatic cancer. Extrapolating results from patients with metastatic pancreatic cancer, most centers nowadays offer eligible patients FOLFIRINOX with or without radiotherapy (preferably SABR). Whether FOLFIRINOX plus SABR is superior to FOLFIRINOX alone will hopefully be answered by the PANCRS trial from Stanford, USA (NCT01926197), which has been recruiting patients for several years now. If adding SABR proves superior, the standard of care probably becomes FOLFIRINOX plus SABR for eligible patients.

Anticipating on these results the prospective, multicenter, multinational, phase III, randomized controlled trial called the CROSSFIRE trial (NCT02791503) compares the efficacy of chemotherapy (preferably FOLFIRINOX) plus IRE (experimental arm) to the efficacy of chemotherapy plus stereotactic ablative radiotherapy or SABR (control arm) in patients with locally advanced, non-resectable, non-metastasized, pancreatic cancer in terms of overall survival from randomization. Primary participating centers are the VU University Medical Center (Amsterdam, the Netherlands) and the Miami Miller School of Medicine (University of Miami, Miami, Florida, USA). The trial started including patients in July of 2016.

There is an increasing evidence that margin accentuation for borderline resectable pancreatic cancer, performing open IRE of the resection margin prior to resection, is effective with an increase in local progression-free survival, distant progression-free survival, and overall survival compared to historic controls [44]. One group from Berne is focusing on the impact of margin accentuation as compared to a historic control group (NCT02952859).

IRE enhances delivery of gemcitabine to pancreatic adenocarcinoma [57]. Investigators from Texas will examine how well electrochemotherapy works at treating people with stage III pancreatic adenocarcinoma (NCT02592395). Electrochemotherapy is a treatment that combines electroporation and chemotherapy administration. Electroporation uses an electric current to produce holes in pancreatic tumor, which causes the tumor cells to die or take up a higher concentration of administered chemotherapy agent. This study will test the safety and look at the effect of electrochemotherapy in the treatment of stage III pancreatic adenocarcinoma.

Another group from Guangzhou will study the impact of IRE on immune response in patients diagnosed with unresectable pancreatic cancers smaller than 5.0 cm (NCT02343835). It will profile the immune response to IRE of unresectable pancreatic cancers. The intra-tumoral and systemic immune response to IRE will be determined and compared to pre-ablated pancreatic cancer specimens and historical control specimens.

A probe with two electrodes on a single needle (single insertion device) is currently being developed by AngioDynamics. The advantage of only having to place a single needle in the middle of a tumor seems self-evident for many pancreatic and other tumors. A group from Utrecht, the Netherlands, is evaluating IRE with two parallel plate electrodes (paddles, personal communication). This would theoretically lead to less needle-based complications such as pancreatic fistula, bile or pancreatic fluid leakage, and hemorrhage and result in a more homogenous energy delivery for open procedures.

---

## References

1. Bilimoria KY, et al. Validation of the 6th edition AJCC pancreatic cancer staging system – report from the National Cancer Database. *Cancer*. 2007;110(4):738–44.
2. Callery MP, et al. Pretreatment assessment of resectable and borderline resectable pancreatic cancer: expert consensus statement. *Ann Surg Oncol*. 2009;16(7):1727–33.
3. Pandya GJ, Shelat VG. Radiofrequency ablation of pancreatic ductal adenocarcinoma: the past, the present and the future. *World J Gastrointest Oncol*. 2015;7(2):6–11.
4. Pezzilli R, et al. Radiofrequency ablation for advanced ductal pancreatic carcinoma is this approach beneficial for our patients? A systematic review. *Pancreas*. 2011;40(1):163–5.
5. Pansky B. Anatomy of the pancreas – emphasis on blood-supply and lymphatic drainage. *Int J Pancreatol*. 1990;7(1–3):101–8.
6. Ibukuro K. Vascular anatomy of the pancreas and clinical applications. *J Gastrointest Cancer*. 2001;30(1–2):87–104.
7. Cesmebasi A, et al. The surgical anatomy of the lymphatic system of the pancreas. *Clin Anat*. 2015;28(4):527–37.
8. OMorchoe CCC. Lymphatic system of the pancreas. *Microsc Res Tech*. 1997;37(5–6):456–77.
9. Bilina C. Dorland's electronic medical dictionary, 28th ed. *Lab Med*. 2000;31(1):51.
10. Ionescu-Tirgoviste C, et al. A 3D map of the islet routes throughout the healthy human pancreas. *Sci Rep*. 2015;5:14634.
11. Olson SH, et al. Weight loss, diabetes, fatigue, and depression preceding pancreatic cancer. *Pancreas*. 2016;45(7):986–91.
12. Worni M, et al. Modest improvement in overall survival for patients with metastatic pancreatic cancer: a trend analysis using the surveillance, epidemiology, and end results registry from 1988 to 2008. *Pancreas*. 2013;42(7):1157–63.
13. Maisonneuve P. Epidemiology and risk factors of pancreatic cancer. *Eur J Cancer*. 2016;57:S4.
14. Freelove R, Walling AD. Pancreatic cancer: diagnosis and management. *Am Fam Physician*. 2006;73(3):485–92.
15. Siegel R, Naishadham D, Jemal A. Cancer statistics, 2013. *CA Cancer J Clin*. 2013;63(1):11–30.
16. Neoptolemos JP, et al. Adjuvant chemotherapy with fluorouracil plus Folinic acid vs gemcitabine following pancreatic cancer resection a randomized controlled trial. *J Am Med Assoc*. 2010;304(10):1073–81.
17. Howard TJ, et al. A margin-negative R0 resection accomplished with minimal postoperative complications is the surgeon's contribution to long-term survival in pancreatic cancer. *J Gastrointest Surg*. 2006;10(10):1338–45. discussion 1345–6.

18. Lopez NE, Prendergast C, Lowy AM. Borderline resectable pancreatic cancer: definitions and management. *World J Gastroenterol.* 2014;20(31):10740–51.
19. Poplin E, et al. Phase III, randomized study of gemcitabine and oxaliplatin versus gemcitabine (fixed-dose rate infusion) compared with gemcitabine (30-minute infusion) in patients with pancreatic carcinoma E6201: a trial of the Eastern Cooperative Oncology Group. *J Clin Oncol.* 2009;27(23):3778–85.
20. Louvet C, et al. Gemcitabine in combination with oxaliplatin compared with gemcitabine alone in locally advanced or metastatic pancreatic cancer: results of a GERCOR and GISCAD phase III trial. *J Clin Oncol.* 2005;23(15):3509–16.
21. Conroy T, et al. FOLFIRINOX versus gemcitabine for metastatic pancreatic cancer. *N Engl J Med.* 2011;364(19):1817–25.
22. Faris JE, et al. FOLFIRINOX in locally advanced pancreatic cancer: the Massachusetts General Hospital Cancer Center experience. *Oncologist.* 2013;18(5):543–8.
23. Gunturu KS, et al. FOLFIRINOX for locally advanced and metastatic pancreatic cancer: single institution retrospective review of efficacy and toxicity. *Med Oncol.* 2013;30(1):361.
24. Metges JP, et al. Efficacy and safety of FOLFIRINOX in patients with pancreatic metastatic cancer. *J Clin Oncol.* 2013;31(4):248–248.
25. Moorcraft SY, et al. FOLFIRINOX for locally advanced or metastatic pancreatic ductal adenocarcinoma: the royal Marsden experience. *Clin Colorectal Cancer.* 2014;13(4):232–8.
26. Neha C, et al. The impact of Folfirinox chemotherapy on the treatment pattern of patients with pancreas cancer seen at a tertiary referral Centre in the UK. *Ann Oncol.* 2014;25:75.
27. Sadot E, et al. FOLFIRINOX induction therapy for stage 3 pancreatic adenocarcinoma. *Ann Surg Oncol.* 2015;22(11):3512–21.
28. Walsh EMA, et al. FOLFIRINOX in pancreatic cancer: can results be reproduced outside the clinical trial setting? *J Clin Oncol.* 2014;32(15):e15236.
29. Hosein PJ, et al. A retrospective study of neoadjuvant FOLFIRINOX in unresectable or borderline-resectable locally advanced pancreatic adenocarcinoma. *BMC Cancer.* 2012;12:199.
30. Johung K, Saif MW, Chang BW. Treatment of locally advanced pancreatic cancer: the role of radiation therapy. *Int J Radiat Oncol Biol Phys.* 2012;82(2):508–18.
31. Gurka MK, et al. Stereotactic body radiation therapy with concurrent full-dose gemcitabine for locally advanced pancreatic cancer: a pilot trial demonstrating safety. *Radiat Oncol.* 2013;8:44.
32. Chuong MD, et al. Stereotactic body radiation therapy for locally advanced and borderline resectable pancreatic cancer is effective and well tolerated. *Int J Radiat Oncol Biol Phys.* 2013;86(3):516–22.
33. Schellenberg D, et al. Single-fraction stereotactic body radiation therapy and sequential gemcitabine for the treatment of locally advanced pancreatic cancer. *Int J Radiat Oncol Biol Phys.* 2011;81(1):181–8.
34. Seo Y, et al. Stereotactic body radiation therapy boost in locally advanced pancreatic cancer. *Int J Radiat Oncol Biol Phys.* 2009;75(5):1456–61.
35. Macchia G, et al. Quality of life and toxicity of stereotactic radiotherapy in pancreatic tumors: a case series. *Cancer Investig.* 2012;30(2):149–55.
36. Rombouts SJ, et al. Systematic review of innovative ablative therapies for the treatment of locally advanced pancreatic cancer. *Br J Surg.* 2015;102(3):182–93.
37. Scheffer HJ, et al. Irreversible electroporation for nonthermal tumor ablation in the clinical setting: a systematic review of safety and efficacy. *J Vasc Interv Radiol.* 2014;25(7):997–1011. quiz 1011.
38. Scheffer HJ, et al. Percutaneous irreversible electroporation of locally advanced pancreatic carcinoma using the dorsal approach: a case report. *Cardiovasc Intervent Radiol.* 2015;38(3):760–5.
39. Martin RC. Irreversible electroporation of stage 3 locally advanced pancreatic cancer: optimal technique and outcomes. *J Vis Surg.* 2015;1(4):1–9.
40. Scheffer HJ, et al. Ablation of locally advanced pancreatic cancer with percutaneous irreversible electroporation: results of the phase I/II PANFIRE study. *Radiology.* 2017;282(2):585–97.
41. Thomson KR, et al. Investigation of the safety of irreversible electroporation in humans. *J Vasc Interv Radiol.* 2011;22(5):611–21.

42. Narayanan G, et al. Percutaneous irreversible electroporation for downstaging and control of unresectable pancreatic adenocarcinoma. *J Vasc Interv Radiol.* 2012;23(12):1613–21.
43. Martin RC, et al. Irreversible electroporation of unresectable soft tissue tumors with vascular invasion: effective palliation. *BMC Cancer.* 2014;14:540.
44. Martin RC 2nd, et al. Treatment of 200 locally advanced (stage III) pancreatic adenocarcinoma patients with irreversible electroporation: safety and efficacy. *Ann Surg.* 2015;262(3):486–94. discussion 492–4.
45. Martin RC 2nd, et al. Irreversible electroporation in locally advanced pancreatic cancer: potential improved overall survival. *Ann Surg Oncol.* 2013;20(Suppl 3):S443–9.
46. Vroomen LG, et al. MR and CT imaging characteristics and ablation zone volumetry of locally advanced pancreatic cancer treated with irreversible electroporation. *Eur Radiol.* 2016; 27:2521–31.
47. Kleeff J, et al. Surgery for recurrent pancreatic ductal adenocarcinoma. *Ann Surg.* 2007;245(4):566–72.
48. Lavu H, et al. Reoperative completion pancreatectomy for suspected malignant disease of the pancreas. *J Surg Res.* 2011;170(1):89–95.
49. Miyazaki M, et al. Repeat pancreatectomy for pancreatic ductal cancer recurrence in the remnant pancreas after initial pancreatectomy: is it worthwhile? *Surgery.* 2014;155(1):58–66.
50. Thomas RM, et al. Selective reoperation for locally recurrent or metastatic pancreatic ductal adenocarcinoma following primary pancreatic resection. *J Gastrointest Surg.* 2012;16(9):1696–704.
51. Paiella S, et al. Safety and feasibility of Irreversible Electroporation (IRE) in patients with locally advanced pancreatic cancer: results of a prospective study. *Dig Surg.* 2015;32(2):90–7.
52. Kluger MD, et al. Single-institution experience with irreversible electroporation for T4 pancreatic cancer: first 50 patients. *Ann Surg Oncol.* 2016;23(5):1736–43.
53. Lambert L, et al. Treatment of locally advanced pancreatic cancer by percutaneous and intra-operative irreversible electroporation: general hospital cancer center experience. *Neoplasma.* 2016;63(2):269–73.
54. Mansson C, et al. Percutaneous irreversible electroporation for treatment of locally advanced pancreatic cancer following chemotherapy or radiochemotherapy. *Eur J Surg Oncol.* 2016;42(9):1401–6.
55. Mansson C, et al. Safety and preliminary efficacy of ultrasound-guided percutaneous irreversible electroporation for treatment of localized pancreatic cancer. *Anticancer Res.* 2014;34(1):289–93.
56. Belfiore MP, et al. Percutaneous CT-guided irreversible electroporation followed by chemotherapy as a novel neoadjuvant protocol in locally advanced pancreatic cancer: our preliminary experience. *Int J Surg.* 2015;21(Suppl 1):S34–9.
57. Bhutiani N, et al. Irreversible electroporation enhances delivery of gemcitabine to pancreatic adenocarcinoma. *J Surg Oncol.* 2016;114(2):181–6.

Eva Roos, Laurien G.P.H. Vroomen, Eran van Veldhuisen, Robert-Jan Coelen, Thomas M. van Gulik, and Martijn R. Meijerink

---

## 12.1 Introduction

The overall prognosis for patients with perihilar cholangiocarcinoma (PHC) is dismal. Resection of the tumor remains the only curative treatment, but only 10–20% of patients have resectable disease at the time of diagnosis [1]. The majority of patients present with locally advanced disease or lymph node metastases upon presentation or during exploratory laparotomy which makes resection not amenable. As the prognosis of patients with locally advanced PHC (LAPHC) or PHC with lymph node metastases in the palliative setting is significantly better compared to patients with organ metastases [2], ablative therapies may be of use for symptom palliation and potential survival benefit. Unfortunately, current ablative techniques for LAPHC are limited by serious side effects. These limitations may be overcome by irreversible electroporation (IRE), of which the safety and feasibility have been demonstrated in the presence of main bile ducts and large vascular structures [3–5].

---

E. Roos • R.-J. Coelen • T.M. van Gulik

Department of Experimental Surgery, Academic Medical Center, Meibergdreef 9, Amsterdam, The Netherlands

L.G.P.H. Vroomen

Department of Interventional Radiology, Memorial Sloan Kettering Cancer Center, New York, NY, USA

E. van Veldhuisen

Department of Surgery, Academic Medical Center, Meibergdreef 9, Amsterdam, The Netherlands

M.R. Meijerink (✉)

Department of Radiology and Nuclear Medicine, VU University Medical Center, de Boelelaan 1117, 1081 HV Amsterdam, The Netherlands

e-mail: [mr.meijerink@vumc.nl](mailto:mr.meijerink@vumc.nl)

## 12.2 Anatomical and Physiological Considerations

PHC, also known as Klatskin tumor, is a rare biliary malignancy originating at or near the hepatic duct confluence with an overall incidence of 1.2/100,000 individuals. Two-thirds of the cases occur in patients over the age of 65, with a near tenfold increase in patients over 80 years of age. The incidence is similar in both men and women.

The typical location of PHC in the liver hilum and proximal bile ducts causes biliary obstruction with concomitant jaundice. Surgical resection of PHC, consisting of a combined extrahepatic bile duct resection and partial liver resection, is the only curative treatment and offers the best chance for long-term survival with a reported median overall survival of 19–39 months and 5-year survival rates of 13–40% in large series [6]. Unfortunately, only a subset of patients is eligible to undergo surgical resection as almost 50% of patients have unresectable disease at presentation, and during exploratory laparotomy, another 40% have locally advanced or metastasized tumors [2]. Of all patients with ultimately unresectable disease, approximately 50% of tumors are considered locally advanced because of unreconstructable vascular or extensive biliary involvement [2, 7]. Liver transplantation in these cases is only performed in a few experienced centers worldwide with very strict selection criteria and extensive preoperative workup including neoadjuvant treatment. Unfortunately, high dropout rates up to 30% prior to transplantation are reported [8, 9].

Systemic chemotherapy is the mainstay of treatment for patients who are not candidates for curative resection or neoadjuvant therapy followed by liver transplantation. Currently, the combination of gemcitabine and cisplatin is the preferred regimen in this setting and offers a median progression-free survival of 8 months. However, despite palliative treatment with biliary stenting to relieve cholestasis, patients eventually often die due to cholangitis, sepsis, and/or liver failure (median overall survival of 12 months) [2, 10].

Although the overall prognosis of unresectable PHC is poor, patients with LAPHC or lymph node metastases beyond the hepatoduodenal ligament (N2) have significant longer survival compared to patients with organ metastases [2]. Some 13% of these patients even survive for more than 36 months. This particular subgroup of PHC patients may therefore benefit from ablative therapies that counteract tumor growth and potentially improve biliary stent patency and survival [11].

### 12.2.1 Ablative Strategies for Advanced PHC

Several ablative therapies for the treatment of advanced PHC have been investigated. Therapies that are currently applied in the context of pilot studies and early clinical trials are stereotactic body radiation therapy (SBRT), photodynamic therapy (PDT), (intraductal) radiofrequency ablation (RFA), brachytherapy, and microwave ablation (MWA). These modalities generally show variable success and high complication rates. Following photodynamic therapy (PDT), a treatment

that uses photosensitizing agents plus a particular type of light to produce a form of oxygen that kills nearby cells, up to 30% of patients experience serious cutaneous phototoxicity. Thermal ablative methods in the region of the portal triad are not only associated with an unacceptable proportion of biliary tract injuries but also considered less effective due to an imperative heat sink effect caused by the large vessels running through the liver hilum [12]. These limitations may be overcome by irreversible electroporation (IRE), of which the safety and feasibility have been demonstrated in the presence of main bile ducts and large vascular structures [13, 14].

Although the literature on IRE in PHC is limited, *in vivo* studies in the liver and pancreas of healthy pigs show sharp demarcations of the margins between ablated and non-ablated parenchyma including good efficacy adjacent to large vascular structures. Importantly, no signs of arterial or venous thrombosis were seen [15–18]. While these results seem promising, clinical results have to be awaited since safety and feasibility have not yet been established in human LAPHC.

Up until now, 17 clinical studies have been published regarding IRE for locally advanced pancreatic adenocarcinoma (LAPC), hepatocellular carcinoma (HCC), and colorectal liver metastases (CRLM). Among these studies, a total of 486 patients with unresectable tumors, unsuitable for thermal ablation due to their proximity to major vessels, bile ducts, or other organs, were treated with either open or percutaneous IRE [3]. These studies showed good results concerning safety and feasibility. Morbidity related to the IRE procedure consisted mainly of duodenal leakage (in patients with transduodenal needle placement or stent removal), pancreatic leakage, bile leakage, (progression of) portal vein thrombosis, local post-procedural pain, and transient urinary retention. In one clinical study, the effect of IRE on vessel patency in close proximity to the ablation zone was evaluated and showed that 151 of 158 major vessels were patent, whereas only seven vessels had signs of thrombosis or mild narrowing [19]. In another study, it was observed that tumors in close proximity to major bile ducts could be safely treated with IRE as 26 of 28 evaluated bile ducts were patent 1 month after treatment (one occlusion occurred) [4].

Although the aforementioned studies suggest that IRE can be safely used in HPB tumors and can provide a treatment benefit in terms of improved disease-free and overall survival, it is difficult to determine whether this benefit is substantial because of selection, low patient number, and short follow-up in these studies. Secondly, although results in other HPB tumors are promising, there is only little evidence for the use of IRE in the treatment for PHC. The group of Meijerink et al. was the first to successfully treat a patient with unresectable PHC with percutaneous IRE [20]. The 66-year-old female with a 3.8 cm PHC presented with unresectable disease due to bilateral extension into the secondary order bile ducts (Figs. 12.1 and 12.2). There were no radiological signs of nodal or vascular involvement. A metal wall stent was present in the common bile duct. IRE was performed with the patient under general anesthesia in the supine position, and a total of six monopolar needle electrodes were placed under CT-fluoroscopy guidance. Eighty treatment pulses were successfully and safely delivered. After removal of all six needles, CT demonstrated that the portal



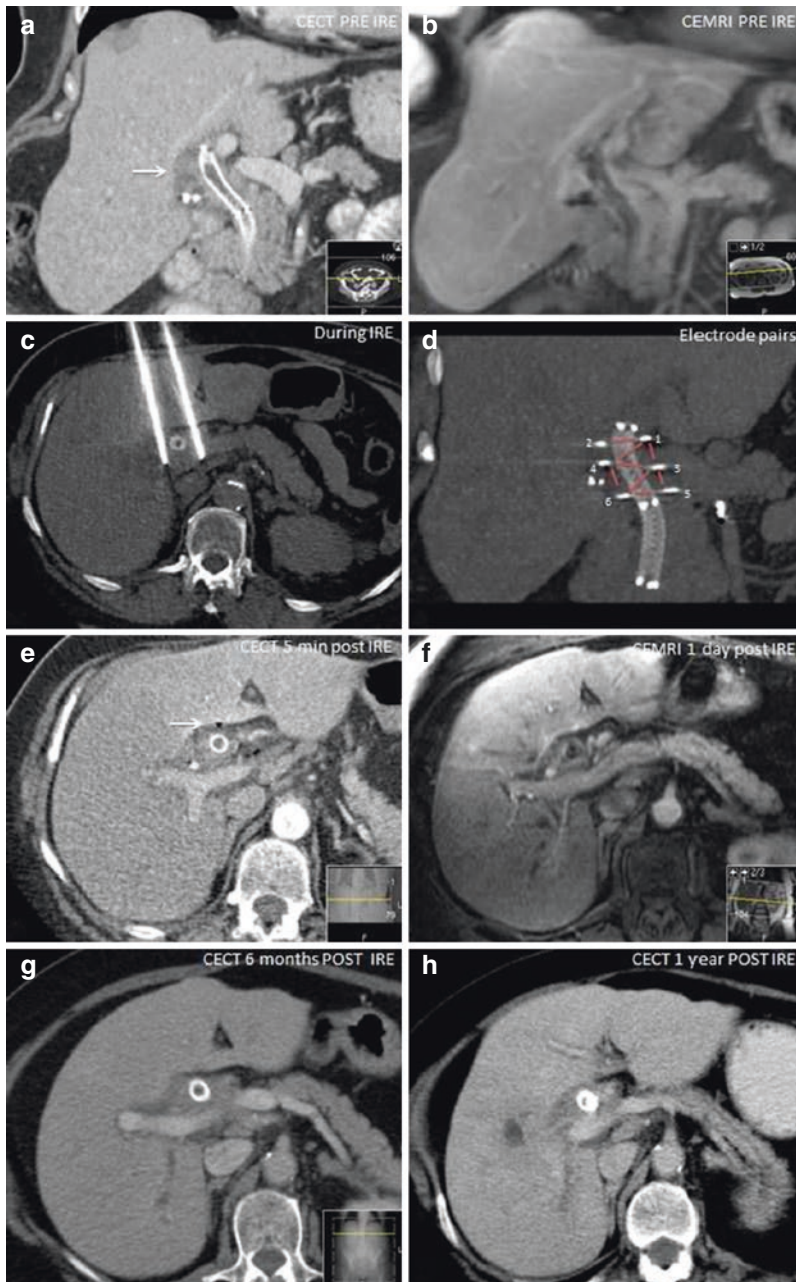


**Fig. 12.1** Adapted from Melenhorst et al. (a) Coronal ceCT image pre-IRE with a hilar cholangiocarcinoma (*arrow*) surrounding a metallic Wallstent present in the common bile duct. (b) ceMRI image demonstrating an enhancing mass in the liver hilum surrounding the common bile duct. (c) Axial CT image of two electrodes placed alongside the Wallstent. (d) Coronal CT view demonstrating all six electrodes and eight electrode pairs during the ablation (*red lines*). (e) ceCT immediately after IRE demonstrating patent vessels and gas bubbles in the ablated area (*arrow*). (f) ceMRI 1 day post-IRE with no signs of complications. (g, h) ceCT 6 months and 1 year after IRE demonstrating no tumor progression [20]

**Fig. 12.2** Adapted from Melenhorst et al. 3D reconstruction with a catheter in the common hepatic artery (*asterisk*) and six electrode places alongside the metallic Wallstent [20]



vein and surrounding arteries were patent and the intrahepatic bile ducts appeared unremarkable. Post-procedural recovery was uneventful, and the patient was discharged on the fourth day after IRE in good clinical condition. Follow-up CT after 4, 6, and 12 months showed no tumor progression or metastatic disease.

Further information about safety and efficacy of IRE in advanced PHC is currently lacking. The authors' treatment centers in Amsterdam (AMC and VUmc) have joined forces and are currently collaborating in the ongoing prospective phase I/II trial on IRE for advanced PHC (the ALPACA trial, NL56231.018.15)

---

## 12.3 Patient Selection

Given the paucity of results regarding safety and efficacy, the authors strongly recommend to only treat patients in the setting of prospective clinical trials or at least prospective registries, preferably in highly experienced and high-volume centers. Patients with either advanced PHC (locally advanced or N2 nodal metastases) based on imaging or staging laparoscopy or potentially resectable PHC but ultimately advanced disease during exploratory laparotomy may prove suitable candidates as well as patient with late-onset resection-site recurrence. For patients with initial unresectability, percutaneous IRE seems favorable over an open approach, given the lower complication rate and less-invasive nature. In case of intraoperative unresectability, "open" IRE may prove preferable.

---

## 12.4 Indications and Contraindications

### 12.4.1 Indications for IRE

Patients with LAPHC, defined as bilateral second-order biliary branch involvement, unilateral second-order biliary branch involvement plus arterial or portal encasement contralateral to this side, or (N2) lymph nodes on imaging or during staging laparoscopy, in the absence of metastatic disease to distant organs, may qualify for IRE. Patients who undergo explorative laparotomy and have inoperable vascular ingrowth or lymph node (N2) involvement are deemed unsuitable for resection and

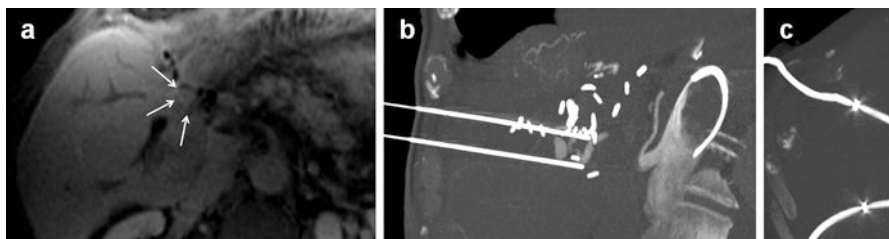


**Fig. 12.3** Example of a patient with a pathology proven local resection-site recurrence diagnosed two years after left-sided hemihepatectomy. (a) T1-weighted gadolinium enhanced MRI clearly demarcating the recurrence. (b) CT-guided IRE with two electrodes in an oblique-coronal plane. (c) Follow-up ceCT at six weeks post-IRE showing two PTC drains, placed prior to the IRE procedure, and a recent status after placing two self-expandable metal Wallstents (SEMS) at the biliodigestive anastomosis four weeks after the IRE procedure. The PTC drains were safely removed hereafter

may also benefit from local treatment [21]. In these cases, open ultrasound-guided IRE can be considered. Patients with late-onset (>6 months after the initial surgery) resection-site recurrence represent a third group of patients that may eventually prove suitable for IRE (Fig. 12.3). The diagnosis of PHC or lymph node metastases must be confirmed with cytology or histopathology using endoscopic or percutaneous brush cytology, endoscopic or percutaneous biopsy, or biopsy during laparoscopy.

#### 12.4.2 Contraindications for IRE

IRE is aimed at patients with LAPHC. Patients with resectable PHC or organ metastasized PHC at surgical exploration should be excluded from treatment with IRE. Furthermore, patients with PHC >5 cm, metastases to peritoneum, liver, or other organs, a history of ventricular cardiac arrhythmias, a recent history of myocardial infarction, uncontrolled hypertension, and uncontrolled infections, and a history of epilepsy, partial portal vein thrombosis, and narrowing of both the portal vein and either the common hepatic artery, celiac trunk, or superior mesenteric artery of >50% do not qualify for treatment with IRE. Extensive vascular involvement of the main branches of the portal vein and/or hepatic artery may result in complete occlusion of the artery or vein when IRE is performed. This might lead to liver ischemia, a deadly complication.

### 12.5 Patient Workup and Treatment Planning

Additional biliary drainage is indicated when serum bilirubin level exceeds 50  $\mu\text{mol/L}$ . These patients will preferably receive placement of percutaneous transhepatic biliary drains (PTCDs) under antibiotic prophylaxis (Fig. 12.4). A percutaneous approach allows for more selective segmental biliary drainage compared to endoscopic drainage. The PTCD technique involves placement of a thin Chiba needle, and a 0.014 in. guidewire under ultrasound guidance to gain access to the

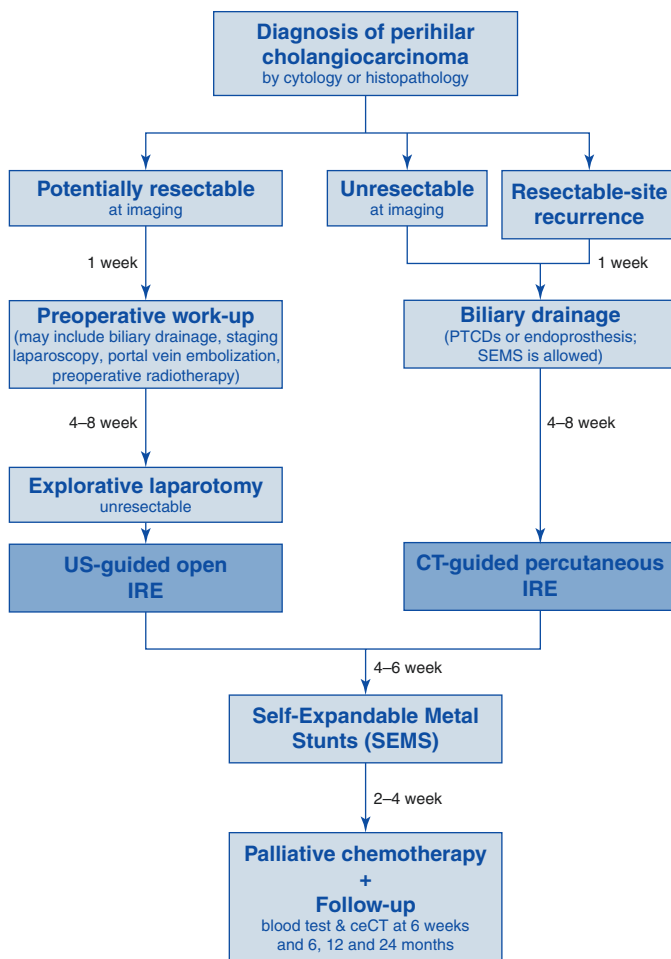


**Fig. 12.4** Flowchart of patient workup

biliary system. Antegrade cholangiography will be used to localize the site of obstruction. The guidewire is then maneuvered through the stenosis, and a catheter is placed with its distal end in the duodenum for internal-external drainage. Externally draining bile is collected in a drain bag during the first 24–48 h, after which the catheter is closed in order to achieve internal drainage. Patients should only receive IRE when serum bilirubin levels are below 50  $\mu\text{mol/L}$ .

Patients scheduled for open IRE should have undergone endoscopic (if already done in referring hospital) or percutaneous biliary drainage of at least the future liver remnant, but preferably of the whole liver. This will ensure adequate drainage post-IRE. Patients scheduled for percutaneous IRE should have adequate biliary drainage of all liver segments, which may require placement of two to three drains depending on tumor extension into the biliary branches.

A metal biliary stent is not considered to represent an absolute contraindication for IRE if there is no contact with the duodenum and as long as a no-touch technique is pursued (IRE electrodes are not in contact with the metal stent, as this would lead to instant overcurrent and generator shutdown). However, metal stents may cause incomplete ablation of tumor tissue, as cell survival was observed surrounding the metal stent in an IRE experiment in the liver by Scheffer et al. [22]. In addition, this experiment showed that higher temperatures are reached at the electrode tips, which is why careful electrode placement is warranted if thermally vulnerable structures (e.g., bile ducts) are in close proximity of the IRE ablation zone.

---

## 12.6 Approach, Image Guidance, and Technique

Antibiotic prophylaxis should always be administered, preferable within 1 h prior to the procedure. The IRE procedure is performed under general anesthesia with complete muscle paralysis and under cardiac gating either in the operation room or in the interventional radiology (CT) room. During the procedure, the cardiac rhythm will be closely monitored, and a defibrillator will be present at all times. IRE should be performed by a trained interventional radiologist, either percutaneously or during explorative laparotomy.

Prior to percutaneous IRE, a pigtail catheter can be placed in the common hepatic artery in the CT suite entering from the right common femoral artery, for administration of small amounts of intra-arterial contrast during IRE. This allows the repeated and real-time visualization of the vessels adjacent to or encasing the tumor and the tumor enhancement pattern, thereby improving the safety and accuracy of electrode placement, while reducing the total dose of contrast administered. Next, the patient is transported to the CT scan. Percutaneous procedures should be performed using CT fluoroscopy guidance and/or ultrasonographic guidance. The procedure is conducted under general anesthesia and epidural analgesia with muscle relaxants to prevent patient motion and under cardiac gating (using the AccuSync). After correct patient positioning, a contrast-enhanced CT scan of the abdomen will be performed under general anesthesia to confirm correct staging and exact tumor size measurement and for planning of electrode placement.

For clinical application of IRE, the Nanoknife<sup>®</sup> system (Angiodynamics Inc., Latham, New York, USA) is set up to produce 90 microsecond high-voltage (1,500–3,000 V) direct-current (25–45 A) electrical pulses. Typically, at least 90 pulses should be delivered between paired unipolar electrodes, with an exposed tip of 15–20 mm. The voltage setting for each electroporation will be determined by the distance between each pair of electrodes, with the intent to generate at least 1,000 V between electrodes. The electrodes will be placed in and around the tumor aiming at a macroscopic complete ablation with a 5 mm margin, with the inter-electrode distances 12–24 mm and the maximum angulation between electrodes 15°.

All pulses will be administered in the absolute refractory period with the use of electrocardiographic (ECG) synchronization to avoid triggering ventricular arrhythmia. If the lesion is larger or has a different shape than the area that one set of probes can cover (according to manufacturer's guidelines), multiple ablations should be performed, until the whole tumor area is ablated. The generator is programmed to stop delivery and recharge if the current flow exceeds 50 A. Pullbacks should be performed if the target treatment zone is greater than 2 cm in the direction of needle placement, and treatment is repeated to cover the entire target.

Specific attention should be paid to the placement of electrodes close to bile ducts as previous research demonstrated that biliary strictures may occur when needles are placed within 3 mm of the bile ducts [23].

---

## 12.7 Follow-Up and Response Evaluation

Plastic PTC drains should be exchanged for self-expandable metal stents in the days or weeks following the IRE procedure to ensure adequate drainage and to prevent clogging of the plastic drains by debris caused by the IRE procedure. In case of bilateral biliary tract involvement the simultaneous placement of two dedicated biliary stents (kissing stent procedure) should be considered. Bile ducts to atrophic liver lobes do not require drainage.

Postoperatively, patients should undergo treatment in an enhanced recovery program. Patients should be monitored on the recovery and the surgical ward daily, according to current medical practice. Patients with advanced PHC generally need optimal palliative chemotherapy (gemcitabine/cisplatin) starting within 6 weeks after the procedure. Follow-up is performed within the routine palliative care with measurements of serum markers and contrast-enhanced CT and/or MR scans.

---

## References

1. Khan SA, et al. Cholangiocarcinoma. *Lancet*. 2005;366(9493):1303–14.
2. Ruys AT, et al. Long-term survival in hilar cholangiocarcinoma also possible in unresectable patients. *World J Surg*. 2012;36(9):2179–86.
3. Scheffer HJ, et al. Irreversible electroporation for nonthermal tumor ablation in the clinical setting: a systematic review of safety and efficacy. *J Vasc Interv Radiol*. 2014;25(7):997–1011. quiz 1011.
4. Kingham TP, et al. Ablation of perivascular hepatic malignant tumors with irreversible electroporation. *J Am Coll Surg*. 2012;215(3):379–87.
5. Silk MT, et al. Percutaneous ablation of peribiliary tumors with irreversible electroporation. *J Vasc Interv Radiol*. 2014;25(1):112–8.
6. Popescu I, et al. Curative-intent surgery for hilar cholangiocarcinoma: prognostic factors for clinical decision making. *Langenbecks Arch Surg*. 2014;399(6):693–705.
7. Matsuo K, et al. The Blumgart preoperative staging system for hilar cholangiocarcinoma: analysis of resectability and outcomes in 380 patients. *J Am Coll Surg*. 2012;215(3):343–55.
8. Gores GJ, et al. Liver transplantation for perihilar cholangiocarcinoma. *Dig Dis*. 2013;31(1):126–9.

9. Darwish MS, et al. Predictors of pretransplant dropout and posttransplant recurrence in patients with perihilar cholangiocarcinoma. *Hepatology*. 2012;56(3):972–81.
10. Valle J, et al. Cisplatin plus gemcitabine versus gemcitabine for biliary tract cancer. *N Engl J Med*. 2010;362(14):1273–81.
11. Cheon YK, et al. Longterm outcome of photodynamic therapy compared with biliary stenting alone in patients with advanced hilar cholangiocarcinoma. *HPB (Oxford)*. 2012;14(3):185–93.
12. Goldberg SN, et al. Percutaneous radiofrequency tissue ablation: does perfusion-mediated tissue cooling limit coagulation necrosis? *J Vasc Interv Radiol*. 1998;9(1):101–11.
13. Silk MT, et al. Percutaneous ablation of peribiliary tumors with irreversible electroporation. *J Vasc Interv Radiol*. 2014;25(1):112–8.
14. Kingham TP, et al. Ablation of perivascular hepatic malignant tumors with irreversible electroporation. *J Am Coll Surg*. 2012;215(3):379–87.
15. José A, et al. Irreversible electroporation shows efficacy against pancreatic carcinoma without systemic toxicity in mouse models. *Cancer Lett*. 2012;317(1):16–23.
16. Garon EB, et al. In vitro and in vivo evaluation and a case report of intense nanosecond pulsed electric field as a local therapy for human malignancies. *Int J Cancer*. 2007;121(3):675–82.
17. Bower M, et al. Irreversible electroporation of the pancreas: definitive local therapy without systemic effects. *J Surg Oncol*. 2011;104(1):22–8.
18. Charpentier KP, et al. Irreversible electroporation of the pancreas in swine: a pilot study. *HPB (Oxford)*. 2010;12(5):348–51.
19. Narayanan G, et al. Vessel patency post irreversible electroporation. *Cardiovasc Intervent Radiol*. 2014;37(6):1523–9.
20. Melenhorst MC, et al. Percutaneous irreversible electroporation of unresectable hilar cholangiocarcinoma (Klatskin tumor): a case report. *Cardiovasc Intervent Radiol*. 2016;39(1):117–21.
21. Coelen RJ, et al. Diagnostic accuracy of staging laparoscopy for detecting metastasized or locally advanced perihilar cholangiocarcinoma: a systematic review and meta-analysis. *Surg Endosc*. 2016;30(10):4163–73.
22. Scheffer HJ, et al. The Influence of a metal stent on the distribution of thermal energy during irreversible electroporation. *PLoS One*. 2016;11(2):e0148457.
23. Lu DS, et al. Irreversible electroporation: ready for prime time? *Tech Vasc Interv Radiol*. 2013;16(4):277–86.

Jim Koukounaras, Helen Kavnoudias,  
and Kenneth R. Thomson

---

## 13.1 Introduction

Surgical excision is still considered the optimal treatment for malignant renal tumours [1, 2]. However, before the advent of computed tomography, renal mass lesions smaller than 4 cm were difficult to detect and TNM staging used 4 cm as the maximum size of T1a lesions. As a result of increased detection of small, often asymptomatic, mass lesions, routine nephrectomy has become less desirable. Nephron-sparing nephrectomy with or without laparoscopy has become a routine procedure for T1a and some T1b lesions. More recently thermal ablative techniques have been employed for T1a lesions particularly when the lesion is exophytic. One of the major limitations of these ablative techniques is thermal damage to adjacent organs and the collecting system and heat sink effects which limit the efficacy of the techniques adjacent to blood vessels. As a result of these limitations, the most suitable lesion for thermal ablation is <4 cm in diameter, polar, cortical and distant from the renal hilum and collecting system. These limitations also apply to a great extent to nephron-sparing surgery.

Percutaneous irreversible electroporation (IRE) is ideally suited to treatment of small renal mass lesions because it is a nonthermal method of soft tissue ablation which is unaffected by local blood flow and it does not disturb the collagenous structure of the target tissue. The kidney is easily accessible by percutaneous image-guided techniques to facilitate the use of IRE, and non-polar, hilar lesions adjacent to the ureter and calyces are not a contraindication to the use of IRE. Provided the lesion is carefully targeted by IRE, lesions larger than 3 cm can be treated effectively and safely.

---

J. Koukounaras • H. Kavnoudias • K.R. Thomson (✉)  
Radiology Department, Alfred Hospital, Melbourne, VIC, Australia  
e-mail: [xrayvision4@gmail.com](mailto:xrayvision4@gmail.com)



## 13.2 Physiological and Anatomical Considerations

The kidneys are paired retroperitoneal structures surrounded by Gerota's fascia that is normally located between the transverse processes of T12–L3 vertebrae, with the left kidney typically somewhat more superior in position than the right. The upper poles are normally oriented more medially and posteriorly than the lower poles. The adrenal glands are situated at the upper pole of each kidney and the lower portion of each kidney is closely related to the colon. There are one or more renal arteries to each kidney arising directly from the abdominal aorta and venous drainage is to the inferior vena cava. The left renal vein passes anterior to the aorta about the level of the second part of the duodenum. Urine is secreted into the calyces of the collecting system and transported via the ureter to the urinary bladder by ureteric peristalsis.

The kidneys serve important functions, including filtration and excretion of metabolic waste products, regulation of electrolytes and fluid, acid-base balance and stimulation of red blood cell production. They regulate blood pressure via the renin-angiotensin-aldosterone system, controlling reabsorption of water and maintaining intravascular volume. The kidneys also reabsorb glucose and amino acids and have endocrine functions via erythropoietin, calcitriol and vitamin D activation.

## 13.3 Diseases

The differential diagnosis of a small (<4 cm) renal mass lesion includes benign cyst, angiomyolipoma, lymphoma, metastasis, benign mesenchymal tumour, renal sarcoma, renal cell carcinoma, adenoma, oncocytoma, abscess and haematoma. The differentiation of these and exclusion of volume averaging artefacts in the renal hilum require high-quality triple phase contrast-enhanced computed tomography (CT) (Fig. 13.1), supplemented by ultrasound, magnetic resonance imaging (MRI) and sometimes biopsy [3–7]. Since most lesions are slow growing, short interval repeat imaging may not be helpful. However, in an elderly unfit person with a very small (<2 cm) exophytic renal mass, a repeat CT scan after 12 months is a reasonable approach. In most cases a definitive diagnosis can be made based on the imaging findings



**Fig. 13.1** Renal tumour. A solid mass with abnormal vascularity in arterial phase is typical of a renal cell carcinoma. Sometimes, however, the vascularity may be difficult to detect. See Fig. 13.2

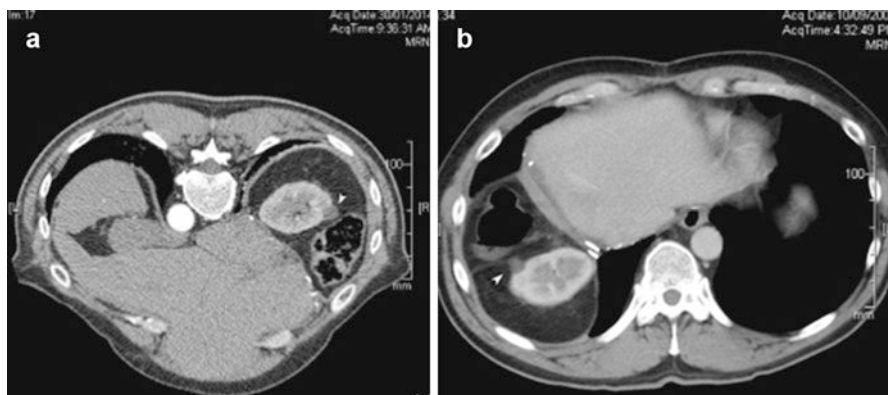


**Fig. 13.2** Small indeterminate exophytic lesion. (a) A small poorly enhancing exophytic lesion (*arrowhead*) in a patient status post liver resection for colon cancer metastasis (2007). (b) By 2014, there was evidence of some growth in size. On biopsy this proved to be a clear cell renal carcinoma. The prior adjacent surgery, diaphragmatic sulcus and proximity of the colon were indications for IRE of this lesion (*arrowhead*)

(Fig. 13.2), but lesions <1.5 cm are unlikely to cause significant morbidity at least in the short term.

Biopsy is recommended before any indeterminate mass lesion is treated by an ablative technique. There is a very small (0.01%) risk of seeding of the biopsy track with malignant tumours and this may limit the enthusiasm for biopsy. It is worth noting that tumour seeding may also occur after laparoscopic nephron-sparing surgery. The electric field immediately adjacent to the active IRE electrode is lethal to cells and this may inhibit seeding.

---

### 13.4 Current and Future Indications

IRE is indicated for soft tissue ablation and is suited to focal renal masses of malignant potential. IRE does have advantages when compared to partial nephrectomy as the IRE is not dependent on the anatomical relationships of the tumour such as blood supply or venous drainage. However, this is an area with a large number of therapeutic options, and more long-term data is required to establish the final place of IRE in the kidney.

---

### 13.5 Contraindications

Provided the patient is able to tolerate a general anaesthetic with muscle paralysis, there are almost no contraindications to IRE once a tumour of malignant potential has been identified in the kidney. Treatment of nonfocal malignancy such as transitional cell carcinoma is not recommended even though it is probably possible.

Patients with pacemakers and pacemaker-defibrillators should be reviewed by a cardiologist prior to an IRE procedure. We prefer to use cardiac-gated delivery of IRE in all procedures. In some cases the defibrillator may need to be deactivated during the procedure, but a standard demand pacemaker has, in our experience, not provided any problem in terms of aberrant rhythm or generation of abnormal currents through the pacemaker leads.

---

### **13.6 Patient Workup and Treatment Planning (Multidisc Meetings, Histology, Imaging, Lab, Antibiotics, Pre-procedural Safety Procedures, Modelling)**

In our institution all renal tract malignancies are reviewed by a multidisciplinary committee comprising urologists, radiologists, radiation oncologists and medical oncologists. Laboratory results, including renal function, cardiorespiratory status, past and recent imaging (CT, ultrasound or magnetic resonance) and histology, are presented and a decision is made on the most appropriate treatment for each particular patient. Lesions which are technically difficult for partial nephrectomy are usually quite accessible for a focal ablative treatment such as IRE.

Once a decision for IRE has been made, the lesion is studied on the available cross-sectional imaging or if necessary further cross-sectional imaging is obtained. The kidney is relatively accessible from a prone or oblique approach for percutaneous procedures like IRE. Because the kidney will move significantly from a supine position to a prone or oblique position, often the final targeting planning will not occur until the patient is positioned and anaesthetised for the IRE procedure. It is, however, still useful to plan the procedure in general terms so that the tumour and a margin of normal tissue can be effectively targeted (Fig. 13.3). Decisions such as the number of electrodes, length of active electrode exposure and distance between electrodes can be made prior to the procedure to ensure that a complete ablation can be achieved. The electrode placement should be designed so that if possible, the distance between electrodes is between 1.0 and 2.5 cm. The effective electroporation field extends about 5 mm from the outer margin of the electrode so that provided adequate current is achieved, a 2.5 cm electrode will cover a 3.0 cm diameter tumour. Ideally the electrodes should sit at the margin of the tumour so that a margin can be achieved with confidence. If desired this planning can be transferred to the AngioDynamics generator to view the electrode siting. This is however only a single-plane diagram. Planning can also be performed using the Visifield planning software which provides a more robust estimate of the electric field that will be generated [[Visifield.com](http://Visifield.com)].

---

### **13.7 Approach and Image Guidance**

The major decision to be made at the time of the procedure is whether to place the arms alongside the abdomen or to raise the arms above the imaging field. There is an increased risk of brachial plexus injury if the arms are extended forcibly for long

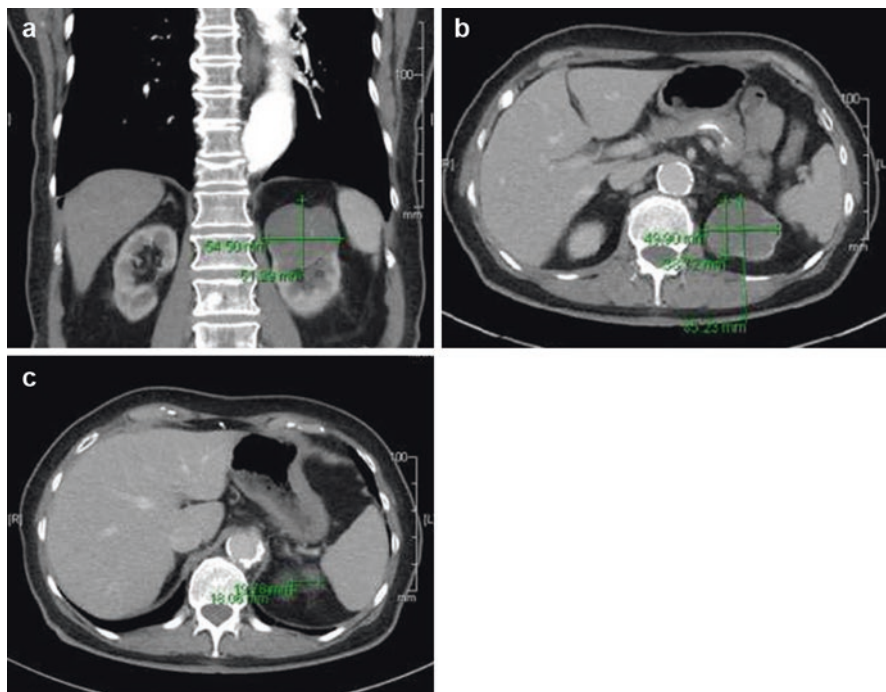


**Fig. 13.3** Planning the electrode siting. Using axial images select the *top* (a) and *bottom* (b) of the tumour, and with a coronal image (c), select the largest region of the tumour. Note the dimensions and calculate what electrode spacing and how many electrodes will be required. Even though the tumour position will change as the patient is turned from supine to prone, the tumour size will be the same



**Fig. 13.4** Patient positioning. In the prone position, the kidney moves forward. As the patient is usually on a support to protect the venous return, the arms may be positioned alongside the patient below the level of interest. In this example the right arm is only just visible and image degradation is acceptable

periods even when the patient is in a prone oblique position. In most cases the CT artefact produced by the arms is below the imaging field of the kidneys (Fig. 13.4). We have used the Perfint positioning robot (Fig. 13.5) to aid positioning of IRE electrodes and to assist planning of the electrode array when an oblique electrode

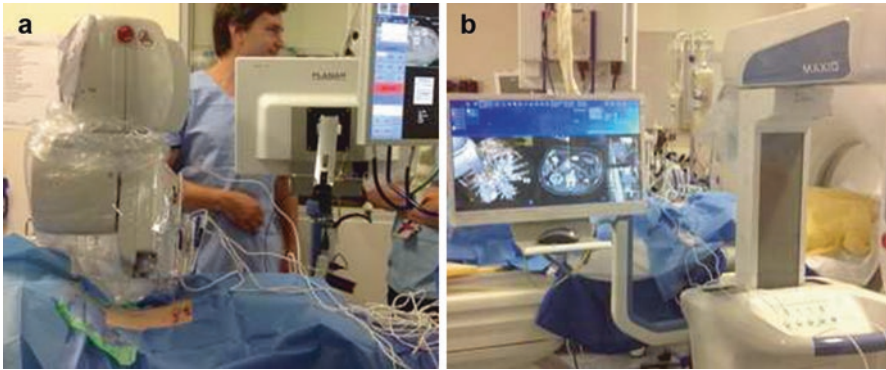


**Fig. 13.5** Perfint robot. (a) CT data is transmitted to the Perfint robot and the electrode placement is planned on the Perfint workstation. Once planning is complete, the robot arm indicates the position at which the electrode should be introduced. The operator inserts the electrode through the guide. (b) The Perfint robot is in position and the last electrode is about to be inserted. CT fluoroscopy is used after placement to confirm accurate positioning

path is required, but normally for a renal tumour, the electrode path is in the axial plane and less difficult than, for instance, a placement through the intercostal spaces for a liver tumour.

In our experience it is easier to confirm placement of IRE electrodes in the renal target area with CT rather than ultrasound. If ultrasound is used, because the position of the patient is likely to be different to that of the diagnostic CT examinations, CT/ultrasound fusion may not be possible with older fusion technology.

### 13.8 Technique (General Technique, Tips and Tricks, Procedural Safety Procedures)

Normally the patient is anaesthetised in the supine position, and ECG and blood pressure monitoring is established, often with a radial arterial pressure line. ECG dots are required for two sets of monitors if cardiac-gated delivery of the electro-poration is to be used. A Foley catheter is inserted into the urinary bladder, and the patient is then positioned prone or prone oblique according to the prior plan. All imaging should be performed in expiration as this is the most consistent phase for an anaesthetised and paralysed patient. A contrast-enhanced CT in arterial and excretion phase is obtained with a skin-marking sheet over the area of interest. Once images are obtained, the table position of the upper and lower border of the target zone is recorded and a mark made on the patient's skin. The medial and lateral borders of the target zone are also marked after calculations from the skin-marking sheet. During placement and adjustment of electrodes, respiration is off so that a consistent respiratory position is achieved.

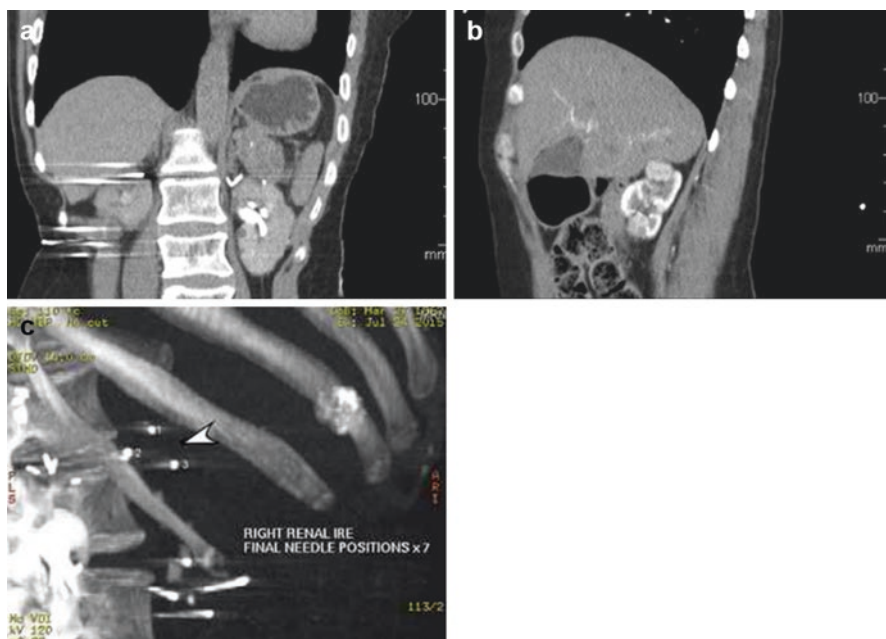


**Fig. 13.6** Electrode measurements. (a) Pre-electrode placement. CT sagittal reconstruction showing tumours at the upper pole and the lower pole in a patient with Von Hippel Lindau disease. (b) CT reconstruction in short axis of the electrode to allow accurate measurements of electrode separation. (c) CT reconstruction in long axis of the electrodes to confirm electrodes are truly parallel to one another

Electrodes are exposed by withdrawing the insulation sleeve and inserted at sites according to the prior plan to ensure that the target zone is completely covered. As each electrode is placed, the position should be confirmed using a few CT slices or CT fluoroscopy. Each electrode cable should be labelled using the numbered labels supplied with the blue activator electrode.

Once electrode placement is completed, a non-contrast CT through the target kidney is performed and displayed on the workstation. The actual distance between each electrode is determined by a stack of images perpendicular to the long axis of the electrodes (Fig. 13.6). These measurements are then transferred to the AngioDynamics generator. Use of a Faraday probe allows a direct display of the current with each pulse and a more aggressive application of the electroporation energy without causing the generator to shut down because of excessive current (Fig. 13.7). Alternatively a set of ten pulses at a low energy such as 1,200 V/cm can be delivered through each electrode pair and the results viewed on the AngioDynamics generator monitor after the delivery is complete (Fig. 13.8). Low currents require either increase in volts/cm generally or selectively for each electrode pair. High currents or pulses showing spikes require reduction in the energy to be delivered. A

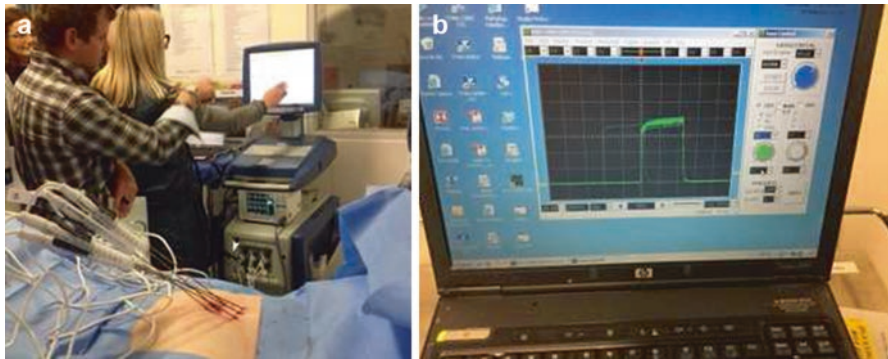


**Fig. 13.7** Monitoring the IRE pulse. (a) Use of a Faraday current probe. A general view showing multiple electrodes in position. The Faraday probe is switched from one electrode pair to another as the sets of electric pulses are delivered. It is attached to electrode 5 in this image. (b) This oscilloscope display shows a series of pulses around 20 amperes. Each successive pulse in the set of 10 is slightly lower in current as the voltage falls slightly with each discharge from the capacitor in the Nanoknife generator. The shape of this current is ideal

further group of about 70–90 pulses are then delivered at the new settings and the results displayed for evaluation. Further adjustments are made as necessary and a final set of 70–90 pulses delivered. The total number of pulses delivered should be about 100 with currents at or above about 35 A. If a single pair of electrodes proves difficult to energise with the rest of the array, they can be deleted and activated separately.

For each set of activations, the electrode number, volts/cm, and current achieved are recorded on a worksheet (Fig. 13.9). Careful recording is critical when there are a large number of electrodes, and care should be taken to ensure every possible combination of electrodes is activated. These recordings are also important if there is a shutdown because of overvoltage. To force the generator to change voltage, the distance specified on the generator may be increased or decreased without actually changing the relative electrode positions in the patient. The data recorded by the AngioDynamics generator should be saved to a USB only at the end of the procedure.

Once the ablation is considered complete, a final CT scan with electrodes in position is performed. For best evaluation, contrast is required but this depends on the renal function. The ablation zone is of lower attenuation than normal kidney and contains a few bubbles of gas. There will be normally minor soft tissue change in the perinephric fat as a result of electrode placement. If there is any doubt the ablation is incomplete, the electrodes should be repositioned or some of the electroporation repeated.

After the patient is conscious, a trial of void is performed and the indwelling urinary catheter removed. If there is a history of prostatism, the catheter is left in position until the following day. Even in cases of electroporation reaching the hilum of the kidney, significant haematuria is unusual.

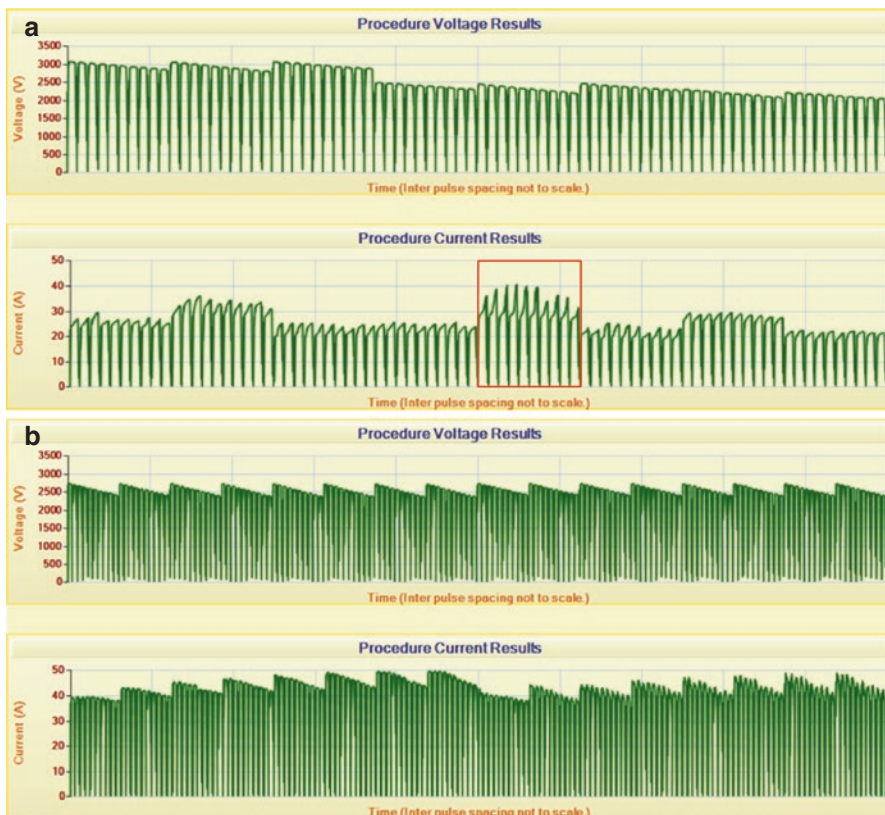


**Fig. 13.8** Electric pulse delivery. **(a)** Abnormal “spikey” current display. Although the current and voltage are well under cut-off levels, the shape of the pulses indicates that the electric field is not uniform. This may be due to very inhomogeneous tumour or due to excessive electrode separation. Repositioning of one or more electrodes may be required. **(b)** Completion display of IRE electric pulses at the limits of tolerance. Real-time monitoring allows more aggressive current delivery with less chance of overcurrent shutdown as the delivery can be aborted just before the generator shuts down



IRE Worksheet									
PATIENT NAME		JAMES BLOGGS			ORGAN	LEFT KIDNEY UPPER POLE			
ID NUMBER		1			GUIDANCE	CT	PERFINT	U/S	FUSION
DATE		JULY 4 2016							
Turnour size (CM)	X	1.5			POSITION OF ELECTRODES		1		2
	Y	1.3						3	
	Z	1.5							
#1	PAIRS	DISTANCE	VOLTS/CM	VOLTAGE	CURRENT	NO PULSES			
	1/2	1.8	1200	2160	15	40			
	1/3	2.0	1200	2400	20	40			
	2/3	1.5	1200	1800	15	40			
#2	PAIRS	DISTANCE	VOLTS/CM	VOLTAGE	CURRENT	NO PULSES			
	1/2	1.8	1500	2700	25	80			
	1/3	2.0	1500	3000	30	80			
	2/3	1.5	1500	2250	20	80			
#3	PAIRS	DISTANCE	VOLTS/CM	VOLTAGE	CURRENT	NO PULSES			
	2/1	1.8	1800	3000	38	80			

**Fig. 13.9** Worksheet for renal tumour. It is important to record the voltage, separation, number of pulses delivered and the current achieved for each pair of electrodes each time any parameters are changed. Ideally an increase in current of 15–20 amperes is desirable for IRE. Note that in this example, the highlighted distance between electrodes 2 and 3 in sequence #3 has been increased artificially to force a higher voltage. The electrode was not physically moved

### 13.9 Complications (Related to Needles, Related to Energy Delivery or Related to the General Procedure)

Complications after renal electroporation are very infrequent in our experience. The most surprising outcome is that haematuria is most uncommon and has been very limited even with deep insertion of the IRE electrodes. The incidence of bleeding in our experience, even though it is limited, is equal to or less than the risk after renal biopsy.

Even with cardiac gating, long sequences of electroporation pulses may result in an increase in blood pressure during the procedure. This is possibly related to diaphragmatic contractions and increased venous return to the heart but in truth we have no exact cause. The blood pressure is easily controlled by the anaesthetist during the procedure and we have not seen persistent hypertension after the procedure.

In one case the left adrenal gland was unintentionally included in the electroporation field, and this resulted in severe hypertension easily controlled with alpha and beta blockade without late sequelae.

Direct puncture damage caused by an electrode is possible with any IRE procedure, but we do not need to introduce fluids to separate adjacent organs and we have not employed urinary cooling to protect the collecting system and ureter.

The major complication is an incomplete ablation, but this is part of a learning curve in planning deployment of electrodes and ensuring the ablative electric field encompasses the entire tumour and a margin.

### 13.10 (Neo)adjuvant Treatment and Supportive Procedures (Renal Failure Support, Urine Cooling, etc.)

Although there is theoretically some advantage in adjuvant chemotherapy with IRE in other regions, principally skin tumours, this is not routine practice due to the lack of an effective therapeutic agent. Adequate hydration and minimization of contrast media is employed as with any CT contrast procedure as the aim of the IRE procedure is to preserve renal function. The lack of thermal effects makes urine cooling and tissue separation unnecessary.

### 13.11 Follow-Up and Response Evaluation (Imaging, Lab)

Standard follow-up protocols as for any other treatment method for renal tumour are used. This may be CT or ultrasound as desired. We performed a contrast CT or an ultrasound at 1–2 months post IRE in all our patients with further follow-up at 6- and then 12-month intervals. Where renal function was reduced, contrast-enhanced MR imaging is also suitable (Fig. 13.10).

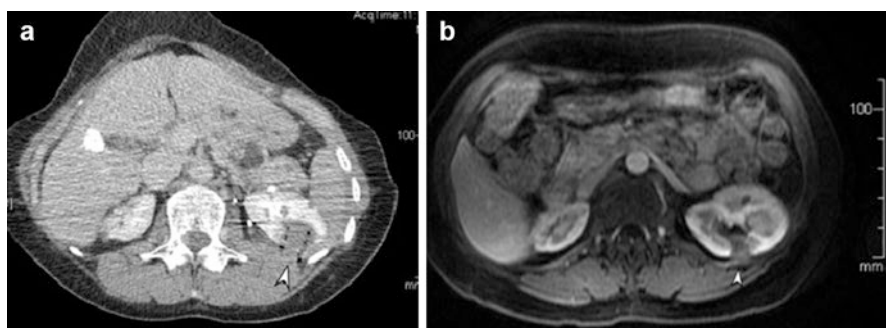


**Fig. 13.10** Follow-up. (a) Prone CT image at completion of IRE and removal of electrodes. Gas in the line of the electrodes is related to hydrolysis. (b) MR with contrast (axial 3 phase LAVA sequence) in the same patient at 6 months post IRE. The tumour mass has decreased in size and is non-enhancing. Note the IRE ablation extended to the central portion of the left kidney

### 13.12 Disease Recurrence (Residual Disease, Local Site Recurrence or Distant Disease Recurrence)

Residual disease indicates a failure of the original index IRE procedure and is more frequent in the early experience of the operator. Following successful (complete) ablation, we have not seen evidence of local or distal site recurrence. One of our patients has Von Hippel Lindau disease and develops tumours in other renal sites. We have performed three procedures and she has had two partial nephrectomies for separate tumours.

Our results were presented at SIR 2016 in Vancouver, BC. Nineteen patients of ages ranging from 43 to 85 years (mean 70 years) with a total of 27 tumours were treated between 2008 and 2015. Six of the 19 patients were undertaken on a salvage compassionate basis under an ethics-approved trial to evaluate the safety of the IRE technique. Of the 13 other patients, there has been no recurrence of ablated tumours where a complete ablation was achieved. Overall, including the salvage patients, this experience resulted in an ablation rate of 88% for tumours <3 cm and 63% for tumours >3 cm. However seven of the tumours without recurrence were >3 cm in diameter. There was no difference in results by site (central or peripheral).

---

### 13.13 Results from Literature

Pech et al. first reported human experience of IRE for renal tumour in an “ablate and resect” research project, but the interval between ablation and nephrectomy was too short to establish any IRE effect [8, 10]. A new Dutch study protocol has been proposed by Wagstaff et al. where the interval between IRE and radical nephrectomy will be 4 weeks which will provide data on the histologic changes after IRE [9].

Trimmer et al. reported a small cohort of renal tumours treated by IRE, but their selection was for tumours of a smaller size (average 2.9 cm) and a peripheral location distant from critical structures [11]. Their study reported no complications and ablation rates similar to those achieved with thermal ablation.

Wehle et al. considered that “watchful waiting” and serial CT scan management of small renal masses (average 1.83 cm) in patients unsuitable for surgery or thermal ablation are appropriate [12]. This is a widely held view among urologists, but “watchful waiting” as a management strategy has not been thoroughly evaluated.

Health technology assessment ([www.nice.org.uk](http://www.nice.org.uk)) of renal IRE is that current evidence on the safety and efficacy of IRE for treating renal cancer is inadequate in quality and quantity and that this procedure should only be used in the context of research. NICE also stated that studies should report the effect of the procedure on local tumour control and patient survival.

Our opinion is that IRE, in experienced hands, is as effective as other ablative methods but has far wider application within the renal parenchyma with less restrictions on its use.

## References

1. American Cancer Society. Cancer facts and figures 2000. Atlanta: American Cancer Society; 2000. p. 4.
2. Russo P. Renal cell carcinoma: presentation, staging, and surgical treatment. *Semin Oncol.* 2000;27:160–76. Medline.
3. Cohan RH, Sherman LS, Korobkin M, Bass JC, Francis IR. Renal masses: assessment of corticomedullary-phase and nephrographic-phase CT scans. *Radiology.* 1995;196:445–51. Link.
4. Kopka L, Fischer U, Zoeller G, Schmidt C, Ringert RH, Grabbe E. Dual-phase helical CT of the kidney: value of the corticomedullary and nephrographic phase for evaluation of renal lesions and preoperative staging of renal cell carcinoma. *AJR Am J Roentgenol.* 1997;169:1573–8. CrossRef, Medline.
5. Szolar DH, Kammerhuber F, Altziebler S, et al. Multiphasic helical CT of the kidney: increased conspicuity for detection and characterization of small (<3-cm) renal masses. *Radiology.* 1997;202:211–7. Link.
6. Yuh BI, Cohan RH. Different phases of renal enhancement: role in detecting and characterizing renal masses during helical CT. *AJR Am J Roentgenol.* 1999;173:747–55. CrossRef, Medline.
7. Silverman SG, Lee BY, Seltzer SE, Bloom DA, Corless CL, Adams DF. Small (<3-cm) renal masses: correlation of spiral CT features and pathologic findings. *AJR Am J Roentgenol.* 1994;163:597–605. CrossRef, Medline.
8. Pech M1, Janitzky A, Wendler JJ, Strang C, Blaschke S, Dudeck O, Ricke J, Liehr UB. Irreversible electroporation of renal cell carcinoma: a first-in-man phase I clinical study. *Cardiovasc Intervent Radiol.* 2011;34:132–8.
9. Wagstaff P, de Bruin DM, Zondervan PJ, Heijink CD, Engelbrecht MRW, van Delden OM, van Leeuwen TG, Wijkstra H, de la Rosette JJ, Pes MP. The efficacy and safety of irreversible electroporation for the ablation of renal masses: a prospective, human, in-vivo study protocol. *BMC Cancer.* 2015;15:165.
10. Deodhar A, Monette S, Single GW Jr, Hamilton WC Jr, Thornton R, Maybody M, Coleman JA, Solomon SB. Renal tissue ablation with irreversible electroporation. Preliminary results in a porcine model. *Urology.* 2011;77:754–60.
11. Trimmer CK, Khosla A, Morgan M, Stephenson SL, Ozayar A, Cadeddu JA. Minimally invasive percutaneous treatment of small renal tumours with irreversible electroporation: a single centre experience. *JVIR.* 2015;26:1465–71.
12. Wehle MJ, Thiel DD, Petrou SP, Young PR, Frank I, Karsteadt N. Conservative management of incidental contrast-enhancing renal masses as safe alternative to invasive therapy. *Urology.* 2004;64:49–52.

Matthijs Scheltema and Jean de la Rosette

## Abbreviations

AS	Active surveillance
CROES	Clinical Research Office of the Endourological Society
HIFU	High-intensity focused ultrasound
IRE	Irreversible electroporation
(mp)MR	(Multiparametric) magnetic resonance imaging
PCa	Prostate cancer
PSA	Prostate-specific antigen
TRUS	Transrectal ultrasound
TTMB	Transperineal template-mapping biopsies
V	Volt

---

## 14.1 Introduction on Focal Therapy for Prostate Cancer

The incidence of prostate cancer (PCa) is increasing mainly due to a higher life expectancy and the more frequent use of prostate-specific antigen (PSA) testing. The increased search for PCa is often accompanied by early-stage diagnosis. At present the recommended therapies by guideline for localized PCa are radical prostatectomy, radiotherapy with either brachytherapy or external beam radiotherapy, and active surveillance [9, 14, 18]. Radical treatment is associated with high incidence of side effects resulting in impairment of the quality of life of PCa patients. Functional outcomes vary, with rates of urinary incontinence between 3.2% and 18.3%, urinary

---

M. Scheltema (✉) • J. de la Rosette  
Department of Urology, AMC University Hospital, Meibergdreef 9,  
1105 AZ Amsterdam, The Netherlands  
e-mail: [m.j.scheltema@amc.nl](mailto:m.j.scheltema@amc.nl); [j.j.delarosette@amc.uva.nl](mailto:j.j.delarosette@amc.uva.nl)

**Table 14.1** Defined risk groups in prostate cancer

	Low-risk	Intermediate-risk	High-risk
Gleason score	GS 6	GS 7	GS >7
PSA	PSA $\leq$ 10 ng/mL	PSA 10–20 ng/mL	PSA $\geq$ 20 ng/mL
TNM	cT1c-2a	cT2b-2c	>cT3a

Defined risk groups according to the D'Amico classification [2]. If any of the three determinants (Gleason score, PSA, TNM) are positive, patients are upgraded to the corresponding risk group

irritation or obstruction, bowel symptoms (rectal urgency, frequency, pain, hematochezia, or fecal incontinence) in 2.9–34%, and erections insufficient for intercourse in 60.8–78.8% [16, 17]. Moreover, the adjuvant hormonal therapy in radiotherapy is related with hot flashes, fatigue, depression, gynecomastia, and weight change. Some of these symptoms even persisted up to 2 years after the withdrawal of hormonal therapy [17]. Active surveillance (AS) is an interesting PCa management option for low-risk PCa patients since patients that harbor low-risk PCa have low PCa-specific mortality (for risk classification see Table 14.1) [3]. AS comprises regular PSA testing and follow-up systematic random biopsies, postponing and selecting definite treatment for patients that show PCa progression or upgrading. However, intermediate- to high-risk PCa is sometimes missed due to the inherent errors in current PCa diagnostics. In a large series, upgrading to intermediate- or high-risk PCa was seen in 44% of radical prostatectomy specimen for low-grade PCa [5]. Apart from disease progression or upgrading, up to 20% of patients choosing for AS dropped out by preference, highlighting the psychological burden that some patients experience [7].

The rationale for focal therapy in prostate cancer derived from the combination of the aforementioned limitations experienced in current treatment options. In focal therapy the tumor lesion is targeted while sparing adjacent anatomical structures that are of importance for urinary, bowel, and sexual function. Especially damage to either the neurovascular bundle(s), connective tissue within the prostate, supplying prostatic blood vessels, the urethra or the rectal wall may impair functional outcomes (see Figs. 14.1 and 14.2 for adjacent anatomical structures). Several ablative modalities have been studied, including cryosurgery, radiofrequency ablation (RFA), focal brachytherapy, high-intensity focused ultrasound (HIFU), laser ablation, photodynamic therapy, microwave ablation, interstitial laser thermotherapy, focal radiotherapy with the CyberKnife, and irreversible electroporation (IRE). In a systematic review on focal therapy ( $n = 2,350$ ) in localized PCa, it was shown that focal therapy is a safe treatment option, with the most frequent complications being urinary retention (0–17%), urethral stricture (0–5%), and urinary tract infection (0–17%). Functional outcomes were promising with pad-free continence rates of 95–100% and leak-free continence of 83–100%, erectile function (sufficient for penetration) was preserved in 54–100%, and bowel symptoms were infrequent (0–1%) [22]. No long-term data exists on PCa-specific survival despite one trial treating low- to high-risk PCa with cryosurgery, indicating a 87% PCa-specific survival after 10 years [1]. In the aforementioned systematic review, mandatory post-focal therapy biopsies were performed in nine series and showed an absence of clinically significant PCa in 83–100% and of any PCa in 50–96% of patients [22].

**Fig. 14.1** Overview surrounding organs and structures (Copied with permission from Porter and Wolff [15])

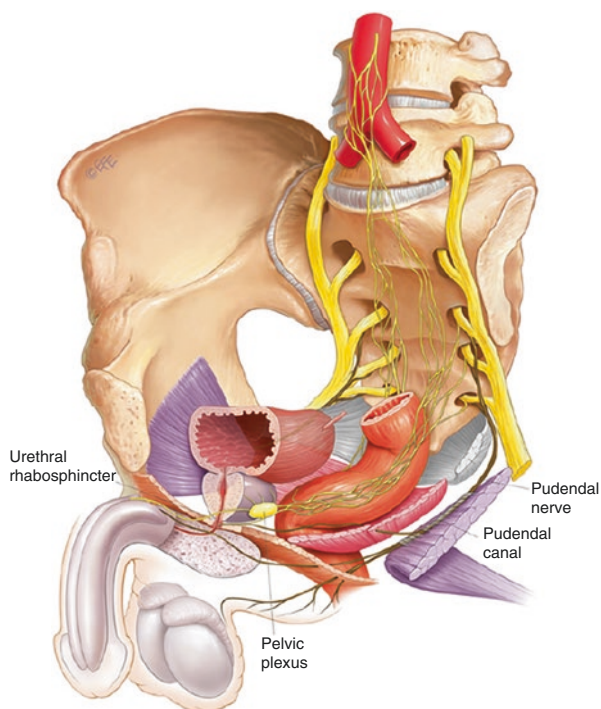
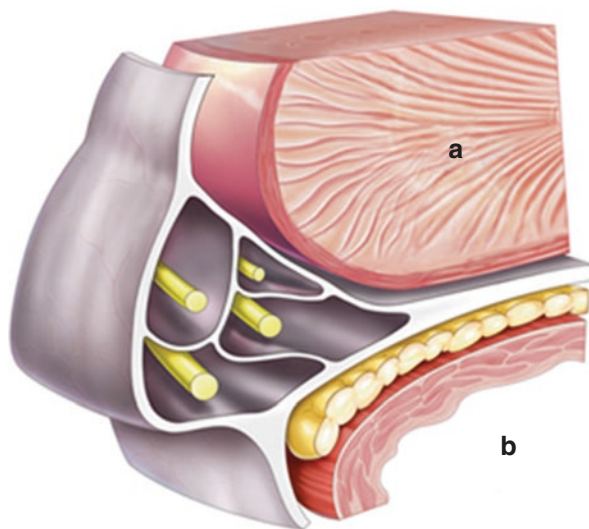


**Fig. 14.2** Neurovascular bundle. Relationship of the left neurovascular bundle with the prostate (a) and rectal wall (b) (Copied with permission from Porter and Wolff [15])



## 14.2 Patient Selection

In focal prostate cancer therapy, only the affected prostatic tissue is targeted, leaving untreated prostate tissue unharmed. Since many of the prostate tumors are of multifocal origin and current imaging techniques do not have the ability to accurately

detect all prostate cancer foci, adequate patient selection for PCa is challenging. In a review including 12 series on post-radical prostatectomy specimen, unilateral PCa was only found in 18–33% [8]. Especially high-grade (Gleason sum score >7) or high-volume PCa (>15% of prostate) is often multifocal [10]. In TRUS-guided biopsies, selective sampling of the prostate often misses PCa foci and several studies showed a poor concordance of tumor grade and volume between transrectal ultrasound (TRUS)-obtained biopsies and radical prostatectomy specimen [6]. Therefore transperineal template-mapping biopsies (TTMB) are the current “golden” standard for patient selection in focal therapy. Thirty cores are taken in TTMB, systematically sampling the prostate with a 5 mm inter-biopsy distance by using the same transperineal grid used for brachytherapy seed placement.

An international consensus meeting on patient selection agreed that potential candidates should have unilateral and low- to intermediate-risk PCa with a clinical stage  $\leq$ T2a and a minimum life expectancy of more than 10 years [4]. Patients with prior pelvic/prostatic surgery or radiotherapy should be counseled with caution. Other factors that could complicate focal therapy are prostate calcifications or cysts, inflammatory bowel disease, and bleeding disorders.

### 14.3 Treatment Procedures and Peri- and Postoperative Complications

In a regular treatment procedure, patients are admitted the day before the IRE procedure and will receive antibiotic prophylaxis before the procedure. The procedure is performed under general anesthesia, and patients receive a strong muscle relaxant to prevent uncontrolled muscle contraction. Up to six IRE electrodes are placed using ultrasound guidance in the predetermined target zone with use of the transperineal grid used for brachytherapy seed placement (Fig. 14.3). The predetermined

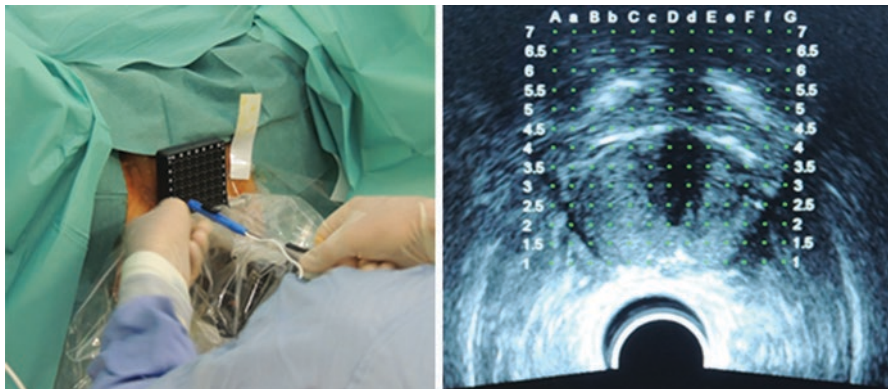


**Fig. 14.3** *Left plane*, IRE electrode placement through a transperineal brachygrid. *Right plane*, the transperineal brachygrid projected on the digital screen of the ultrasound machine to guide electrode placement



target zone is based on the topography and number of positive biopsy cores after TTMB. A total of 90 consecutive pulses (1,500 V/cm) are delivered per tumor focus, resulting in current between 20 and 50 A. Total ablation time is between 3 and 5 min and total procedure time is about 1 h. To prevent cardiac arrhythmias, pulses are synchronized with the cardiac rhythm using an electrocardiogram synchronizer. Among the perioperative complications are cardiac arrhythmias, severe muscle contraction, extended muscle blockage, anesthetic drug toxicity or allergy, and damage to adjacent structures by incorrect/displaced electrodes. After the procedure patients receive a transurethral catheter for up to 24 h to prevent urinary retentions. Patients are usually discharged 24 h after the procedure. The most frequent complications following IRE ablation in the prostate are urinary retention, irritable bladder symptoms, hematuria, and urinary tract infections.

---

#### 14.4 Follow-Up After Irreversible Electroporation

In contrast to radical treatment, PSA levels after focal therapy remain detectable. Follow-up usually consists of serial PSA testing and periodic prostate biopsies with either TRUS guidance or transperineal template mapping. It is recommended to perform PSA testing every 3 months for the first year, biannual for the second year, and thereafter annually [4]. Follow-up biopsies are performed at least once at 6 months or 1 year after the IRE procedure, by preference of the conducting center. When clinical suspicion arises, extra prostate biopsies can be performed. Multiparametric MRI (mpMRI) is performed 6 months after the IRE ablation and subsequent annually up to 5 years. It has been shown that mpMRI imaging is a feasible tool to visualize IRE ablation effects, ablated area, and possible residual PCa 4 weeks after IRE ablation of PCa foci [24].

---

#### 14.5 Current Results in Localized Prostate Cancer

The first safety and feasibility trials [12, 21] with IRE in the prostate were conducted in Beagle dogs. All procedures went uneventful with no episodes of urinary retention. Potency was preserved after bilateral focal ablation. Pathological analysis showed fibrosis in the ablation zone, without any damage to adjacent structures (e.g. capsule, urethra, rectal wall, blood vessels, and neurovascular bundle). IRE for localized treatment-naïve PCa has been performed in a number of phase 1–2 trials [11, 13, 20, 23, 26]. A total of 100 patients have been treated with low- to intermediate-risk (Gleason sum score of 6 or 7), organ-confined PCa. None of these trials reported major complications but demonstrated IRE as a safe and effective treatment modality for focal therapy in localized PCa. Functional outcomes were promising, with all patients being pad-free continent after the IRE procedure. Potency was preserved in 56–95% of the patients with a good erectile function prior to the IRE procedure. It has been shown that IRE effectively ablates all tumor within the ablation zone. Sixteen patients underwent a scheduled radical prostatectomy

4 weeks after an IRE ablation of their PCa lesion(s). Histopathological analysis after radical prostatectomy ( $n = 16$ ) showed necrotic/fibrotic tissue and no residual tumor within the target zone [26]. In line, TTMB after the IRE procedure ( $n = 21$ ) revealed no residual tumor within the ablation zone, but showed significant disease outside the ablation zone in five patients [20]. Hypothetically this could be explained by sampling error since not all patients received TTMB prior to their IRE procedure, and although TTMB have been shown to have a high negative predictive value (92–96%), significant PCa foci can still be missed [19]. In another trial ( $n = 34$ ), six patients showed clinical suspicion for possible residual tumor on mpMRI, but histopathological verification was only performed in one patient [23]. Although short-term oncological control is hopeful, long-term data are warranted to establish IRE as an effective treatment modality for tumor ablation in PCa.

---

## 14.6 Ongoing Trials and Future Perspectives

The Clinical Research Office of the Endourological Society (CROES) is conducting the first multicenter randomized controlled trial (NCT01835977) in the area of focal therapy for localized prostate cancer. IRE will be performed with either a focal or extended ablation scheme in 200 patients with unilateral, organ-confined, low- to intermediate-risk (Gleason 6 or 7) PCa. The patient will be evaluated on functional outcomes with the use of standardized questionnaires and their quality of life. Oncological control will be determined by serial PSA testing, TTMB 6 months after the procedure, and follow-up mpMRI. Patients that do not meet the inclusion criteria, e.g., bilateral disease, may receive an IRE treatment that will not be in the scope of this study. Results will be recorded and evaluated by use of the CROES registry system.

Another field of focal therapy that received increasing interest is salvage ablative therapy after primary radiotherapy for PCa. Potential patients have a biochemical recurrence or recurrence on imaging, without any evidence of local or distant metastases. Prior to salvage ablative therapy, verification of PCa recurrence should be performed by (image-guided) prostate biopsies. Follow-up should include mpMRI, prostate biopsies after 1 year, and serial PSA testing [25]. At present, most experience with salvage ablative therapy is obtained with high-intensity focused ultrasound and cryosurgery. However it is expected that IRE will be a feasible ablative modality, and future trials on salvage ablative therapy with IRE are anticipated. Likewise, it is expected that in the near future, trials on salvage ablative therapy will commence on local recurrent or residual PCa after primary focal therapy with IRE.

---

### Conclusion

Focal ablation with irreversible electroporation holds great promise for the treatment of localized PCa. The phase 1–2 trials evaluating the safety and efficacy of IRE in PCa showed encouraging results on functional preservation and oncological control. However long-term data are warranted to establish IRE as an effective treatment modality for tumor ablation in PCa.

## References

1. Cheetham P, Truesdale M, Chaudhury S, et al. Long-term cancer-specific and overall survival for men followed more than 10 years after primary and salvage cryoablation of the prostate. *J Endourol*. 2010;24:1123–9. doi:[10.1089/end.2010.0130](https://doi.org/10.1089/end.2010.0130).
2. D'Amico AV. Cancer-specific mortality after surgery or radiation for patients with clinically localized prostate cancer managed during the prostate-specific antigen era. *J Clin Oncol*. 2003;21:2163–72. doi:[10.1200/JCO.2003.01.075](https://doi.org/10.1200/JCO.2003.01.075).
3. Dall'Era MA, Albertsen PC, Bangma C, et al. Active surveillance for prostate cancer: a systematic review of the literature. *Eur Urol*. 2012;62:976–83. doi:[10.1016/j.eururo.2012.05.072](https://doi.org/10.1016/j.eururo.2012.05.072).
4. de la Rosette J, Ahmed H, Barentsz J, et al. Focal therapy in prostate cancer-report from a consensus panel. *J Endourol*. 2010;24:775–80. doi:[10.1089/end.2009.0596](https://doi.org/10.1089/end.2009.0596).
5. Dinh KT, Mahal BA, Ziehr DR, et al. Incidence and predictors of upgrading and up staging among 10,000 contemporary patients with low risk prostate cancer. *J Urol*. 2015;194:343–9. doi:[10.1016/j.juro.2015.02.015](https://doi.org/10.1016/j.juro.2015.02.015).
6. Jayram G, Eggener SE. Patient selection for focal therapy of localized prostate cancer. *Curr Opin Urol*. 2009;19:268–73. doi:[10.1097/MOU.0b013e328329eb3c](https://doi.org/10.1097/MOU.0b013e328329eb3c).
7. Loeb S, Bruinsma SM, Nicholson J, et al. Active surveillance for prostate cancer: a systematic review of clinicopathologic variables and biomarkers for risk stratification. *Eur Urol*. 2015;67:619–26. doi:[10.1016/j.eururo.2014.10.010](https://doi.org/10.1016/j.eururo.2014.10.010).
8. Meiers I, Waters DJ, Bostwick DG. Preoperative prediction of multifocal prostate cancer and application of focal therapy: review 2007. *Urology*. 2007;70:3–8. doi:[10.1016/j.urology.2007.06.1129](https://doi.org/10.1016/j.urology.2007.06.1129).
9. Mottet N, Bellmunt J, Bolla M, et al. EAU-ESTRO-SIOG Guidelines on Prostate Cancer. Part 1: Screening, Diagnosis, and Local Treatment with Curative Intent. *Eur Urol*. 2017;71(4):618–29. doi:[10.1016/j.eururo.2016.08.003](https://doi.org/10.1016/j.eururo.2016.08.003).
10. Mouraviev V, Mayes JM, Sun L, et al. Prostate cancer laterality as a rationale of focal ablative therapy for the treatment of clinically localized prostate cancer. *Cancer*. 2007;110:906–10. doi:[10.1002/cncr.22858](https://doi.org/10.1002/cncr.22858).
11. Neal RE, Millar JL, Kavounoudias H, et al. In vivo characterization and numerical simulation of prostate properties for non-thermal irreversible electroporation ablation. *Prostate*. 2014;74:458–68. doi:[10.1002/pros.22760](https://doi.org/10.1002/pros.22760).
12. Onik G, Mikus P, Rubinsky B. Irreversible electroporation: implications for prostate ablation. *Technol Cancer Res Treat*. 2007;6:295–300. doi:[10.1016/j.juro.2008.08.003](https://doi.org/10.1016/j.juro.2008.08.003).
13. Onik G, Rubinsky B. First patient experience focal therapy of prostate cancer. *Irreversible Electroporation*. 2010:235–47.
14. Parker C, Gillessen S, Heidenreich A, Horwich A. Cancer of the prostate: ESMO clinical practice guidelines for diagnosis, treatment and follow-up. *Ann Oncol*. 2015;24:mdv222. doi:[10.1093/annonc/mdv222](https://doi.org/10.1093/annonc/mdv222).
15. Porter C, Wolff E. Prostate ultrasound. Current practice and future directions. New York: Springer-Verlag; 2015.
16. Resnick MJ, Koyama T, Fan K-H, et al. Long-term functional outcomes after treatment for localized prostate cancer. *N Engl J Med*. 2013;368:436–45. doi:[10.1056/NEJMoa1209978](https://doi.org/10.1056/NEJMoa1209978).
17. Sanda MG, Dunn RL, Michalaski J, et al. Quality of life and satisfaction with outcome among prostate cancer survivors. *N Engl J Med*. 2008;358:1250–61.
18. Thompson I, Thrasher J, Gunnar Aus M, et al. (2009) Guideline for the management of clinically localized prostate cancer: 2007 update.
19. Thompson JE, Moses D, Shnier R, et al. Multiparametric magnetic resonance imaging guided diagnostic biopsy detects significant prostate cancer and could reduce unnecessary biopsies and over detection: a prospective study. *J Urol*. 2014;192:67–74. doi:[10.1016/j.juro.2014.01.014](https://doi.org/10.1016/j.juro.2014.01.014).
20. Ting F, Tran M, Böhm M, et al. Focal irreversible electroporation for prostate cancer: functional outcomes and short-term oncological control. *Prostate Cancer Prostatic Dis*. 2015:1–7. doi:[10.1038/pcan.2015.47](https://doi.org/10.1038/pcan.2015.47).

21. Tsivian M, Polascik TJ. Bilateral focal ablation of prostate tissue using low-energy direct current (LEDC): a preclinical canine study. *BJU Int.* 2013;112:526–30. doi:[10.1111/bju.12227](https://doi.org/10.1111/bju.12227).
22. Valerio M, Ahmed HU, Emberton M, et al. The role of focal therapy in the management of localised prostate cancer: a systematic review. *Eur Urol.* 2013;66:732–51. doi:[10.1016/j.eururo.2013.05.048](https://doi.org/10.1016/j.eururo.2013.05.048).
23. Valerio M, Stricker PD, Ahmed HU, et al. Initial assessment of safety and clinical feasibility of irreversible electroporation in the focal treatment of prostate cancer. *Prostate Cancer Prostatic Dis.* 2014;17:343–7. doi:[10.1038/pcan.2014.33](https://doi.org/10.1038/pcan.2014.33).
24. van den Bos W, de Bruin DM, Jurhill RR, et al. The correlation between the electrode configuration and histopathology of irreversible electroporation ablations in prostate cancer patients. *World J Urol.* 2015; doi:[10.1007/s00345-015-1661-x](https://doi.org/10.1007/s00345-015-1661-x).
25. van den Bos W, de Bruin DM, van Randen A, et al. MRI and contrast-enhanced ultrasound imaging for evaluation of focal irreversible electroporation treatment: results from a phase I–II study in patients undergoing IRE followed by radical prostatectomy. *Eur Radiol.* 2015; doi:[10.1007/s00330-015-4042-3](https://doi.org/10.1007/s00330-015-4042-3).
26. van den Bos W, Muller BG, de Bruin DM, et al. Salvage ablative therapy in prostate cancer: international multidisciplinary consensus on trial design. *Urol Oncol Semin Orig Investig.* 2015;33:495.e1–495.e7. doi:[10.1016/j.urolonc.2015.06.015](https://doi.org/10.1016/j.urolonc.2015.06.015).

Martijn R. Meijerink, Nicole van Grieken,  
and Laurien G.P.H. Vroomen

---

## 15.1 Introduction

Malignancies that are notorious for their recurrence within the lesser pelvis following radiotherapy and/or surgery are female and male urogenital tract tumors and locoregional recurrences from gastrointestinal origin such as anorectal carcinomas [1, 2]. Due to ingrowth in or compression on peripheral nerves, these relapsing malignancies can cause aggravating pain and neural function loss. The presence of extensive adhesions induced by previous surgical procedures and the risk of radiation-induced toxicity in a previously irradiated area precludes radical local treatment options such as repeat surgery [3] and stereotactic ablative body radiation therapy (SABR) [4–6]. The risk of severe treatment-induced morbidity does not seem to outweigh clinical benefit [2, 7, 8]. In general, therapy for this specific patient population primarily aims at prolonging the – preferably quality-preserved – life span, and most patients will be referred to medical oncologists for either palliative chemotherapy or best supportive care. Selected patients can be offered other local treatment modalities such as radiofrequency ablation (RFA) or cryotherapy [9–11]. One important drawback of these thermal treatment modalities is the high risk of inducing thermal damage to important neural structures like the sciatic nerve or presacral plexus, as well as to the intestines, ureters, and large vessels [12, 13].

---

M.R. Meijerink (✉) • N. van Grieken • L.G.P.H. Vroomen  
Department of Radiology and Nuclear Medicine, VU University Medical Center,  
de Boelelaan 1117, 1081 HV Amsterdam, The Netherlands  
e-mail: [mr.meijerink@vumc.nl](mailto:mr.meijerink@vumc.nl)

## 15.2 Anatomical and Physiological Considerations

The pelvis is a body cavity bounded by the pelvic bones (Fig. 15.1). The pelvic inlet (cranial opening of the pelvis) is the oblique roof and the pelvic floor is the caudal boundary. The cavity contains reproductive organs, the urinary bladder and distal ureters, the pelvic colon, and the rectum and major arteries, veins, muscles, and nerves. In the female, the uterus and vagina occupy the interval between these viscera. The structures work together in a crowded space that can be affected by many diseases in different ways. The lesser pelvis or true pelvis is the space enclosed by the pelvic girdle and below the pelvic brim: between the pelvic inlet and the pelvic floor. This cavity is a short, curved canal, deeper on its posterior than on its anterior wall. The greater pelvis (or “false pelvis”) is the space enclosed by the pelvic girdle above and in front of the pelvic brim. It is bounded on either side by the ilium; in front it is incomplete, presenting a wide interval between the anterior borders of the ilia; behind is a deep notch on either side between the ilium and the base of the sacrum. The greater pelvis is generally considered the caudal part of the abdominal cavity (this is why it is sometimes called the false pelvis). For example, the femoral nerve from L2 to L4 is located within the greater pelvis, but not in the lesser pelvis.

Extensive knowledge about the pelvic nervous system anatomy is quintessential to prevent unnecessary morbidity and to make a well thought-out therapeutic decision, since both thermal and nonthermal ablative therapies can cause irreversible and complete nerve function loss. The fourth and fifth lumbar spinal nerves form the

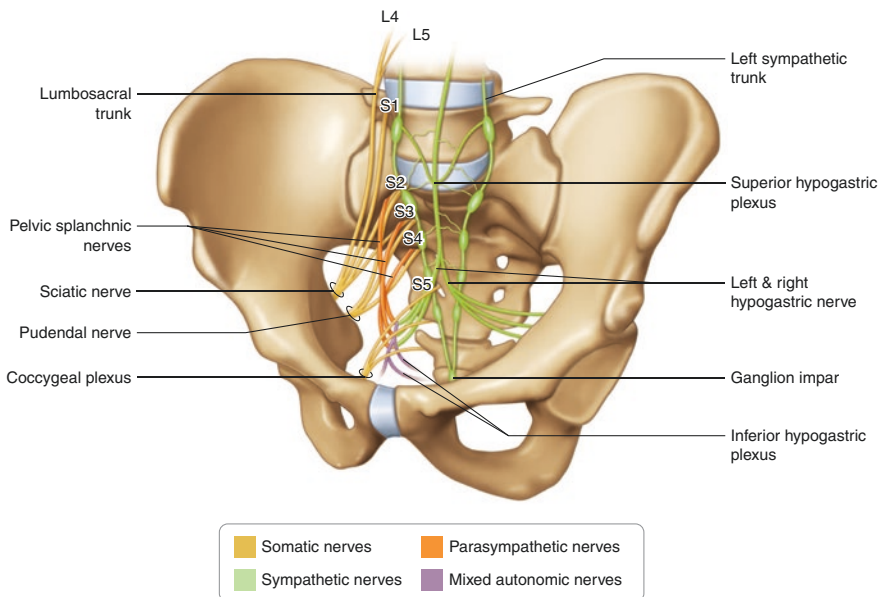


**Fig. 15.1** Pelvic nervous system anatomy. The somatic nerves are displayed in *orange*, the sympathetic and parasympathetic in *yellow* and *blue*, and the mixed autonomic fibers in *green*

lumbosacral trunk. The lumbosacral trunk goes on to join the first through fourth sacral nerves as they exit the sacrum to form the sacral plexus.

The obturator nerve arises from the *lumbar plexus* and doesn't innervate anything in the pelvis, but it runs through the pelvis to the medial thigh.

The *sacral plexus* runs down on the posterior pelvic wall anterior to the piriformis muscle. Nerves that stem from the sacral plexus include the sciatic nerve; the pudendal nerve; the gluteal, quadratus femoris, internal obturator, and piriform nerves; the posterior femoral cutaneous nerve; the perforating cutaneous nerve; and the pelvic splanchnic nerves. The sciatic nerve, formed by the fourth lumbar through the third sacral spinal nerves, leaves the pelvis through the greater sciatic foramen to enter the gluteal area. The pudendal nerve, formed from the second through the fourth spinal sacral nerves, exits the pelvis through the greater sciatic foramen and enters the perineum through the lesser sciatic foramen to innervate the muscles and skin of the perineum. The superior and inferior gluteal nerve, formed by, respectively, the fourth lumbar through the first sacral and the fifth lumbar through the second sacral spinal nerves, leave the greater sciatic foramen to innervate gluteal muscles. The nerve to the quadratus femoris and internal obturator muscle, formed from the fourth lumbar through the second sacral spinal nerves, leaves the greater sciatic foramen to innervate hip muscles. The piriformis muscle nerve stems from the first and second sacral spinal nerves. The posterior femoral cutaneous nerve and the perforating cutaneous nerve formed from the second and third sacral spinal nerves to innervate the skin of the perineum, thigh, leg, and buttock.

The *coccygeal* plexus of nerve fibers is formed by the fourth and fifth sacral spinal nerves and the coccygeal nerves. It supplies the coccygeus and levator ani muscles and the sacrococcygeal joint. Anococcygeal nerves innervate the skin between the coccyx and anus.

The *pelvic autonomic nerves* that innervate the pelvic cavity can be subdivided into the sacral sympathetic trunk, the superior and inferior hypogastric plexus, and the pelvic splanchnic nerves (S2–S4). The sacral sympathetic trunks are a continuation of the lumbar sympathetic trunks that run in front of the sacrum and behind the rectum. The right and left sacral sympathetic trunks unite anterior to the coccyx at the ganglion impar. These trunks provide fibers to the hypogastric plexus and postganglionic sympathetic fibers to the sacral plexus that innervate the lower extremities. The superior hypogastric plexus sits in front of the sacral promontory and contains sympathetic fibers from the aortic plexus. It descends into the pelvis and divides into the left and right hypogastric nerves. The inferior hypogastric plexuses are formed when the right and left hypogastric nerves are joined by pre-ganglionic parasympathetic fibers from the pelvic splanchnic nerves. The plexuses are located on each side of the rectum and the base of the bladder. They contain both sympathetic and parasympathetic fibers. The pelvic splanchnic nerves are pre-ganglionic parasympathetic fibers that originate from the second, third, and fourth sacral spinal segments. They join the hypogastric nerves to form the inferior hypogastric plexuses.

## 15.3 Malignant Tumor Recurrences Within the Pelvic Cavity

Despite advances achieved in the radical treatment of primary colorectal and urogenital cancer, locoregional relapse remains a major therapeutic concern. Although the list of primary malignancies capable of recurring within the lower abdomen is long, the most frequently encountered are recurring rectal cancer, recurring gynecological tumors, and recurring prostate cancer. The latter has been extensively discussed in Chap. 14.

### 15.3.1 Recurring Rectal Cancer

Over the past decades, the oncological outcome for primary rectal cancer has improved due to refinements in chemotherapy, (chemo)radiation, and surgery. Despite this, there still is a 10% rate of local recurrence and this recurrence threatens survival and quality of life of the affected patient [14]. Local recurrence is defined as any non-nodal tumor recurrence within the pelvic cavity, including the neorectum, mesentery, pelvic viscera, pelvic sidewall structures, and bone. Risk factors associated with local control are more bulky tumors (T3/T4), node positivity, and adverse pathology such as lymphovascular invasion or perineural invasion [15, 16]. Technical failures in the performance of total mesorectal excision are likely to account for a considerable number of locally recurrent rectal cancers. Neoadjuvant therapy has shown to decrease the risk of local recurrence at the cost of certain risks, as perioperative morbidity is higher in patients who receive radiotherapy, whether it is given preoperatively or postoperatively [17]. Due to the variable anatomy and heterogeneous clinical presentation, the detection and clinical management remains complex.

Several groups have attempted to characterize patterns of recurrence. One study describes a classification based on anatomical location within the pelvis, defining recurrence as either [1] *axial* (anastomotic, mesorectal, or perirectal soft tissue or perineum); [2] *anterior*, involving the genitourinary (GU) tract; or [3] *posterior*, involving the sacrum and presacral fascia; or [4] *lateral* bony pelvis [18].

Without treatment, many patients will suffer from invalidating symptoms such as pain, obstruction, hemorrhage, and sepsis, and they will rarely survive beyond 5 years. Approximately 50% of these local recurrences are limited to the pelvis and can be considered for curative re-excision [1, 14]. The objectives of re-excision – complete tumor resection, preservation of function, and avoidance of complications – are equal to those of the initial surgery but considerably more challenging to achieve. The surgical field has been disrupted and often irradiated; the tumors are frequently adherent to critical adjacent organs and structures. While aggressive resections offer the best opportunity for local control, palliation, and cure, they also carry a high risk of complications and long-term morbidity [15].



### 15.3.2 Recurring Gynecological Cancer

Gynecological cancers (cancers affecting the ovaries, uterus, cervix, vulva, and vagina) are among the most common cancers in women. Globally, a woman's risk of developing cancer of the cervix, ovaries, or uterus by the age of 65 is 2.2%; cancers of the vulva and vagina are less common [2]. Since the biology of ovarian cancer differs from that of other gynecological cancers and since focal ablative therapies for primary ovarian carcinomas or local recurrences are rarely indicated, we will focus on malignant tumor recurrences from primary cervical, endometrial, and vulvar cancer.

Endometrial cancer is the most common genital tract cancer among women in developed countries. The worldwide risk that a woman will develop cancer of the uterus by the age of 65 is 0.59%. The treatment standard of women with endometrial cancer is surgery, followed, in some patients, by radiotherapy, with or without chemotherapy. The prognosis for women with early-stage disease is good. Women who present with advanced or recurrent disease have a much poorer prognosis, with a median overall survival of approximately 10 months [19, 20].

Cervical cancer is the second most common cancer in women up to 65 years of age, and it is the most frequent cause of death from gynecological cancers worldwide. Women with cervical cancer are treated primarily by surgery or chemoradiotherapy; a small number require both modalities. For small volume early-stage disease, surgery and radiotherapy appear to be equally effective, and concurrent chemoradiation is more effective than radiation alone [21]. Surgery may be more beneficial in younger women, in whom ovaries can be preserved, and vaginal atrophy, stenosis, and other long-term sequelae of radiotherapy can be avoided [2].

Cancer of the vulva is rare; when combined with cancer of the vagina, it accounts for less than 1% of all cancer cases and 8% of gynecological cancers [22]. Management of women with vulvar cancer usually involves surgery to stage and control the disease and to prevent local recurrence. Chemoradiotherapy may be given as the initial treatment in women with larger, more advanced lesions involving the urethra/bladder or anal canal/rectum or who are considered unsuitable for surgery. It may also be used as an adjunct to surgery in patients who have inadequate surgical resection margins or lymph nodes involved with cancer.

Unfortunately, in some women with gynecological cancer, the disease will return (recur) or progress after initial treatment. Although the surgical management of early cancers is relatively straightforward, with lower associated morbidity and mortality, the surgical management of advanced and recurrent cancer is significantly more complicated, often requiring very extensive operations. Pelvic exenterative surgery involves removal of some or all of the pelvic organs, including the lower bowel (rectum with or without the sigmoid colon and sometimes the anal canal), the bladder, reproductive organs (including womb, fallopian tubes, ovaries, vagina, and vulva), the pelvic peritoneum (the membrane that lines the pelvis and pelvic organs), and sometimes the perineum (external area around the vagina and anus), with reconstruction.

## 15.4 Patient Selection

For recurring cancers within the pelvic cavity, the aim of exenterative surgery should be resection of all tumors with clear histological margins with the intent of cure. It is a radical, often mutilating, surgery that is associated with significant postoperative side effects (morbidity) and risk of death (mortality), and it is a major undertaking for both the patient and surgeon. The number of patients eligible for exenterative surgery is small, especially since the presence of nearby anatomical structures renders them unsuitable for complementary radical procedures [8, 18]. Generally, the maximum tolerable radiation dose has already been reached during treatment of the primary tumor. In these cases, re-irradiation is often precluded due to the high risk of radiation-induced complications [4].

In the past two decades, thermal ablation has worked its way into everyday clinical practice. Apart from the (potentially) curative possibilities, thermal ablation can be valuable in the palliative setting to achieve cytoreduction and pain relief [9–11]. For example, palliative CT-guided RFA for painful pelvic recurrences of rectal cancer is considered a feasible and effective treatment in selected cases where the recurrence is located at a safe distance from major nerves, intestines, and urogenital tract structures [9, 23–25].

Since irreversible electroporation (IRE) is regarded to leave supporting tissue largely unaffected, the structural integrity of large blood vessels, the bladder and ureters, and the intestines is thought to be preserved [26, 27]. Moreover, initially damaged axons may regenerate with complete recovery of function, according to preclinical animal studies [28–30]. For these reasons, IRE may prove a safe and feasible treatment option for patients with malignant tumor recurrences in the lesser pelvis that are considered unsuitable for established focal therapies.

Because of the relatively high morbidity involved in the radical ablative treatment of tumors within the pelvic cavity, patient selection is fundamental. Patients must be motivated and understand that recovery may be prolonged, and quality of life and function compromised, even following a successful procedure. Physicians should take patient comorbidities and overall performance status into account. Patients with poor functional reserve at baseline are not good candidates. Patients should be evaluated with detailed and appropriate pre-procedural workup, including medical, cardiac, and pulmonary clearance, and optimized prior to the intervention. The treatment plan should ideally be made by a multidisciplinary team that includes interventional radiologists, surgeons, medical and radiation oncologists, abdominal diagnostic radiologists, and gastroenterologists or gynecologists.

Because of the high risk of occult multifocal disease and the difficulty in controlling recurrence by surgery alone, neoadjuvant therapy with either chemoradiotherapy or chemotherapy alone should be considered in all cases of recurrent cancer. Many patients will have been previously irradiated. As a result, administering additional doses of radiation may prove unsafe or unfavorable. Delivery of chemotherapy and/or radiotherapy is generally best when given pre-procedurally as neo-adjuvant or induction therapy primarily aimed at size reduction or to

induce a presumed synergistic effect, as adjuvant treatment may be poorly tolerated.

IRE may represent a suitable technique to treat pathology-proven locoregional pelvic tumor recurrences that are truly unsuitable for established treatments such as surgical excision, (re)irradiation, and thermal ablation. Although with IRE radical destruction seems achievable for smaller lesions, this currently is unrealistic for patients presenting with larger tumors. For these patients, symptom prevention and pain relief should be the primary aim.

---

## 15.5 Indications and Contraindications

Adult patients with a good performance status (WHO 0–1) and preferably small, well-delineated, and pathology-proven tumor recurrence may qualify for percutaneous IRE. For smaller tumors ( $\leq 3$  cm), a radical ablation to improve oncological outcome seems feasible. For larger lesions or for patients with extensive extra-pelvic disease, the intent should be symptom prevention and pain relief. The indication should always be made in the setting of a multidisciplinary tumor board. Patients need to comprehend the risks associated with the procedure and be willing to sign a written informed consent. High-quality cross-sectional imaging should be performed maximum 6 weeks prior to the procedure to exclude multifocal pelvic and extra-pelvic disease and for treatment planning. The lesions should be unsuitable for surgical excision and radical stereotactic body radiation therapy. Further systemic therapy, either palliative or neo-adjuvant to induce size reduction, should be considered unfavorable.

Transmucosal tumor invasion into surrounding intestines or extensive involvement (complete encasement) of the intestines, ureters, bladder, or urethra, pregnancy, a history of ventricular arrhythmias, congestive heart failure (>NYHA class 2), uncontrolled hypertension, and any implanted cardiac stimulation devices are considered absolute contraindications. Coronary artery disease (defined as myocardial infarction within 6 months prior to screening), atrial fibrillation, the presence of metallic foreign objects in the ablation zone, and having received chemo- or immunotherapy maximum 4 weeks prior to the procedure are considered relative contraindications [31]. If the anatomical location of the tumor would necessitate advancing needles through bony structures, intestines, or major blood vessels, the use of safety-enhancing procedures such as pneumo-, hydro-, or balloon dissections or laparoscopic surgical assistance may be considered. For such procedures, extensive experience with percutaneous image-guided tumor ablation is mandatory.

---

## 15.6 Patient Workup and Treatment Planning

For tumors that are likely to show tracer uptake, a baseline  $^{18}\text{F}$ -FDG PET (CT) scan is recommended to rule out extra-pelvic disease and to be able to assess local response or local tumor residue/recurrence after treatment. For bony involvement,

MRI with at least T1, T2, high b-value DWI, and contrast-enhanced sequences are recommended to evaluate the extent of the ingrowth and to reliably establish the boundaries of the lesion. The size and shape of the tumor should determine the number and configuration of the needle electrodes aiming at a tumor-free margin of 0.5–1.0 cm. Eligible patients should be suitable for general anesthesia by anesthetic review with special attention to cardiac history and include electrocardiography (ECG) [32]. Routine blood samples should include electrolyte and creatinine testing, complete blood count, and coagulation studies. For patients taking anticoagulant or antiplatelet drugs, the risk of stopping the medication must be balanced against the risk of harm if treatment is stopped. For low-risk procedures, aspirin can be continued. Clopidogrel and warfarin should be stopped although this may require bridging anticoagulation with unfractionated or low molecular weight heparin. Consultation with a cardiologist is particularly recommended for patients with coronary artery stents.

---

## 15.7 Approach, Image Guidance, and Technique

All procedures are performed under general anesthesia in prone, side-lying, or supine position depending on the tumor location and the intended needle track. Prior to the procedure, two defibrillation pads are placed and connected to a defibrillator as a precautionary measure. With no data about open or laparoscopic procedures within the pelvic cavity, the preferred approach is percutaneous. Given the real-time superior three-dimensional evaluation of the nonmoving target tissue and the electrodes, combined with the much less invasive nature of the procedure, it seems unlikely that a surgical approach will ever prove superior for ablations in the pelvic cavity. To define the three-dimensional measurements of the tumor and its vicinity to vital structures, a contrast-enhanced (ce) CT or cone-beam CT scan should always be performed prior to the ablation, preferably using multiplanar image reconstruction to verify and if necessary adjust the treatment plan. Needle electrodes with an exposure length of 20 mm will be advanced in and around the tumor under CT fluoroscopy guidance, aiming at an inter-needle distance of 15–24 mm. Using the only commercially available system currently out there (NanoKnife, AngioDynamics Inc., Queensbury, NY), at least 100 pulses of 1,000–1,500 V/cm with a 90  $\mu$ s pulse length are delivered for each electrode pair. An ECG-gating device is connected to a 5-lead ECG to allow IRE pulses to be synchronized with the refractory period of the heart to avoid arrhythmias. Immediately before IRE, complete muscle relaxation is confirmed using a peripheral nerve stimulator to assess neuromuscular transmission. When necessary, additional doses to block the neuromuscular cascade can be administered by the anesthesiology team. For larger tumors, the electrodes need to be repositioned or pulled back for one or more overlapping ablations. Immediately after the procedure, a second ceCT scan will assess the ablation zone and detect crucial early complications such as an active perilesional hemorrhage.

## 15.8 Complications

With only one retrospective case series reporting results after IRE of eight patients (nine tumors) and one case report, reporting on a very large tumor recurrence involving the sacral bone, safety for IRE in the pelvic cavity has not yet been established [39, 40]. There were no deaths within 90 days post-IRE. One patient experienced a delayed hemorrhage after restarting anticoagulation therapy 3 days after the procedure (CTCAE grade III). Eight CTCAE grade II complications occurred in six out of eight patients. Three patients showed lower limb motor loss (all PNI type: II [axonotmesis]), with partial recovery in one patient. Two patients developed a hypotonic bladder (PNI type: I [neurapraxia] and PNI type: II [axonotmesis]) with complete recovery in one patient. Two patients showed upper limb motor loss, with partial recovery in both patients (PNI type: II [axonotmesis]). One patient developed a vagino-tumoral fistula following the IRE procedure. Procedure-related details including complications are summarized in Tables 15.1, 15.2, and 15.3.

**Table 15.1** Classification based on location and involvement of other structure by Jimenez et al. [18]

Patterns of tumor recurrence within the pelvic cavity based on location and involvement of other structures	1. Axial, which can be subdivided into anastomotic, mesorectal or perirectal soft tissue, or perineum following APE
	2. Anterior, involving the GU tract including the bladder, vagina, uterus, seminal vesicles, and prostate
	3. Posterior, involving the sacrum and presacral fascia, and lateral, involving the soft tissues of the pelvic sidewall and lateral bony pelvis
	4. Lateral, involving the soft tissues of the pelvic sidewall and lateral bony pelvis

**Table 15.2** Seddon's classification [33]

	Score	Tissue injured	Clinical findings	Prognosis
Neurapraxia	I	Myelin	Profound motor loss, paralysis lasting days to months	Excellent
			Normal to minimal sensory involvement	
Axonotmesis	II	Myelin, axon	Complete motor loss with sensory involvement	
	Fair		OR Complete motor loss with normal sensation	
Neurotmesis	III	Connective sheath damage ranges from partial to complete nerve disruption.	Complete motor loss	Poor
			Complete sensation loss	

**Table 15.3** Adapted from Vroomen et al. Procedure details, clinical and radiologic outcome [40]

	# probes	# pullbacks	Complications (CTCAE grade)	Complication characteristics	Seddon's classification	Affected nerve(s)	Recovery neural function	Follow-up (months)	Time to progression	
									TLP	TDP
Pt. 1	5	1	-	-	-	-	-	36 <sup>a</sup>	4/ <sup>b</sup>	3
Pt. 2	6	2	II	Lower limb motor loss + sensory involvement	Axonotmesis	Sciatic nerve	Partial	11 <sup>a</sup>	5	-
			II	Vagino-tumoral fistula						
Pt. 3	6	2	II	Hypotonic bladder	Neurapraxia	Pudendal plexus S2-S4	Completely	21 <sup>a</sup>	5	5
			II	Lower limb motor loss + sensory involvement	Axonotmesis	Sciatic nerve	None			
Pt. 4	4	1	II	Slight deterioration of preexisting lower limb motor loss + sensory involvement	Axonotmesis	Sciatic nerve	None	12 <sup>a</sup>	6	6
			III	Hemorrhage	-					
Pt. 5	6	1	II	Hypotonic bladder	Axonotmesis	Pudendal plexus S2-S4	None	17	7	-
			-	-	-	-	-	-	-	-
Pt. 6	4	1	-	-	-	-	-	9	-	9
		0								
Pt. 7	3	0	II	Upper limb motor loss + sensory involvement	Axonotmesis	Femoral nerve	Partial	9	-	-
			II	Upper limb motor loss + sensory involvement	Axonotmesis	Femoral nerve	Partial	4	-	-

TLP time to local progression, TDP time to distant progression

<sup>a</sup>Diseased

<sup>b</sup>Patient developed a marginal recurrence which was successfully retreated with percutaneous IRE (see text)

---

## 15.9 Follow-Up and Response Evaluation

The fibrotic scar tissue will substitute the electroporated tumor cells (Fig. 15.2d). This physiological process lasts several weeks to months and is often associated with a reactive inflammatory immune response at the margins of the ablation zone, which makes assessment with  $^{18}\text{F}$ -FDG PET (CT) in the first weeks to months less reliable. The ablated tissue should show lack of contrast enhancement (Fig. 15.3). Because of the limited size reduction, conventional or revised response evaluation criteria in solid tumors (RECIST) appear inappropriate [34, 35]. More sophisticated response evaluation criteria such as the PET response criteria in solid tumors (PERCIST) [36], modified RECIST [37], or Choi criteria [38] seem favorable.

---

## 15.10 Disease Recurrence

One of the major advantages of both thermal and nonthermal tumor ablation is the ability to retreat residual vital tumor tissue or recurring lesions. Re-IRE should be considered if the recurring or residual tumor tissue is limited to a solitary and well-demarcated area and if the aim for retreatment, either to improve oncological outcome pursuing a radical ablation or to induce symptom relief, remains attainable. Controlling early or multifocal recurrences may prove demanding. In these cases, the biological meaningfulness should be readdressed in a multidisciplinary oncology board. Given the difficulties to distinguish recurring tissue from reactive inflammatory tissue post-IRE, we suggest to confirm the presence of the vital tumor tissue using core biopsies.

---

## 15.11 Results from Literature

In the series from the authors, after a median follow-up of 12 months (range 4–36), four patients were still alive and four had deceased, respectively, 11, 12, 21, and 36 months after IRE [40]. Although no LSRs have been objectified according to conventional RECIST so far, unequivocal LSR was observed in five patients (five lesions) using PERCIST criteria. For lesions with a largest tumor diameter of  $\leq 3$  cm (five out of nine), up until now, one LSR has been detected (29 mm) (Fig. 15.3). Contrarily, all (four out of eight) lesions with a diameter of  $>3$  cm recurred. CT-guided core biopsy confirmed tumor relapse in one patient who was successfully retreated with percutaneous IRE 16 months after the first treatment; hereafter no local recurrence was detected until his death (Patient 1, Fig. 15.2). Tumor recurrence distant from the pelvic treatment site was present in three out of seven patients: cerebral ( $n = 1$ ) and lung ( $n = 2$ ). The lesion-based primary efficacy rate was 38% (three out of eight) and the assisted efficacy rate was 50% (four out of eight). Prior to IRE, three patients reported debilitating pain; 3 months after IRE, pain perception had remained unchanged in one patient (VAS score 5; patient 2) and had improved slightly (VAS score 5–4; patient 5) and considerably (VAS score 6–3; patient 3) in the other two.

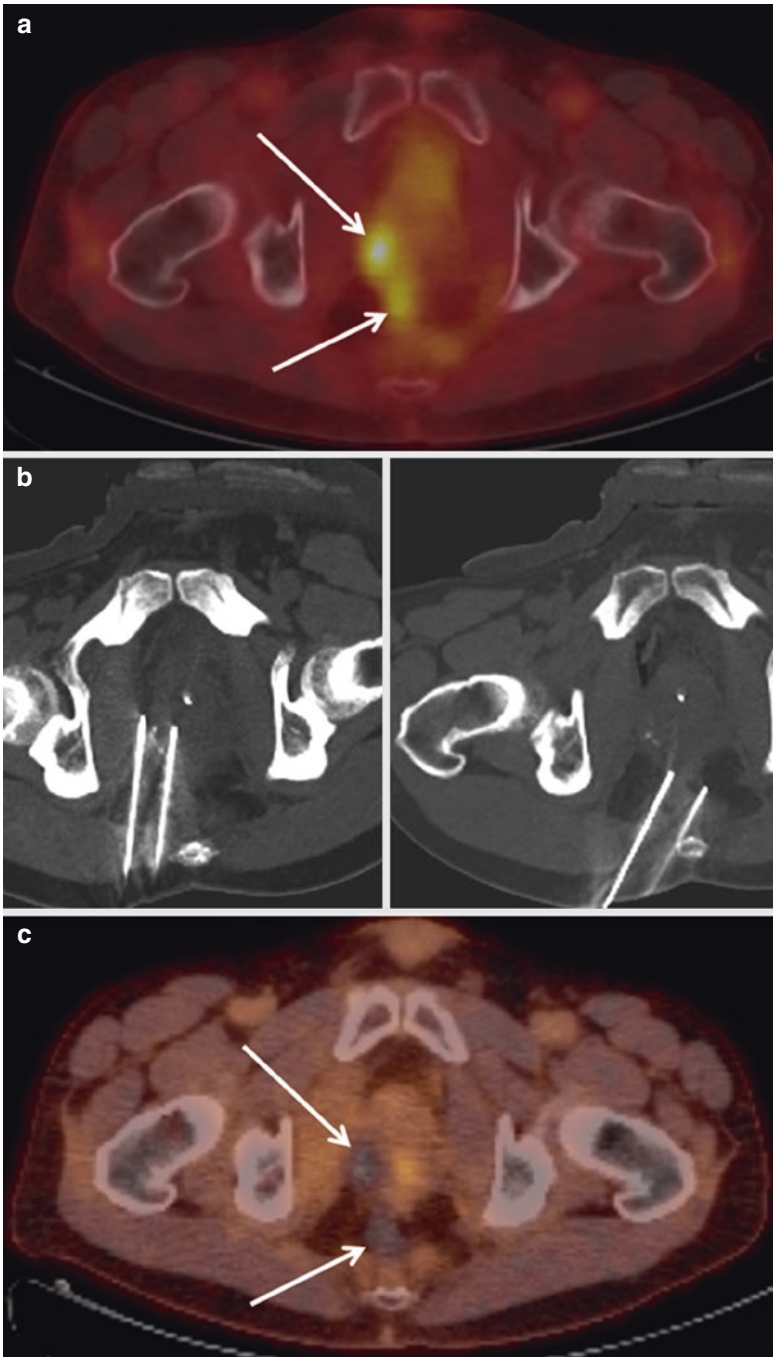


**Fig. 15.2** 18F-FDG PET-CT image of a 48-year-old male patient with two small pathologically proven locoregional recurrences (*arrows*) of primary rectal adenocarcinoma in the precoccygeal and right peri-prostatic area (**a**). Nonenhanced CT scan showing the inserted needle electrodes prior to pulse delivery (**b**). 18F-FDG PET-CT image 3 months after IRE showing no signs for residual or recurring disease (**c**) (Reprinted with permission from Vroomen LG et al. *Cardiovasc Intervent Radiol* 2017) [40]



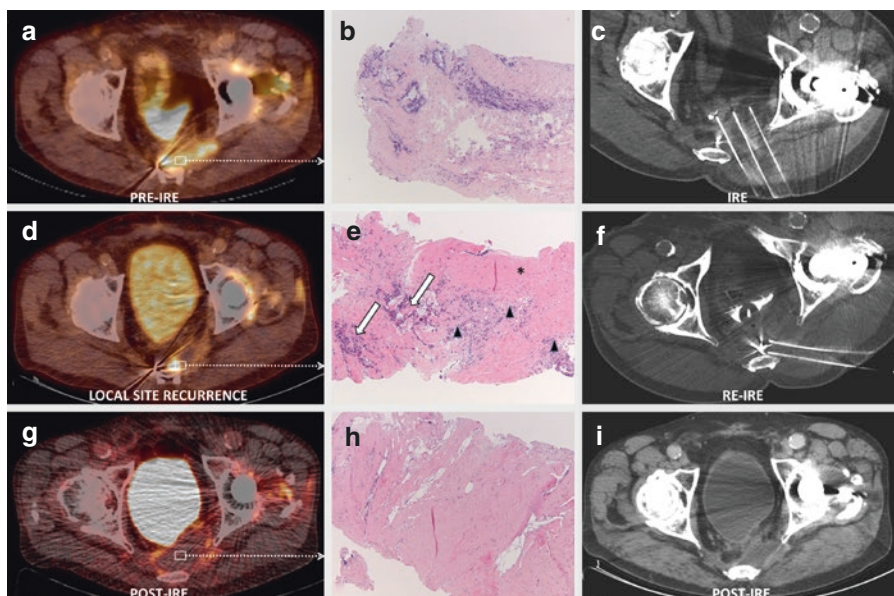


**Fig. 15.3** 18F-FDG PET-CT image (a) of a 70-year-old male patient with an 18F-FDG avid 60-mm pathologically proven locoregional recurrence (arrows) of primary rectal adenocarcinoma in the left parasacral area. Pre-IRE biopsy (b) of the initial LSR showing malignant cells on hematoxylin and eosin (HE) staining. Nonenhanced CT scan (c) showing three of the inserted needle electrodes prior to pulse delivery during the initial IRE procedure. 18F-FDG PET-CT image (d) 4 months after the initial IRE procedure showing a LSR. Pre-IRE biopsy (e) of the LSR prior to the second IRE procedure showing malignant cells (white arrows) encompassed by inflammatory cells (arrow heads); both embedded in the fibrotic tissue (asterisks) on HE staining. Nonenhanced CT scan (f) showing two of the inserted needle electrodes just before pulse delivery during the second IRE procedure. 18F-FDG PET-CT image (g) 3 months after the second IRE procedure showing no signs for residual or recurring disease. Post-IRE biopsy (h) of the ablated area after the second IRE procedure showing fibrotic tissue on HE staining. Nonenhanced CT scan (i) 6 months after the second IRE showing no signs of LSR (Reprinted with permission from Vroomen LG et al. *Cardiovasc Intervent Radiol* 2017) [40]

In the case report by Niessen et al. [39], a patient suffering from a huge advanced local recurrence of endometrial cancer ( $11.9 \times 11.6 \times 14.9$  cm) (Fig. 15.2a) with infiltration of the sacral bone and nerve plexus was treated with percutaneous IRE for palliative purposes. Due to the immediate proximity to the sacral plexus, the patient could neither undergo surgical therapy nor a second radiation therapy. Only minor temporary impairment of the neural function occurred, even though a large infiltrating tissue volume ( $941 \text{ cm}^3$ ) was ablated (Fig. 15.4).

In conclusion, IRE may represent a suitable technique to treat well-selected locoregional pelvic tumor recurrences; however, as opposed to preclinical animal studies, permanent neural function loss can occur. Although radical ablation seems achievable for smaller lesions, this currently seems unrealistic for patients presenting with larger tumors. For these patients, symptom prevention and pain relief should be the focus of future clinical studies.

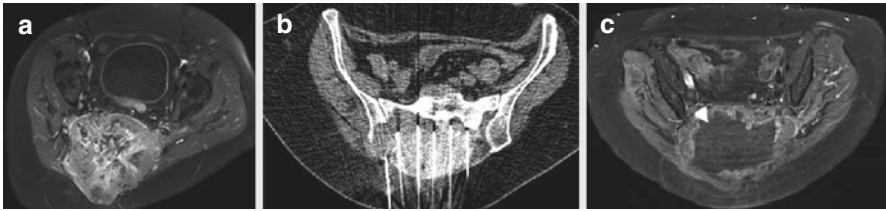


**Fig. 15.4** Baseline postcontrast T1-weighted magnetic resonance images (**a**: axial plane; **b**: sagittal plane). Preinterventional images depicting the large (11.9×11.6×14.9 cm) viable tumor mass with infiltration and destruction of the os sacrum as well as infiltration of the sacral nerve plexus (**a**). Intraoperative computed tomography fluoroscopy image showing the six ablation electrodes in the tumor mass (**b**). Follow-up postcontrast T1-weighted magnetic resonance images at 8 weeks after second intervention. Only peripheral parts of the tumor mass show viable enhancing tumor tissue (*arrow*). Central parts of the tumor are necrotic (*arrow head*) (**c**) (Reprinted with permission from Niessen et al. *J Med Case Rep* 2013 [39])

## 15.12 Ongoing and Future Clinical Trials

Given the heterogeneity of tumor type and tumor size, anatomical location, and treatment indication (symptom palliation or disease control), it may prove difficult to setup prospective safety and early efficacy studies for the abovementioned specific indications. For these reasons, we suggest to include all patients in prospective registries if treated outside the setting of controlled clinical trials.

## References

1. Yeo HL, Paty PB. Management of recurrent rectal cancer: practical insights in planning and surgical intervention. *J Surg Oncol*. 2014;109(1):47–52.
2. Ang C, et al. Exenterative surgery for recurrent gynaecological malignancies. *Cochrane Database Syst Rev*. 2014;2:CD010449.
3. Colibaseanu DT, et al. Extended sacropelvic resection for locally recurrent rectal cancer: can it be done safely and with good oncologic outcomes? *Dis Colon Rectum*. 2014;57(1):47–55.
4. Koom WS, et al. Reirradiation to the pelvis for recurrent rectal cancer. *J Surg Oncol*. 2012;105(7):637–42.
5. Cai G, et al. Accelerated hyperfractionated intensity-modulated radiotherapy for recurrent/unresectable rectal cancer in patients with previous pelvic irradiation: results of a phase II study. *Radiat Oncol*. 2014;9:278.
6. Sole CV, et al. External-beam radiation therapy after surgical resection and intraoperative electron-beam radiation therapy for oligorecurrent gynecological cancer. Long-term outcome. *Strahlenther Onkol*. 2014;190(2):171–80.
7. Mohiuddin M, Marks G, Marks J. Long-term results of reirradiation for patients with recurrent rectal carcinoma. *Cancer*. 2002;95(5):1144–50.
8. Hahnloser D, et al. Curative potential of multimodality therapy for locally recurrent rectal cancer. *Ann Surg*. 2003;237(4):502–8.
9. Pusceddu C, et al. Painful pelvic recurrence of rectal cancer: percutaneous radiofrequency ablation treatment. *Abdom Imaging*. 2013;38(6):1225–33.
10. Mylona S, et al. Palliative treatment of rectal carcinoma recurrence using radiofrequency ablation. *Cardiovasc Intervent Radiol*. 2012;35(4):875–82.

11. Kvorning Ternov K, et al. Salvage cryotherapy for local recurrence after radiotherapy for prostate cancer. *Scand J Urol*. 2015;49(2):115–9.
12. Boss A, et al. Thermal damage of the genitofemoral nerve due to radiofrequency ablation of renal cell carcinoma: a potentially avoidable complication. *AJR Am J Roentgenol*. 2005;185(6):1627–31.
13. Atwell TD, et al. Complications following 573 percutaneous renal radiofrequency and cryoablation procedures. *J Vasc Interv Radiol*. 2012;23(1):48–54.
14. Heriot AG, et al. Extended radical resection: the choice for locally recurrent rectal cancer. *Dis Colon Rectum*. 2008;51(3):284–91.
15. Bouchard P, Efron J. Management of recurrent rectal cancer. *Ann Surg Oncol*. 2010;17(5):1343–56.
16. Wu ZY, et al. Risk factors for local recurrence of middle and lower rectal carcinoma after curative resection. *World J Gastroenterol*. 2008;14(30):4805–9.
17. Guillem JG, et al. Long-term oncologic outcome following preoperative combined modality therapy and total mesorectal excision of locally advanced rectal cancer. *Ann Surg*. 2005;241(5):829–36. discussion 836–8.
18. Jimenez RE, et al. Contemporary outcomes of total pelvic exenteration in the treatment of colorectal cancer. *Dis Colon Rectum*. 2003;46(12):1619–25.
19. McMeekin DS, et al. The relationship between histology and outcome in advanced and recurrent endometrial cancer patients participating in first-line chemotherapy trials: a Gynecologic Oncology Group study. *Gynecol Oncol*. 2007;106(1):16–22.
20. Thigpen T, et al. Tamoxifen in the treatment of advanced or recurrent endometrial carcinoma: a Gynecologic Oncology Group study. *J Clin Oncol*. 2001;19(2):364–7.
21. Yin YJ, et al. The treatment of pelvic Locoregional recurrence of cervical cancer after radical surgery with intensity-modulated radiation therapy compared with conventional radiotherapy: a retrospective study. *Int J Gynecol Cancer*. 2015;25(6):1058–65.
22. van der Velden J, et al. Squamous cell cancer of the vulva with occult lymph node metastases in the groin: the impact of surgical technique on recurrence pattern and survival. *Int J Gynecol Cancer*. 2004;14(4):633–8.
23. Kalil AN, et al. Radiofrequency ablation in the treatment of pelvic recurrence of rectal cancer. *Hepato-Gastroenterology*. 2003;50(54):1937–9.
24. Machtinger R, et al. MRgFUS for pain relief as palliative treatment in recurrent cervical carcinoma: a case report. *Gynecol Oncol*. 2008;108(1):241–3.
25. Lefevre JH, et al. Radiofrequency ablation for recurrent pelvic cancer. *Color Dis*. 2008;10(8):781–4.
26. Deodhar A, et al. Renal tissue ablation with irreversible electroporation: preliminary results in a porcine model. *Urology*. 2011;77(3):754–60.
27. Phillips MA, et al. Irreversible electroporation on the small intestine. *Br J Cancer*. 2012;106(3):490–5.
28. Li W, et al. The effects of irreversible electroporation (IRE) on nerves. *PLoS One*. 2011;6(4):e18831.
29. Schoellnast H, et al. Acute and subacute effects of irreversible electroporation on nerves: experimental study in a pig model. *Radiology*. 2011;260(2):421–7.
30. Schoellnast H, et al. The delayed effects of irreversible electroporation ablation on nerves. *Eur Radiol*. 2013;23(2):375–80.
31. Scheffer HJ, et al. Irreversible electroporation for nonthermal tumor ablation in the clinical setting: a systematic review of safety and efficacy. *J Vasc Interv Radiol*. 2014;25(7):997–1011. quiz 1011.
32. Nielsen K, et al. Anaesthetic management during open and percutaneous irreversible electroporation. *Br J Anaesth*. 2014;113(6):985–92.
33. Seddon HJ. Three types of nerve injury. *Brain*. 1943;66(4):237–88.
34. Jaffe CC. Measures of response: RECIST, WHO, and new alternatives. *J Clin Oncol*. 2006;24(20):3245–51.

35. Eisenhauer EA, et al. New response evaluation criteria in solid tumours: revised RECIST guideline (version 1.1). *Eur J Cancer*. 2009;45(2):228–47.
36. Wahl RL, et al. From RECIST to PERCIST: evolving considerations for PET response criteria in solid tumors. *J Nucl Med*. 2009;50(Suppl 1):122S–50S.
37. Lencioni R, Llovet JM. Modified RECIST (mRECIST) assessment for hepatocellular carcinoma. *Semin Liver Dis*. 2010;30(1):52–60.
38. Choi H. Response evaluation of gastrointestinal stromal tumors. *Oncologist*. 2008;13(Suppl 2):4–7.
39. Niessen C, et al. Palliative treatment of presacral recurrence of endometrial cancer using irreversible electroporation: a case report. *J Med Case Rep*. 2013;7:128.
40. Vroomen LGPH, Scheffer HJ, Melenhorst MCA M, van Grieken N, van den Tol MP, Meijerink MR. Irreversible Electroporation to Treat Malignant Tumor Recurrences Within the Pelvic Cavity: A Case Series. *CardioVascular and Interventional Radiology*.

H. Kodama, Govindarajan Srimathveeravalli,  
and S.B. Solomon

---

## 16.1 Introduction

Lung and bronchial cancer has the second highest incidence of new diagnosis in cancer patients and is the cause of the largest number of patient deaths due to cancer in the last decade. In addition to primary disease, lung is a common site for metastatic disease from colorectal cancer, breast cancer, and melanoma [1]. Partial (lobectomy) or complete resection of the lung remains the gold standard for treating this disease. However, surgery reduces lung capacity and results in significant reduction in quality of life in the postsurgical setting. Image-guided ablation is a suitable alternative to patients for whom surgery is contraindicated as this treatment approach can preserve lung volume and function and allow re-treatment in case of recurrent or metachronous disease. Ablation can be performed as a same day discharge procedure with minimal loss of lung function. When used as palliation, ablation will not impact quality of life associated with recovery from a surgical procedure. Unlike surgery, chemotherapy need not be interrupted, and image-guided therapy may also support treatment at earlier time points while avoiding risk of undesirable symptoms. Finally, ablation presents a lower technical burden to physicians and resource limited hospitals and therefore may be well suited for wider use. Ablation techniques that induce significant alterations in temperature of the targeted tissue are currently used to treat tumors in the lung. Such thermal ablation techniques pose certain efficacy limitations and risks that necessitate investigation of alternate ablation therapies for use in the lung. Irreversible electroporation (IRE) has the potential to overcome these limitations and serve as an important option for treatment of primary and metastatic disease in the lung.

---

H. Kodama • G. Srimathveeravalli • S.B. Solomon (✉)  
Department of Radiology, Memorial Sloan Kettering Cancer Center, New York, NY, USA  
e-mail: [solomonS@mskcc.org](mailto:solomonS@mskcc.org)

---

## 16.2 Physiological and Anatomical Considerations

IRE and radiofrequency ablation (RFA) both rely on application of electric fields for tissue ablation; however, the working mechanism of IRE is substantially different from RFA. IRE achieves cell death through loss of cell homeostasis, not requiring sustained increases in tissue temperature for tissue necrosis [2], and thus can be considered to be a “nonthermal” ablation technique [3]. Because of this working principle, IRE is generally not affected by the heat sink effect from the presence of large blood vessels or airways that negatively impacts thermal ablation of tumors in the lung [4, 5]. Further, IRE does not appear to have any obvious effect on the extracellular matrix and collagenous structures within the ablation zone. Thermal ablation denatures proteins and collagen within the ablation zone, resulting in loss of airways and smaller blood vessels. IRE ablations are marked by sharp boundary regions, with large blood vessels and bronchi within the ablation region appearing intact in the posttreatment setting [4, 5]. Preservation of bronchi in the lung may help avoid complications such as bronchopleural fistula that can arise following thermal ablation in lung. These results indicate that IRE may be well suited for increased preservation of lung capacity and minimize complications through sparing of bronchi in the ablative or peri-ablative regions.

---

## 16.3 Disease Indication

As per NCCN and ESMO guidelines, surgery remains the definitive therapy for primary of different lung tumors as long as the patient can tolerate treatment and the disease has not metastasized beyond the lung. Radiation is the second line of treatment, often used with patients in the postsurgical setting for control of secondary disease sites and for treatment of regional metastasis. The role of ablation is limited to treatment of smaller tumors (<2 cm) and commonly performed on patients who are not eligible for surgery. Similar guidelines to treatment are followed for patients with metastatic breast or colon cancer to the lung. IRE can therefore be expected to fulfill a similar role in patients with either primary tumors or metastatic disease in the lung. Diffuse tumors can be especially challenging to treat with ablation therapy and pose a challenge to establishing clear ablation margins. Such patients are contraindicated to receive therapy with IRE.

---

## 16.4 Contraindications

IRE requires the application of high-voltage electric pulses for tumor ablation. Applications of such pulses carry the known risks of neuromuscular stimulation and can affect normal electrophysiological functions in the heart. Therefore, patients

with cardiac dysrhythmia, heart failure, pacemaker or defibrillator, and stents within the ablation in-field should not be considered for treatment with IRE. Location of the tumor within 5 cm of the heart is also a contraindication to use of IRE [6]. As metal implants like stents can affect efficacy of IRE, patients with such implants in the proximity of the tumor may not be eligible to receive treatment. IRE also presents the risk of hemorrhage and bleeding due to needle placement and electric pulse delivery. Patients on anticoagulants must therefore be able to temporarily stop medication during the perioperative period.

---

## 16.5 Pretreatment Work-Up

Routine physical examination with laboratory tests, pulmonary function test, and imaging studies including chest radiograph and chest CT should be performed as patient work-up. EKG work-up must be performed to exclude patients at risk of cardiac events. Ideal tumor size or location for IRE treatment is not well known but tumors 1–3 cm in size may be suitable targets for therapy. Successful tumor ablation with IRE is predicated on covering the entire tumor with an electric field of intensity of 800 V/cm or higher. Therefore, needle placement and choice of electrical pulse parameters is crucial to obtaining good treatment outcomes. The electric field distribution during IRE can be modeled mathematically, and the expected ablation zone can be predicted with some certainty (Fig. 16.1). Therefore, numerical simulations can assist in planning of needle placement and selection of electrical parameters for treatment.

---

## 16.6 Intervention

Patient positioning and approach can be as per physician preference and location of tumor. Probe placement can be performed under CT, cone beam CT, or CT fluoroscopic guidance referring to the planning images. Due to the softness of surrounding normal lung tissue or pneumothorax caused by puncture of probes, tumor location or distance from the critical structure can change during the procedure. Intra-procedural imaging is therefore critical for accurate needle placement. Care must be taken to place needles directly into the tumor for best results. Placement of needles bracketing the tumor or in adjacent normal lung may not yield adequate results. The electrical impedance can vary substantial based on aeration of lung. Deflated lung may provide more homogenous electrical conductivity around the tissue, improving treatment outcomes and increasing size of the ablation (Fig. 16.1). Parallel placement of electrodes is important for achieving uniform field effects within the tumor, and imaging must be performed to ensure proper needle geometry before pulse delivery (Fig. 16.2). Experiments in large animal models [5] indicate

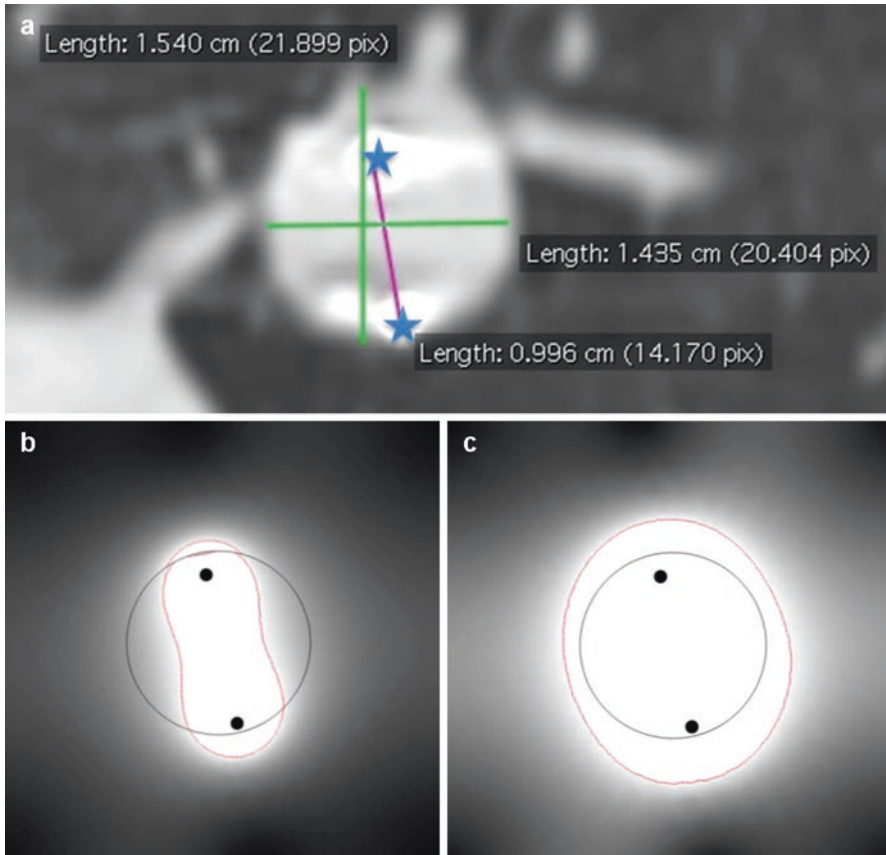


**Fig. 16.1** (a) Placement of needle electrodes for pulse delivery into a lung nodule. Electrodes (*asterisk*), tumor measurements, and electrode spacing are shown. Contingent on the electric field strength used and the relative difference in electrical conductivity of the tumor and surrounding normal lung, numerical simulation can determine whether (b) inadequate or (c) adequate tumor coverage can be achieved (a Courtesy Prof. Thierry de Baere, Institut Gustave Roussy, France)

needle spacing and exposure <math>< 1.5\text{ cm}</math>, 70 or more pulses delivered at a field strength of



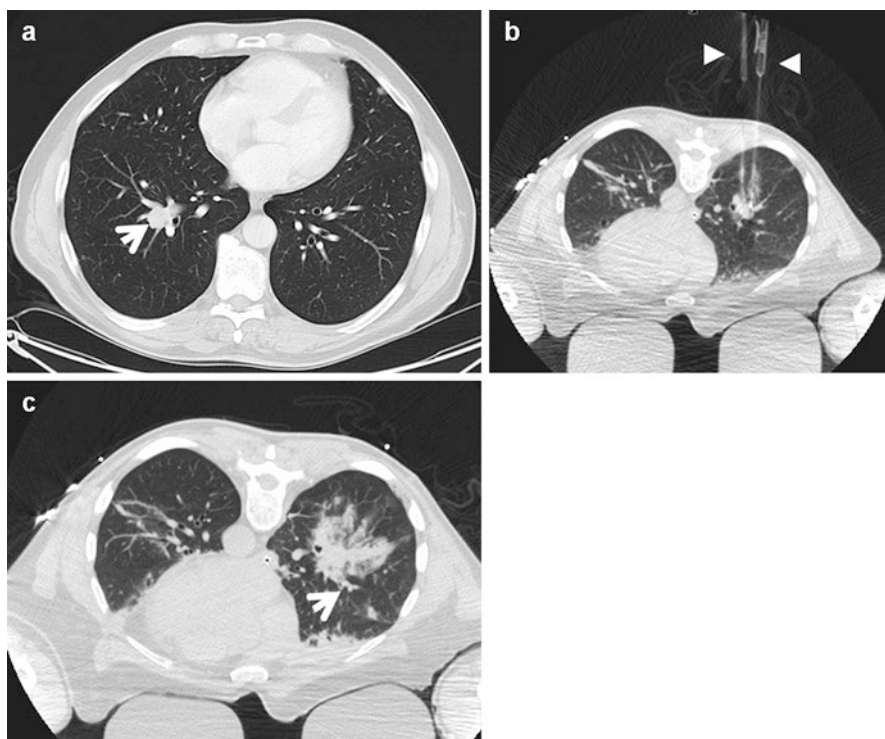


**Fig. 16.2** Patient treated with IRE. (a) Lung nodule (*arrow*) abutted by blood vessels and large airway. (b) Parallel placement of two IRE electrode needles (*arrowheads*) within the tumor. (c) Immediate post ablation image shows large hemorrhagic zone (*arrow*) in the peritreatment region. The large airway seems patent

## 16.7 Complications

There are no prospective studies reporting safety of IRE in patient lung. According to the one study [7] with a small patient number ( $n = 23$ ), chest tube placement was required due to pneumothorax in 35 %, and tumor seeding along the needle tract was seen in 13 %. Complication rate, especially tumor seeding, is quite high. Reported tumor seeding rate after lung RFA (radiofrequency ablation) is 0.1 % [8]. Pulmonary hemorrhage can be seen frequently because of increased permeability of vessels after IRE; however, no severe hemoptysis has been reported so far. Postoperative abscess formation, hemothorax, thrombosis, air embolism, or arrhythmia can be seen which are reported in the literature of IRE for the other organs, or lung ablation therapy. [9, 10]. Typical IRE treatments require more needle placements than RFA for adequate tumor coverage. Multiple adjustments to needle

placement may be required to ensure that electrodes are placed parallel to each other. These considerations may contribute to increased risk of pneumothorax and bleeding during IRE of tumors in the lung. Preclinical evidence following IRE of normal lung suggests there may be remodeling of large airways with some narrowing of the lumen. Clinical studies of IRE in other organs such as the liver suggest increased risk of thrombus formation and occasional stenosis in large veins [9, 10].

---

## 16.8 Follow-Up and Response Assessment

Similar to RFA, lab tests and imaging are recommended every 3–6 months post-intervention. There is significant edema post-IRE (Fig. 16.2) and the treatment region can enlarge in size in the first few weeks posttreatment. This can confound accurate measurements during early follow-up. Therefore, functional imaging tools such as FDG-PET/CT should be employed whenever possible to improve early detection of residual disease or recurrence.

---

## 16.9 Clinical Experience

There is a single prospective study looking at efficacy and safety following IRE of tumors in the lung, and the study reports a local tumor control of <39 %. This study was terminated early due to high disease recurrence following treatment [7]. Usman et al. [11] reported two cases treated with lung IRE where both tumors demonstrated recurrence. Given that the local control rate of RFA or microwave ablation is 57.9–93.8 % [12, 13], further refinement may be required prior to wider use of IRE in the lung.

---

## References

1. Cancer Facts and Figures, American Cancer Society. <http://www.cancer.org/research/cancer-factsstatistics/cancerfactsfigures2016/index>. April 2016.
2. Miller L, Leof J, Rubinsky B. Cancer cells ablation with irreversible electroporation. *Technol Cancer Res Treat*. 2005;4:699–706.
3. Davlos RV, Rubinsky B. Temperature considerations during irreversible electroporation. *Int J Heat Mass Transf*. 2008;51:5617–22.
4. Dupuy DE, Aswad B, Ng T. Irreversible electroporation in a Swine lung model. 2011.
5. Deodhar A, Monette S, Single GW Jr, Hamilton WC Jr, Thornton RH, Sofocleous CT, Maybody M, Solomon SB. Percutaneous irreversible electroporation lung ablation: preliminary results in a porcine model. *Cardiovasc Intervent Radiol*. 2011;34:1278–87.
6. Deodhar A, Dickfeld T, Single GW, Hamilton WC Jr, Thornton RH, Sofocleous CT, Maybody M, Gónen M, Rubinsky B, Solomon SB. Irreversible electroporation near the heart: ventricular arrhythmias can be prevented with ECG synchronization. *AJR Am J Roentgenol*. 2011;196(3):W330–5.

7. Ricke J, Jürgens JH, Deschamps F, Tselikas L, Uhde K, Kosiek O, De Baere T. Irreversible electroporation (IRE) fails to demonstrate efficacy in a prospective multicenter phase II trial on lung malignancies: the ALICE trial. *Cardiovasc Intervent Radiol*. 2015;38:401–8.
8. Kashima M, Yamakado K, Takaki H, Kodama H, Yamada T, Uraki J, Nakatsuka A. Complications after 1000 lung radiofrequency ablation sessions in 420 patients: a single center's experiences. *AJR Am J Roentgenol*. 2011;197(4):W576–80.
9. Dollinger M, Beyer LP, Haimerl M, Niessen C, Jung EM, Zeman F, Stroszczyński C, Wiggermann P. Adverse effects of irreversible electroporation of malignant liver tumors under CT fluoroscopic guidance: a single-center experience. *Diagn Interv Radiol*. 2015;21(6):471–5.
10. Kluger MD, Epelboym I, Schrope BA, Mahendraraj K, Hecht EM, Susman J, Weintraub JL, Chabot JA. Single-institution experience with irreversible electroporation for T4 pancreatic cancer: first 50 patients. *Ann Surg Oncol*. 2016;23(5):1736–43.
11. Usman M, Moore W, Talati R, Watkins K, Bilfinger TV. Irreversible electroporation of lung neoplasm: a case series. *Med Sci Monit*. 2012;18:CS43–7.
12. de Baère T, Palussière J, Aupérin A, Hakime A, Abdel-Rehim M, Kind M, Dromain C, Ravaud A, Tebboune N, Boige V, Malka D, Lafont C, Ducreux M. Midterm local efficacy and survival after radiofrequency ablation of lung tumors with minimum follow-up of 1 year: prospective evaluation. *Radiology*. 2006;240(2):587–96.
13. Pennathur A, Luketich JD, Abbas G, Chen M, Fernando HC, Gooding WE, Schuchert MJ, Gilbert S, Christie NA, Landreneau RJ. Radiofrequency ablation for the treatment of stage I non-small cell lung cancer in high-risk patients. *J Thorac Cardiovasc Surg*. 2007;134(4):857–64.

---

## **Part V**

# **Future Perspectives**

---

# From Local to Systemic Treatment: Leveraging Antitumor Immunity Following Irreversible Electroporation

# 17

Anita G.M. Stam and Tanja D. de Gruijl

---

## 17.1 Introduction: Local Ablation Techniques, the Abscopal Effect, and Systemic Antitumor Immunity

The clinical success of immune checkpoint inhibitors is set to change the landscape of cancer therapy by making immunotherapy part of the standard therapeutic arsenal in the war on cancer. For immune checkpoint blockade to be clinically efficacious, a previously induced and ongoing or dormant antitumor T cell response that can be unleashed by subsequent immune checkpoint blockade is essential. Recent studies have demonstrated that neo-epitopes arising from non-synonymous mutations are preferentially targeted by antitumor T cells that are (re)activated by immune checkpoint inhibitors [1, 2]. As these epitopes vary widely from individual to individual, it is very costly and logistically challenging to devise personalized therapies such as custom-made vaccines based on an individual tumor's mutanome. Alternatively, autologous tumors can be used as source of all possibly relevant antigens, including unique neo-antigens. This may be achieved by generating ex vivo vaccines based on DNA, mRNA, lysates, apoptotic blebs, or necroptotic fragments from surgically removed tumors [3] or by inducing immunogenic antigen release in vivo, a process sometimes referred to as in vivo vaccination [4]. Such antigen release, resulting from a process known as immunogenic cell death, can be easily combined with immune checkpoint blockade to achieve effective triggering of antitumor immunity. Immunogenic cell death may be achieved by conventional means such as chemotherapy or radiotherapy or by more novel and experimental therapies such as oncolytic virotherapy or local tumor ablation [5, 6].

---

A.G.M. Stam • T.D. de Gruijl (✉)

Immunotherapy Laboratory, Department of Medical Oncology, VU University Medical Center – Cancer Center Amsterdam, De Boelelaan 1117, 1081 HV Amsterdam, The Netherlands  
e-mail: [td.degruijl@vumc.nl](mailto:td.degruijl@vumc.nl)

Local ablative therapies have been developed for the treatment of isolated tumors and metastases. These local therapies are mostly based on thermal ablation, i.e., destruction of tumor cells by heat induction. Through the local application of extreme temperatures, either high or low, irreversible tissue damage is achieved leading to tumor cell apoptosis and coagulative necrosis. Such percutaneous high-energy-based ablation techniques have been applied to numerous tumor types, including the liver, bone, lung, kidney, breast, adrenal glands, prostate, and head and neck [7]. Minimally invasive interventional techniques for in situ tumor destruction are gaining ground clinically. Unlike surgery, the treated malignancy is not removed from the body, but apoptotic or necrotic cell remnants, induced by the ablative technique, remain available to be taken up by phagocytes. If apoptosis induction is accompanied by the release of damage-associated molecular patterns (DAMPs), like ATP and high-mobility group protein B1 [HMGB1], which serve as so-called “find me” and “eat me” signals for phagocytes, infiltrating antigen-presenting cells (APCs) will become activated and transport tumor fragments to draining lymph nodes where adaptive immune activation can take place [4, 7, 8]. In effect this local ablation, through, e.g., thermal techniques or radio frequency ablation (RFA), thus serves to achieve in vivo tumor vaccination – comprehensively reviewed by Chu and Dupuy [7], O’Brien et al. [8], and Bastianpillai et al. [6]. As a result, such local therapies can induce a durable and systemic antitumor T cell response that in turn can induce regression in distant, non-treated metastases, a phenomenon known as the abscopal effect. In keeping with this notion, case reports of spontaneous regression of metastases following RFA of a primary tumor and enhancement of tumor-specific T cell responses have been reported [9].

While the exact mechanism of the abscopal effect in image-guided thermal ablation is not fully understood, it most likely involves the activity of specialized APCs, the so-called dendritic cells (DCs). DCs, depending on their maturation state, regulate tolerance versus immunity [4, 10]. Immature DCs residing in tissues are extremely proficient in antigen uptake; however, in this state, they are poor stimulators of T cells. As DCs mature after exposure to microbial components or, in the case of local thermal ablation, endogenous danger signals released by dying cells, i.e. DAMPs, they lose their ability to take up antigens and gain T cell stimulatory function. On the other hand, if a DC does not receive maturation signals, it becomes tolerogenic, a characteristic that prevents it from inducing autoimmunity to self-antigens but rather effects the expansion of an immunosuppressive T cell subset, the regulatory T cells (Tregs) [4, 10]. Thus, exposure to sufficient quantities of antigens, combined with maturation signals, can generate DCs capable of inducing robust immune responses. These characteristics of DCs have led investigators to develop DC-based immunotherapies that target tumors. For example, DC vaccines have been developed that use autologous DCs loaded with tumor antigens generated ex vivo. While yielding some evidence of tumor responses, clinical trials testing these DC vaccines so far have largely shown them to be ineffective [10]. This may be a result of using suboptimal DC subsets, their inadequate maturation induction, insufficient co-stimulatory signals, and/or the inability of the injected DCs to travel to the lymph nodes to effectively prime T cells. While our understanding of these

matters is deepening and will result in superior vaccine designs in the near future, in vivo vaccination approaches may also be used to effectively achieve DC-based antitumor immunization [10]. Ablative tumor therapies such as radiofrequency ablation (RFA) result in massive tumor cell death, leading to the release of antigens, which are taken up by DCs, leading to effective antitumor immunity [11, 12]. Furthermore, a study by Zerbinì and colleagues showed that extracts of RFA-treated liver comprising hepatocarcinoma cells could promote the maturation of DCs [13]. This is most likely due to the release of DAMPs like heat shock proteins (HSP70 and HSP96), ATP, calreticulin, and HMGB1, which can bind DAMP receptors on DCs, e.g., Toll-like receptors (TLRs), and subsequently induce DC maturation and activation [6, 10]. In this regard, the type of cellular stress induced by the tumor ablation in large part determines the DAMP repertoire and the immunogenicity of the released antigens; the DNA damage response and endoplasmic reticulum (ER) stress are two examples of such processes known to elicit immunogenic responses [8, 14, 15]. Properly activated DCs will gain the ability to migrate to the tumor-draining lymph nodes (TDLN) where they may encounter and (re)activate tumor antigen-specific T cells which can subsequently home to more distant sites in the body and eliminate (micro)metastases, thus accounting for the observed abscopal effect. These observations hold true for intrinsically immunogenic tumors (i.e., with high mutation rates and high neo-antigen load, such as lung tumors), but are much less pronounced in weakly immunogenic tumors (e.g. prostate tumors) [2]. The latter may benefit from therapies combining local ablation with immune stimulation, e.g., by intratumoral delivery of Toll-like receptor ligands (TLR-L) and/or perioperative immune checkpoint inhibition [7, 8]. Indeed, despite the increase in antigen availability and ability to mature DCs, RFA of non-immunogenic tumors does not usually induce systemic immunity. However, combining thermal ablation with therapies that increase intratumoral DC (ITDC) numbers and maturation levels has been successful in mediating immunogenic rejection of tumor metastases in mouse models [16]. Therefore, high-energy-based local ablation techniques combined with (local) immune potentiation have the potential to turn a patient's tumor into an endogenous tumor vaccine.

Currently, the most commonly used thermal techniques use image-guided technologies to target and destroy tumors. They comprise RFA and microwave ablation (MWA), which are high-temperature-based modalities, and cryoablation, which is a low-temperature-based modality. Newer technologies, such as high-intensity focused ultrasound (HiFU) and laser ablation, are conceptually similar to high-temperature-based ablation but are less intensely studied. HiFU is the only noninvasive local ablation modality. It involves the use of ultrasound beams that are focused on a selected tumor area to generate high temperatures (up to 60 °C) through acoustic energy, causing coagulative necrosis [6, 7]. In contrast to these thermal ablation techniques, irreversible electroporation (IRE) is a new imaging-guided technique which is not primarily based on heat induction but causes formation of small defects in the cell membrane by the application of high-voltage electric pulses. This causes loss of homeostatic properties of the cell, leading to cell death through apoptosis [17, 18]. IRE is based on the pulsatile application of electric energy delivered

between several paired electrodes that are placed around the tumor [19]. IRE is believed to destroy all cells within the ablation zone, but – due to its primarily non-thermal mechanism of action – to leave supporting extracellular matrix structures unaffected. As a result, larger blood and lymphatic vessels should remain intact, facilitating efficient immune infiltration and lymph drainage to and from the tumor ablation zone, respectively. This should greatly enhance immunogenicity of the IRE-induced antigen release. In the next few paragraphs, we will review the various thermal ablation techniques in relation to their ability to induce a systemic antitumor immune response, followed by a brief review of what has been observed so far in this regard for IRE and a brief discussion of how in the future IRE may be combined with immune-modulating therapies to further increase its *in vivo* vaccination efficacy.

---

## **17.2 Thermal Tumor Ablation: Evidence of the Generation of Antitumor Immunity**

### **17.2.1 Radiofrequency Ablation (RFA)**

Radiofrequency ablation (RFA) utilizes an alternating radiofrequency current to generate heat and is one of the most widely used thermal tumor ablation techniques. Considering its widespread use in clinical practice, actual evidence for the induction of an immune response following RFA is surprisingly sparse. Nevertheless, reports that have appeared in literature are promising. The first study that set out to study an RFA-induced antitumor immune response was carried out in 2003 by Wisniewski and colleagues, who applied RFA to an induced hepatic tumor in rabbits and harvested lymphocytes and collected liver tissue biopsies for further analysis. They found that a tumor-specific T cell response was elicited 2 weeks after treatment and reported a significantly prolonged survival rate to be associated with treatment. Their findings strongly suggested an immunological effect involved in curbing tumor growth [20]. Den Brok et al. also demonstrated a tumor-specific immune response following RFA in a murine melanoma model and were able to further augment this response through CTLA-4 immune checkpoint blockade [21]. In a murine colon cancer model, it was shown that RFA, when combined with a tumor vaccine, could cause regression of both local and distal tumors [22]. Dromi et al. showed increased DC infiltration in the tumor ablation site as well as systemic induction of both CD4<sup>+</sup> and CD8<sup>+</sup> T cell responses post-RFA in a murine urothelial carcinoma model and, remarkably, tumor rejection upon tumor rechallenge, a clear sign of the successful induction of a memory immune response [23]. Zerbini and colleagues investigated immune responses following RFA in patients with hepatocellular carcinoma (HCC). They observed enhanced responses of both CD4<sup>+</sup> and CD8<sup>+</sup> T cells to recall antigens, suggestive of a generalized improvement in overall immune status, possibly related to reduced tumor-induced immune suppression [24]. Indeed, a decrease in CD4<sup>+</sup>CD25<sup>+</sup> forkhead box protein P3 (FoxP3)<sup>+</sup> Tregs in response to RFA has been reported in patients with HCC [25], confirming that one of the



antitumor mechanisms may be the reduction of peripheral tolerance to tumor antigens. In the transitional zone, which forms adjacent to the central area of RFA-induced coagulative necrosis, studies have reported inflammatory infiltrates that consist of neutrophils, macrophages, DCs, natural killer (NK) cells, and B and T cells with tumor specificity [7, 20, 23, 26]. These infiltrating immune subsets have also been observed in distant, untreated tumors [27], and their frequencies and activation state in peripheral blood were modulated by RFA [25, 28, 29]; these observations are again suggestive of a generalized immune activation by RFA. Increased frequencies of tumor-specific T cells have been detected post-RFA in cancer patients [24, 30], which appeared to effect increased tumor-free survival in some patients [30]. These (memory) T cells can also cause resistance to tumor rechallenge in animal models [23]. The mechanism by which RFA is able to induce or boost tumor-specific systemic immunity is likely due to the release of HSPs following RFA treatment [8]. Lysates derived from RFA-treated tumor cells indeed induced DC maturation [13] and combined with cytokine-induced killer cells induced an efficient tumor response [12].

### 17.2.2 Microwave Ablation (MWA)

Microwave ablation (MWA) therapy harnesses the thermal effect of high-frequency energy to induce tissue coagulation. Percutaneous MWA was first used for HCC in 1994 by Seki et al. [31]. Subsequent immune response induction was first documented in the B16 melanoma model as enhanced NK cell infiltration following local microwave hyperthermia [32]. Zhang and colleagues demonstrated local invasion of T cells, NK cells, and macrophages subsequent to MWA [33]. Szmigielski et al. showed both infiltration of T cells and increased CD4/CD8 ratios in MWA-treated prostate cancer [34]. MWA is a relatively weak stimulator of local inflammation and as a consequence of innate and acquired antitumor immunity [7]. Indeed, the induction of pro-inflammatory cytokines, including IL-1 $\beta$  and IL-6 [35], by MWA is minimal compared with that by other ablative techniques, as is the release of HSP70 [36]. Even so, the extent of inflammatory immune infiltrates in the ablated tissue of HCC was shown to be inversely correlated with clinical outcome in terms of overall survival and risk of local recurrence [37]. This observation thus provides evidence of a clinical response resulting from MWA-induced immune stimulation.

### 17.2.3 Cryoablation

Cryoablation, i.e., the destruction of tumor cells by subzero temperatures (of at least  $-40$  °C), was developed as a treatment for inoperable liver tumors. The low temperatures are achieved by inserting a probe into the lesion with circulating liquid nitrogen or through the expansion of argon gas [38]. The formation of ice crystals within the cell causes the cell membrane to rupture, thus inducing rapid cell death.

The observation that metastatic tumors would sometimes regress subsequent to cryoablation of the primary tumor has been reported in the form of multiple case studies since this technique was first used to treat prostate cancer in the 1970s [39, 40]. Early experimental *in vivo* data showed tumor-specific seroconversion to occur after cryoablation [41, 42]. In addition, NK cell activity [43], tumor-specific T cell responses in regional lymph nodes [43], and frequencies of systemically circulating T cells [44, 45] have all been shown to increase after cryoablation. Indeed, cryoablation induces a notably higher post-ablative immunogenicity than other focal ablative techniques [7, 44]. After cryoablation, pro-inflammatory cytokines, including IL-1 $\beta$ , IL-6, and TNF $\alpha$ , are released in higher quantities than after RFA or MWA [35, 46], and antigen accumulation in DCs was also greater after cryoablation than after RFA of melanoma tumors in a murine model [11]. Whereas 7 % of DCs in the tumor ablation site draining lymph nodes were occupied by intratumorally injected model tumor antigens after RFA, 20 % were occupied following *in situ* cryoablation [11]. These studies indicate that cryoablation facilitates improved antigen presentation and possibly T cell priming. The exact mechanism by which cryoablation induces a favorable immune response may be explained by the observed induction of extracellular HMGB 1 and nucleotides (both known DAMPs), released from dying cells [8, 47].

### 17.2.4 High-Intensity Focused Ultrasound (HiFU)

High-intensity focused ultrasound (HiFU) therapy entails the noninvasive use of ultrasound for local ablation of solid tumors. Two main mechanisms of action have been identified [6, 7]: (1) mechanical energy from the sound waves is converted into heat, causing coagulation necrosis; (2) HiFU treatment generates small pockets of air (bubbles) in the tissue, a phenomenon referred to as acoustic cavitation. These bubbles expand and collapse, leading to mechanical tissue destruction. Additionally, it may also damage vasculature, leading to ischemia and necrosis [48]. Zhou et al. found that levels of immunosuppressive cytokines in the circulation of cancer patients were significantly reduced after HiFU [49]. Hu and colleagues were able to compare the two mechanisms involved in HiFU, thermal and mechanical, by predominantly inducing one or the other *in vitro* [50]. They observed that mechanical tumor destruction induced a more potent immune stimulation than thermal destruction and speculated that the coagulative necrosis induced by thermal tumor ablation led to incomplete endogenous danger signal release and that these DAMPs might even be structurally compromised by thermal stress. Notably, they were also the first to report the release of DAMPs (hsp60 and ATP) following HiFU treatment and showed up-regulation of co-stimulatory molecules, signaling HiFU-induced DC activation [50]. In a follow-up study, they demonstrated that mechanical lysis stimulated a superior protective effect upon tumor rechallenge, produced more effective DC migration, and incited enhanced cytotoxic T cell activity, as compared to thermal tumor destruction [51].

### 17.2.5 Photodynamic Therapy (PDT)

Photodynamic therapy (PDT) involves the application of light on intratumorally administered photosensitive compounds to generate reactive oxygen species, resulting in cell death. Evans et al. were the first to describe the stimulation of cytokine (TNF) release by macrophages following PDT [52]. Sublethal doses of PDT have also been shown to cause macrophage activation [53]. Moreover, PDT was shown to induce tumor-specific antibody responses, regression of metastases, and resistance to tumor rechallenge in in vivo models of metastatic mammary cancer [54, 55]. In a clinical setting, PDT was shown to enhance immune recognition of tumor-associated antigens and to induce a more powerful immune response than conventional surgery [56]. PDT exerts antitumor activity through two main mechanisms [6]: (1) the direct mechanism involves the generation of reactive oxygen species (ROS) which irrevocably damage cells, leading to apoptosis and necrosis [57]; (2) the indirect antitumor effect results from damage to the endothelium of blood vessels, resulting in ischemia. The PDT-induced ROS cause an ER stress response that may contribute to the inherent immunogenicity of this therapy [8]. PDT causes the release of various DAMPs, among which are calreticulin, ATP, HSP70, and HSP90 and CRT [58–60]. These DAMPs may explain the observed DC maturation, IL-12 production, and activation of macrophages, upon exposure to PDT-derived tumor lysates [8, 61]. GM-CSF, acting by increasing DC recruitment, maturation, and survival, and imiquimod, a known TLR7 agonist, have been shown to further augment the antitumor effect of PDT [62, 63]. While PDT clearly leads to immunogenic cell death, it has one obvious drawback: its application is limited to superficially located tumors that are accessible to light [8], unless it is applied intraoperatively.

### 17.2.6 Stereotactic Radiotherapy

Radiation therapy involves the use of ionizing radiation to damage cellular DNA, either through direct ionization or the generation of free radicals. Stereotactic body irradiation therapy (SBRT) relies on focused radiation beams targeting a well-defined tumor, through detailed imaging and computerized three-dimensional treatment planning to deliver the radiation dose with extreme accuracy. It allows for the delivery of a high dose of radiation to the tumor in a short amount of time. Although its efficacy has long been attributed to its direct effect on tumor cells, a growing body of evidence suggests the involvement of a secondary immune component. Clinically, this was evidenced by the effects on metastases distant from the irradiated field, i.e., the aforementioned abscopal effect, which was first identified in this particular context [64]. A study of the abscopal effect in mice with implanted Lewis lung carcinomas and fibrosarcomas showed the tumor-specific inhibition of distant tumor growth to increase with higher irradiation doses-per-fraction [65]. Various reported studies have shown that radiation therapy causes the release of DAMPs and pro-inflammatory cytokines from dying cells, thus effectively inducing immunogenic cell death.

Calreticulin, the potent “eat me” signal causing uptake by APCs, is released from irradiated tumor cells, facilitating efficient antigen presentation to T cells [66, 67]. In addition, HMGB1 and ATP are released, both inflammatory molecules with the ability to bind and activate DCs, causing the release of IL-1 $\beta$  and facilitating T cell priming [68–70]. An important role for the TLR4-L HMGB1 in the efficacy of radiotherapy was demonstrated by compelling evidence from a study conducted by Apetoh and colleagues who showed that patients with a loss-of-function TLR4 allele had higher rates of relapse following radiotherapy [68].

### 17.2.7 Electrochemotherapy (ECT)

Electroporation, also known as electropermeabilization, is a term used to describe permeabilization of the cell membrane as a consequence of the application of short and intense electric fields across the cell membrane, e.g., in tissues [71]. This method was first reported in the early 1970s. The increase in membrane permeability is associated with the formation of nanopores in the cell membrane, hence the term “electroporation” [18]. The process of electroporation, when used in a reversible fashion, has been used clinically for high-efficiency drug delivery into cells [72]. Platinum-based drugs, such as oxaliplatin, and various anthracyclines (most notably doxorubicin) have been shown to induce the release of DAMPs from dying tumor cells, including calreticulin, HSPs, ATP, and HMGB1 [66, 68, 73–76]. Indeed, seminal work from Kroemer, Zitvogel, and colleagues demonstrated that the clinical efficacy of many cytostatic drugs relied on a secondarily induced anti-tumor immune response. From these studies, originally the term “immunogenic cell death” was coined. The immunogenic potential of chemotherapy may be even more efficiently harnessed by the use of electrochemotherapy (ECT). ECT involves the focal application of an electric field to tumor tissues in combination with chemotherapy, resulting in temporary formation of pores in the tumor cell membrane (electroporation) and subsequent high-efficiency uptake of a chemotherapeutic agent [72, 77]. Of note, Gerlini et al. observed both the local recruitment and activation of DCs and the induction of their migration toward draining lymph nodes following ECT of melanoma lesions [72, 78]. In various murine tumor models, ECT was shown to attract an inflammatory immune infiltrate (including CD11c<sup>+</sup> DCs and CD11b<sup>+</sup> macrophages) and to induce a systemic antitumor immune response, offering protection upon rechallenge [79, 80]. Moreover, the combination of ECT with the TLR9-L CpG (a choice based on the observation of increased TLR9 expression post-ECT) further enhanced this systemic antitumor immunity, thus potentially offering protection against the outgrowth of distant metastases [79, 80]. Of note, a recent retrospective study showed remarkably high complete response rates in five patients with metastatic melanoma who were treated by ECT subsequent to IFN $\alpha$  treatment, suggesting enhancement of ECT efficacy by prior immune conditioning of the tumors, possibly by optimizing DC and T cell infiltration and activation [81].

### 17.3 IRE: A Form of In Vivo Vaccination?

Irreversible electroporation (IRE) is a new imaging-guided technique which induces nanopore formation in the cell membrane by the application of high-voltage electric pulses and provides a promising alternative to heat-induced tumor ablation. Depending on the amplitude and duration of the electric pulses, electroporation of the cell membrane is reversible after which the cell survives, or irreversible, resulting in apoptosis [17, 18]. Due to its primarily nonthermal mechanism of action, IRE leaves the structural integrity of inlying and adjacent accessory tissue structures, like vessels, intact [18]. This allows for the selective ablation of diffusely growing malignancies that surround such structures, as is typically the case for, e.g., locally advanced pancreatic cancer (LAPC). Moreover, for immune effector cells, it should allow for easy access to, and migration from, the tumor ablation site.

As yet relatively little is known about the immunological response to IRE. An early study from Al-Sakere and colleagues [71] on the effects of IRE up to 6 h after treatment in a subcutaneously injected murine tumor model did not show immune infiltration into the treated tissue. However, this might well have been due to the short time period during which recruitment of an immune infiltrate could effectively take place as well as the subcutaneous localization of these transplanted tumors which are generally poorly vascularized, thus complicating immune effector cell infiltration. More encouraging observations were subsequently reported. For instance, Rubinsky et al. reported rapid resolution of cellular debris following IRE in a canine prostate tumor, which they interpreted to indicate intact and functional draining lymph vessels; they also noticed lymph node reactivity in the ablation drainage area, indicative of IRE-induced immune activation [18]. In a rat osteosarcoma model, increased T cell infiltration and reduced levels of the immunosuppressive cytokine IL-10 were reported following IRE [82]. José and colleagues [83] observed extensive areas of necrosis in a xenograft model of intra-pancreatically injected tumors, with infiltrating lymphocytes and histiocytes by day 7 after IRE, and further increased infiltration by day 14. Of particular interest are the observations made by Neal and colleagues who studied the effects of IRE in an immune competent versus immune compromised mouse model [84]. Post-IRE tumor responses were substantially more durable in the immune competent mice as compared to the immune-deficient mice, with decreased tumor burden and increased progression-free survival. IRE-treated tumors in the immune competent mice were marked by robust T cell infiltration rates at the ablation border. Importantly, tumor rechallenge in the immune competent mice resulted in an increased delay in tumor outgrowth or even complete prevention of tumor growth, clearly pointing to a protective memory immune response induced by IRE [84]. In a recent report, Bulvik and colleagues have compared the effects of IRE with those of RFA and found higher levels of systemic IL-6 post-IRE, which might have resulted from DAMP-mediated immune activation [85]. In a s.c. HCC model, superior delayed tumor outgrowth was observed after IRE. Moreover, in the border zone surrounding the treated lesions, leukocyte infiltration into the ablation zone was demonstrated in

IRE-treated, but not in RFA-treated, lesions. This led the authors to conclude that not only larger vessels but also the microvasculature was preserved post-IRE, which should greatly facilitate leukocyte trafficking [85].

Thus far evidence of post-IRE-induced antitumor immunity in man has been lacking. We have therefore studied the effects of IRE on systemic immunity in a pilot study of ten patients with locally advanced pancreatic cancer (LAPC) who participated in the PANFIRE-I phase I study (NCT01939665, [clinicaltrials.gov](https://clinicaltrials.gov)), in which the safety of percutaneous IRE for LAPC was investigated (Scheffer et al. in press). Overall, the complications observed in this trial were acceptable. There were no deaths directly attributable to IRE and 12 minor (grade I/II) and 11 major (nine grade III, two grade IV) complications were recorded. Findings further suggested prolonged time to local recurrence, and consequently overall survival, as compared to chemotherapy or no treatment (Scheffer et al. in press). Pancreatic carcinoma appears to be moderately immunogenic and to barely induce spontaneous antitumor immune responses [86]. Experimental evidence is accumulating to suggest that this may in part be caused by local and systemic immune suppression [87, 88] with Tregs playing a key role [89]. Nevertheless, pancreatic tumors are amenable to immunotherapy with clinical benefit demonstrated after tumor-specific vaccination approaches [90–92]. The use of IRE in LAPC results in apoptosis and a decrease in tumor load, which may lead to a reduction in tumor-associated immune suppression and the simultaneous release of immunogenic apoptotic tumor fragments. This could conceivably lead to the generation of antitumor immunity. To test this hypothesis, we monitored Tregs and activation of (tumor-specific) effector T cells in the peripheral blood of the IRE-treated LAPC patients (Scheffer et al. submitted). Our findings are encouraging in that they confirm a transient and moderate decrease in systemic Treg rates, accompanied by a transient increase in frequencies of proliferating CD8<sup>+</sup> T cells. Similar decreases in systemic frequencies of Tregs were previously reported after RFA [25]. The post-IRE systemic decrease in Treg rates also coincided with systemic T cell responses to WT-1, detectable by IFN $\gamma$  Elispot assay, which in turn were more prominent in patients with above median overall survival (OS) (Scheffer et al. submitted). WT-1 has been reported to be expressed in 75 % of pancreatic tumors and not at all in healthy pancreatic tissues [93], confirming its relevance as an immune target antigen. In some patients, we found evidence of pre-treatment T cell reactivity to WT-1, which is promising as such natural immunity may be boosted to enhance antitumor efficacy. Indeed, we found evidence of boosted as well as de novo-induced T cell responses to WT-1 in multiple patients following IRE (see Fig. 17.1). Although caution is warranted due to the small number of studied patients, the seeming relationship between WT-1 responsiveness and above median OS is particularly exciting. It suggests a relationship between (induced) antitumor immunity and a measure of protection against outgrowth of local and distant micrometastases.

In summary (see Fig. 17.2), IRE may aid in the generation of effective antitumor immunity through (1) the release of immunogenic (i.e., DAMP and [neo-]antigen comprising) apoptotic tumor cell remnants; (2) reduction of tumor-associated immune suppression; (3) enhanced immunogenicity by infiltration of innate immune

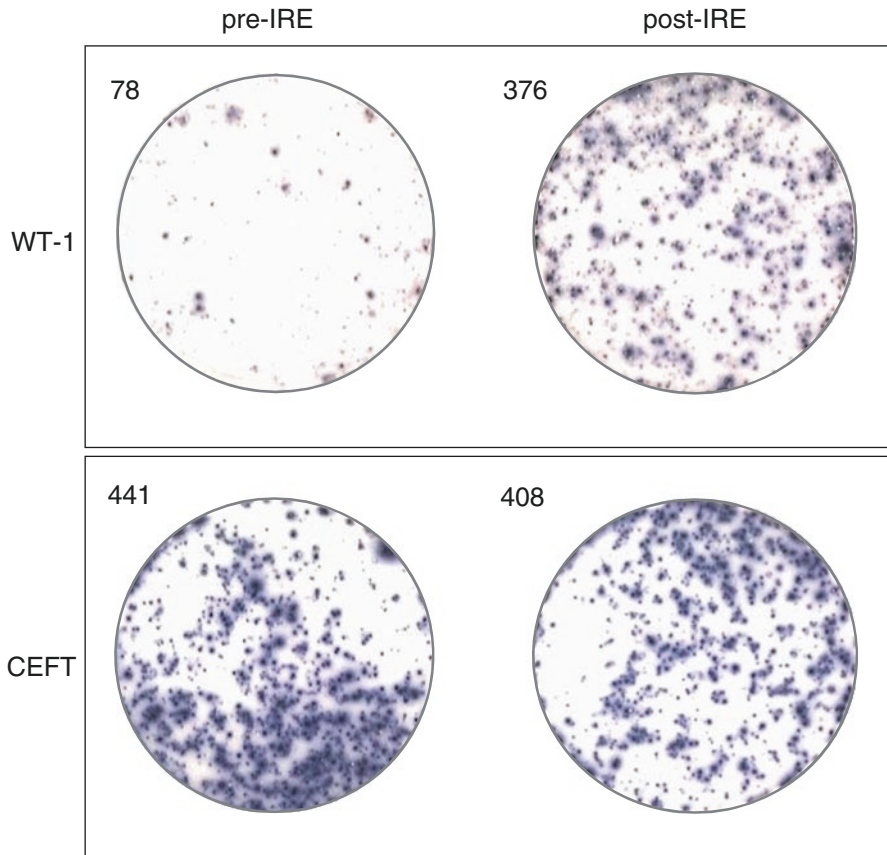


**Fig. 17.1** Specific increase in WT-1 reactive T cells from peripheral blood after irreversible electroporation of a locally advanced pancreatic tumor. Pre- and post (3 month)-IRE IFN $\gamma$  Elispot results are shown after in vitro restimulation with peripheral blood-derived mononuclear cells, against a 15aa overlapping peptide pool covering full-length WT-1 or a peptide pool containing MHC-I and MHC-II epitopes from CMV-, EBV-, flu-, and tetanus- derived recall antigens (CEFT). Representative wells are shown (one out of  $n = 6$  for WT-1 and one out of  $n = 3$  for CEFT). Numbers of IFN $\gamma$  forming spots listed are per 250,000 seeded T cells for WT-1 and per 50,000 T cells for CEFT

effector cells, including DCs, releasing pro-inflammatory cytokines and chemokines and carrying antigens to the draining lymph nodes; (4) subsequent generation of antitumor T cell immunity in the draining lymph nodes resulting either from passive draining of apoptotic remnants (taken up by lymph node resident DCs) or active transport from the tumor site by DCs; and (5) primed killer T cells may subsequently home back to the treated tumor site and aid in the clearance of remaining tumor cells or provide protection against distant metastases.

The exact mechanisms underlying the potential immunogenic qualities of IRE remain to be further unraveled. For example, what DAMPs are released and are

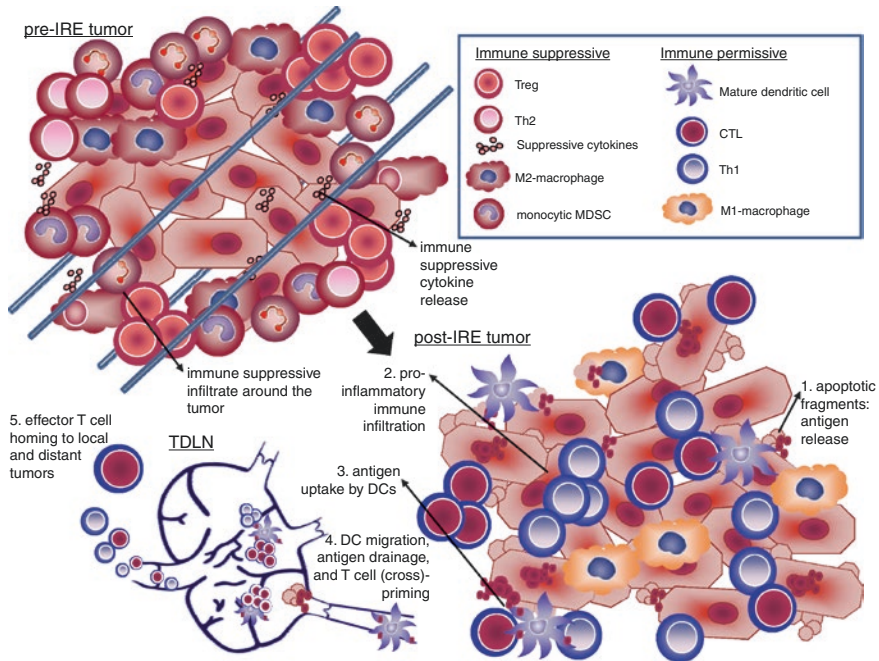


**Fig. 17.2** Irreversible electroporation (IRE) may lead to the generation of effective antitumor immunity. An essentially immune suppressed tumor microenvironment pre-IRE may be converted to an immune permissive environment through the induction of immunogenic tumor cell death leading to decreased immune suppression and an influx of pro-inflammatory immune effector cells. Systemic tumor-specific T cell immunity may eventually be achieved through (1) the release of immunogenic apoptotic tumor cell remnants; (2) reduction of tumor-associated immune suppression and recruitment of a pro-inflammatory immune infiltrate, including DCs; (3) antigen uptake and activation of infiltrating DCs through damage-associated molecular patterns (DAMPs); (4) subsequent generation of antitumor T cell immunity in the draining lymph nodes resulting either from passive draining of immunogenic apoptotic remnants (subsequently taken up by lymph node resident DCs) or active transport from the tumor site by DCs; and (5) primed killer T cells homing back to the treated tumor site to eliminate remaining tumor cells or providing systemic protection against outgrowth of distant metastases. The captioned legend shows the various depicted immune suppressive or permissive immune subsets and immune suppressive cytokines

they more structurally conserved due to the essentially nonthermal mechanism of action of IRE [7, 18]? Do the preserved blood and lymph vessels indeed allow for the emigration of antigen carrying DCs or the direct drainage of released antigens and associated DAMPs? Does this result in efficient priming of high avidity antitumor effector T cells in the draining lymph nodes? Knowledge of these processes may aid in the optimized design of IRE-based in vivo vaccination approaches. Recent developments in the immunotherapy of cancer have now opened up ways in which to further boost the IRE-induced antitumor immunity through combination therapies.



## 17.4 A Peek into the Future: Combined IRE and Local Immune Modulation

Harnessing the immune system in combination with local tumor ablation is an approach that may effectively marry local with systemic anticancer efficacy. There is increasing evidence that the pretreatment immune status influences the outcome even of conventional cancer treatments such as chemo- and radiotherapy. High rates of tumor-infiltrating lymphocytes (TILs) and type I IFN response signatures are related to higher clinical response rates and represent favorable prognostic factors in patients with various tumor types [93–97]. To optimally leverage the immune response triggered by local tumor ablation techniques like IRE, it is important to attract an immune infiltrate to the primary and metastatic tumor sites and to ensure efficient T cell priming in the lymph nodes draining the tumor ablation site. This may be achieved by peri-ablative administration of TLR-L and/or immune checkpoint inhibitors.

In particular, TLR-Ls or DAMPs that induce the release of type I IFNs may provide the “push” needed to kick-start or reawaken an effective antitumor immune response. As elegantly shown by Gajewski and colleagues in multiple publications [95, 96, 98], type I IFNs released by properly stimulated DCs (in man plasmacytoid DCs being the most powerful type I IFN producers) activate infiltrating T and NK effector cells and activate and recruit a myeloid DC subset with superior cross-priming abilities. In mice, this cross-presenting DC subset with a superior ability to prime high-avidity cytotoxic CD8<sup>+</sup> T cells is characterized by CD8 $\alpha$  expression, in man by expression of CD141/BDCA3 and CLEC9A [10]. These DCs in turn can prime a new generation of tumor antigen-specific cytotoxic effector T cells in the draining lymph nodes. Multiple studies convincingly demonstrated the prognostic as well as predictive power of type I IFN response signatures, e.g., in predicting clinical outcome of MAGE-A3 vaccination in melanoma patients [94]. One way in which type I IFN release can efficiently be achieved is through plasmacytoid DC activation by the TLR agonist CpG [99]. The immunological efficacy of local injection of unmethylated CpG type B oligodeoxynucleotides (CpG-B ODNs) in melanoma [100–102] clearly indicates the potential of using CpG ODNs as intratumoral immune-activating and therapeutic agents, also in combination with local tumor ablation. In two single-blinded randomized phase II clinical trials, we evaluated the immunological effects of local injections of CpG-B at the primary tumor excision site in clinical stage I–II melanoma patients by comparing immune parameters in CpG-B-treated patients to patients who received a saline placebo [100–102]. We found that administration of CpG-B resulted in larger TDLNs and activation in the TDLN of lymph node-resident DC subsets [100, 102]. Recruitment to the TDLN of a BDCA3/CD141<sup>+</sup>CLEC9A<sup>+</sup> myeloid DC subset with T cell-stimulatory and cross-priming abilities was markedly increased following treatment with the combination of CpG-B and GM-CSF [102]. Importantly, post-CpG-B treatment increases in tumor-specific CD8<sup>+</sup> T cells were observed in peripheral blood, consistent with enhanced systemic protection [101]. These findings are consistent with those from an in vivo mouse study showing the rapid induction of systemic T cell responses against melanoma-associated antigens

upon intratumoral delivery of CpG-B [103]. This effect was also shown to hinge on the activation of plasmacytoid DC [103]. Kortylewski and colleagues showed that although CpG can activate immune cells and induce antitumor efficacy in vivo, ligation of TLR9 by CpG also induces activation of the signal transducer STAT3, resulting in IL-10 and IL-6 production and down-modulation of the antitumor immune response [104, 105]. In keeping with this notion, our group showed, concurrent with the induction of a type I antitumor immune response, the functional activation of Tregs by CpG-B [106]. Application of CpG-STAT3 siRNA complexes, counteracting CpG-induced immune suppression, might further improve the antitumor response [105]. Another pathway that is emerging as a major player in the induction of a type I IFN response and that is associated with the induction of spontaneous antitumor immunity as well as tumor regression after therapy is the STING pathway, which is activated in DC upon cytosolic binding of cyclic dinucleotides (CDNs) derived from dying tumor cells [98, 107]. Indeed, targeting the STING pathway may prove to be a more desirable route to induce activation and recruitment of cross-priming DC than through TLR ligation since it may induce immune-activating type I IFN without activating the suppressive STAT3 pathway [108]. CpG ODNs have been successfully combined with local tumor ablation techniques to achieve in vivo vaccination in various tumor models and in first-in-man clinical trials. Veenstra and colleagues [109] carried out a comprehensive evaluation of innate immunity and specific immune responses to Her2/*neu* induced after cryoablation. They found peritumoral administration of CpG ODNs following cryoablation to significantly improve treatment outcome in all tested mouse strains. Den Brok and colleagues similarly showed that TLR9-mediated activation of DCs enhanced cross-priming of tumor-specific cytolytic T cells in the lymph nodes draining the cryoablation site and synergized with cryoablation to arrive at a superior “in vivo DC vaccine” [110]. The same group studied the ability of CpG ODNs to enhance antitumor immunity in combination with cryoablation in a melanoma model when administered via different routes: peritumoral, intravenous, and subcutaneous but distant from the tumor. Their data clearly showed peritumoral administration to be superior in the activation of DCs, the induction of tumor-specific cytotoxic T cells, and long-lasting tumor protection [111]. This observation was borne out by two clinical trials subsequently conducted by Levy and colleagues. They combined localized irradiation of a tumor site with intratumoral injections of CpG-B ODNs and showed increased systemic T cell immunity accompanied by abscopal responses in distant, untreated tumors in patients with indolent B cell lymphoma [112] or mycosis fungoides [113].

Besides the “push” provided by type I IFN-inducing TLR- or STING-Ls, the “pull” provided by immune checkpoint inhibitors may help overcome tumor-imposed immune suppression at the T cell level. Indeed, CTLA-4 blockade has been effectively combined with local tumor ablation to enhance efficacy of subsequent in vivo immunization [7]. As CTLA-4 blockade is particularly important in lifting suppressive barriers in the priming phase of the adaptive immune response, it makes sense to combine it with local tumor ablation as this approach can be leveraged to induce antitumor immunity in the draining lymph nodes [114]. A preclinical proof-of-concept study in a murine prostate cancer model showed that CTLA-4 blockade in combination with cryoablation of the primary tumor could slow or even prevent the

outgrowth of tumors after rechallenge at distant sites [115]. These distant tumors were highly infiltrated by CD4<sup>+</sup> and CD8<sup>+</sup> T cells and had a significantly higher ratio of effector T cells to Treg cells as compared to the situation after cryoablation alone. Similarly, systemic CTLA-4 blockade enhanced the antitumor efficacy of MWA treatment of subcutaneous HCC tumors, intratumorally injected with GM-CSF-carrying microspheres [116]. Local administration of anti-CTLA-4 may be an attractive therapeutic option when combined with local tumor ablation, as a murine study in a melanoma model has shown that this approach carries equal antitumor efficacy without the unwanted, and at times severe, side effects of systemic CTLA-4 blockade [117]. We have conducted a first-in-man clinical trial of local low-dose administration of anti-CTLA4/tremelimumab in stage I/II melanoma patients and were able to show increased systemic levels of tumor-specific T cells and decreased systemic rates of Tregs (van Pul et al. manuscript in preparation). In particular, the latter observation advocates the combined local administration of CpG ODNs and anti-CTLA-4, with the latter counteracting unwanted suppressive effects of the former, and together synergistically enhancing the in vivo vaccination effects of local tumor ablation.

In conclusion, future exploration of clinical strategies combining IRE with local immune potentiation may ultimately yield a very effective in vivo vaccination approach. IRE has the added advantage over thermal ablation techniques of post-ablative preservation of the blood and lymph vasculature, thus ensuring effective immune infiltration of the ablation site as well as migration of (neo-) antigen-carrying DCs to the draining lymph nodes. Indeed, the first preclinical and clinical studies have provided evidence for post-IRE immune infiltration and the induction of tumor-specific systemic T cell immunity. These promising characteristics may be further exploited by combining IRE with local administration of immune stimulatory agents like type I IFN-inducing TLR-Ls and/or immune checkpoint inhibitors. A recent study even hinted at the possibility of a gene therapy-based approach. Hepatic arterial infusion of two doses of a naked human GM-CSF plasmid immediately following liver localized IRE led to systemically detectable levels of hGM-CSF within 24 h of IRE in pigs and was accompanied by a denser macrophage infiltrate surrounding the ablation zone [118]. Lower intensity electrical fields in the periphery of the ablation zone were presumed to be responsible for a localized reversible electroporation, leading to the observed transgene expression rather than the apoptosis effected by IRE in the central ablation zone. This would allow for the exciting possibility of the local delivery and expression of immune modulatory transgenes in aid of the in vivo immunization induced by IRE. Translational studies in the near future will have to demonstrate whether immune-adjuvanted IRE can deliver on its considerable promise.

---

## References

1. Mcgranahan N, Furness AJ, Rosenthal R, Ramskov S, Lyngaa R, Saini SK, Jamal-Hanjani M, Wilson GA, Birnbak NJ, Hiley CT, Watkins TB, Shafi S, Murugaesu N, Mitter R, Akarca AU, Linares J, Marafioti T, Henry JY, Van Allen EM, Miao D, Schilling B, Schadendorf D, Garraway LA, Makarov V, Rizvi NA, Snyder A, Hellmann MD, Merghoub T, Wolchok JD, Shukla SA, Wu CJ, Peggs KS, Chan TA, Hadrup SR, Quezada SA, Swanton C. Clonal

- neoantigens elicit T cell immunoreactivity and sensitivity to immune checkpoint blockade. *Science*. 2016;351(6280):1463–9.
2. Schumacher TN, Schreiber RD. Neoantigens in cancer immunotherapy. *Science*. 2015;348(6230):69–74.
  3. Aaes TL, Kaczmarek A, Delvaeye T, De Craene B, De Koker S, Heyndrickx L, Delrue I, Taminau J, Wiernicki B, De Groote P, Garg AD, Leybaert L, Grooten J, Bertrand MJ, Agostinis P, Berx G, Declercq W, Vandenabeele P, Krysko DV. Vaccination with necroptotic cancer cells induces efficient anti-tumor immunity. *Cell Rep*. 2016;15(2):274–87.
  4. Garg AD, Romano E, Rufo N, Agostinis P. Immunogenic versus tolerogenic phagocytosis during anticancer therapy: mechanisms and clinical translation. *Cell Death Differ* 2016. [10.1038/cdd.2016.5](https://doi.org/10.1038/cdd.2016.5). [Epub ahead of print].
  5. de Gruijl TD, Janssen AB, van Beusechem VW. Arming oncolytic viruses to leverage antitumor immunity. *Expert Opin Biol Ther*. 2015;15(7):959–71.
  6. Bastianpillai C, Petrides N, Shah T, Guillaumier S, Ahmed HU, Arya M. Harnessing the immunomodulatory effect of thermal and non-thermal ablative therapies for cancer treatment. *Tumour Biol*. 2015;36(12):9137–46.
  7. Chu KF, Dupuy DE. Thermal ablation of tumours: biological mechanisms and advances in therapy. *Nat Rev Cancer*. 2014;14(3):199–208.
  8. O'Brien MA, Power DG, Clover AJ, Bird B, Soden DM, Forde PF. Local tumour ablative therapies: opportunities for maximising immune engagement and activation. *Biochim Biophys Acta*. 2014;1846(2):510–23.
  9. Dromi SA, Walsh MP, Herby S, Traugotter B, Xie J, Sharma KV, et al. Radiofrequency ablation induces antigen-presenting cell infiltration and amplification of weak tumor-induced immunity. *Radiology*. 2009;251:58–66.
  10. Palucka K, Banchereau J. Dendritic-cell-based therapeutic cancer vaccines. *Immunity*. 2013;39(1):38–48.
  11. den Brok MHMG, Suttmuller RPM, Nierkens S, Bennink EJ, Frielink C, Toonen LWJ, et al. Efficient loading of dendritic cells following cryo and radiofrequency ablation in combination with immune modulation induces anti-tumour immunity. *Br J Cancer*. 2006;95(7):896–905.
  12. Shan CC, Shi LR, Ding MQ, Zhu YB, Li XD, Xu B, Jiang JT, Wu CP. Cytokine-induced killer cells co-cultured with dendritic cells loaded with the protein lysate produced by radiofrequency ablation induce a specific antitumor response. *Oncol Lett*. 2015;9(4):1549–56.
  13. Zerbini A, Pilli M, Fagnoni F, Pelosi G, Pizzi MG, Schivazappa S, Laccabue D, Cavallo C, Schianchi C, Ferrari C, Missale G. Increased immunostimulatory activity conferred to antigen-presenting cells by exposure to antigen extract from hepatocellular carcinoma after radiofrequency thermal ablation. *J Immunother*. 2008;31(3):271–82.
  14. Gasser S, Orsulic S, Brown EJ, Raulet DH. The DNA damage pathway regulates innate immune system ligands of the NKG2D receptor. *Nature*. 2005;436(7054):1186–90.
  15. Panaretakis T, Kepp O, Brockmeier U, Tesniere A, Bjorklund AC, Chapman DC, Durchschlag M, Joza N, Pierron G, van Endert P, Yuan J, Zitvogel L, Madeo F, Williams DB, Kroemer G. Mechanisms of pre-apoptotic calreticulin exposure in immunogenic cell death. *EMBO J*. 2009;28(5):578–90.
  16. Waitz R, Solomon SB. Can local radiofrequency ablation of tumors generate systemic immunity against metastatic disease? *Radiology*. 2009;251(1):1–2.
  17. Lee EW, Loh CT, Kee ST. Imaging guided percutaneous irreversible electroporation: ultrasound and immunohistological correlation. *Technol Cancer Res Treat*. 2007;6(4):287–94.
  18. Rubinsky B, Onik G, Mikus P. Irreversible electroporation: a new ablation modality – clinical implications. *Technol Cancer Res Treat*. 2007;6(1):37–48.
  19. Lee EW, Thai S, Kee ST. Irreversible electroporation: a novel image-guided cancer therapy. *Gut Liver*. 2010;4(Suppl 1):S99–S104.
  20. Wissniewski TT, Hänslér J, Neureiter D, Frieser M, Schaber S, Esslinger B, Voll R, Strobel D, Hahn EG, Schuppan D. Activation of tumor-specific T lymphocytes by radio-frequency ablation of the VX2 hepatoma in rabbits. *Cancer Res*. 2003;63(19):6496–500. Erratum in: *Cancer Res*. 2003 Nov 1;63(21):7543

21. den Brok MH, Suttmuller RP, van der Voort R, Bennink EJ, Figdor CG, Ruers TJ, Adema GJ. In situ tumor ablation creates an antigen source for the generation of antitumor immunity. *Cancer Res.* 2004;64(11):4024–9.
22. Gameiro SR, Higgins JP, Dreher MR, Woods DL, Reddy G, Wood BJ, Guha C, Hodge JW. Combination therapy with local radiofrequency ablation and systemic vaccine enhances antitumor immunity and mediates local and distal tumor regression. *PLoS One.* 2013;8(7):e70417.
23. Dromi SA, Walsh MP, Herby S, Traughber B, Xie J, Sharma KV, Sekhar KP, Luk A, Liewehr DJ, Dreher MR, Fry TJ, Wood BJ. Radiofrequency ablation induces antigen-presenting cell infiltration and amplification of weak tumor-induced immunity. *Radiology.* 2009;251(1):58–66.
24. Zerbini A, Pilli M, Penna A, Pelosi G, Schianchi C, Molinari A, Schivazappa S, Zibera C, Fagnoni FF, Ferrari C, Missale G. Radiofrequency thermal ablation of hepatocellular carcinoma liver nodules can activate and enhance tumor-specific T-cell responses. *Cancer Res.* 2006;66(2):1139–46.
25. Fietta AM, Morosini M, Passadore I, Cascina A, Draghi P, Dore R, Rossi S, Pozzi E, Meloni F. Systemic inflammatory response and downmodulation of peripheral CD25+Foxp3+ T-regulatory cells in patients undergoing radiofrequency thermal ablation for lung cancer. *Hum Immunol.* 2009;70(7):477–86.
26. Zerbini A, Pilli M, Laccabue D, Pelosi G, Molinari A, Negri E, Cerioni S, Fagnoni F, Soliani P, Ferrari C, Missale G. Radiofrequency thermal ablation for hepatocellular carcinoma stimulates autologous NK-cell response. *Gastroenterology.* 2010;138(5):1931–42.
27. Nijkamp MW, Borren A, Govaert KM, Hoogwater FJ, Molenaar IQ, van Diest PJ, Kranenburg O, Borel Rinkes IH. Radiofrequency ablation of colorectal liver metastases induces an inflammatory response in distant hepatic metastases but not in local accelerated outgrowth. *J Surg Oncol.* 2010;101(7):551–6.
28. Rughetti A, Rahimi H, Rossi P, Frati L, Nuti M, Gaspari A, Danza FM, Ercoli L. Modulation of blood circulating immune cells by radiofrequency tumor ablation. *J Exp Clin Cancer Res.* 2003;22(4 Suppl):247–50.
29. Ali MY, Grimm CF, Ritter M, Mohr L, Allgaier HP, Weth R, Bocher WO, Endrulat K, Blum HE, Geissler M. Activation of dendritic cells by local ablation of hepatocellular carcinoma. *J Hepatol.* 2005;43(5):817–22.
30. Hiroishi K, Eguchi J, Baba T, Shimazaki T, Ishii S, Hiraide A, Sakaki M, Doi H, Uozumi S, Omori R, Matsumura T, Yanagawa T, Ito T, Imawari M. Strong CD8(+) T-cell responses against tumor-associated antigens prolong the recurrence-free interval after tumor treatment in patients with hepatocellular carcinoma. *J Gastroenterol.* 2010;45(4):451–8.
31. Seki T, Wakabayashi M, Nakagawa T, Itho T, Shiro T, Kunieda K, Sato M, Uchiyama S, Inoue K. Ultrasonically guided percutaneous microwave coagulation therapy for small hepatocellular carcinoma. *Cancer.* 1994;74(3):817–25.
32. Nakayama J, Kokuba H, Kobayashi J, Yoshida Y, Hori Y. Experimental approaches for the treatment of murine B16 melanomas of various sizes. II: injection of ethanol with combinations of beta-interferon and microwavall hyperthermia for B16 melanomas with a size of greater than 10 mm in diameter. *J Dermatol Sci.* 1997;15(2):82–8.
33. Zhang J, Dong B, Liang P, Yu X, Su L, Yu D, Ji X, Yu G. Significance of changes in local immunity in patients with hepatocellular carcinoma after percutaneous microwave coagulation therapy. *Chin Med J.* 2002;115(9):1367–71.
34. Szmigielski S, Sobczynski J, Sokolska G, Stawarz B, Zielinski H, Petrovich Z. Effects of local prostatic hyperthermia on human NK and T cell function. *Int J Hyperth.* 1991;7(6):869–80.
35. Ahmad F, Gravante G, Bhardwaj N, Strickland A, Basit R, West K, Sorge R, Dennison AR, Lloyd DM. Changes in interleukin-1 $\beta$  and 6 after hepatic microwave tissue ablation compared with radiofrequency, cryotherapy and surgical resections. *Am J Surg.* 2010;200(4):500–6.
36. Ahmad F, Gravante G, Bhardwaj N, Strickland A, Basit R, West K, Sorge R, Dennison AR, Lloyd DM. Renal effects of microwave ablation compared with radiofrequency, cryotherapy and surgical resection at different volumes of the liver treated. *Liver Int.* 2010;30(9):1305–14.

37. Dong BW, Zhang J, Liang P, Yu XL, Su L, Yu DJ, Ji XL, Yu G. Sequential pathological and immunologic analysis of percutaneous microwave coagulation therapy of hepatocellular carcinoma. *Int J Hypertherm*. 2003;19(2):119–33.
38. Kulaylat MN, Gibbs JF. Thermoablation of colorectal liver metastasis. *J Surg Oncol*. 2010;101(8):699–705.
39. Ablin RJ, Soanes WA, Gonder MJ. Prospects for cryo-immunotherapy in cases of metastasizing carcinoma of the prostate. *Cryobiology*. 1971;8(3):271–9.
40. Gursel E, Roberts M, Veenema RJ. Regression of prostatic cancer following sequential cryotherapy to the prostate. *J Urol*. 1972;108(6):928–32.
41. Ablin RJ. Cryosurgery of the rabbit prostate. Comparison of the immune response of immature and mature bucks. *Cryobiology*. 1974;11(5):416–22.
42. Ablin RJ, Jagodzinski RV, Prox C, Williams RW, Gonder MJ, Soanes WA. Cryosurgery of the monkey (macaque) prostate. I. Humoral immunologic responsiveness following cryostimulation. *Cryobiology*. 1976;13(1):47–53.
43. Sabel MS, Nehs MA, Su G, Lowler KP, Ferrara JL, Chang AE. Immunologic response to cryoablation of breast cancer. *Breast Cancer Res Treat*. 2005;90(1):97–104.
44. Jansen MC, van Hillegersberg R, Schoots IG, Levi M, Beek JF, Crezee H, van Gulik TM. Cryoablation induces greater inflammatory and coagulative responses than radiofrequency ablation or laser induced thermotherapy in a rat liver model. *Surgery*. 2010;147(5):686–95.
45. Gravante G, Sconocchia G, Ong SL, Dennison AR, Lloyd DM. Immunoregulatory effects of liver ablation therapies for the treatment of primary and metastatic liver malignancies. *Liver Int*. 2009;29(1):18–24.
46. Chapman WC, Debelak JP, Wright Pinson C, Washington MK, Atkinson JB, Venkatakrishnan A, Blackwell TS, Christman JW. Hepatic cryoablation, but not radiofrequency ablation, results in lung inflammation. *Ann Surg*. 2000;231(5):752–61.
47. Beyer C, Stearns NA, Giessel A, Distler JH, Schett G, Pisetsky DS. The extracellular release of DNA and HMGB1 from Jurkat T cells during in vitro necrotic cell death. *Innate Immun*. 2012;18(5):727–37.
48. Wu F, Zhou L, Chen WR. Host antitumor immune responses to HIFU ablation. *Int J Hypertherm*. 2007;23(2):165–71.
49. Zhou Q, Zhu XQ, Zhang J, Xu ZL, Lu P, Wu F. Changes in circulating immunosuppressive cytokine levels of cancer patients after high intensity focused ultrasound treatment. *Ultrasound Med Biol*. 2008;34(1):81–7.
50. Hu Z, Yang XY, Liu Y, Morse MA, Lysterly HK, Clay TM, Zhong P. Release of endogenous danger signals from HIFU-treated tumor cells and their stimulatory effects on APCs. *Biochem Biophys Res Commun*. 2005;335(1):124–31.
51. Hu Z, Yang XY, Liu Y, Sankin GN, Pua EC, Morse MA, Lysterly HK, Clay TM, Zhong P. Investigation of HIFU-induced anti-tumor immunity in a murine tumor model. *Transl Med*. 2007;5:34.
52. Evans S, Matthews W, Perry R, Fraker D, Norton J, Pass HI. Effect of photodynamic therapy on tumor necrosis factor production by murine macrophages. *J Natl Cancer Inst*. 1990;82(1):34–9.
53. Steubing RW, Yeteru S, Tuccillo A, Sun CH, Berns MW. Activation of macrophages by Photofrin II during photodynamic therapy. *J Photochem Photobiol B*. 1991;10(1–2):133–45.
54. Chen WR, Zhu WG, Dynlacht JR, Liu H, Nordquist RE. Long-term tumor resistance induced by laser photo-immunotherapy. *Int J Cancer*. 1999;81(5):808–12.
55. Korbelik M, Krosli G, Krosli J, Dougherty GJ. The role of host lymphoid populations in the response of mouse EMT6 tumor to photodynamic therapy. *Cancer Res*. 1996;56(24):5647–52.
56. Kabinu E, Oseroff AR, Wilding GE, Gollnick SO. Enhanced systemic immune reactivity to a basal cell carcinoma associated antigen following photodynamic therapy. *Clin Cancer Res*. 2009;15(13):4460–6.
57. Oleinick NL, Evans HH. The photobiology of photodynamic therapy: cellular targets and mechanisms. *Radiat Res*. 1998;150(5 Suppl):S146–56.
58. Garg AD, Krysko DV, Verfaillie T, Kaczmarek A, Ferreira GB, Marysael T, Rubio N, Firczuk M, Mathieu C, Roebroek AJ, Annaert W, Golab J, de Witte P, Vandenebeeke P, Agostinis P. A

- novel pathway combining calreticulin exposure and ATP secretion in immunogenic cancer cell death. *EMBO J*. 2012;31(5):1062–79.
59. Garg AD, Krysko DV, Vandenabeele P, Agostinis P. DAMPs and PDT-mediated photo-oxidative stress: exploring the unknown. *Photochem Photobiol Sci*. 2011;10(5):670–80.
  60. Garg AD, Krysko DV, Vandenabeele P, Agostinis P. Hypericin-based photodynamic therapy induces surface exposure of damage-associated molecular patterns like HSP70 and calreticulin. *Cancer Immunol Immunother*. 2012;61(2):215–21.
  61. Castano AP, Mroz P, Hamblin MR. Photodynamic therapy and anti-tumour immunity. *Nat Rev Cancer*. 2006;6(7):535–45.
  62. Krosli G, Korbek M, Krosli J, Dougherty GJ. Potentiation of photodynamic therapy-elicited antitumor response by localized treatment with granulocyte-macrophage colony-stimulating factor. *Cancer Res*. 1996;56(14):3281–6.
  63. Papakostas D, Stockfleth E. Topical treatment of basal cell carcinoma with the immune response modifier imiquimod. *Future Oncol*. 2015;11(22):2985–90.
  64. Mole RH. Wholebody irradiation; radiobiology or medicine? *Br J Radiol*. 1953;26(305):234–41.
  65. Camphausen K, Moses MA, Ménard C, Sproull M, Beecken WD, Folkman J, O'Reilly MS. Radiation abscopal antitumor effect is mediated through p53. *Cancer Res*. 2003;63(8):1990–3.
  66. Obeid M, Tesniere A, Ghiringhelli F, Fimia GM, Apetoh L, Perfettini JL, Castedo M, Mignot G, Panaretakis T, Casares N, Métivier D, Larochette N, van Endert P, Ciccocanti F, Piacentini M, Zitvogel L, Kroemer G. Calreticulin exposure dictates the immunogenicity of cancer cell death. *Nat Med*. 2007;13(1):54–61.
  67. Obeid M, Panaretakis T, Joza N, Tufi R, Tesniere A, van Endert P, Zitvogel L, Kroemer G. Calreticulin exposure is required for the immunogenicity of gamma-irradiation and UVC light-induced apoptosis. *Cell Death Differ*. 2007;14(10):1848–50.
  68. Apetoh L, Ghiringhelli F, Tesniere A, Obeid M, Ortiz C, Criollo A, Mignot G, Maiuri MC, Ullrich E, Saulnier P, Yang H, Amigorena S, Ryffel B, Barrat FJ, Saftig P, Levi F, Lidereau R, Nogues C, Mira JP, Chompret A, Joulin V, Clavel-Chapelon F, Bourhis J, André F, Delaloge S, Tursz T, Kroemer G, Zitvogel L. Toll-like receptor 4-dependent contribution of the immune system to anticancer chemotherapy and radiotherapy. *Nat Med*. 2007;13(9):1050–9.
  69. O'Brien-Ladner A, Nelson ME, Kimler BF, Wesselius LJ. Release of interleukin-1 by human alveolar macrophages after in vitro irradiation. *Radiat Res*. 1993;136(1):37–41.
  70. Hong JH, Chiang CS, Tsao CY, Lin PY, McBride WH, Wu CJ. Rapid induction of cytokine gene expression in the lung after single and fractionated doses of radiation. *Int J Radiat Biol*. 1999;75(11):1421–7.
  71. Al-Sakere B, Bernat B, André F, Connault E, Opolon P, Davalos RV, et al. A study of the immunological response to tumor ablation with irreversible electroporation. *Technol Cancer Res Treat*. 2007;6(4):301–5.
  72. Gerlini G, Sestini S, Di Gennaro P, Urso C, Pimpinelli N, Borgognoni L. Dendritic cells recruitment in melanoma metastasis treated by electrochemotherapy. *Clin Exp Metastasis*. 2013;30(1):37–45.
  73. Ghiringhelli F, Apetoh L, Tesniere A, Aymeric L, Ma Y, Ortiz C, Vermaelen K, Panaretakis T, Mignot G, Ullrich E, Perfettini JL, Schlemmer F, Tasdemir E, Uhl M, Génin P, Civas A, Ryffel B, Kanellopoulos J, Tschopp J, André F, Lidereau R, McLaughlin NM, Haynes NM, Smyth MJ, Kroemer G, Zitvogel L. Activation of the NLRP3 inflammasome in dendritic cells induces IL-1beta-dependent adaptive immunity against tumors. *Nat Med*. 2009;15(10):1170–8.
  74. Michaud M, Martins I, Sukkurwala AQ, Adjemian S, Ma Y, Pellegatti P, Shen S, Kepp O, Scazecz M, Mignot G, Rello-Varona S, Tailler M, Menger L, Vacchelli E, Galluzzi L, Ghiringhelli F, di Virgilio F, Zitvogel L, Kroemer G. Autophagy-dependent anticancer immune responses induced by chemotherapeutic agents in mice. *Science*. 2011;334(6062):1573–7.
  75. Fucikova J, Kralikova P, Fialova A, Brtnicky T, Rob L, Bartunkova J, Spisek R. Human tumor cells killed by anthracyclines induce a tumor-specific immune response. *Cancer Res*. 2011;71(14):4821–33.

76. Panaretakis T, Joza N, Modjtahedi N, Tesniere A, Vitale I, Durchschlag M, Fimia GM, Kepp O, Piacentini M, Froehlich KU, van Endert P, Zitvogel L, Madeo F, Kroemer G. The co-translocation of ERp57 and calreticulin determines the immunogenicity of cell death. *Cell Death Differ.* 2008;15(9):1499–509.
77. Mir LM, Orłowski S, Belehradec J Jr, Paoletti C. Electrochemotherapy potentiation of anti-tumour effect of bleomycin by local electric pulses. *Eur J Cancer.* 1991;27(1):68–72.
78. Gerlini G, Di Gennaro P, Borgognoni L. Enhancing anti-melanoma immunity by electrochemotherapy and in vivo dendritic-cell activation. *Oncoimmunology.* 2012;1(9):1655–7.
79. Roux S, Bernat C, Al-Sakere B, Ghiringhelli F, Opolon P, Carpentier AF, Zitvogel L, Mir LM, Robert C. Tumor destruction using electrochemotherapy followed by CpG oligodeoxynucleotide injection induces distant tumor responses. *Cancer Immunol Immunother.* 2008;57(9):1291–300.
80. Keisari Y, Hochman I, Confino H, Korenstein R, Kelson I. Activation of local and systemic anti-tumor immune responses by ablation of solid tumors with intratumoral electrochemical or alpha radiation treatments. *Cancer Immunol Immunother.* 2014;63(1):1–9.
81. Hribernik A, Cemazar M, Sersa G, Bosnjak M, Snoj M. Effectiveness of electrochemotherapy after IFN- $\alpha$  adjuvant therapy of melanoma patients. *Radiol Oncol.* 2016;50(1):21–7.
82. Li X, Xu K, Li W, Qiu X, Ma B, Fan Q, Li Z. Immunologic response to tumor ablation with irreversible electroporation. *PLoS One.* 2012;7:e48749.
83. Jose A, Sobrevals L, Ivorra A, Fillat C. Irreversible electroporation shows efficacy against pancreatic carcinoma without systemic toxicity in mouse models. *Cancer Lett.* 2012;317:16–23.
84. Neal RE II, Rossmeisl JH Jr, Robertson JL, Arena CB, Davis EM, Singh RN, Stallings J, Davalos RV. Improved local and systemic anti-tumor efficacy for irreversible electroporation in immunocompetent versus immunodeficient mice. *PLoS One.* 2013;8:e64559.
85. Bulvik BE, Rozenblum N, Gourevich S, Ahmed M, Andriyanov AV, Galun E, Goldberg SN. Irreversible electroporation versus radiofrequency ablation: a comparison of local and systemic effects in a small-animal model. *Radiology.* 2016;280:413–24.
86. Lutz ER, Wu AA, Bigelow E, Sharma R, Mo G, Soares K, Solt S, Dorman A, Wamwea A, Yager A, Laheru D, Wolfgang CL, Wang J, Hruban RH, Anders RA, Jaffee EM, Zheng L. Immunotherapy converts nonimmunogenic pancreatic tumors into immunogenic foci of immune regulation. *Cancer Immunol Res.* 2014;2:616–31.
87. Sideras K, Braat H, Kwekkeboom J, van Eijck CH, Peppelenbosch MP, Sleijfer S, Bruno M. Role of the immune system in pancreatic cancer progression and immune modulating treatment strategies. *Cancer Treat Rev.* 2014;40:513–22.
88. Schnurr M, Duewell P, Bauer C, Rothenfusser S, Lauber K, Endres S, Kobold S. Strategies to relieve immunosuppression in pancreatic cancer. *Immunotherapy.* 2015;7:363–76.
89. Hiraoka N, Onozato K, Kosuge T, Hirohashi S. Prevalence of FOXP3+ regulatory T cells increases during the progression of pancreatic ductal adenocarcinoma and its premalignant lesions. *Clin Cancer Res.* 2006;12:5423–34.
90. Koido S, Homma S, Okamoto M, Takakura K, Mori M, Yoshizaki S, Tsukinaga S, Odahara S, Koyama S, Imazu H, Uchiyama K, Kajihara M, Arakawa H, Misawa T, Toyama Y, Yanagisawa S, Ikegami M, Kan S, Hayashi K, Komita H, Kamata Y, Ito M, Ishidao T, Yusa S, Shimodaira S, Gong J, Sugiyama H, Ohkusa T, Tajiri H. Treatment with chemotherapy and dendritic cells pulsed with multiple Wilms' tumor 1 (WT1)-specific MHC class I/II-restricted epitopes for pancreatic cancer. *Clin Cancer Res.* 2014;20:4228–39.
91. Le DT, Wang-Gillam A, Picozzi V, Gretten TF, Crocenzi T, Springett G, Morse M, Zeh H, Cohen D, Fine RL, Onners B, Uram JN, Laheru DA, Lutz ER, Solt S, Murphy AL, Skoble J, Lemmens E, Grous J, Dubensky T Jr, Brockstedt DG, Jaffee EM. Safety and survival with GVAX pancreas prime and listeria monocytogenes-expressing mesothelin (CRS-207) boost vaccines for metastatic pancreatic cancer. *J Clin Oncol.* 2015;33:1325–33.
92. Le DT, Lutz E, Uram JN, Sugar EA, Onners B, Solt S, Zheng L, Diaz LA Jr, Donehower RC, Jaffee EM, Laheru DA. Evaluation of ipilimumab in combination with allogeneic pancreatic tumor cells transfected with a GM-CSF gene in previously treated pancreatic cancer. *J Immunother.* 2013;36:382–9.



93. Oji Y, Nakamori S, Fujikawa M, Nakatsuka S, Yokota A, Tatsumi N, Abeno S, Ikeba A, Takashima S, Tsujie M, Yamamoto H, Sakon M, Nezu R, Kawano K, Nishida S, Ikegame K, Kawakami M, Tsuboi A, Oka Y, Yoshikawa K, Aozasa K, Monden M, Sugiyama H. Overexpression of the Wilms' tumor gene WT1 in pancreatic ductal adenocarcinoma. *Cancer Sci.* 2004;95:583–7.
94. Ulloa-Montoya F, Louahed J, Dizier B, Gruselle O, Spiessens B, Lehmann FF, Suciu S, Kruit WH, Eggermont AM, Vansteenkiste J, Brichard VG. Predictive gene signature in MAGE-A3 antigen-specific cancer immunotherapy. *J Clin Oncol.* 2013;31(19):2388–95.
95. Fuertes MB, Kacha AK, Kline J, Woo SR, Kranz DM, Murphy KM, Gajewski TF. Host type I IFN signals are required for antitumor CD8+ T cell responses through CD8{alpha}+ dendritic cells. *J Exp Med.* 2011;208(10):2005–16.
96. Fuertes MB, Woo SR, Burnett B, Fu YX, Gajewski TF. Type I interferon response and innate immune sensing of cancer. *Trends Immunol.* 2013;34(2):67–73.
97. Zitvogel L, Galluzzi L, Kepp O, Smyth MJ, Kroemer G. Type I interferons in anticancer immunity. *Nat Rev Immunol.* 2015;15(7):405–14.
98. Woo SR, Corrales L, Gajewski TF. The STING pathway and the T cell-inflamed tumor microenvironment. *Trends Immunol.* 2015;36(4):250–6.
99. Krieg AM. CpG still rocks! Update on an accidental drug. *Nucleic Acid Ther.* 2012;22(2):77–89.
100. Molenkamp BG, van Leeuwen PAM, Meijer S, Sluijter BJR, Wijnands PGJTB, Baars A, van den Eertwegh AJM, Scheper RJ, de Gruijl TD. Intradermal CpG-B activates both plasmacytoid and myeloid dendritic cells in the sentinel lymph node of melanoma patients. *Clin Cancer Res.* 2007;13(10):2961–9.
101. Molenkamp BG, Sluijter BJR, van Leeuwen PAM, Santegoets SJAM, Meijer S, Wijnands PGJTB, Haanen JBAG, van den Eertwegh AJM, Scheper RJ, de Gruijl TD. Local administration of PF-3512676 CpG-B instigates tumor-specific CD8+ T-cell reactivity in melanoma patients. *Clin Cancer Res.* 2008;14(14):4532–42.
102. Sluijter BJR, van den Hout MFCM, Koster BD, van Leeuwen PAM, Schneiders FL, van de Ven R, Molenkamp BG, Vosslander S, Verweij CL, van den Tol MP, van den Eertwegh AJM, Scheper RJ, de Gruijl TD. Arming the melanoma sentinel lymph node through local administration of CpG-B and GM-CSF: recruitment and activation of BDCA3/CD141+ dendritic cells and enhanced cross-presentation. *Cancer Immunol Res.* 2015;3(5):495–505.
103. Lou Y, Liu C, Lizée G, Peng W, Xu C, Ye Y, Rabinovich BA, Hailemichael Y, Gelbard A, Zhou D, Overwijk WW, Hwu P. Antitumor activity mediated by CpG: the route of administration is critical. *J Immunother.* 2011;34(3):279–88.
104. Kortylewski M, Xin H, Kujawski M, Lee H, Liu Y, Harris T, Drake C, Pardoll D, Yu H. Regulation of the IL-23 and IL-12 balance by Stat3 signaling in the tumor microenvironment. *Cancer Cell.* 2009;15(2):114–23.
105. Kortylewski M, Swiderski P, Herrmann A, Wang L, Kowolik C, Kujawski M, Lee H, Scuto A, Liu Y, Yang C, Deng J, Soifer HS, Raubitschek A, Forman S, Rossi JJ, Pardoll DM, Jove R, Yu H. In vivo delivery of siRNA to immune cells by conjugation to a TLR9 agonist enhances antitumor immune responses. *Nat Biotechnol.* 2009;27(10):925–32.
106. van den Hout MF, Sluijter BJ, Santegoets SJ, van Leeuwen PA, van den Tol MP, van den Eertwegh AJ, Scheper RJ, de Gruijl TD. Local delivery of CpG-B and GM-CSF induces concerted activation of effector and regulatory T cells in the human melanoma sentinel lymph node. *Cancer Immunol Immunother.* 2016;65(4):405–15.
107. Woo SR, Fuertes MB, Corrales L, Spranger S, Furdyna MJ, Leung MY, Duggan R, Wang Y, Barber GN, Fitzgerald KA, Alegre ML, Gajewski TF. STING-dependent cytosolic DNA sensing mediates innate immune recognition of immunogenic tumors. *Immunity.* 2014;41(5):830–42.
108. Zhu Q, Man SM, Gurung P, Liu Z, Vogel P, Lamkanfi M, Kanneganti T-D. Cutting edge: STING mediates protection against colorectal tumorigenesis by governing the magnitude of intestinal inflammation. *J Immunol.* 2014 15;193(10):4779–82.
109. Veenstra JJ, Gibson HM, Freytag S, Littrup PJ, Wei WZ. In situ immunization via non-surgical ablation to prevent local and distant tumor recurrence. *Oncimmunology.* 2015;4(3):e989762.

110. den Brok MH, Suttmuller RP, Nierkens S, Bennink EJ, Toonen LW, Figdor CG, Ruers TJ, Adema GJ. Synergy between in situ cryoablation and TLR9 stimulation results in a highly effective in vivo dendritic cell vaccine. *Cancer Res.* 2006;66(14):7285–92.
111. Nierkens S, den Brok MH, Roelofsen T, Wagenaars JA, Figdor CG, Ruers TJ, Adema GJ. Route of administration of the TLR9 agonist CpG critically determines the efficacy of cancer immunotherapy in mice. *PLoS One.* 2009;4(12):e8368.
112. Brody JD, Ai WZ, Czerwinski DK, Torchia JA, Levy M, Advani RH, Kim YH, Hoppe RT, Knox SJ, Shin LK, Wapnir I, Tibshirani RJ, Levy R. In situ vaccination with a TLR9 agonist induces systemic lymphoma regression: a phase I/II study. *J Clin Oncol.* 2010;28(28):4324–32.
113. Kim YH, Gratzinger D, Harrison C, Brody JD, Czerwinski DK, Ai WZ, Morales A, Abdulla F, Xing L, Navi D, Tibshirani RJ, Advani RH, Lingala B, Shah S, Hoppe RT, Levy R. In situ vaccination against mycosis fungoides by intratumoral injection of a TLR9 agonist combined with radiation: a phase I/2 study. *Blood.* 2012;119(2):355–63.
114. Marabelle A, Kohrt H, Levy R. Intratumoral anti-CTLA-4 therapy: enhancing efficacy while avoiding toxicity. *Clin Cancer Res.* 2013;19(19):5261–3.
115. Waitz R, Solomon SB, Petre EN, Trumble AE, Fassò M, Norton L, Allison JP. Potent induction of tumor immunity by combining tumor cryoablation with anti-CTLA-4 therapy. *Cancer Res.* 2012;72(2):430–9.
116. Chen Z, Shen S, Peng B, Tao J. Intratumoural GM-CSF microspheres and CTLA-4 blockade enhance the antitumour immunity induced by thermal ablation in a subcutaneous murine hepatoma model. *Int J Hyperth.* 2009;25(5):374–82.
117. Fransen MF, van der Sluis TC, Ossendorp F, Arens R, Melief CJ. Controlled local delivery of CTLA-4 blocking antibody induces CD8+ T-cell-dependent tumor eradication and decreases risk of toxic side effects. *Clin Cancer Res.* 2013;19(19):5381–9.
118. Au JT, Mitra A, Song TJ, Cavnar M, Jun K, Carson J, Gholami S, Haddad D, Gaujoux S, Monette S, Ezell P, Wolchok J, Fong Y. Irreversible electroporation facilitates gene transfer of a GM-CSF plasmid with a local and systemic response. *Surgery.* 2013;154(3):496–503.

Martijn R. Meijerink, Hester J. Scheffer, and  
Govindarajan Naranayan

---

## 18.1 Introduction

Modern medicine is constantly developing less invasive methods for treatment of disease. While some of the research regarding tissue ablation was documented over 100 years ago, the majority of the investigative efforts have taken place within the past 20 years. Since its first introduction in 1990, the efficacy of thermal ablation techniques, such as radiofrequency ablation (RFA) and microwave ablation (MWA), has greatly improved due to technological advancements in image guidance, resulting in real-time tumor localization and accurate needle targeting. Technical advances of the thermal devices such as the development of more powerful generators and better-quality probe designs have further improved the efficacy, creating larger, more spherical, and more predictable ablation zones.

In the rapidly changing climate of tumor ablation, irreversible electroporation (IRE) is the newest kid on the block. Over the past years, IRE has been increasingly used in clinical practice because the hypothetical advantages over thermal ablation seem intuitive and self-evident. However, hard evidence regarding the actual working mechanism and – more importantly – regarding the established safety and efficacy is lacking and conclusions drawn from the available data may very well be prejudiced.

Preclinical and clinical research has demonstrated proof of concept that IRE is capable of creating complete cell death of in situ malignant tumors in humans, without creating major thermal coagulation necrosis. Based on our results, we can further conclude that IRE has an acceptable safety profile, considering the treatment of

---

M.R. Meijerink (✉) • H.J. Scheffer  
Department of Radiology and Nuclear Medicine, VU University Medical Center,  
de Boelelaan 1117, 1081 HV Amsterdam, The Netherlands  
e-mail: [mr.meijerink@vumc.nl](mailto:mr.meijerink@vumc.nl)

G. Naranayan  
Department of Radiology and Nuclear Medicine, Miami, FL, USA

difficult-to-reach tumors that are not suitable for surgical resection and thermal ablation. The toxicity profile, the focal treatment site efficacy, and the currently reported oncological outcome after IRE mandates the setup of larger-scale phase II and III clinical trials for tumors within the liver, biliary tract, pancreas, and prostate.

Nonetheless, many aspects of IRE still need to be unraveled. IRE suffers from several growing pains that need to be addressed in the following years in order to improve its efficacy and further decrease the risk for collateral damage.

---

## 18.2 Knowledge Gaps in Irreversible Electroporation

One of the difficulties encountered in clinical practice is the lack of properly validated tumor-specific standardized treatment protocols, since the current ablation protocols are mainly based on animal studies investigating the effect of IRE on healthy liver tissue. Recent papers have questioned IRE's ability to destroy tumor tissue in the same way it destroys normal tissue. Qin et al. found that even at 1,300 V/cm with 99 pulses, a pulse duration of 100  $\mu$ s, and 10 Hz, there were still islands of viable tumor cells seen [1]. This brings into question a potential flaw in the assumption that tumor tissue will have the same response to IRE as normal tissue. The mechanism of cell death following IRE relies on cell apoptotic responses to loss of homeostasis from pore formation. Tumor cells, known to be resistant to apoptotic pathways, may require higher thresholds to be adequately treated, analogous to increased chemotherapy levels required for tumor cell death [2]. Electric field dose-response studies for tumor-specific tissues are scarce, and much remains unknown about the clinical possibilities to destroy malignant tissues with irregular geometries and heterogeneous properties. An interesting topic to this extent is the study from Appelbaum and colleagues, who showed that multiple shorter cycles of energy application create larger ablation zones [3]. The authors hypothesized that the increase in electrical conductivity induced by an IRE pulse persists after the initial pulse and that longer overall exposure results in an increased shift of cellular contents caused by the membrane permeabilization, thereby enhancing the ablation zone. Apart from their findings, we showed that sequential pulsing simultaneously leads to a lower temperature increase, which improves procedural safety. The model of sequential pulsing needs to be validated in further animal and clinical studies, but could represent a big step forward toward improved safety and efficacy of IRE. Researchers are faced with the challenging task to identify the optimal treatment algorithms of different tumor types with heterogeneous electrical properties, strong enough to create complete tumor cell death while avoiding thermal damage in areas where this can have detrimental effects.

Another shortcoming of IRE that likely reduces procedural efficacy is the lack of well-defined intraprocedural endpoints that can be used to confirm effective ablation. With RFA, tissue necrosis is achieved as the tissue gradually desiccates and eventually loses its ability to conduct current, which is signaled by a precipitous rise

in impedance (“roll-off”), which has been shown to be a significant predictor of local control. With IRE, the current should lie between 20 and 40 A during pulse delivery, but there is no reliable feedback to inform the clinician whether all tissue has been effectively electroporated. Especially with pancreatic IRE, exact delineation of the irreversible damaged ablation zone with intraprocedural ultrasound or CT is not feasible because of the development of edema and gas pockets. Since it has been postulated that increased current is a direct derivative of increased membrane permeabilization [4, 5], the group of Martin and colleagues advises a current increase of 12–15 A from baseline for each electrode pair [6]. If this increase is not reached after the initial 90 pulses, the protocol should be repeated until the desired current change is achieved. However, as shown in the chapter on pancreatic IRE, there is a steady temperature rise during IRE that is also accompanied by a rise in amperage – in an acellular model; caution should be taken when repeating the electroporation protocol, as the accumulated energy may cause thermal damage to the heat-susceptible structures in the vicinity of the ablated region. IRE would benefit from the establishment of solid intraprocedural endpoints that can be used to confirm effective ablation.

A third issue that needs to be addressed is the difficulty of planning the desired three-dimensional geometry of the ablation zone and subsequent electrode placement. At the moment, the NanoKnife® generator converts the three-dimensional tumor measurements (width, height, and depth) into a two-dimensional oval or circle, reducing the tumor to a perfect oval- or circle-shaped “tube,” in which the planned electrode configuration is then drawn. In reality, the shape and size of deep-seated tumors and the subsequent planning of electrode placement is much more complex, and the current software does not take this into account. Recently, a web-based treatment-planning software tool of electroporation-based treatments was developed, including algorithms for automatic tissue segmentation and generation of a 3D model of the tissue [7]. The procedure allows the user to define how the electrodes will be inserted. Finally, electric field distribution is computed, the position of electrodes and the voltage to be applied are optimized using the 3D model, and a downloadable treatment plan is made available to the user. This new software tool may improve treatment planning and subsequent accuracy of IRE delivery.

Last, the geometry of zones of cell death produced by IRE is a complex issue. Placement of multiple electrodes at a 1.5–2.0 cm interelectrode distance while carefully maneuvering past vessels and bile ducts has proven laborious and time-consuming. Misplacement of the probes by a margin of millimeters can already result in residual tumor. Placement of larger probe arrays with multiple repositionings to treat larger tumors has proven even more difficult, and local failure rates of tumors >3 cm are too high. As has been successfully done with thermal ablation, emphasis should be put on the development of electrodes that are capable of creating larger ablation zones, resulting in fewer electrode repositionings, thereby reducing the risk of misplacement. The bipolar probe that is currently being developed is therefore eagerly awaited.

## 18.3 IRE and Cancer Care: Where Do We Go?

### 18.3.1 Colorectal Liver Metastases

In their ablate and resect COLDFIRE-1 study, Scheffer et al. proved that IRE is able to radically destroy in situ colorectal liver metastases [8]. The safety of IRE in the liver has been well documented in the literature; however, the local control rate remains inferior compared to thermal ablation techniques, especially for lesions >3 cm [9–12]. On the other hand, considering that these patients represent a group for which no curative treatment option used to be available, a fair chance of complete tumor destruction already has major implications. Results of the prospective COLDFIRE-2 study are eagerly awaited and will be published at the end of 2017 (Fig. 18.1). Until local control rates improve, IRE should be reserved for well-selected patients with relatively small hepatic tumors that are truly unsuitable for resection and thermal ablation. In general this means tumors abutting the portal triad or the hepatic venous pedicle, where thermal ablation is considered unsafe and less effective. A study comparing IRE to stereotactic body radiation therapy for small-size colorectal liver metastases, which are unsuitable for surgical resection and thermal ablation, is currently being constructed (COLDFIRE-3).

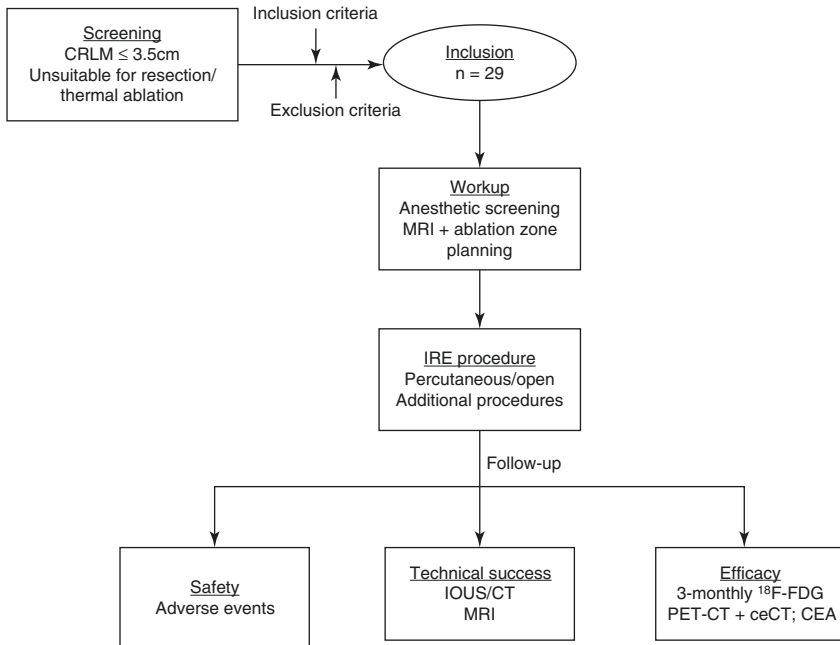
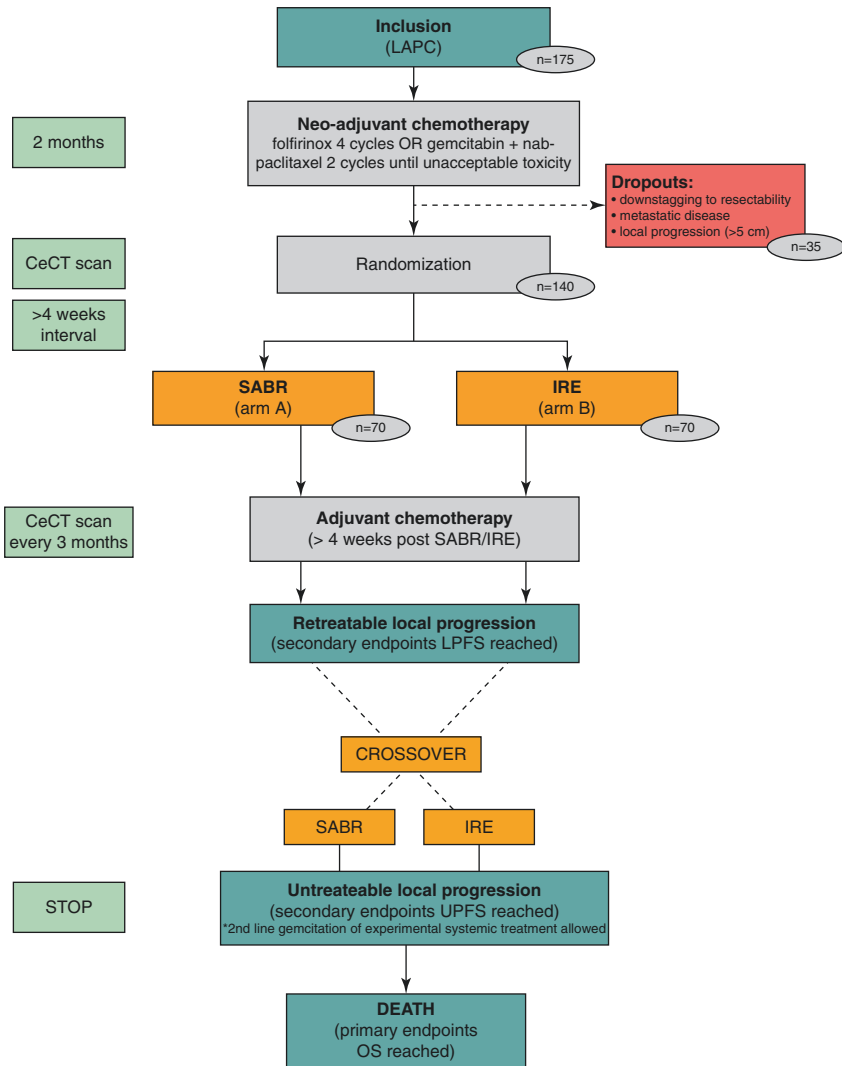


**Fig. 18.1** Flowchart of the COLDFIRE-2 trial study design. The COLDFIRE-2 trial is an ongoing phase I/II trial on IRE for patients with small (<3.5 cm) colorectal liver metastases that are unsuitable for surgery and thermal ablation [13]

### 18.3.2 Pancreatic Cancer

Although ablation of unresectable CRLM is nowadays considered standardized practice, pancreatic tumor ablation raises more questions. Rather than pursuing cure, pancreatic ablation aims to prolong life expectancy while preserving quality of life. Previous studies investigating the safety of IRE reported relatively low complication rates [14–16], although the prospective Amsterdam PANFIRE (percutaneous IRE) and IMPALA (open IRE) trials revealed a significantly higher number of complications. Although a few suggestions were given to reduce IRE-associated morbidity, these complications weigh heavily when considering IRE for LAPC. On the other hand pancreatic IRE shows a promising event-free and overall survival. Whether the assumed survival benefit truly outweighs the morbidity associated with pancreatic IRE – in a patient population that is considered technically incurable – needs to be further assessed. Importantly, the possible role of immune induction yields promise for further improved survival. Besides the introduction of IRE, the traditional cornerstones of LAPC treatment – chemotherapy and radiation – are also subject to alterations. Recently, the landscape for systemic therapy for pancreatic cancer has improved with the advent of folfirinox. In LAPC, folfirinox with or without additional chemoradiation showed improved survival and in some instances even led to downstaging to resectability [17–19]. Additionally, a study in 2013 revealed a survival benefit when nab-paclitaxel was combined with gemcitabine as compared to gemcitabine alone [20]. Improving chemotherapeutic options for pancreatic adenocarcinoma remains an active area of research with multiple ongoing studies. Although the standard treatment regimen of LAPC generally includes radiation, survival data of randomized trials regarding the role of external beam radiation therapy for patients with LAPC have been conflicting [21]. Besides, the use of large radiation fields inevitably delivers a high percentage of the radiation dose to the surrounding tissue, leading to significant toxicity. This limits the delivery of the intended radiation dose to the tumor, increasing the chance for local failure [22]. In order to maximize survival benefit and minimize toxicity, stereotactic ablative body radiotherapy (SABR) recently came on stage. SABR is capable of delivering higher doses of radiation with improved precision using four-dimensional diagnostic imaging, resulting in decreased toxicity and dose-escalation to the tumor [23, 24]. In a disease with so many systemic manifestations, it is hard to see the impact of localized therapy on survival without obtaining some control of metastatic spread with systemic therapy. Besides, there is a growing body of literature that suggests that a multimodal approach combining systemic chemotherapy with focal tumor destruction offers great promise to improved survival of LAPC [25]. The next step toward implementation of IRE in the treatment of LAPC is therefore to compare it with the current standard of care, which consists of folfirinox and radiation. This is the aim of the CROSSFIRE-trial, an international cross-Atlantic multicenter randomized study with overall survival as the primary endpoint, and safety and progression-free survival as secondary endpoints, that started accrual early 2016. In the CROSSFIRE-trial, patients with de

Flow chart of the CROSSFIRE study



Type of study: phase III RCT; design; intention-to-treat; max crossover allowed; 10%; per patient analysis will replace intension-to-treat in case of trend (adding patients); RPSFT analysis in case of dissimilar crossover numbers

**Fig. 18.2** Flowchart of the CROSSFIRE-trial study design. The CROSSFIRE-trial is an ongoing international cross-Atlantic multicenter randomized controlled phase III trial comparing FOLFIRINOX plus SABR to FOLFIRINOX plus IRE

novo LAPC will receive four cycles of folfirinox, after which 70 patients will be randomized to SABR and 70 to IRE. After completion of local treatment, additional folfirinox will be given until progressive disease or maximum toxicity (Fig. 18.2).



### 18.3.3 Perihilar Cholangiocarcinoma

The indications for IRE may extend beyond the liver and the pancreas. A disease where IRE may also show potential is perihilar cholangiocarcinoma (PHC). The location of PHC in the liver hilum and proximal bile ducts causes biliary obstruction with concomitant jaundice. Despite palliative treatment with biliary stenting to relieve cholestasis, patients eventually die of cholangitis, sepsis, or liver failure. As with LAPC, approximately 50% of tumors are considered locally advanced because of unreconstructable vascular or extensive biliary involvement and during exploratory laparotomy another 40% have locally advanced or metastasized tumors [26, 27]. Liver transplantation is the only chance for cure for these patients but has strict selection criteria [28]. Several ablative strategies for the treatment of PHC have been investigated, such as photodynamic therapy, intraductal RFA, brachytherapy, and MWA, but without great success, mostly due to the heat-sink effect. The successful case report by Melenhorst et al. [29] stimulated us to develop the ALPACA-trial, a joint effort between the VU University Medical Center and the Academic Medical Center in Amsterdam. In this pilot study, ten patients with upfront unresectable PHC will be treated with percutaneous IRE, whereas another ten patients that are found to have advanced PHC intraoperatively are treated with IRE during the same surgical exploration session. Rather than placing a metal stent for biliary protection, which may leave a rim of vital tissue behind as shown in Chap. 11, percutaneous biliary drainage using plastic stents will be performed prior to IRE for biliary protection. The primary aim of the ALPACA-trial is to investigate the safety and feasibility of IRE for advanced PHC; secondary endpoints are progression-free and overall survival and quality of life (see Fig. 18.3 for the flowchart of the ALPACA-trial).

## 18.4 Future Perspectives

As interventional oncologic therapies evolve, they are combined with other treatments in a multimodality approach to treating cancer. Combined therapy of ablation with embolization, radiation with embolization, or chemotherapy with ablation are just a few examples of treatment options that show the promise of this multifaceted approach to increase treatment effect.

Directly after IRE a margin of reversibly electroporated tissue exists between the irreversibly damaged ablation zone and the normal tissue. During this temporary permeability of the cell membranes, macromolecules such as chemotherapeutics can travel freely into the cells within this zone, a process known as electrochemotherapy. Capitalizing on this principle, if IRE were combined with systemic or intratumorally injected chemotherapy, marginal remnant viable tumor cells within this zone could be eradicated with electrochemotherapy. The therapeutic advantage of combinatorial irreversible electroporation and electrochemotherapy is the focus of current studies [30].

On another level, we have proven that besides inducing local tumor destruction, the mechanism through which IRE operates also results in a systemic effect. This local immune response could result in the destruction of micrometastases in the

Flow chart of the ALPACA study

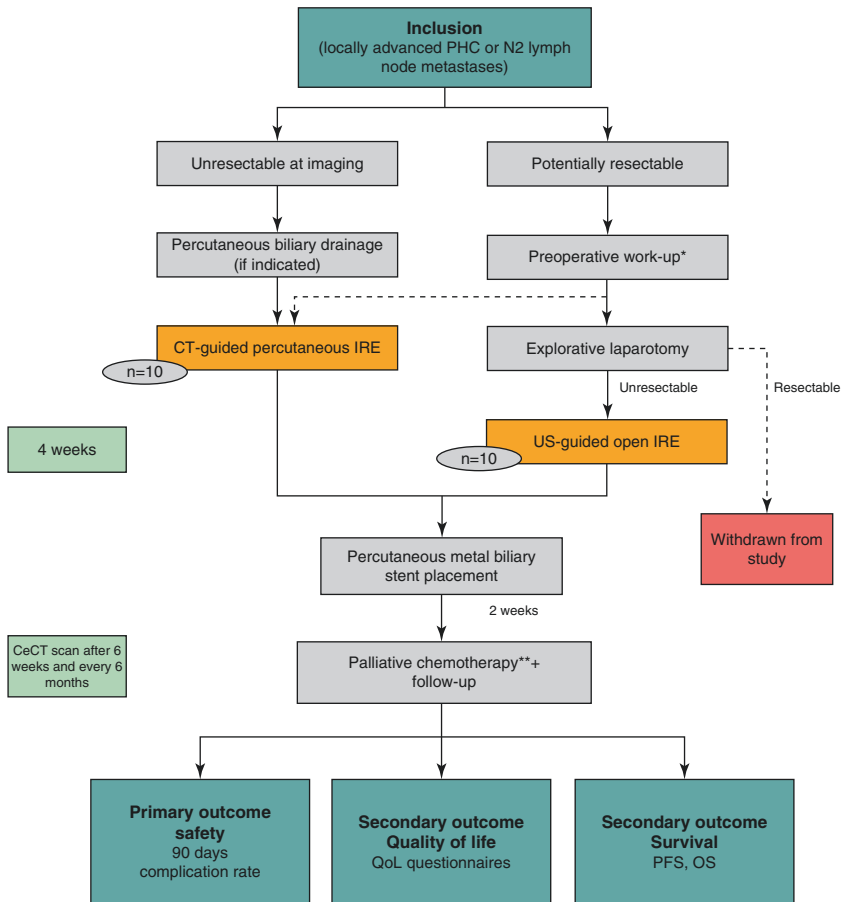


**Fig. 18.3** Flowchart of the ALPACA-trial study design. The ALPACA-trial is an ongoing phase I/II pilot study investigating the safety and feasibility of IRE for patient with locally advanced perihilar cholangiocarcinomas (Klatskin)

affected lymph nodes, which could positively affect survival. More importantly, locally generated antitumor T-cell responses could ultimately provide protection against outgrowth of distant metastases and may lead to memory responses, potentially providing long-term immune protection against tumor outgrowth. Our data suggest that IRE offers an attractive and effective in situ vaccination platform to combine with immunotherapeutic approaches. In the coming years, this approach will be further investigated. A similar potential to recruit the immune system has been suggested for RFA [31]. Therefore, although it is paramount that the thermal effect of IRE should not exceed the threshold for thermal damage near heat-susceptible structures, the thermal and the electrical element of IRE may have a synergistic effect and may induce the greatest antitumor effect together. The immunologic potential of electrical and thermal ablation is the current focus of several trials.

Harnessing the immune system to enhance both local and systemic treatment effect is yet another approach that warrants study and may one day offer the bridge between local and systemic treatment. The detectable and durable T-cell responses point to a protective antitumor immune response induced by IRE. Combining IRE with immune stimulation may represent another therapeutic platform for improved survival and will be the focus of future studies.

Other indications for IRE that show promise but which are not covered in this book are thyroid cancer and intracerebral gliomas [30, 32]. The feasibility of using pulsed electric fields to permeabilize the endothelial cells of the blood-brain barrier was recently demonstrated. This allows for increased drug transport across the blood-brain barrier through the transcellular pathway and may be used in combination with IRE for brain tumors [33]

The aims of this book are (1) to provide better insight in the working mechanism of IRE with respect to the thermal component simulating different clinical scenarios and (2) to provide solid data on the specific safety and efficacy of IRE for current and future clinical indications. To this extent we can conclude that the clinical treatment protocols for IRE generate considerable heat and every physician should take this into account when performing IRE. IRE is capable of creating irreversible cell death and to achieve macroscopic complete tumor eradication without inducing thermal coagulation necrosis.

As with any new technique, more questions have been raised than answers have been given. The technique is still in its infancy, and we are just starting to understand the exact working mechanism of IRE and its side effects. Technical improvements of the ablation device and increasing knowledge about tissue-specific electrical properties should result in improved efficacy in the future.

The foundation has been laid for the next grand challenge for IRE: to prove its efficacy in large randomized controlled trials. Until then, the technique should be reserved for well-selected patients with relatively small tumors that are truly unsuitable for resection and thermal ablation.

Nevertheless, based on the available literature and their early clinical experience, the authors and editors expect IRE to prove a valuable fortification in the armory of interventional oncologists treating patients with cancer in the near future.

---

## References

1. Qin Z, et al. Irreversible electroporation: an in vivo study with dorsal skin fold chamber. *Ann Biomed Eng.* 2013;41(3):619–29.
2. Silk M, et al. The state of irreversible electroporation in interventional oncology. *Semin Interv Radiol.* 2014;31(2):111–7.
3. Appelbaum L, et al. Irreversible electroporation ablation: creation of large-volume ablation zones in in vivo porcine liver with four-electrode arrays. *Radiology.* 2014;270(2):416–24.
4. Ivorra A, Rubinsky B. In vivo electrical impedance measurements during and after electroporation of rat liver. *Bioelectrochemistry.* 2007;70(2):287–95.
5. Ivorra A, et al. In vivo electrical conductivity measurements during and after tumor electroporation: conductivity changes reflect the treatment outcome. *Phys Med Biol.* 2009;54(19):5949–63.
6. Dunki-Jacobs EM, Philips P, Martin RC 2nd. Evaluation of resistance as a measure of successful tumor ablation during irreversible electroporation of the pancreas. *J Am Coll Surg.* 2014;218(2):179–87.

7. Pavliha D, et al. Planning of electroporation-based treatments using web-based treatment-planning software. *J Membr Biol.* 2013;246(11):833–42.
8. Scheffer HJ, et al. Ablation of colorectal liver metastases by irreversible electroporation: results of the COLDFIRE-I ablate-and-resect study. *Eur Radiol.* 2014;24(10):2467–75.
9. Eller A, et al. Local control of perivascular malignant liver lesions using percutaneous irreversible electroporation: initial experiences. *Cardiovasc Intervent Radiol.* 2015;38(1):152–9.
10. Cannon R, et al. Safety and early efficacy of irreversible electroporation for hepatic tumors in proximity to vital structures. *J Surg Oncol.* 2013;107(5):544–9.
11. Kingham TP, et al. Ablation of perivascular hepatic malignant tumors with irreversible electroporation. *J Am Coll Surg.* 2012;215(3):379–87.
12. Silk MT, et al. Percutaneous ablation of peribiliary tumors with irreversible electroporation. *J Vasc Interv Radiol.* 2014;25(1):112–8.
13. Scheffer HJ, et al. Colorectal liver metastatic disease: efficacy of irreversible electroporation – a single-arm phase II clinical trial (COLDFIRE-2 trial). *BMC Cancer.* 2015;15:772.
14. Paiella S, et al. Safety and feasibility of irreversible electroporation (IRE) in patients with locally advanced pancreatic cancer: results of a prospective study. *Dig Surg.* 2015;32(2):90–7.
15. Martin RC 2nd, et al. Irreversible electroporation therapy in the management of locally advanced pancreatic adenocarcinoma. *J Am Coll Surg.* 2012;215(3):361–9.
16. Narayanan G, et al. Percutaneous irreversible electroporation for downstaging and control of unresectable pancreatic adenocarcinoma. *J Vasc Interv Radiol.* 2012;23(12):1613–21.
17. Faris JE, et al. FOLFIRINOX in locally advanced pancreatic cancer: the Massachusetts General Hospital cancer Center experience. *Oncologist.* 2013;18(5):543–8.
18. Hosein PJ, et al. A retrospective study of neoadjuvant FOLFIRINOX in unresectable or borderline-resectable locally advanced pancreatic adenocarcinoma. *BMC Cancer.* 2012;12:199.
19. Suker M, et al. FOLFIRINOX for locally advanced pancreatic cancer: a systematic review and patient-level meta-analysis. *Lancet Oncol.* 2016;17(6):801–10.
20. Von Hoff DD, et al. Increased survival in pancreatic cancer with nab-paclitaxel plus gemcitabine. *N Engl J Med.* 2013;369(18):1691–703.
21. Loehrer PJ Sr, et al. Gemcitabine alone versus gemcitabine plus radiotherapy in patients with locally advanced pancreatic cancer: an Eastern Cooperative Oncology Group trial. *J Clin Oncol.* 2011;29(31):4105–12.
22. Gurka MK, et al. Stereotactic body radiation therapy with concurrent full-dose gemcitabine for locally advanced pancreatic cancer: a pilot trial demonstrating safety. *Radiat Oncol.* 2013;8:44.
23. Berber B, et al. Emerging role of stereotactic body radiotherapy in the treatment of pancreatic cancer. *Expert Rev Anticancer Ther.* 2013;13(4):481–7.
24. Lax I, et al. Stereotactic radiotherapy of malignancies in the abdomen. *Methodological aspects. Acta Oncol.* 1994;33(6):677–83.
25. Auriemma WS, et al. Locally advanced pancreatic cancer. *Semin Oncol.* 2012;39(4):e9–22.
26. Matsuo K, et al. The Blumgart preoperative staging system for hilar cholangiocarcinoma: analysis of resectability and outcomes in 380 patients. *J Am Coll Surg.* 2012;215(3):343–55.
27. Ruys AT, et al. Long-term survival in hilar cholangiocarcinoma also possible in unresectable patients. *World J Surg.* 2012;36(9):2179–86.
28. Darwish Murad S, et al. Predictors of pretransplant dropout and posttransplant recurrence in patients with perihilar cholangiocarcinoma. *Hepatology.* 2012;56(3):972–81.
29. Melenhorst MC, et al. Percutaneous irreversible electroporation of Unresectable hilar cholangiocarcinoma (Klatskin tumor): a case report. *Cardiovasc Intervent Radiol.* 2016;39(1):117–21.
30. Neal RE 2nd, et al. In vitro and numerical support for combinatorial irreversible electroporation and electrochemotherapy glioma treatment. *Ann Biomed Eng.* 2014;42(3):475–87.
31. Rombouts SJ, et al. Systematic review of innovative ablative therapies for the treatment of locally advanced pancreatic cancer. *Br J Surg.* 2015;102(3):182–93.
32. Meijerink MR, et al. Percutaneous irreversible electroporation for recurrent thyroid cancer – a case report. *J Vasc Interv Radiol.* 2015;26(8):1180–2.
33. Bonakdar M, et al. Electroporation of brain endothelial cells on chip toward permeabilizing the blood-brain barrier. *Biophys J.* 2016;110(2):503–13.

---

# Index

## A

- Ablative techniques, 105–106
- Ablative tumor therapies, 251
- Abscopal effect, 250
- Active surveillance (AS), 216
- AngioDynamics, 70, 188, 207
- Angulation, 58
- Animal electricity, 17
- Anisotropic tissue, 59
- Anode break excitation, 20
- Anterior inferior pancreaticoduodenal artery, 169
- Antitumor immunity, 249
  - cryoablation, 253–254
  - ECT, 256
  - HiFU, 254
  - IRE
    - in vivo vaccination, 257–260
    - and local immune modulation, 261
  - MWA, 253
  - PDT, 255
  - RFA, 252
  - SBRT, 255
- Arrhenius integral, 128
- Arterial blood supply, 142
- Artificial inhomogeneities, 129
- Automatic segmentation, 69
- Avalanche breakdown, 25

## B

- Bilayer lipid membranes (BLM),
  - pore generation
  - in, 54, 55
- Biliary endoprosthesis, 111
- Biliary system
  - clinical studies, 84–86
  - preclinical studies, 84

## Blood vessels

- clinical studies, 83–84
  - preclinical studies, 82–83
- Bowing, 58

## C

- Calcium electroporation, 23
- Celiac plexus, 169
- Cervical cancer, 227
- CEUS, 152. *See* Contrast-enhanced US (CEUS)
- Claude Couinaud's segment, 141
- Clinical target volume (CTV), 67
- Coccygeal plexus, 225
- Color Doppler ultrasound, 29
- Colorectal liver metastases, 274
- Computed tomography (CT), 151, 235
  - liver tumors, 156
  - PHC, 198
- Conductive implants, 62
- Conductivity, 47
- Contrast-enhanced CT (ceCT), 118
- Contrast-enhanced US (CEUS), 31, 116, 119, 150, 152
- Cryoablation, 253
- Cryotherapy, 8
- CT hepatic angiography (CTHA), 152

## D

- Damage-associated molecular patterns (DAMPs), 250, 251, 254, 255, 259, 261
- Dendritic cells (DCs), 250
- Diffusion-weighted imaging (DWI), 118
- Disease recurrence, 158
- Dorsal pancreatic artery, 169
- Dynamic conductivity, 60

**E**

- 18F-FDG PET-CT, 234
- Electric fields, 42, 57
  - artificial inhomogeneities, 129
  - electrode geometry, deviations in, 58
  - Joule heating, 60
  - Laplace's equation, 48
  - natural inhomogeneities, 128
  - Ohm's law, 44
    - electrical conductivity, 45
    - permittivity, 46
    - shape functions, 48
    - pulse characteristics, 43
- Electrical conductivity, 45
- Electrochemotherapy (ECT), 22, 187, 256
- Electrode arrays, 63
- Electrode geometry, deviations
  - anisotropic tissue, 59
  - bowing and angulation, 58
  - shape functions, 49
  - skewness, 59
  - tissue inhomogeneity, 59
  - vascularization and perfused tissue, 60
- Electrodes, 207
- Electrofusion, 23
- Electrogenotherapy, 24
- Electromagnetic navigation, 76
- Electroporation, 13
  - historical review, 14
  - Lichtenberg phenomenon, 17–18
  - pulsed electric fields
    - and medicine, 20–31
    - and water sterilization, 18–19
- Endocrine pancreas, 170
- Endometrial cancer, 227
- Endoscopic placement, 112
- Endoscopic retrograde
  - cholangiopancreatography (ERCP), 111
- External beam radiation (EBR), 172
- External beam radiation therapy (EBRT), 146

**F**

- Finite element method (FEM), 42, 69
- Focal nodular hyperplasia (FNH), 143
- Foley catheter, 206

**G**

- Gene delivery, 24
- Greater pelvis, 224
- Gross tumour volume (GTV), 67
- Gynecological cancers, 227

**H**

- Health technology assessment, 212
- Hemangioma, 143
- Henriques–Moritz damage model, 128
- Hepatocellular adenoma (HCA), 143
- Hepatocellular carcinoma (HCC), 147
- High-intensity focused ultrasound (HiFU), 8, 251, 254
- Human tumor ablation, 28
- Hypogastric plexuses, 225

**I**

- Image-guided tumor ablation
  - cryoablation, 8
  - HIFU, 8
  - laser ablation, 8, 9
  - percutaneous ethanol ablation, 6
  - RFA, 7
- Immune checkpoint inhibitors, 249
- Immunogenic cell death, 256
- Infection, 106
- Intrahepatic bile ducts, 142
- Intraoperative neurophysiologic monitoring (IONM), 90
- Intravenous contrast agent, 108
- Irreversible electroporation (IRE), 13, 24
  - ablation monitoring and endpoint assessment, 117–119
  - applications, 31
  - colorectal liver metastases, 274
  - effects, 27–28
  - human tumor ablation, 28
  - indications, 279
  - interventional oncologic therapies, 277
  - in vivo vaccination, 257, 260
  - knowledge gaps, 272–273
  - needle insertion and image guidance, 116–117
  - numerical methods and models, 67–68
    - different pulse parameters, 70–72
    - evaluating treatment outcomes, statistical methods, 75–76
    - fusion with navigation systems, 76
    - treatment plans, optimization, 72
    - 2D vs 3D modelling and treatment planning tools, 72–75
  - pancreatic cancer, 275–276
  - PHC, 277–278
  - preclinical and clinical research, 271
  - pulsed electrical fields, nonthermal spectrum of, 123
  - risk prevention, 106–107
    - probe placement, 107–110
    - pulsed electrical field exposure, 110–112
    - site-specific AEs, 110

- theoretical mechanism, 122–123
- thermal effects, 124–127
- treatment planning, 115
- Ischemia, 23
- Islet cell tumors, 171
  
- J**
- Joule heating
  - conductive implants, 62
  - dynamic conductivity, 60
  - electrode arrays and pulse sequences, 63
  - electrode exposure length, 63
  - pulse number, 62
  
- K**
- Kidney tumours
  - approach and image guidance, 204–206
  - complications, 210–211
  - contraindications, 203
  - disease recurrence, 212
  - diseases, 202, 203
  - follow-up and response evaluation, 211
  - health technology assessment, 212
  - indications, 203
  - (neo)adjuvant treatment and supportive procedures, 211
  - patient workup and treatment planning, 204, 205
  - technique, 206–209
- Klatskin tumor. *See* Perihilar cholangiocarcinoma (PHC)
- Knowledge gaps, 272
  
- L**
- Laplace's equation, 48
  - parallel plate electrodes, 50
  - two cylindrical electrodes, 51
- Laser ablation, 8
- Laser-induced interstitial thermotherapy, 8
- Lever technique, 107–110
- Liver tumors
  - clinical studies, 160
  - complications, 152–155
  - computed tomography, 156
  - control rates, 161
  - disease recurrence, 158–159
  - follow-up and response evaluation, 155–154
  - general technique, approach and image guidance, 150–153
  - indications
    - benign, 148
    - contraindications, 149
    - malignant, 148–149
  - limitations, 160
  - MRI, 157–158
  - organ-specific disease
    - FNH, 143
    - HCA, 143
    - HCC, 147
    - hemangioma, 143
    - liver metastases, 144–147
  - patient workup and treatment planning, 149–150
  - PET, 156
  - portal triad, 142
  - segments, 140–141
  - venous drainage, 142
- Local ablative therapies, 250
- Local immune modulation, 261
- Locally advanced pancreatic carcinoma (LAPC), 258
  - chemotherapy, 172
  - new local ablative therapies, 173
  - radiotherapy, 172
- Lumbar plexus, 225
- Lung tumors
  - clinical experience, 244
  - complications, 243
  - contraindications, 240–241
  - disease indication, 240
  - follow-up and response assessment, 244
  - intervention, 241–243
  - nonthermal ablation technique, 240
  - pretreatment work-up, 241, 242
  
- M**
- Magnetic resonance imaging (MRI), 118, 152, 156, 157
- Microwave ablation (MWA), 9, 10, 253
- Modern electrodynamic theory, 42
  
- N**
- NanoKnife generator, 115
- Nanoknife® system, 198
- Natural inhomogeneities, 128
- Neodymium:yttrium-aluminum-garnet (Nd:YAG) laser system, 8
- Nerves
  - clinical studies, 89–90
  - preclinical studies, 89
- Neurovascular bundle, 217
- Nonthermal irreversible electroporation, tissue ablation, 26

**O**

## Ohm's law

- electrical conductivity, 45
- permittivity, 46
- shape functions, 48

**P**

## Pancreas

- bile duct, 168
- celiac plexus, 169
- clinical studies, 86–88
- glands, 170
- pancreaticoduodenal arterial arcades, 168
- preclinical studies, 86
- superior and inferior lymphatic vessels, 169
- uncinate process, 168
- venous drainage, 169

## Pancreatic adenocarcinoma, 170–171

## Pancreatic malignancies

- complications, 179–181
- disease recurrence
  - IRE, local recurrence after, 185–186
  - pancreaticoduodenectomy, local recurrence after, 184–185
- follow-up and response evaluation, 182–184
- image guidance, and technique, 175–176
  - open approach, 176–177
  - percutaneous CT-guided approach, 178–179
  - percutaneous US-guided approach, 177–178
- Islet cell tumors, 171
- ongoing and clinical trials, 187–188
- overall and progression-free survival, 186
- pancreatic adenocarcinoma, 170
- patient selection, indications and contraindications, 173–174
- patient workup and treatment planning, 174–175
- QoL, 185
- treatment, 171–172
  - chemotherapy, 172
  - new local ablative therapies, 173
  - radiotherapy, 172–173

## Pancreaticoduodenectomy, local recurrence after, 184

## Parallel plate electrodes, 50

## Parallelism, 68

## Patient selection, 110–112

PCa. *See* Prostate cancer (PCa)

## Peleg-Fermi model, 76

## Pelvic autonomic nerves, 225

## Pelvic tumors, within pelvic cavity

- approach, image guidance and technique, 230
- case report, 233–236
- complications, 231–232
- disease recurrence, 233
- follow-up and response evaluation, 233–235
- gynecological cancers, 227
- indications and contraindications, 229
- ongoing and clinical trials, 236
- patient selection, 228–229
- patient workup and treatment planning, 229
- rectal cancer, 226

## Pelvis, 224–225

## Pennes' bioheat equation, 70

## Percutaneous ethanol ablation, 6–7

## Percutaneous transhepatic biliary drains (PTCDs), 196

## Percutaneous tumor ablation, 107

## Perfused tissue, 60

## Perihilar cholangiocarcinoma (PHC), 191, 277

- ablative strategies, 192–195
- contraindications, 196
- follow-up and response evaluation, 199
- image guidance, and technique, 198–199
- indications, 195
- location of, 192
- patient selection, 195
- patient workup and treatment planning, 196–197
- prognosis, 192
- systemic chemotherapy, 192

## Perioperative peripheral nerve injury (PPNI), 107

## Permittivity, 46

## Photodynamic therapy (PDT), 192, 255

## Planning target volume (PTV), 67

## Pneumodissection, 108

## Portal triad, 142

## Portal vein, 142

## Portal vein embolization (PVE), 144

## Portal vein stenting, 111

## Positron emission tomography (PET), liver tumors, 156

## Prostate cancer (PCa)

- focal therapy, 215–217
- follow-up, 219
- functional outcomes, 219
- ongoing trials, 220
- patient selection, 217–218
- potency, 219



- risk groups, 220
  - short-term oncological control, 220
  - treatment procedures and peri- and postoperative complications, 218–219
- Pulsed electric fields
- exposure, 110
  - and food industry, 19
  - and medicine, 20–22
    - animals, IRE effects, 27
    - applications, IRE, 31–32
    - electrofusion, 23
    - electrogenotherapy, 24
    - IRE, human tumor ablation, 28
    - irreversible electroporation, 24–26
    - tissue ablation, nonthermal irreversible electroporation, 26–27
  - and water sterilization, 18
  - nonthermal spectrum of, 123–124
- Pulse sequences, 63
- Pyknosis, 124
- Q**
- Quality of life (QoL), 185
- R**
- Radiation-induced liver disease (RILD), 146
- Radiofrequency ablation (RFA), 7, 129, 145, 240, 252, 253
- Radiotherapy, 68
- Reactive oxygen species (ROS), 255
- Rectal cancer, 226
- S**
- Sacral plexus, 225
- Schwan equation, 52
- Sequential pulsing, 112
- Skewness, 59
- Skin electroporation, 22
- Splenic artery, 169
- Stereotactic ablative body radiotherapy (SABR/SBRT), 146, 172, 255, 275
- Superior pancreaticoduodenal arteries, 168
- Surgical resection, 81
- T**
- Thermal ablation, 81
- Thermal energy
- artificial inhomogeneities, 129
  - contributory element, 130
  - natural inhomogeneities, 128
  - potentially dangerous side effect, 129
- 3-D medical imaging modalities, 42
- 3D modelling, 72
- Tissue ablation, nonthermal irreversible electroporation, 26
- Tissue inhomogeneity, 59
- Toll-like receptor ligands (TLR-L), 251, 261, 263
- Transmembrane potential, 52, 54
- Transperineal template-mapping biopsies (TTMB), 218
- Treatment planning, 115–116
- Two cylindrical electrodes, 51
- 2D modelling, 72
- U**
- Urinary tract
- clinical studies, 88–89
  - preclinical studies, 88
- Urine, 202
- V**
- Vascular lock, 23
- Vascular smooth muscle cells (VSMC), 27
- Vascularization, 60
- Venous drainage, 142
- Visceral arteries, abdominal aorta
- cranial, 109
- Visualization, 41
- Vulvar cancer, 227
- W**
- Water sterilization, 18
- X**
- X-rays, 5